22 July 2005

Science

Vol. 309 No. 5734
Pages 521–652 $10

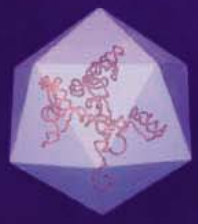

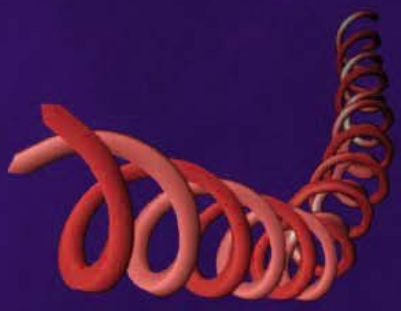

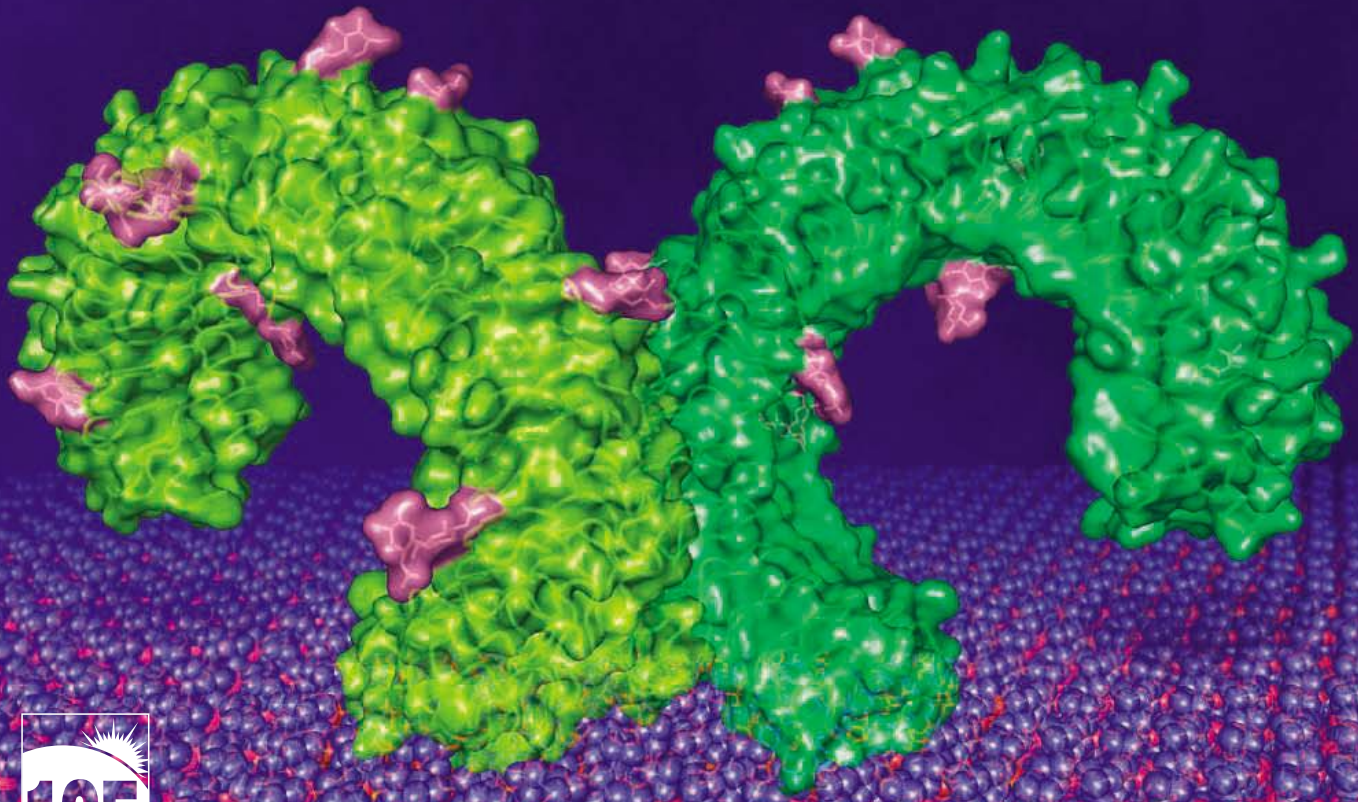

Now Available!
Gene Expression Data for Primary Cells
Visit the What's New section at www.cambrex.com/bioproducts

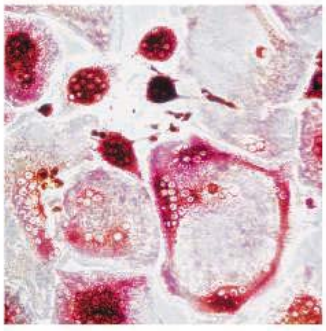
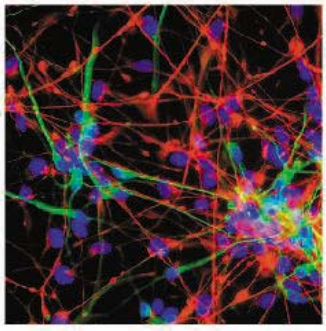
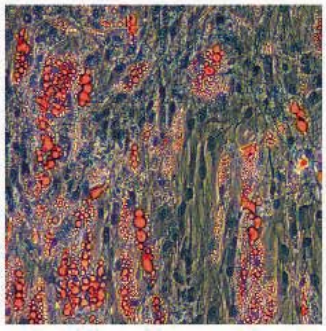
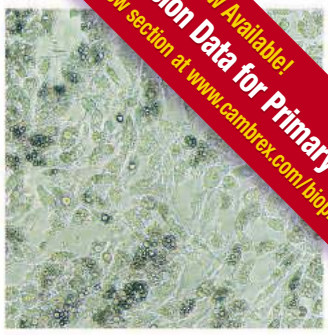

Primary. Human. Ready to Use.

Poietics™ Differentiating Cell Systems

Bone, Adipose, Neural Cells and Media Kits

- Osteoclast precursors that stain positive for TRAP and resorb bone upon differentiation.
- Preadipocytes isolated from subcutaneous and visceral fat.
- Neural progenitors stained positive for β-tubulin III and GFAP.

Hematopoietic Progenitor Cells

- Fresh unprocessed bone marrow from a wide donor selection.
- Progenitors include $CD34^+$, $CD133^+$, mononuclear cells, and erythroid progenitors.
- Sources include mobilized and normal peripheral blood, bone marrow, and cord blood.

Mesenchymal Stem Cells

- Highly homogeneous MSC population tested and guaranteed in 3 different lineages.
- Media kits available for the expansion of MSCs, and the differentiation of osteoblasts, chondrocytes, and adipocytes.

Immune Cells

- $CD14^+$ Monocytes.
- Dendritic cells and precursors.
- $CD4^+$ T cells and $CD19^+$ B cells from cord blood.

Cambrex, the source for Clonetics® and Poietics™ Cell Systems, BioWhittaker™ Classical Media, SeaPlaque® and NuSieve® Agarose, and PAGEr® *Precast Gels.*

For more information contact us at:
www.cambrex.com
U.S. **800-638-8174** | Europe **32 (0) 87 32 16 09**

Cambrex Bio Science Walkersville, Inc.
8830 Biggs Ford Road | Walkersville, MD 21793

CAMBREX
Innovation. Experience. Performance.

Obviously influenced by the microarray software movement.

Relate your microarray data into biological pathways with Stratagene's software solutions.

In addition to developing innovative reagents and instrumentation, Stratagene now offers software solutions for life science researchers. We engineer our software so that it is powerful but extremely easy to use, allowing you to focus on your research.

Our Interaction Explorer™ Software (PathwayAssist) enables the building of pathway/biological association networks extracted from scientific literature, while our ArrayAssist® and GeneTraffic® software are specifically designed for analyzing microarray data.

- **Interaction Explorer™ Software (PathwayAssist) – turning microarray data into pathways**
- **ArrayAssist® Software – for complete microarray data analysis**
- **GeneTraffic® Software – data management and analysis for microarray core facilities**

Need More Information? Give Us A Call:

Stratagene USA and Canada
Order: (800) 424-5444 x3
Technical Services: (800) 894-1304

Stratagene Europe
Order: 00800-7000-7000
Technical Services: 00800-7400-7400.

Stratagene Japan K.K.
Order: 03-5159-2060
Technical Services: 03-5159-2070

www.stratagene.com

Ask us about these great products:

Visit **www.stratagene.com/softwaresolutions** for more information or to download trial versions of our software.

STRATAGENE

GE Healthcare

Ni Sepharose™

4x greater binding capacity in histidine-tagged protein purification

Ni Sepharose™ products from GE Healthcare give you the highest binding capacity available for histidine-tagged protein purification. With up to four times the binding capacity, it's no longer pure imagination to dramatically increase your yield, while saving time and costs. Maximum target protein activity is assured, thanks to tolerance of a wide range of additives and negligible nickel ion leakage. The flexibility to use a variety of protocols ensures the highest possible purity. Ni Sepharose 6 FF is excellent for manual procedures such as gravity/batch and easy scale-up, while the HP version is designed for high-performance in automated purification systems – both are available in different formats, including prepacked columns. Outstanding performance has never been easier to achieve.

www.amershambiosciences.com/his

imagination at work

GE10-05

Science

Volume 309
22 July 2005
Number 5734

COVER A surface representation of human Toll-like receptor 3, derived from the x-ray crystal structure and shown on a cell membrane. The glycosylated Toll-like receptor dimer (green with pink sugars) recognizes double-stranded RNA (orange) from microbial pathogens such as viruses (lavender). Binding of the RNA to the receptor activates the innate immune system. The structure is described on page 581. [Image: J. Choe, M. Pique, and I. A. Wilson]

DEPARTMENTS

NEWS OF THE WEEK

NEWS FOCUS

548

561

564

LETTERS

BOOKS *ET AL.*

POLICY FORUMS

PERSPECTIVES

REVIEW

Contents continued

EndNote. Where millions of researchers, librarians and students begin.

Learn about new tools for your research and publishing—

Onfolio™
Organize RSS feeds and Web research

RefViz™
Visualize references

sciPROOF™
Proof your manuscript

800-722-1227 • 760-438-5526
Fax: 760-438-5573
rs.info@thomson.com

EndNote, used by millions of researchers, students, professors, librarians and writers worldwide, is known for introducing innovative features such as the ability to search online bibliographic databases, organize references and images, and create instant bibliographies. With EndNote 9, you can work faster with increased performance, connect to more data sources worldwide, and share customized libraries with colleagues easily. EndNote is easy to use, easy to learn and is seamlessly compatible with Microsoft® Word for Windows® and Mac® OSX. There simply is no better way to manage your references and build instant bibliographies.

Download your Free demo or buy online today.
www.endnote.com

Science

SCIENCE EXPRESS www.sciencexpress.org

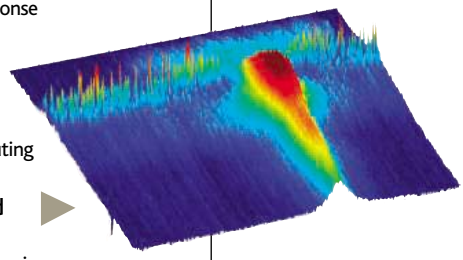

TECHNICAL COMMENT ABSTRACTS

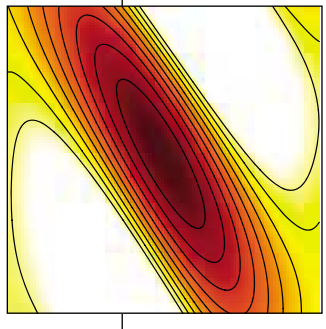

565 & 586

BREVIA

RESEARCH ARTICLES

REPORTS

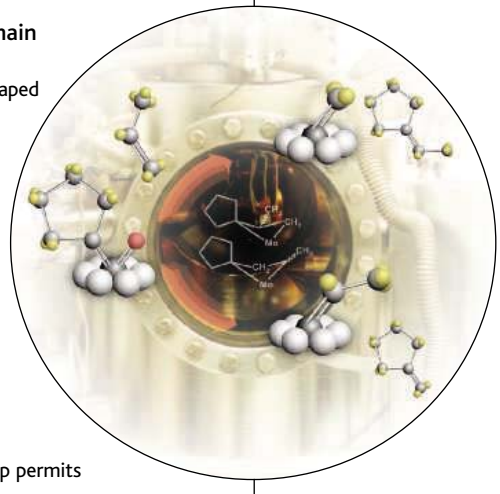

588 & 591

Contents continued

Spend less time looking for antibodies and more time doing research...

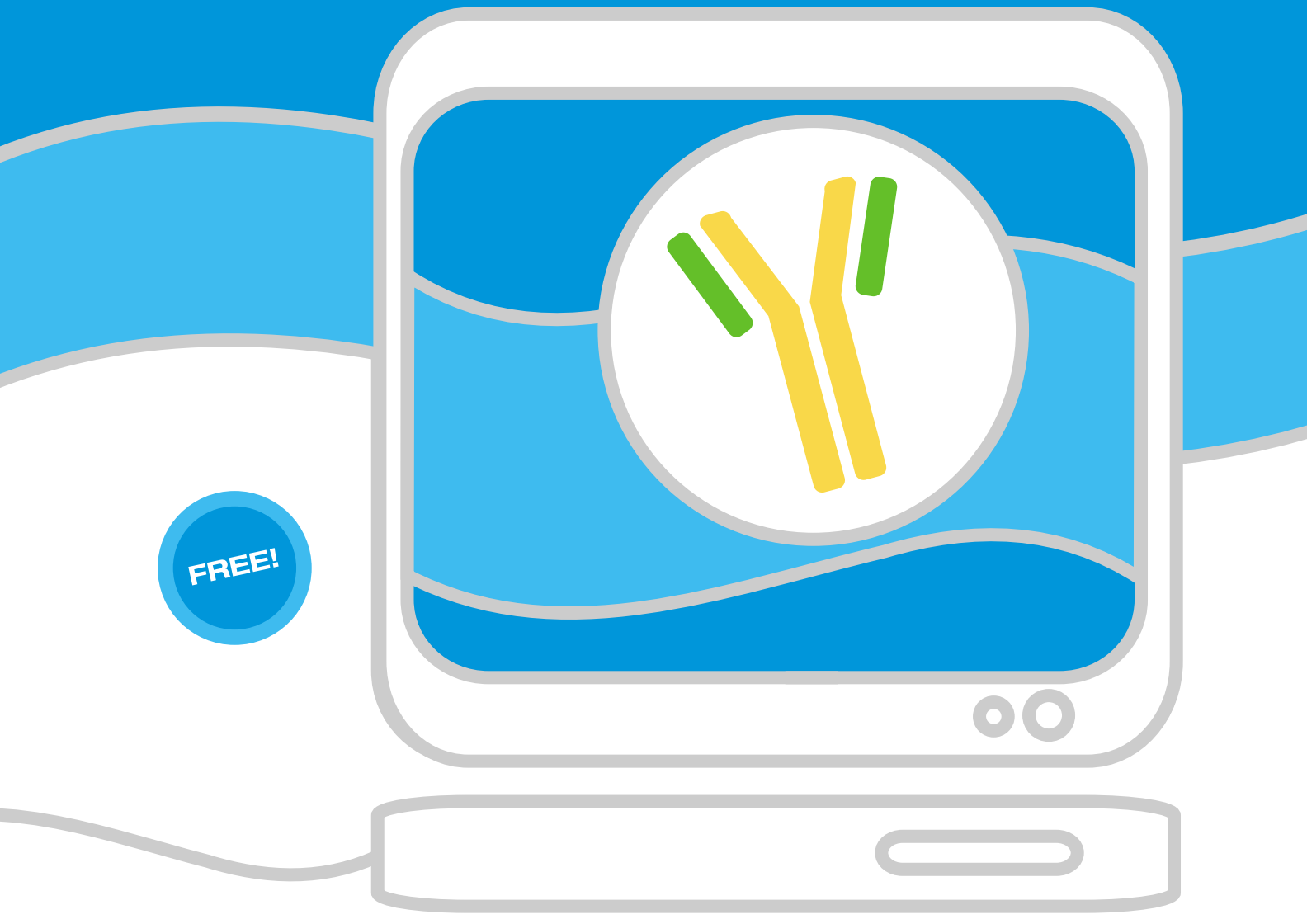

FREE!

Find Antibodies Online

Search over 130,000 antibodies from over 100 companies by antigen, species reactivity, and application... free and online.

- Over 130,000 Antibodies
- Over 100 Antibody Companies
- No Registration Required
- Full Product Specifications
- Over 225,000 Research Products and Instruments
- Direct Access to Product Pages on Company Websites

biocompare®

The Buyer's Guide for Life Scientists™

www.biocompare.com

REPORTS CONTINUED

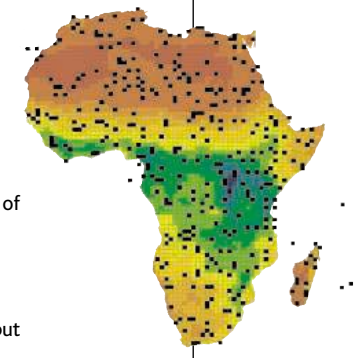

546 & 603

617

AAAS
ADVANCING SCIENCE, SERVING SOCIETY

SCIENCE (ISSN 0036-8075) is published weekly on Friday, except the last week in December, by the American Association for the Advancement of Science, 1200 New York Avenue, NW, Washington, DC 20005. Periodicals Mail postage (publication No. 484460) paid at Washington, DC, and additional mailing offices.

Domestic individual membership and subscription (51 issues): $135 ($74 allocated to subscription). Domestic institutional subscription (51 issues): $550; Foreign postage extra: Mexico, Caribbean (surface mail) $55; other countries (air assist delivery) $85. First class, airmail, student, and emeritus rates on request. Canadian rates with GST available upon request, GST #1254 88122. Publications Mail Agreement Number 1069624. **Printed in the U.S.A.**

Change of address: allow 4 weeks, giving old and new addresses and 8-digit account number. **Postmaster:** Send change of address to *Science*, P.O. Box 1811, Danbury, CT 06813–1811. **Single copy sales:** $10.00 per issue prepaid includes surface postage; bulk rates on request. **Authorization to photocopy** material for internal or personal use under circumstances not falling within the fair use provisions of the Copyright Act is granted by AAAS to libraries and other users registered with the Copyright Clearance Center (CCC) Transactional Reporting Service, provided that $15.00 per article is paid directly to CCC, 222 Rosewood Drive, Danvers, MA 01923. The identification code for *Science* is 0036-8075/83 $15.00. *Science* is indexed in the *Reader's Guide to Periodical Literature* and in several specialized indexes.

Contents continued

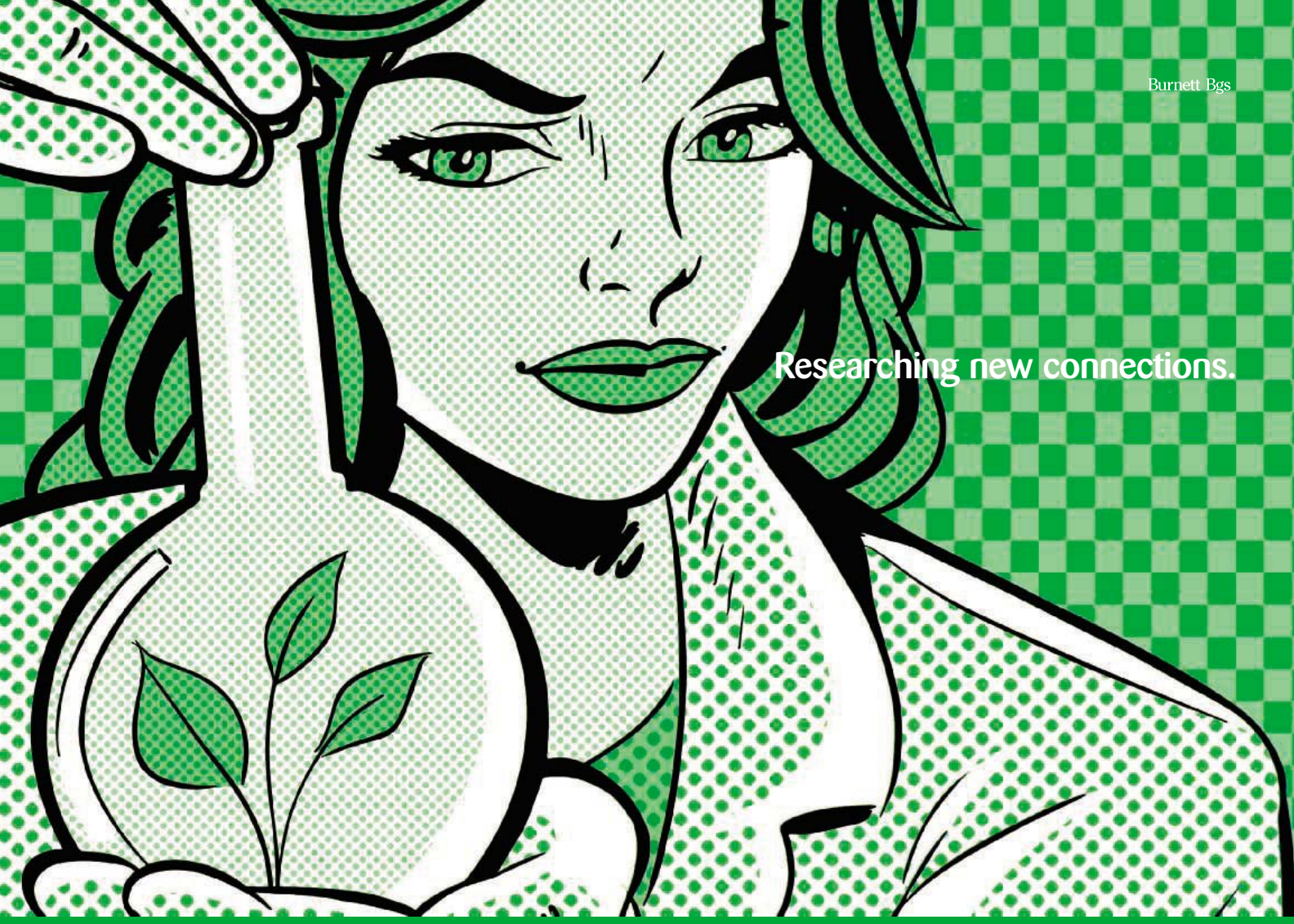

2005 EDITION

PREMIO ITALGAS
energia & ambiente

It is natural for Italgas to link energy with respect for the environment. For this reason, the best research projects on an international level have been awarded prizes since 1987. During these years, many scientists and young researchers have achieved this important acknowledgement. The very high standard of the projects has enabled the attainment of a concrete contribution to the sustainability of development for a better quality of life.

The 2005 Edition of the Italgas Prize is divided into four different areas:

- Prize "Science and Environment", reserved for scientists and researchers;
- Prize "Projects for the Environment", for companies, local authorities and organisations;
- Prize "Popularisation of Science", for people working in informative or communication activities;
- Prize "Debut in the research", for graduates, authors of Research Doctorate Theses.

Candidatures for the Prizes must be submitted by 23 September 2005. All details regarding the modality of participation, and other information, are available on the Web Site.

Enl GROUP

www.premioitalgas.it

italgas

Science
www.scienceonline.org

sciencenow www.sciencenow.org Daily News Coverage

Ducks Help Spread Asian Bird Flu
Animals can harbor and shed H5N1 virus for up to 17 days.

Sticky Valves and Broken Hearts
Mutant gene links at least two major causes of heart valve disease.

Don't Call It Junk
Gene-free DNA of higher organisms may make complex bodies possible.

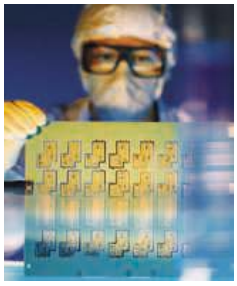

Making it in nanotechnology.

science's next wave www.nextwave.org Career Resources for Young Scientists

Canada: Doing Big Science on a Small Scale—Working in Nanotechnology *A. Fazekas*
Next Wave talks to an up-and-coming nanotechnologist about his own professional journey.

UK: Published but Unpaid *P. Dee*
Phil Dee may be away from the bench, but the opportunity to publish has never been better.

Global: On Balance *I. S. Levine*
How difficult is it for scientists to maintain a balance between work and the rest of life?

MiSciNet: Educated Woman, Chapter 41—Fear and Feedback *M. P. DeWhyse*
A graduate student wonders how to get honest feedback about her progress from her adviser.

MiSciNet: Naira Rezende—A Principal Investigator in Training *E. Francisco*
A graduate of Hunter College talks about her love for science and her dream of running her own lab.

science's sage ke www.sageke.org Science of Aging Knowledge Environment

Perspective: Allelic Variation and Human Longevity *A. Nebel and S. Schreiber*
Careful study design is key to the search for genetic differences that impact longevity.

News Focus: Error Prone *R. J. Davenport*
Mitochondrial mutations might speed aging through rampant cell suicide.

News Focus: Bombshell *M. Leslie*
Radioactive dating reveals cellular ages.

Searching populations for longevity genes.

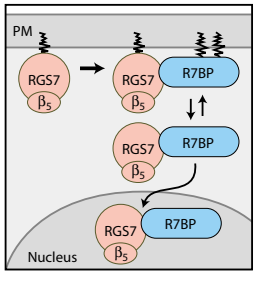

Shuttling Gβ_5 to the nucleus.

science's stke www.stke.org Signal Transduction Knowledge Environment

Perspective: Adult Bone Marrow Stem/Progenitor Cells (MSCs) Are Pre-Conditioned by Microenvironmental "Niches" in Culture—A Two-Stage Hypothesis for Regulation of MSC Fate *C. A. Gregory, J. Ylostalo, D. J. Prockop*
Multipotent mesenchymal stem cells from a single colony are not all identical.

Perspective: R7BP—A Surprising New Link Between G Proteins, RGS Proteins, and Nuclear Signaling in the Brain *J. R. Hepler*
Reversible palmitoylation of R7BP may allow Gβ_5 to function in the nucleus.

Teaching Resource: Chromatin Remodeling *N. F. Lue*
Prepare a graduate-level class on the mechanisms of chromatin remodeling.

Separate individual or institutional subscriptions to these products may be required for full-text access.

edited by Stella Hurtley and Phil Szuromi

Management Opportunities in Land Use

Human activities now appropriate more than one-third of the Earth's terrestrial ecosystem production. **Foley *et al.*** (p. 570) review the local and global impacts of land-use change on ecosystem function and services, the latter including the provision of fresh water and maintenance of soil fertility. Although increasing land use has caused deterioration in the capacity of ecosystems to provide such services, certain land-use strategies could lead to win-win-win opportunities for conservation, economics, and social development.

Mantle Versus Meteorites

Earth's silicate composition is thought to be similar to that of chondritic meteorites, the likely building blocks of the terrestrial planets. Thus, differences in isotopic composition of the crust from that of chondrites have been interpreted as requiring complementary reservoirs in Earth's mantle, and these data, particular for Nd isotopes, have been the basis of many models of Earth's interior. **Boyet and Carlson** (p. 576, published online 16 June 2005; see the 17 June news story by **Kerr**) now show that chondritic meteorites have a different relative abundance of ^{142}Nd—the daughter of short-lived ^{146}Sm—than sampled rocks on Earth, Moon, and Mars. The best explanation for this finding is that Earth's mantle was differentiated within about 30 million years of its formation. A small portion of the mantle, enriched in certain elements, has remained isolated and has not formed additional crust. The bulk of the mantle, now with a different composition from that of chondrites, formed Earth's continental and oceanic crust, as well as the Moon.

Solid-State Quantum Computing Made Simple?

Proposals for solid-state quantum computing have so far relied on two-qubit gates as the elementary units, but controlling the coupling interaction between qubits presents a significant challenge for real implementations. Taking cues from the quantum optics community, which has shown that quantum information processing could be carried out using only linear optics, **Engel and Loss** (p. 586; see the Perspective by **Egues**) propose a solid-state protocol that does not require interacting two-qubit gates. Using electron spins in a double quantum dot system, they argue that a Bell-state measurement of the spin-parity (converted to a charge-state for easy readout) should allow for a simpler and scalable solid-state quantum computer scheme.

Bear's Witness

The study of DNA in ancient remains can be hampered by contamination that ranges from bacterial to human. However, **Noonan *et al.*** (p. 597, published online 2 June 2005) present the results of a metagenomic approach to analyze large amounts of ancient genomic DNA sequence from extracts of 40,000-year-old cave bear bones. Because of the extensive information that is already available from comparative genomics, the genuine bear sequences could be distinguished from contaminants. In addition, the evolutionary relationship between extinct and modern bears was elucidated.

Olefin Metathesis at Metal Surfaces

Stable bonding of organic molecules to metals is often achieved via thiol-gold chemistry. Although robust, it is difficult to do any further reactions with this saturated bonding arrangement. Two groups report on olefin metathesis reaction performed at carbene groups attached to metallic substrates. **Siaj and McBreen** (p. 588) attached cyclopentylidene groups on Mo_2C surfaces, which are stable to very high temperatures. They can grow polynorbornene from this alkylidene site through ring-opening metathesis conducted at ~230°C. **Tulevski *et al.*** (p. 591) reacted diazomethane derivatives with clean ruthenium films to form surface carbene groups that are stable under ambient conditions to temperatures of 160°C. When formed on Ru particles, these carbene groups underwent olefin metathesis reactions. These reaction chemistries may also find application in forming surface polymers.

Toll-Like Receptor Structure Revealed

Binding of diverse ligands initiates various signaling pathways that play a role in the immune response. Human Toll-like receptor 3 (TLR3) is activated by double-stranded RNA, such as those associated with many viruses. The lack of a three-dimensional structure for any TLR has hampered the design of experiments to define their mode of signaling. **Choe *et al.*** (p. 581, published online 16 June 2005; see the cover) have determined the TLR3 ectodomain structure at 2.1 angstrom resolution. The ectodomain forms a horseshoe-shaped solenoid that comprises 23 leucine-rich repeats. The inner concave surface and a large portion of the outer surface are covered by carbohydrate. One face is glycosylation-free, which suggests that it may play a role in ligand binding and oligomerization.

Overcoming Cultural Barriers

Hepatitis C virus (HCV) is a major cause of chronic liver disease, with over 170 million persistently infected individuals worldwide. The development of drugs for HCV has been slowed by the absence of a cell culture system for studying viral replication. **Lindenbach *et al.*** (p. 623, published online 9 June 2005) constructed a full-length HCV genome using sequences from two different viral strains and found that the chimeric virus can replicate to high titers in cultured human liver cells. The virus spread from cell to cell and could be partially neutralized by an antibody against a viral glycoprotein and by a soluble form of a cellular surface protein involved in viral entry.

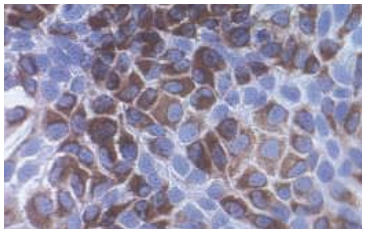

CREDITS (TOP TO BOTTOM): JEAN CLOTTES/FRENCH MINISTRY OF CULTURE AND COMMUNICATION; LINDENBACH *ET AL.*

Room to Roam

An evaluation by **Ceballos *et al.*** (p. 603; see the news story by **Stokstad**) of global conservation priorities and conflicts for an entire animal group, the land mammals, shows that at least 15% of Earth's land surface is needed for the conservation of 10% of the geographic ranges of the great majority of mammal species. A variety of approaches to conservation will be necessary in different areas and for different taxa, ranging from protected reserves to management of human-dominated landscapes. How is animal population size regulated? **Sibly *et al.*** (p. 607; see the Perspective by **Reynolds and Freckleton**) analyze population time series from 1780 data sets that cover four of the major taxonomic groups of animals. Most populations do not grow exponentially to carrying capacity, as previously assumed. Instead, growth rate is strongly adjusted by density-dependent factors and slows long before carrying capacity is achieved. Despite the differences in evolutionary history, metabolism, and body size, species in all four groups generally show strong density dependence at low population levels that falls off at high population levels.

Hippocampal Memory Formation Revisited

What is the role of the hippocampus in spatial representation versus representation of episodic and other nonspatial information? **Leutgeb *et al.*** (p. 619; see the Perspective by **Buzsáki**) find that hippocampal neurons have independent coding schemes for location and for what happens at a location. Changes in spatial location are represented as changes in location of firing in hippocampal place cells, whereas changes in cue configuration at a single location are represented by changes in firing rate. These results explain how, depending on the choice of dependent variables, different results have been obtained. The combination and integration of spatial and nonspatial information in the hippocampal output may form the neural basis for the role of the hippocampus in episodic memory.

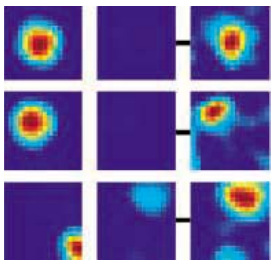

CREDITS: LEUTGEB *ET AL.*

Considering Chromosome Rearrangements

What are the causes, constraints, and consequences of chromosome rearrangements? **Murphy *et al.*** (p. 613) used genome sequences and high-density comparative maps from eight species within five mammalian orders to infer evolutionary processes influencing chromosome dynamics. Chromosomal breakpoints tended to be reused during evolution, and there has been an increase in the rates of mammalian chromosome breakage since the Late Cretaceous period. Centromeres tended to be associated with reuse breakpoints. Forty breakpoints were identified as primate-specific, and nearly all involved segmental duplications.

Drab and Glam Together

The males and females of *Eclectus roratus*, a parrot of the Australian rainforest, are so different in their plumage that they were long regarded as separate species. In contrast to the normal pattern in sexually dimorphic birds, males are drab while females are brightly colored. An 8-year field study by **Heinsohn *et al.*** (p. 617) has revealed that the reversed sexual dichromatism in *Eclectus* is not a result of sex-role reversal, the standard explanation for this phenomenon. Instead, it seems that contrasting selection pressures are acting on males (avoiding predation) and females (competition with other females).

Just in Time

A circadian clock serves to manage internal physiology in a cyclical manner. **Dodd *et al.*** (p. 630) now investigate the advantages conferred by having a circadian clock. *Arabidopsis* plants with cycles closely matched to their environmental light-dark cycle showed improved fitness relative to plants whose cycles did not fit well. The mechanisms may involve production of certain proteins in a "just in time" manner, anticipating daylight soon enough to produce the photosynthetic machinery, but not so much in advance that certain unstable proteins start to degrade.

Career advice, insight and tools.

Turn to the experts for the big picture.
Visit www.ScienceCareers.org

Your career is too important to leave to chance. So to find the right job or get career advice, turn to the experts. At ScienceCareers.org we know science. And we are committed to helping take your career forward. Our knowledge is firmly founded on the expertise of *Science*, the premier scientific journal, and the long experience of AAAS in advancing science around the world. Put yourself in the picture with the experts in science. Visit www.ScienceCareers.org.

ScienceCareers.org
We know science AAAS

Misusing the Nazi Analogy

Sixty years ago, Allied forces brought an end to Adolf Hitler's dream that Germany would rule Europe and dominate the world. The death of Nazi Germany gave birth to a charge that still haunts the scientific community—what might be called "the Nazi analogy." In ethical or policy disputes about science and medicine, no argument can bring debate to a more screeching halt then the invocation of the Nazi comparison.

Whether the subject is stem cell research, end-of-life care, the conduct of clinical trials in poor nations, abortion, embryo research, animal experimentation, genetic testing, or human experimentation involving vulnerable populations, references to Nazi policies or practices tumble forth from critics. "If X is done, then we are on the road to Nazi Germany" has become a commonplace claim in contemporary bioethical debates.

Sadly, too often those who draw an analogy between current behavior and what the Nazis did do not know what they are talking about. The Nazi analogy is equivalent to dropping a nuclear bomb in ethical battles about science and medicine. Because its misuse diminishes the horror done by Nazi scientists and doctors to their victims, it is ethically incumbent upon those who invoke the Nazi analogy to understand what they are claiming.

A key component of Nazi thought was to rid Germany and the lands under German control of those deemed economic drains on the state—the mentally ill, alcoholics, the "feeble-minded," and the demented elderly. They were seen as direct threats to the economic viability of the state, a fear rooted in the bitter economic experience after the First World War. The public health of the nation also had to be protected against threats to its genetic health. These were created when people of "inferior" races intermarried with those of Aryan stock. Threats to genetic health also included, by their very existence, genetic degenerates—Jews and Roma. Theories of race hygiene had gained prominence in mainstream German scientific and medical circles as early as the 1920s.

What is important to keep in mind about these underlying themes that provided the underpinning for Nazi euthanasia and eugenic practices is that they have little to do with contemporary ethical debates about science, medicine, or technology. Take, for instance, the case of Terri Schiavo, a massively brain-damaged patient who was kept alive by means of artificial feeding for more than a decade. When congressmen and religious leaders in the United States commented on her situation during the weeks leading up to her death on 31 March 2005, soon after her feeding tube was removed, they described it as analogous to what the Nazis had done to Jews in concentration camps—a complete misuse of the Nazi analogy. Whatever one thought about the ethical issues raised by the decision to allow the removal of a feeding tube from this woman, the decision had nothing to do with the belief that her continued existence posed a threat to the economic integrity of the United States or that her racial background posed a threat to America's genetic health. The fight over her fate was about who best could represent her wishes so that her self-determination could be respected—a moral principle not afforded those killed by deliberate starvation in the Nazi euthanasia programs.

Similarly, when critics charge that allowing embryonic stem cell research permits the taking of innocent life to serve the common good, and then compare it to Nazi research in concentration camps, the claims of resemblance are deeply flawed; moreover, they demean the immorality of Nazi practices. Concentration camp prisoners were used in lethal experiments because they were seen as doomed to die anyway, were seen as racial inferiors, and, given the conditions of total war that prevailed, they were considered completely expendable in the service of the national security of the Third Reich.

There are many reasons why a practice or policy in contemporary science or medicine might be judged unethical. But the cavalier use of the Nazi analogy in an attempt to bolster an argument is unethical. Sixty years after the fall of the Third Reich, we owe it to those who suffered and died at the hands of the Nazis to insist that those who invoke the Nazi analogy do so with care.

Arthur L. Caplan

Arthur L. Caplan is chair of the Department of Medical Ethics, University of Pennsylvania School of Medicine, Philadelphia, PA 19104, USA.

10.1126/science.1115437

CREDIT: BETTMANN/CORBIS

edited by Gilbert Chin

CLIMATE SCIENCE

Eddies and the Seesaw

A series of warm episodes, each lasting several thousand years, occurred in Antarctica between 90,000 and 30,000 years ago. These events correlated with rapid climate oscillations in the Arctic, with Antarctica warming while the Arctic was cooling or already cold. This bipolar seesaw is thought to have been driven by changes in the strength of the deep overturning circulation in the North Atlantic Ocean, but some have questioned how completely that process can account for the fine details of Antarctic warming events.

Keeling and Visbeck offer an explanation that builds upon earlier suggestions that include the effects of shallow-water processes as well as deep ones. They suggest that changes in the surface salinity gradient across the Antarctic Circumpolar Current were caused by the melting of icebergs discharged from the Arctic, which allowed increased heat transport to Antarctica by ocean eddies. This mechanism produces Antarctic warming of the magnitude observed in ice core records. — HJS

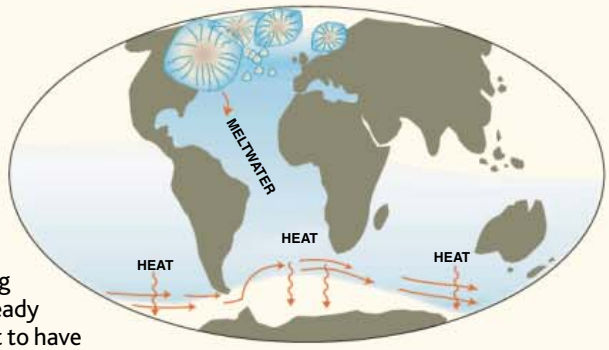

Diagram of the eddy-meltwater explanation.

Quat. Sci. Rev. 10.1016/j/quascirev.2005.04.005 (2005).

CHEMISTRY

Combichem Sensors

The design of fluorescent chemosensors that can be used to detect metal ions often begins by identifying a molecule with an appropriate metal-binding specificity and then derivatizing the compound so that binding initiates a fluorescent signal. However, once the binding scaffold is set, synthetic routes to fluorescent derivatives may be few.

Mello and Finney have approached the problem from the opposite direction by using fluorescence to screen combinatorial libraries. They took advantage of cases where binding of a metal ion restricts torsional motion between aryl groups and hence favors an extended aromatic network. A 2,6-biaryl-4-vinylpyridine core bound to a resin support was functionalized with identical arms that consisted of an amino acid and an acyl end group. Screening an initial library of 198 such compounds with a variety of mono- and divalent cations, they identified a fluorophore that bound Hg^{2+} with an affinity of about 1.8×10^{-6} M^{-1}, which is about an order of magnitude greater than the affinity of K^+ for 18-crown-6 ether. — PDS

J. Am. Chem. Soc. 10.1021/ja043682p (2005).

BIOMEDICINE

Outside Influences

One of the current concepts in cancer research is that tumor epithelial cells do not grow in isolation, but in the context of a stromal microenvironment that can be permissive or nonpermissive for malignancy. Although this hypothesis was proposed many years ago, only recently have microenvironmental influences on tumorigenesis been explored at the level of specific cell types and signaling molecules.

Two papers focus on the cellular microenvironment in breast cancer. Radisky *et al.* describe a cascade of signaling events triggered in mouse mammary epithelial cells that are exposed to matrix metalloproteinase-3 (MMP-3), a stromal enzyme that is overexpressed in human breast cancer and that has been shown to confer tumorigenic potential to normal epithelial cells. These signaling events culminate in the production of reactive oxygen species (ROS) that damage DNA and cause genomic instability in the epithelial cells. Hu *et al.* investigated whether stromal cells in human breast cancer undergo genomic modifications that might influence stromal cell gene expression during tumorigenesis. An assay of genome-wide methylation revealed that epigenetic changes occur in stromal cells in a tumor stage– and cell type–specific manner, supporting the idea that the dialogue between tumor cells and microenvironment evolves as tumors progress. — PAK

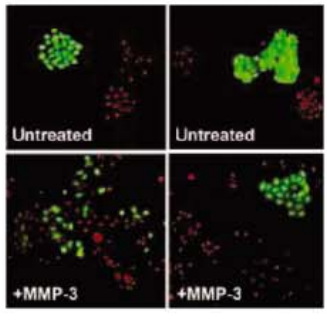

Mitochondrial superoxide dismutase (SOD; right, green cells) blocks the ROS-mediated cell scattering produced by MMP-3, but cytoplasmic SOD does not (left).

Nature **436**, 123 (2005); *Nat. Genet.* 10.1038/ng1596 (2005).

MICROBIOLOGY

What's in a Name?

The human pathogen *Staphylococcus aureus* exhibits a golden hue, which comes from a carotenoid that is made by joining two molecules of farnesyl pyrophosphate, a reaction that is catalyzed by dehydrosqualene synthase (encoded by the gene *crt*M). Liu *et al.* have looked closely at this bacterium and find that its pigment is in fact a defensive weapon. Deleting *crt*M changed *S. aureus* color from gold to pale yellow and increased its sensitivity to being killed by reactive oxygen species (ROS). Conversely, adding this gene to another human pathogen, *Streptococcus pyogenes*, enhanced its color as well as its resistance to singlet oxygen. Survival of *crt*M-deleted *S. aureus* when challenged by human neutrophils or by whole blood from mice and humans was much lower than for wild-type bacteria. Protection could be conferred by an inhibitor of NADPH oxidase, which generates ROS; this was consistent with no difference in the survival of mutant and wild-type bacteria when cocultured with blood from a patient with chronic granulomatous disease (CGD; caused by NADPH oxidase deficiency) or from a mouse model of human CGD. Taken together, these results suggest that

CREDITS: (TOP) KEELING AND VISBECK, *QUAT. SCI. REV.* 10.1016/J/QUASCIREV.2005.04.005 (2005); (BOTTOM) RADISKY *ET AL.*, *NATURE* **436**, 123 (2005)

inhibition of carotenoid synthesis may render *S. aureus* more susceptible to host immune defenses. — GJC

J. Exp. Med. 10.1084/jem.20050846 (2005).

ENVIRONMENTAL SCIENCE

Fouling Deliberately

An ongoing problem in water purification is the fouling of membranes by particulates (such as clay, silt, or algae) and by natural organic matter (NOM), which comes from the biological degradation of plants and humus. NOM typically consists of molecules in the range of 1 to 2 kD, but can form aggregates of much larger size. It has not been clear which components of NOM are responsible for fouling, although it is known that more hydrophobic membranes are more susceptible.

Clark *et al.* turn this problem on its head by using a hydrophobic polymer as the basis for a new adsorbent material that can be used to pretreat water. Polysulfone, a common membrane material, was dissolved in an organic solvent mixture and then injected into water, which is not a solvent for the polymer. The polysulfone formed particles with a diameter around 50 nm, which then rapidly clustered into micrometer-sized colloidal aggregates with large surface area. When added to local drinking water, the aggregates adsorbed only a small fraction of the NOM from the water, but these molecules were the ones responsible for most of the fouling of a 20-kD filtration membrane. — MSL

Langmuir 10.1021/la050186l (2005).

CHEMISTRY

Sizing Rings

Over the past hundred years, chemists have developed numerous methods to squeeze molecules into tight, small rings, despite the inherent strain this places on bond angles. Large rings have little or no strain, but their synthesis poses a different challenge—the ends of long strands must be coaxed to form a loop, instead of linking end-to-end to yield linear oligomers.

Hori *et al.* used π-stacking interactions to help achieve this goal. They prepared a precursor resembling a double key-chain: An oligomer of -OCH_2CH_2O- was capped at both ends by palladium centers complexed to cyclic ligands comprising seven aromatic groups. Adding water to a solution of this compound in dimethyl sulfoxide led to its dimerization, presumably driven by stacking of the large aromatic rings. After they had been brought together, the cyclic ligands became catenated by means of their reversible coordination to Pd, resulting in a very large ring of 238 atoms. — JSY

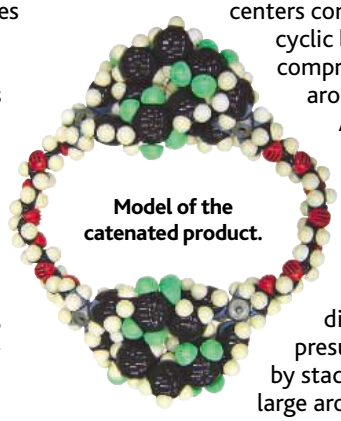

Model of the catenated product.

Angew. Chem. Int. Ed. 10.1002/anie.200501559 (2005).

CREDITS: HORI *ET AL.*, *ANGEW. CHEM. INT. ED.* 10.1002/ANIE.200501559 (2005)

HIGHLIGHTED IN *SCIENCE*'S SIGNAL TRANSDUCTION KNOWLEDGE ENVIRONMENT

Science's STKE www.stke.org

NO Deadly Signal

Reminiscent of mild-mannered Clark Kent, the glycolytic enzyme glyceraldehyde-3-phosphate dehydrogenase (GAPDH) has an alter ego with potent and deadly effects. When translocated to the nucleus, GAPDH has been associated with transcriptional regulation, and Hara *et al.* present results implicating it in cell death. Screening for proteins that interact with GAPDH turned up Siah1, a ubiquitin ligase. In transfected cells, GAPDH moved to the nucleus, an effect that required the nuclear localization signal of Siah1. In human embryonic kidney cells undergoing apoptosis in response to staurosporine, GAPDH underwent modification via *S*-nitrosylation (a consequence of increased intracellular nitric oxide), which enhanced its association with Siah1. In a macrophage cell line undergoing apoptosis in response to lipopolysaccharide, GAPDH became *S*-nitrosylated and associated with endogenous Siah1, and this complex moved to the nucleus. All of these effects could be blocked by an inhibitor of the nitric oxide—generating enzyme iNOS (inducible nitric oxide synthase). Exactly how nuclear Siah1 promotes apoptosis remains to be explored, but its action appears to require its RING finger domain, indicating that Siah1-mediated ubiquitination and consequent degradation of nuclear proteins is one likely mechanism. — LBR

Nat. Cell Biol. **7**, 665 (2005).

www.sciencemag.org

Science

1200 New York Avenue, NW
Washington, DC 20005
Editorial: 202-326-6550, FAX 202-289-7562
News: 202-326-6500, FAX 202-371-9227

Bateman House, 82-88 Hills Road
Cambridge, UK CB2 1LQ
+44 (0) 1223 326500, FAX +44 (0) 1223 326501

SUBSCRIPTION SERVICES For change of address, missing issues, new orders and renewals, and payment questions: 800-731-4939 or 202-326-6417, FAX 202-842-1065. Mailing addresses: AAAS, P.O. Box 1811, Danbury, CT 06813 or AAAS Member Services, 1200 New York Avenue, NW, Washington, DC 20005

INSTITUTIONAL SITE LICENCES please call 202-326-6755 for any questions or information

REPRINTS Ordering/Billing/Status 800-635-7171; Corrections 202-326-6501

PERMISSIONS 202-326-7074, FAX 202-682-0816

MEMBER BENEFITS Bookstore: AAAS/BarnesandNoble.com bookstore www.aaas.org/bn; Car purchase discount: Subaru VIP Program 202-326-6417; Credit Card: MBNA 800-847-7378; Car Rentals: Hertz 800-654-2200 CDP#343457, Dollar 800-800-4000 #AA1115; AAAS Travels: Betchart Expeditions 800-252-4910; Life Insurance: Seabury & Smith 800-424-9883; Other Benefits: AAAS Member Services 202-326-6417 or www.aaasmember.org.

science_editors@aaas.org (for general editorial queries)
science_letters@aaas.org (for queries about letters)
science_reviews@aaas.org (for returning manuscript reviews)
science_bookrevs@aaas.org (for book review queries)

Published by the American Association for the Advancement of Science (AAAS), *Science* serves its readers as a forum for the presentation and discussion of important issues related to the advancement of science, including the presentation of minority or conflicting points of view, rather than by publishing only material on which a consensus has been reached. Accordingly, all articles published in *Science*—including editorials, news and comment, and book reviews—are signed and reflect the individual views of the authors and not official points of view adopted by the AAAS or the institutions with which the authors are affiliated.

AAAS was founded in 1848 and incorporated in 1874. Its mission is to advance science and innovation throughout the world for the benefit of all people. The goals of the association are to: foster communication among scientists, engineers and the public; enhance international cooperation in science and its applications; promote the responsible conduct and use of science and technology; foster education in science and technology for everyone; enhance the science and technology workforce and infrastructure; increase public understanding and appreciation of science and technology; and strengthen support for the science and technology enterprise.

INFORMATION FOR CONTRIBUTORS

See pages 135 and 136 of the 7 January 2005 issue or access www.sciencemag.org/feature/contribinfo/home.shtml

EDITOR-IN-CHIEF **Donald Kennedy**
EXECUTIVE EDITOR **Monica M. Bradford**
DEPUTY EDITORS **R. Brooks Hanson, Katrina L. Kelner**
NEWS EDITOR **Colin Norman**

EDITORIAL SUPERVISORY SENIOR EDITORS Barbara Jasny, Phillip D. Szuromi; **SENIOR EDITORS** Gilbert J. Chin, Lisa D. Chong, Pamela J. Hines, Paula A. Kiberstis (Boston), Beverly A. Purnell, L. Bryan Ray, Guy Riddihough (Manila), H. Jesse Smith, Valda Vinson, David Voss; **ASSOCIATE EDITORS** Marc S. Lavine, Jake S. Yeston; **ONLINE EDITOR** Stewart Wills; **CONTRIBUTING EDITOR** Ivan Amato; **ASSOCIATE ONLINE EDITOR** Tara S. Marathe; **BOOK REVIEW EDITOR** Sherman J. Suter; **ASSOCIATE LETTERS EDITOR** Etta Kavanagh; **INFORMATION SPECIALIST** Janet Kegg; **EDITORIAL MANAGER** Cara Tate; **SENIOR COPY EDITORS** Jeffrey E. Cook, Harry Jach, Barbara P. Ordway; **COPY EDITORS** Cynthia Howe, Alexis Wynne Mogul, Sabrah M. n'haRaven, Jennifer Sills, Trista Wagoner; **EDITORIAL COORDINATORS** Carolyn Kyle, Beverly Shields; **PUBLICATION ASSISTANTS** Chris Filiatreau, Joi S. Granger, Jeffrey Hearn, Lisa Johnson, Scott Miller, Jerry Richardson, Brian White, Anita Wynn; **EDITORIAL ASSISTANTS** Ramatoulaye Diop, E. Annie Hall, Patricia M. Moore, Brendan Nardozzi, Michael Rodewald; **EXECUTIVE ASSISTANT** Sylvia S. Kihara; **ADMINISTRATIVE SUPPORT** Patricia F. Fisher

NEWS SENIOR CORRESPONDENT Jean Marx; **DEPUTY NEWS EDITORS** Robert Coontz, Jeffrey Mervis, Leslie Roberts, John Travis; **CONTRIBUTING EDITORS** Elizabeth Culotta, Polly Shulman; **NEWS WRITERS** Yudhijit Bhattacharjee, Jennifer Couzin, David Grimm, Constance Holden, Jocelyn Kaiser, Richard A. Kerr, Eli Kintisch, Andrew Lawler (New England), Greg Miller, Elizabeth Pennisi, Charles Seife, Robert F. Service (Pacific NW), Erik Stokstad; Carolyn Gramling, Genevra Ornelas, Cathy Tran (interns); **CONTRIBUTING CORRESPONDENTS** Marcia Barinaga (Berkeley, CA), Barry A. Cipra, Adrian Cho, Jon Cohen (San Diego, CA), Daniel Ferber, Ann Gibbons, Robert Irion, Mitch Leslie (NetWatch), Charles C. Mann, Evelyn Strauss, Gary Taubes, Ingrid Wickelgren; **COPY EDITORS** Linda B. Felaco, Rachel Curran, Sean Richardson; **ADMINISTRATIVE SUPPORT** Scherraine Mack, Fannie Groom **BUREAUS:** Berkeley, CA: 510-652-0302, FAX 510-652-1867, New England: 207-549-7755, San Diego, CA: 760-942-3252, FAX 760-942-4979, Pacific Northwest: 503-963-1940

PRODUCTION DIRECTOR James Landry; **SENIOR MANAGER** Wendy K. Shank; **ASSISTANT MANAGER** Rebecca Doshi; **SENIOR SPECIALISTS** Vicki J. Jorgensen, Jessica K. Moshell; **SPECIALISTS** Jay R. Covert, Stacey Ferebee; **PREFLIGHT DIRECTOR** David M. Tompkins; **MANAGER** Marcus Spiegler; **SPECIALIST** Jessie Mudjitaba;

ART DIRECTOR Joshua Moglia; **ASSOCIATE ART DIRECTOR** Kelly Buckheit; **ILLUSTRATOR** Katharine Sutliff; **SENIOR ART ASSOCIATES** Holly Bishop, Laura Creveling, Preston Huey, Julie White; **ASSOCIATE** Nayomi Kevitiyagala; **PHOTO RESEARCHER** Leslie Blizard

***SCIENCE* INTERNATIONAL**

EUROPE (science@science-int.co.uk) **EDITORIAL: INTERNATIONAL MANAGING EDITOR** Andrew M. Sugden; **SENIOR EDITOR/PERSPECTIVES** Julia Fahrenkamp-Uppenbrink; **SENIOR EDITORS** Caroline Ash (Geneva: +41 (0) 222 346 3106), Stella M. Hurtley, Ian S. Osborne, Peter Stern; **ASSOCIATE EDITOR** Stephen J. Simpson; **EDITORIAL SUPPORT** Emma Westgate; Deborah Dennison **ADMINISTRATIVE SUPPORT** Janet Clements, Phil Marlow, Jill White; **NEWS: INTERNATIONAL NEWS EDITOR** Eliot Marshall **DEPUTY NEWS EDITOR** Daniel Clery; **CORRESPONDENT** Gretchen Vogel (Berlin: +49 (0) 30 2809 3902, FAX +49 (0) 30 2809 8365); **CONTRIBUTING CORRESPONDENTS** Michael Balter (Paris), Martin Enserink (Amsterdam and Paris); **INTERN** Mason Inman

ASIA Japan Office: Asca Corporation, Eiko Ishioka, Fusako Tamura, 1-8-13, Hirano-cho, Chuo-ku, Osaka-shi, Osaka, 541-0046 Japan; +81 (0) 6 6202 6272, FAX +81 (0) 6 6202 6271; asca@os.gulf.or.jp **JAPAN NEWS BUREAU:** Dennis Normile (contributing correspondent, +81 (0) 3 3391 0630, FAX 81 (0) 3 5936 3531; dnormile@gol.com); **CHINA REPRESENTATIVE** Hao Xin, + 86 (0) 10 6307 4439 or 6307 3676, FAX +86 (0) 10 6307 4358; haoxin@earthlink.net; **SOUTH ASIA** Pallava Bagla (contributing correspondent +91 (0) 11 2271 2896; pbagla@vsnl.com); **CENTRAL ASIA** Richard Stone (+7 3272 6413 35, rstone@aaas.org)

EXECUTIVE PUBLISHER **Alan I. Leshner**
PUBLISHER **Beth Rosner**

FULFILLMENT & MEMBERSHIP SERVICES (membership@aaas.org) **DIRECTOR** Marlene Zendell; **MANAGER** Waylon Butler; **SYSTEMS SPECIALIST** Andrew Vargo **SENIOR SPECIALIST** Pat Butler; **SPECIALISTS** Laurie Baker, Tamara Alfson, Karena Smith

BUSINESS OPERATIONS AND ADMINISTRATION DIRECTOR Deborah Rivera-Wienhold; **BUSINESS MANAGER** Randy Yi; **SENIOR BUSINESS ANALYST** Lisa Donovan; **BUSINESS ANALYST** Jessica Tierney; **FINANCIAL ANALYST** Michael LoBue, Farida Yeasmin; **RIGHTS AND PERMISSIONS: ADMINISTRATOR** Emilie David; **ASSOCIATE** Elizabeth Sandler; **MARKETING: DIRECTOR** John Meyers; **MEMBERSHIP MARKETING MANAGER** Darryl Walter; **MARKETING ASSOCIATE** Julianne Wielga; **RECRUITMENT MARKETING MANAGER** Allison Pritchard; **ASSOCIATES** Mary Ellen Crowley, Amanda Donathen, Catherine Featherston; **DIRECTOR OF INTERNATIONAL MARKETING AND RECRUITMENT ADVERTISING** Deborah Harris; **INTERNATIONAL MARKETING MANAGER** Wendy Sturley; **MARKETING/MEMBER SERVICES EXECUTIVE:** Linda Rusk; **JAPAN SALES AND MARKETING MANAGER** Jason Hannaford; **SITE LICENSE SALES: DIRECTOR** Tom Ryan; **SALES AND CUSTOMER SERVICE** Mehan Dossani, Catherine Holland, Adam Banner, Yaniv Snir; **ELECTRONIC MEDIA: INTERNET PRODUCTION MANAGER** Lizabeth Harman; **ASSISTANT PRODUCTION MANAGER** Wendy Stengel; **SENIOR PRODUCTION ASSOCIATES** Sheila Mackall, Amanda K. Skelton, Lisa Stanford; **PRODUCTION ASSOCIATE** Nichele Johnston; **LEAD APPLICATIONS DEVELOPER** Carl Saffell

PRODUCT ADVERTISING (science_advertising@aaas.org); **MIDWEST** Rick Bongiovanni: 330-405-7080, FAX 330-405-7081 • **WEST COAST/W. CANADA** B. Neil Boylan (Associate Director): 650-964-2266, FAX 650-964-2267 • **EAST COAST/E. CANADA** Christopher Breslin: 443-512-0330, FAX 443-512-0331 • **UK/SCANDINAVIA/FRANCE/ITALY/BELGIUM/NETHERLANDS** Andrew Davies (Associate Director): +44 (0)1782 750111, FAX +44 (0) 1782 751999 • **GERMANY/SWITZERLAND/AUSTRIA** Tracey Peers (Associate Director): +44 (0) 1782 752530, FAX +44 (0) 1782 752531 **JAPAN** Mashy Yoshikawa: +81 (0) 33235 5961, FAX +81 (0) 33235 5852 **ISRAEL** Jessica Nachlas +9723 5449123 • **TRAFFIC MANAGER** Carol Maddox; **SALES COORDINATOR** Deiandra Simms

CLASSIFIED ADVERTISING (advertise@sciencecareers.org); **U.S.: SALES DIRECTOR** Gabrielle Boguslawski: 718-491-1607, FAX 202-289-6742; **INTERNET SALES MANAGER** Beth Dwyer: 202-326-6534; **INSIDE SALES MANAGER** Daryl Anderson: 202-326-6543; **WEST COAST/MIDWEST** Kristine von Zedlitz: 415-956-2531; **EAST COAST** Jill Downing: 631-580-2445; **LINE AD SALES** Emnet Tesfaye: 202-326-6740; **SENIOR SALES COORDINATOR** Erika Bryant; **SALES COORDINATORS** Rohan Edmonson, Christopher Normile, Joyce Scott, Shirley Young; **INTERNATIONAL: SALES MANAGER** Tracy Holmes: +44 (0) 1223 326525, FAX +44 (0) 1223 326532; **SALES** Christina Harrison, Suitlana Barnes; **SALES ASSISTANT** Helen Moroney; **JAPAN:** Jason Hannaford: +81 (0) 52 789 1860, FAX +81 (0) 52 789 1861; **PRODUCTION: MANAGER** Jennifer Rankin; **ASSISTANT MANAGER** Deborah Tompkins; **ASSOCIATE** Amy Hardcastle; **SENIOR TRAFFICKING ASSOCIATE** Christine Hall; **SENIOR PUBLICATIONS ASSISTANT** Robert Buck; **PUBLICATIONS ASSISTANT** Natasha Pinol

AAAS BOARD OF DIRECTORS RETIRING PRESIDENT, CHAIR Shirley Ann Jackson; **PRESIDENT** Gilbert S. Omenn; **PRESIDENT-ELECT** John P. Holdren; **TREASURER** David E. Shaw; **CHIEF EXECUTIVE OFFICER** Alan I. Leshner; **BOARD** Rosina M. Bierbaum; John E. Burris; John E. Dowling; Lynn W. Enquist; Susan M. Fitzpatrick; Richard A. Meserve; Norine E. Noonan; Peter J. Stang; Kathryn D. Sullivan

AAAS
ADVANCING SCIENCE, SERVING SOCIETY

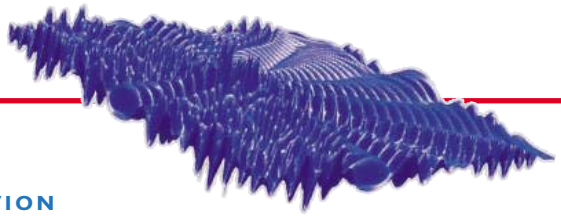

NetWatch

edited by Mitch Leslie

EDUCATION

Bodies in Motion

From Kepler's planetary laws to standing waves, this collection of animations puts concepts from beginning physics and astronomy into motion. Creator Michael Gallis, a physics professor at Pennsylvania State University in Schuylkill, has gathered more than 100 brief movies in categories such as mechanics, electricity and magnetism, and optics. Students can stretch a cylinder to discover how to calculate Young's modulus of elasticity or follow the moon's orbit to learn why eclipses are so rare. Above, interference between two waves that reflect off the walls of a container spawns this rippling pattern.

phys23p.sl.psu.edu/phys_anim/Phys_anim.htm

TOOLS

Where the Fossils Are

Mammal diversity hit its zenith during the Miocene epoch, when horses, camels, rhinos, saber-toothed cats, and a wealth of other furry creatures roamed North America. Researchers who want to tease out patterns in mammal evolution and distribution can dig into The Miocene Mammal Mapping Project from the University of California, Berkeley. The site enables users to pinpoint mammal fossil localities from the Miocene and late Oligocene epochs, between 30 million and 5 million years ago. The database, a 5-year project that was completed last month, houses information on more than 3400 sites in the western United States gleaned from the literature and unpublished records. Users can map fossil finds by categories that include formation, species, and age. Clicking on a locality summons data such as the site's time range, environment type, and mammal groups.

www.ucmp.berkeley.edu/miomap/index.html

IMAGES

Slip Sliding Away

Glaciers the world over are dwindling because of global warming and other factors, but one place where you'll see ice expanding is this gallery from the National Snow and Ice Data Center in Boulder, Colorado. The collection recently tripled in size and now showcases more than 3000 photos of U.S. and Canadian glaciers, snapped between 1883 and 1995. Shots such as this 1931 picture of Alaska's Columbia glacier (left), which has retreated some 15 kilometers in the last 25 years, can provide a historical baseline for studies of climate change and ice dynamics. Visitors can download images or order free high-resolution photos through the site.

nsidc.org/data/glacier_photo

DATABASES

The Other Hepatitis

First identified in 1989, the hepatitis C virus lurks in about 4 million U.S. residents. The insidious pathogen can destroy the liver or provoke cancer; it's responsible for about 50% of liver tumors. This site from Los Alamos National Laboratory in New Mexico offers two databases for researchers interested in the virus. One database lets you troll more than 30,000 full and partial genome sequences from samples collected around the world. You can search by viral subtype, geographic location, route of infection, or other variables. Tools help you build evolutionary trees based on your own sequences and perform other analyses. The site's immunology database lists viral segments that trigger a response from T cells and describes antibodies that latch onto the virus.

hcv.lanl.gov/content/hcv-db/index

RESOURCES

Underwater Invasion

Like more than 7 million people, droves of invasive organisms find the San Francisco Bay area congenial. More than 175 alien species have settled in the bay's waters, making it one of the world's hot spots for aquatic invaders. Meet many of these troublemakers at a new guide from the San Francisco Estuary Institute in Oakland.

The guide aims to help researchers and the general public identify and monitor invasive species. You can consult detailed profiles on new colonists such as the star sea squirt (*Botryllus schlosseri*; above), a European native, and the parasitic flatworm *Austrobilharzia variglandis* from the northern Atlantic Ocean. The pesky worm can incite a rash called swimmer's itch in people who contact it. "This is one of the first cases where we can document that an introduced species is negatively impacting public health" in the Bay Area, says site creator Andrew Cohen. He hopes to enlarge the guide to incorporate all the invasive species that have taken up residence along the West Coast.

www.exoticsguide.org

Send site suggestions to netwatch@aaas.org. Archive: www.sciencemag.org/netwatch

CREDITS (TOP TO BOTTOM): MICHAEL GALLIS; ANDREW N. COHEN/SFEI; WILLIAM O. FIELD/NSIDC

HUMAN SPACE FLIGHT

NASA May Cut Shuttle Flights And Reduce Science on Station

All eyes were on the Florida coast this week as NASA struggled to end a two-and-a-half year hiatus in human space flight by launching the space shuttle Discovery. But behind the scenes, NASA's space transportation system is facing an even bigger challenge. On the table is a plan that could mean as few as a dozen more shuttle flights, even less science on the international space station, and a reengineered shuttle system to carry humans and cargo to the moon by the end of the next decade.

NASA chief Michael Griffin is betting that the plan, which has yet to be approved by the White House and made public, will square with the exploration goals set by U.S. President George W. Bush in 2004 without busting the agency's budget or raiding unrelated science programs. He's also hoping for support from politicians fiercely protective of shuttle-related jobs in their states. But he's constrained by the still-rising costs of returning the shuttle to orbit. And he knows that NASA's European and Japanese partners will almost certainly balk at any attempt to reduce the station's capabilities yet again. "There's going to be a lot of kicking and screaming" over the station's future, predicts one official involved in the discussions.

The transportation report, due out later this month, is one of two internal studies that Griffin requested shortly after taking office in March (*Science*, 18 March, p. 1709). The other, due out late next month, will examine how to assemble the space station using as few shuttle flights as possible.

At the heart of the transportation report, according to officials familiar with it, is a redesigned solid rocket booster that carries the orbiter into space. By adding an upper stage and a capsule, NASA could turn the booster into three distinct vehicles: one to carry a crew of three or so, another to orbit equipment requiring a pressurized cabin, and a third to carry cargo that could withstand the vacuum of space. This "single-stick" option could be ready in 2011, providing crew and cargo services to the space station, according to sources familiar with the study.

Infrequent flyers? NASA is weighing a plan that could mean as few as a dozen more shuttle trips to the space station.

The retirement of the shuttle no later than 2010 would shift attention to a heavy-lift vehicle capable of launching a whopping 100 tons—an order of magnitude more than the single stick. That design also would draw on the shuttle system, essentially replacing the orbiter with a cargo carrier. The unpiloted vehicle would be used later in the decade to launch the pieces of a lunar outpost.

A shuttle-derived vehicle, rather than one based on an existing expendable launcher, has political as well as engineering advantages. Lawmakers in Texas, California, Alabama, and Florida—the site of thousands of shuttle-related jobs—have been reluctant to pull the plug on the shuttle. For them, the single-stick and heavy-lift options promise to keep assembly lines humming after the orbiters are retired. And although Pentagon officials prefer a new launch system based on the department's Atlas or Delta launchers, Griffin won them over by assuring that plenty of science missions would be launched on Delta rockets.

The estimated cost of these new vehicles is from $10 billion to $15 billion through 2015. Operating costs for the single-stick series would run about $3 billion a year—approximately $1 billion less than the shuttle cost before Columbia's failure. NASA hopes to pay the tab from its scheduled modest budget increases and savings from falling shuttle return-to-flight costs. But one official says that those return-to-flight costs will climb as high as $7 billion over 5 years—$2 billion more than previously estimated. That figure would leave little room for new ventures, the cost of which have traditionally been underestimated.

That gloomy budget picture is forcing NASA to consider even more radical cuts to the number of flights needed to finish the space station. NASA had planned 28 more shuttle flights, but the team reexamining the station is officially working to find a way to finish up after 18 to 24. Sources close to the second study say that Griffin and the White House are pressing for as few as a dozen more flights. Last month, Griffin warned his European and Japanese counterparts that the agency may propose other ways to put their laboratory modules into space, such as using expendable launchers, on an extended schedule. "He is softening the beachhead by warning that there may be some deferral," says one source. Japan and Europe have resisted any alternative plan to launch the labs, their primary contribution to the station, because that would force expensive modifications and delays. "The reaction was quite adamant," the official adds.

To honor pledges from the White House to meet its obligations to the station partners, the redesign team is looking at alternatives to reducing shuttle flights. One strong possibility is to minimize the science aboard the U.S. laboratory module. Griffin has already issued ▶

CREDITS: NASA

548 Solar appeal

551 Triggers for puberty

553 Europeans scope the future

such a warning (*Science*, 29 April, p. 610), but fewer shuttle flights could lead to even more dramatic reductions in science equipment and racks. "There isn't a lot of science that could be done on the space station that can't be done later" or on the moon, explains another official familiar with the study.

Not true, says Ian Pryke, a senior fellow at George Mason University in Fairfax, Virginia, and former head of the Washington, D.C., office of the European Space Agency. A centrifuge, he notes, could provide important data on the long-term effect of lunar—or Mars-style—gravity on mammals. Japan is building the centrifuge for NASA, but Griffin already has stated that it likely must be abandoned given space and budgetary constraints.

The station itself seems safe for now. But Griffin's job over the next several months will be to satisfy a White House eager to move beyond the station, placate foreign partners frustrated by delays, and convince lawmakers that he isn't ignoring station science. "With a radically reduced [shuttle] flight rate, the change is going to be traumatic," warns one official. "We're in a mess." That mess may well prove more daunting than a successful return to flight aboard Discovery. **–ANDREW LAWLER**

IMMUNOLOGY

New Virtual Center Aims to Speed AIDS Vaccine Progress

A star-studded team of AIDS researchers from four universities, led by Barton Haynes of Duke, has won a huge award to explore some of the deepest immunologic mysteries confronting the field—part of a bold new effort to speed the search for an HIV vaccine. Haynes will direct the so-called Center for HIV/AIDS Vaccine Immunology (CHAVI), which could receive more than $300 million over the next 7 years from the U.S. National Institute of Allergy and Infectious Diseases (NIAID). "It's big science in the way that the Human Genome Project was," says Peggy Johnston, the top AIDS vaccine official at NIAID, which announced the award last week.

The CHAVI award marks the start of the Global HIV/AIDS Vaccine Enterprise, an ambitious public-private effort spearheaded by the Bill and Melinda Gates Foundation that aims to remove roadblocks hindering the field. "We've all been frustrated by the slow tempo of progress and how difficult a bug this virus is," says Haynes, an immunologist and former chair of Duke's medical school in Durham, North Carolina. "This means a change in the way we do business." Although Haynes and his collaborators—who include Harvard University's Norman Letvin and Joseph Sodroski, Oxford University's Andrew McMichael, and George Shaw of the University of Alabama, Birmingham—beat out three other high-profile teams, at least one competitor doesn't expect the award to divide the field. Harvard immunologist Bruce Walker predicts that the process will have "a lot of collateral positivity."

The enterprise envisions different funders—including the Gates Foundation and other wealthy countries—sponsoring several CHAVI-like consortia. The push for these consortia grows out of the deep frustration about the limits of investigator-initiated research. The enterprise attempts to address those by hewing to a strategic plan to guide the field, standardizing assays so labs can easily compare results, and avoiding unnecessary duplication. CHAVI itself will intensively examine immune responses and the genetic factors that give some people an upper hand against the AIDS virus. In particular, CHAVI investigators will study people who are repeatedly exposed to HIV but remain uninfected, and they will try to unravel why newly infected people vary in their ability to keep the virus in check. Haynes and his collaborators will also explore why some HIV isolates transmit more readily, the structure of anti-HIV antibodies that work best, and why some vaccines work in monkey experiments.

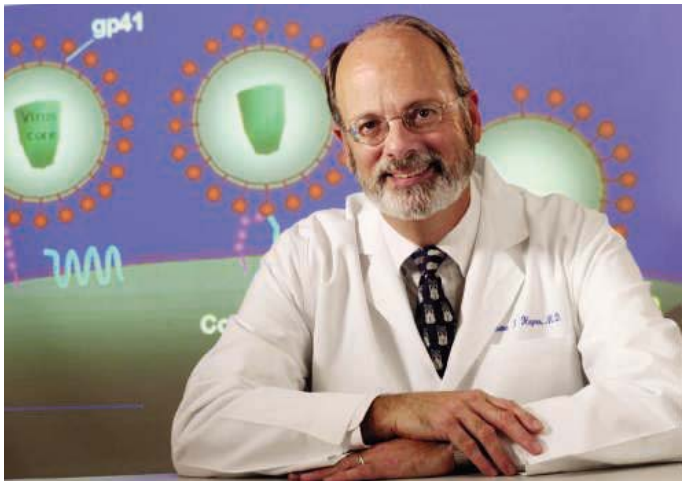

Dream team. Duke's Barton Haynes formed a winning AIDS vaccine consortium, part of the ambitious new Global HIV/AIDS Vaccine Enterprise.

CREDIT: DUKE UNIVERSITY MEDICAL CENTER

The intensely competitive CHAVI application process has been the talk of the field for months. "Everybody who's very active was on one of the applications," says Walker. His group may attempt to fund the projects they proposed through other sources, and Walker's already planning to meet with other also-rans. "My sense is a lot of these groups will continue to pursue the goals that they outlined," he says. Haynes stresses that as CHAVI expands, it might invite researchers from the other teams to join the virtual center. "Our group is just one group," says Haynes. "We don't have all the ideas."

Because money for CHAVI comes solely from NIAID's budget, some basic researchers worry that the institute may cut back on investigator-initiated grants. Anthony Fauci, NIAID's director, says he "can't predict funding from one year to another" but notes that current CHAVI funding taps new money and that NIAID makes it "the highest priority" to protect investigator-initiated research funds. "The field was screaming for some bold new approach," Fauci says.

The CHAVI grant will pay the full amount allocated ($49 million per year) only if the researchers meet specific milestones and move their ideas from the lab to clinical trials. "One of the challenges is going to be how to keep everybody pulling in the same direction," says NIAID's Johnston, who sees CHAVI itself as a grand experiment. "It will either succeed big or fail big, but at least we have tried." **–JON COHEN**

U.K. SCIENCE POLICY

Parliamentary Gadfly Loses His Post

CAMBRIDGE, U.K.—One of the few scientists in Parliament and a blunt critic of the management of U.K. science has been bumped from a committee leadership post by his own Labour Party. Ian Gibson, former dean of biological science at the University of East Anglia, says the party last week gave up control of the Select Committee on Science and Technology, knocking him from the chairmanship, a post he has held for 4 years.

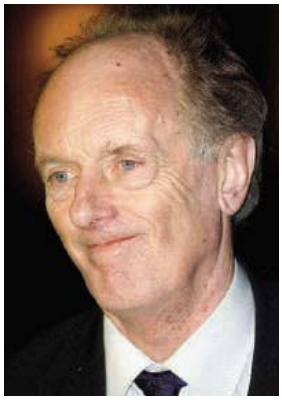

Bumped. Ian Gibson gives up the science committee chair.

After losing seats in the national election in May, Labour was required by parliamentary rules to give up control of at least one committee; it chose the science panel. Gibson says the committee will be headed by an adversary of Labour, Phil Willis, a Liberal Democrat from a constituency 320 kilometers north of London. A former schoolteacher, Willis has handled education issues for his party but is not known to have spoken in Parliament about science, observers say.

Gibson says he is "very disappointed," particularly because he thinks the select committee has sharpened policy by advancing "open access" publishing schemes and probing government research funding. Making last week's decision worse, he says, was a "ridiculous" move by Labour tacticians to stifle dissent: He and other Labour committee members "were more or less blackmailed to accept the choice" of Willis as chair or else lose their own seats on the committee. For this reason, he says, he will not oppose the change, and he expects to remain on the committee. The episode, Gibson adds, "smacks of getting your own back." Party leaders, he believes, punished him for failing to toe the line, for example when he led a revolt against increases in university tuition fees. (The campaign failed.)

The science committee under Gibson did a "valuable" job, according to Peter Cotgreave, director of a London-based lobby group called the Campaign for Science and Engineering. "The committee did some excellent reports," says Cotgreave, including a probe of the Medical Research Council that highlighted management controversies that had been accumulating over many years. He would like to see the committee continue such investigations, perhaps taking on topics such as how science funders should pay for the "full cost" of university research and how to improve links between university and industrial researchers. The Gibson panel "kept the government on its toes," Cotgreave says, adding, "that's the whole point" of Parliament.

—ELIOT MARSHALL

ITALIAN SCIENCE

Carlo Rubbia Dismissed From Energy Agency

ROME—Carlo Rubbia, winner of the 1984 Nobel Prize for work in particle physics, has lost his position as president of Italy's nuclear and alternative energy agency (ENEA) in a battle over leadership. The government dismissed Rubbia last week hours after he published an open letter in *La Repubblica* criticizing the scientific competence of the agency's board.

The government has already named a special commissioner to take over: Luigi Paganetto, economics faculty head at Rome University "Tor Vergata." He will be flanked by two deputies, both former board members: Claudio Regis, a hydrogen engine engineer, and Corrado Clini, director general of the environment ministry and one of Rubbia's fiercest opponents.

ENEA's life has brimmed with controversy since it was set up in 1982 to oversee the nuclear power program. Despite grand ambitions, its agenda has been stalled by boardroom clashes and frequent changes of management. Observers say the agency never recovered from a national referendum in 1987 that pulled the plug on nuclear power. And its niche under the ministry for industry, in collaboration with the environment and research ministries, is top-heavy with bureaucracy.

Slated for dissolution in the 1995 budget, ENEA managed to survive when supporters proposed an overhaul. They called for shifting to new areas such as nuclear fusion and high-performance computing. Rubbia took over as president in 1999, but after clashing with the board, resigned in 2001. He subsequently became ENEA's special commissioner with a mandate to prepare a law governing the agency's future. Under this legislation, Rubbia again became ENEA's president in early 2004.

But Rubbia didn't get far. Board members overruled him on his choice of director general and frequently on scientific matters as well.

Publish and perish. Hours after his letter appeared in print, Rubbia was out.

They requested Rubbia's removal and proffered their own resignations. Early this year, Rubbia took the board to court over its "irregular" procedures—and won the removal of the board's director in mid-June. However, the court suggested placing ENEA under a commissioner. In June, ENEA's 3000 researchers publicly called for an end to the fighting, saying their work was being paralyzed.

Last week, Rubbia complained in his letter that although the law stipulates that ENEA be led by scientists of international repute and high merit, its seven board members were political choices of ENEA's three umbrella ministries and exhibited a "lack of scientific knowledge."

Clini denies that politics lies at the heart of these clashes. He says that, contrary to the board's wishes, Rubbia favored a nuclear waste disposal project that would have spent a large part of ENEA's $440 million budget on French and German researchers.

As to the future, Paganetto wants ENEA to launch new collaborations with Italy's other research institutions and "move quickly to take advantage of European projects." Clini adds that the agency should become the hub for energy and environment research projects related to controlling greenhouse gases under the Kyoto Protocol.

—SUSAN BIGGIN

Susan Biggin is a writer in Trieste, Italy.

CREDITS (TOP TO BOTTOM): DAVID BEBBER/REUTERS; CYBERSPACE GENEVA/REUTERS

SCIENCE AND LAW

Flawed Statistics in Murder Trial May Cost Expert His Medical License

Mangling statistics is a common offense, but in the case of Roy Meadow—a renowned expert on child abuse and co-founder of London's Royal College of Paediatrics and Child Health—it has had uncommon repercussions. As an expert for the prosecution in a 1999 criminal trial, Meadow overstated the low odds of two infants in the same family dying suddenly for unexplained reasons, helping convict a mother of murdering her two sons. On 15 July, a professional panel ruled that Meadow, 72 and retired, should be "erased" from the register of physicians in Britain for his statistical blunder—a decision that some think will deter scientists from testifying as expert witnesses.

The mother, attorney Sally Clark, spent 3 years in prison before her husband (also an attorney) and others organized an appeal that quashed the verdict in 2003. An appeals court found that medical details had been withheld and that the jury may have been swayed by Meadow's testimony. The reversal also prompted an investigation of Meadow by the physicians' governing body, the General Medical Council (GMC).

Censured. Roy Meadow overstated the odds against two SIDS deaths in one family.

A "fitness to practice" panel, headed by GMC lay member Mary Clark-Glass, a former law lecturer, read Meadow its conclusions last week: "You abused your position as a doctor by giving evidence that was misleading, albeit unintentionally, and … you were working outside the limits of your professional competence by straying into the area of statistics. …" It found Meadow "guilty of serious medical misconduct" and meted out the severest penalty. The reason, Clark-Glass explained, was that Meadow's "eminence and authority … carried such great weight," and his errors were "compounded by repetition" in court testimony. Meadow is not commenting to the press at this time.

Meadow's most egregious mistake, according to the inquiry, was to testify that the risk of two infants in the same family dying of unexplained natural causes—sudden infant death syndrome (SIDS)—was one in 73 million. He acknowledged that he got the high number by taking a figure from a draft report of the risk of a single SIDS death in a nonsmoking family like the Clarks (1 in 8543) and squaring it. But according to the GMC, the unpublished report he used was not about the recurrence but the occurrence of SIDS. And the panel found that he was wrong to compute the odds as independent risks. Indeed, the GMC said that information in the draft report showed that the odds went the other way: "There is an elevated risk of a second SIDS death in one family after there has been one such death." The panel faulted Meadow for getting the numbers wrong and for using a bold metaphor (for which he later apologized). He suggested that the likelihood of two children in a family dying this way would be like picking the winning horse in the Grand National 4 years in a row.

Some think it was a mistake for the GMC to focus its ire on Meadow. Richard Horton, editor of *The Lancet*, argued in a 2 July editorial that Meadow had become a "scapegoat" for the failings of the legal system in a series of controversial child abuse cases in which one family convictions have recently been overturned. "Society needs to guard against any crude and oversimplistic settling of scores," he wrote. He proposed a commission to examine how experts should be used in court.

Meadow's friend and colleague Alan Craft, president of the College of Paediatrics, protests that Meadow "did not mean to mislead the jury" but acknowledges that he was "wrong in one small bit of evidence and in the way he presented the statistics." For the GMC to jump from that to serious misconduct was "quite astonishing," Craft says, and will make it "extraordinarily difficult to get experts involved in child protection cases." He thinks the implications for all of medicine "are enormous." Philip Newman, deputy chair of the 1500-strong Academy of Experts in London, says the decision is not necessarily bad: It's a strong reminder that experts must adhere to three I's—"independence, impartiality, and integrity."

Meadow has 28 days to appeal.

–ELIOT MARSHALL

CREDIT: TOBY MELVILLE/REUTERS

ScienceScope

Rip Van Hubble

Keeping the Hubble Space Telescope in orbit until 2030 could save NASA a bundle of money—at least in the short run. Engineers at NASA's Goddard Space Flight Center in Greenbelt, Maryland, say that a canny use of orbital mechanics and the fuel left aboard might allow NASA to avoid attaching a $150 million deorbiting module to the 14-year-old giant telescope. NASA already expects to spend some $200 million on a mission to ensure that Hubble burns up safely—money that would likely come out of science mission budgets. Managers fear that including a deorbiting module for astronauts to attach would make the mission vastly more complex and costly. A decision is pending.

–ANDREW LAWLER

SREL Saved for Now

The Department of Energy (DOE) has thrown a lifeline to the Savannah River Ecology Laboratory (SREL) near Aiken, South Carolina, reversing a White House plan to close the $7.7-million-per-year lab this fall (*Science*, 25 March, p. 1857). But 51 of its 180 employees face layoffs, and its budget will be slashed to $4.3 million.

DOE had planned not to fund the lab in 2006, reflecting a controversial shift away from pollution studies at the surface, the lab's forte. DOE has now pledged some $3 million for the lab, barring direction otherwise from Congress. A department official said a reevaluation had found that the department's needs for surficial science made the turnaround necessary.

–ELI KINTISCH

U.S.-Indian Ties Enhanced

Calling India "a responsible state with advanced nuclear technology," the Bush Administration this week agreed to share U.S. civil nuclear technology with its ally despite India's refusal to sign the Nuclear Nonproliferation Treaty.

A Washington visit by Indian Prime Minister Manmohan Singh also produced a protocol on the contentious issue of intellectual property rights for joint research projects. Export controls between the nations will also be scaled back, agricultural projects boosted, and joint space projects tackled. The United States will endorse India's participation in the International Thermonuclear Experimental Reactor project in France. The agreements require congressional approval.

–PALLAVA BAGLA

UNESCO

U.S. Rules Could Muffle Scientific Voices

The U.S. government has issued new rules on interactions between U.S. citizens and the United Nations Educational, Scientific, and Cultural Organization (UNESCO) that some scientific organizations fear could limit access to the international scientific and cultural body by U.S. experts. But U.S. officials say the changes are intended simply to keep the government in the loop.

"It certainly has the power of acting as a filtering process," says Christopher Keane. He represents the American Geological Institute on the U.S. National Commission to UNESCO, a 100-member body appointed by the U.S. government to coordinate communications between its citizens and UNESCO that was briefed on the directive last month at its first meeting. "But it's a little hard to hang them on it until there's evidence" that the U.S. government is preventing UNESCO from accessing the experts it needs, says Keane.

The 5 May directive, from U.S. Ambassador Louise Oliver to UNESCO Director General Koichiro Matsuura, requires UNESCO to consult U.S. officials before partnering with organizations or citizens in the United States. It also asks UNESCO to check with the U.S. permanent delegation and the commission before planning any U.S. events. U.S. individuals and institutions, it adds, must channel all communications through the commission and avoid direct contact with the UNESCO secretariat in Paris.

U.S. officials say the directive is meant to keep the U.S. government informed about UNESCO's dealings with nongovernmental organizations and is consistent with UNESCO's own regulations. The memo "absolutely does not impose a vetting mechanism," says Andrew Koss, a State Department official who serves as the deputy chief of the U.S. mission. "Advance consultation simply means that if UNESCO comes to us with a list of potential partners, we might offer additional names to help them broaden their horizons." The United States rejoined UNESCO 2 years ago after dropping out in 1984.

Veto power. New directive could restrict U.S. access to meetings such as this one at the International Centre for Theoretical Physics in Trieste, Italy.

But others say the directive goes far beyond the practices of most member states, which only expect UNESCO to inform their national commissions about a given activity after the details have been worked out. "The memo implies that UNESCO's decisions to engage U.S. scientists and engineers—even when they are being selected for their expertise and not as official U.S. representatives—need to be vetted by the U.S. government," says Irving Lerch, chair-elect of the American Physical Society's Forum on International Physics. Lerch, who's also a trustee for Friends of UNESCO, says the procedure would allow the U.S. government to control the flow of scientific opinion from the research community to UNESCO.

The memo has also sparked concern among some managers of UNESCO's scientific programs. "If we were to follow this literally, organizing routine scientific meetings could get very difficult for us," says K. R. Sreenivasan, director of the International Centre for Theoretical Physics in Trieste, Italy, which is a part of UNESCO. "We'd like to invite U.S. scientists who are appropriate for us, not those who have been approved by the U.S. government."

—YUDHIJIT BHATTACHARJEE

ANTITERRORISM

Defense Rules Would Pinch Foreign-Born Scientists

The U.S. Department of Defense (DOD) has proposed a rule that would make it harder for universities to involve foreign nationals in unclassified research projects funded by the agency. The additional security arrangements required by the rule are at odds with traditional practices, say university administrators. The result, they warn, will be fewer opportunities for many researchers born abroad.

The rule, published in the 12 July *Federal Register* (www.access.gpo.gov/su_docs/fedreg/a050712c.html), is intended to beef up DOD's compliance with export-control regulations aimed at restricting the transfer of certain technologies to countries viewed as threats to national security. The Commerce Department earlier this year proposed modifying those regulations so that universities must obtain a license before engaging nationals from a list of countries that includes China, India, and Russia (*Science*, 13 May, p. 938). Universities have traditionally considered themselves exempt from this requirement under what is known as the fundamental research exemption.

By not mentioning the fundamental research exemption, the DOD rule would apply to all DOD-sponsored research. To comply, universities and companies working on defense projects would not only need licenses to enable foreign nationals to participate in the research but would also need to protect export-controlled information through an "access control plan" that includes "unique badging requirements for foreign nationals" and "segregated work areas." The requirements are in line with recommendations last year from DOD's Inspector General, who concluded that the agency did not have "adequate processes to identify unclassified export-controlled technology and to prevent unauthorized disclosure to foreign nationals" (*Science*, 23 April 2004, p. 500).

University officials foresee "draconian clauses" in research contracts that would make it more difficult for them to involve foreign nationals in projects, says Toby Smith, senior federal relations officer for the Association of American Universities in Washington, D.C. Many universities would have to turn down such contracts either because of the cost of additional security or to avoid violating their own nondiscrimination policies, Smith says. "Walling off labs, making foreign graduate students wear badges—it's just not what we do at a university," says Paul Powell, assistant director of the Office of Sponsored Programs at the Massachusetts Institute of Technology in Cambridge.

The comment period closes 12 September.

—YUDHIJIT BHATTACHARJEE

CREDIT: ICTP

NATIONAL INSTITUTES OF HEALTH

Bill Could Restructure Agency And Strengthen Director's Hand

An influential legislator wants to boost the budget authority of the director of the National Institutes of Health (NIH)—and impose a ceiling on the agency's overall growth.

Those controversial suggestions are expected to be part of a bill to streamline management of the biomedical research behemoth. A draft has triggered a mixed reaction from research community leaders, who fear that giving the NIH director too much power could lead to unwise decisions about how to divide resources among NIH's 27 institutes and centers. Meanwhile, a Senate spending panel last week approved a $1.05 billion boost for NIH in 2006, to $29.4 billion. But that level is unlikely to be sustained in the final spending bill because it relies on accounting tricks that are unpopular in the House.

The NIH bill, known as a reauthorization, will soon be introduced by Representative Joe Barton (R–TX), chair of the House Energy and Commerce Committee. NIH's programs were last reauthorized in 1993. A "discussion draft" of the new legislation, which was aired at a committee hearing this week, reflects advice from a 2003 Institute of Medicine (IOM) report on how to address concerns that NIH's sprawling structure makes it less agile and leads to duplicative research across the agency (*Science*, 1 August 2003, p. 574).

Several provisions in the upcoming bill reflect IOM recommendations, such as boosting the 1% of NIH's overall budget that the director can now move from one institute to another or pool for common projects. The bill would also create a new division in the director's office to analyze NIH's overall portfolio and disburse grants for trans-NIH initiatives, and it would require NIH to give Congress detailed spending reports every 2 years. But another key provision came out of left field, observers say: lumping together the annual budgets for NIH's institutes into just two piles—one for 15 "mission-specific" institutes such as cancer and diabetes and a second for nine "science-enabling" institutes such as general medical science and genomics. Smaller piles would go to the director's office and its planning division.

Although giving the NIH director more "flexibility" to move funds is a good idea, says David Moore, head of governmental relations for the Association of American Medical Colleges, Congress should be wary of sanctioning "huge reallocations" because that would override the careful planning that now goes into each institute's appropriation. Research lobbyists worry, too, that the science-enabling institutes could lose out because they don't have patient advocacy groups backing them. Patient groups, for their part, are concerned that eliminating institutes' individual appropriations will make it harder to advocate for funding for particular diseases.

Research leaders are also unhappy that the bill would specify the maximum budget increase NIH could receive from 2007–09, the period of the reauthorization. Legislators typically talk about approving "such sums as necessary" in reauthorization bills to give appropriators full discretion each year.

Barton is believed to be concerned that the doubling of NIH's budget between 1999 and 2003 was not particularly well managed and wants to foreclose such rapid growth. But

Capitol idea. Representative Joe Barton (R–TX) is proposing changes in how NIH manages its money.

"the research community is very concerned about what the overall authorization levels will be. We're watching it very closely," says Patrick White, a lobbyist for the 62-member Association of American Universities.

Barton hopes that the House will pass his measure before the end of the year. There is as yet no equivalent bill in the Senate. And any bill would be vulnerable to members of Congress attaching amendments on controversial topics such as support for human embryonic stem cell research. In the meantime, biomedical research advocates are watching closely what happens in the House.

–JOCELYN KAISER

CREDIT: MANUEL BALCE CENETA/AP PHOTO

ScienceScope

Wanted: More Vet Research

Despite growing threats from animal-based diseases such as avian influenza, the number of veterinarians conducting disease research in the United States is declining, according to a pair of reports released this week by the National Academies. Noting that three-quarters of animal diseases can affect humans, the studies call for more training facilities and government support for animal disease research. One obstacle to progress, they add, is the reluctance of single-mission agencies to support research at the intersection of animal and human health. Legislation introduced this year in the House and Senate would forgive school loans for vets working to regulate agriculture or conduct research. –CATHY TRAN

Barton Draws Critics

Political fires are burning hot over an inquiry by a House panel into a paleoclimate analysis that shows a rise in temperature in the 20th century. "A congressional investigation ... is probably not the best way to resolve a scientific issue," says Ralph Cicerone, the new president of the National Academy of Sciences, in a 15 July letter to Energy and Commerce panel chair Joe Barton (R–TX).

Barton had asked the National Science Foundation and several climate scientists for information on "methodological flaws and data errors" in papers published in 1998 and 1999 by Michael Mann of the University of Virginia, Charlottesville (*Science*, 1 July, p. 31). Other critics of Barton's queries include House Science Committee chair Sherwood Boehlert (R–NY), who calls it "misguided and illegitimate"; AAAS, which publishes *Science*; and 20 prominent U.S. climate scientists who wrote to support Mann's conclusions this week. Barton calls his questions a "routine matter of oversight."

–ELI KINTISCH

European All-Stars

BERLIN—Still without a budget or structure, the proposed European Research Council (ERC) now has 22 eminent scientists to guide its first steps. The newly named scientific council, which includes several Nobel Prize winners, British Royal Society president Robert May, and Polish science minister Michal Kleiber, will determine the initial shape of the ERC. The high-prestige members may also help sell politicians on the concept, says Luc van Dyck of the Initiative for Science in Europe. –GRETCHEN VOGEL

ECOLOGY

Global Analyses Reveal Mammals Facing Risk of Extinction

Two new studies are helping conservation biologists think big—in the case of one of the studies, as big as one-tenth of the continents.

Conservationists typically set goals and priorities for relatively small regions. Although some have come up with priorities for the planet, these have often been wish lists rather than objectives drawn from rigorous analyses. Now a team of researchers, led by mammalogist Gerardo Ceballos of the National Autonomous University of Mexico, has conducted the first global analysis of the conservation status of all known land mammals. On page 630, they report that 25% of known mammal species are at risk of extinction. In order to decrease the risk to mammals worldwide, about 11% of Earth's land should be managed for conservation, the analysis finds.

This is the first time such a global conservation estimate has been calculated for mammals, and although experts are not surprised by these results, they praise the study for its comprehensiveness and detail. "This sets a new standard for global priority-setting analyses," says Peter Kareiva, lead scientist for The Nature Conservancy.

A second conservation study, reported online by *Science* this week (www.sciencemag.org/cgi/content/abstract/1116030), finds that large mammals may be more threatened than their smaller relatives. A team led by Georgina Mace of the Zoological Society of London and Andy Purvis of Imperial College London reports that adult mammals that weigh more than 3 kilograms tend to have biological traits that hike their risk of extinction. "Both of these papers provide us with finer and more detailed insights into threat patterns and processes," says Thomas Brooks of Conservation International in Washington, D.C.

Big risk. Large size significantly ups the odds of extinction for mammals such as elephants and pandas.

The two new analyses rely on massive data sets. Ceballos and his colleagues combed the literature and compiled geographic ranges for all 4795 known species of land mammals. After dividing the world's land into many thousands of cells, each 10,000 square kilometers, they plugged their range data into a conservation planning model, called MARXAN, that identified the least amount of area—all told, 17,020,000 km^2, or 1702 cells—that would conserve at least 10% of the range of each species. Various population models used by conservation biologists typically specify that threshold as the minimum amount of range needed to sustain a healthy population of a species.

This particular analysis won't be used in specific conservation efforts because the scale is much too coarse, but experts say it reveals important points. For example, the analysis shows that the collection of 1702 cells—11% of the total—would provide a resilient and flexible strategy, because almost any cell can be replaced by another cell without an overall loss of species diversity. But about 80% of these high-priority cells have already been affected by agriculture, ▶

CONFLICT OF INTEREST

Forty-Four Researchers Broke NIH Consulting Rules

An internal review of 81 National Institutes of Health researchers who consulted for industry since 1999 has found that 44 did not follow NIH ethics rules for such activities. Nine cases are serious enough to be investigated for possible criminal misdeeds, according to the review.

These results, released last week by the House Energy and Commerce Committee, are part of an examination of NIH ethics rules begun in late 2003 following media reports of large payments by drug and biotech companies to some NIH employees. The furor led NIH earlier this year to temporarily ban all consulting (*Science*, 11 February, p. 824).

The violations show that "the ethical problems are more systemic and severe than previously known," declared Representative Joe Barton (R–TX), chair of the panel that has been investigating NIH. Spokesperson John Burklow says NIH "has been aware of the issues and problems for some time" and is addressing them. Some NIH staffers and observers suggest that the report actually demonstrates how few of the agency's thousands of researchers committed serious violations. Still, "nine is too many," says Howard Garrison, public affairs director of the Federation of American Societies for Experimental Biology in Bethesda, Maryland.

The 81 names appeared on lists that 20 drug companies gave to the committee but not on NIH's own tally of staff consulting activities. Although 37 people were cleared, the rest didn't request approval for their consulting, did the work on company time, and/or did not report the income, according to an 8 July letter from NIH Director Elias Zerhouni to the committee. Eight have since left NIH. Officials have concluded that the consulting in some instances conflicted with the employee's official duties and in other cases traded on "the name of NIH as an affiliation."

Nine cases have been referred to the Department of Health and Human Services' inspector general (IG), the letter says. A few of those names have been reported in the press previously—such as Alzheimer's disease researcher Trey Sunderland, who is still at NIH, and cancer researcher Lance Liotta, who left this spring for George Mason University in Manassas, Virginia. A spokesperson in the IG's office said that former government employees may still be prosecuted.

NIH is still reviewing the cases of 22 staffers. These scientists either admitted not reporting an activity or were named in stories by the *Los Angeles Times* that sparked the ethics overhaul.

—JOCELYN KAISER

CREDIT: PHOTOS.COM

which destroys natural habitat. "We simply are not going to be able to do conservation without making it compatible with some measure of agriculture," notes Kareiva.

The results from Ceballos's team are only for mammals, whose ranges may not overlap with those of other taxa. Adding birds, amphibians, and reptiles would increase the amount of land needed to be conserved. "We need to do much more," says study author Paul Ehrlich, a population biologist at Stanford University. "If you want to add in most biodiversity, you're talking about [conservation of] 30% to 40% of Earth's surface," he speculates. Ehrlich adds that the population size of a species that can survive by preserving 10% of its former range won't be as effective at providing ecosystem goods and services, such as pollination or bush meat.

Similar results about mammal ranges and conservation, not yet published, will come from John Gittleman, an evolutionary biologist at the University of Virginia, Charlottesville. His group spent 4 years collecting range maps and biological data for all known land mammals. "There's a nice convergence," he says. "It's very reassuring."

The report by Mace, Purvis, and their colleagues relies on information from Gittleman's group as well as other data sets such as the so-called World Conservation Union's Red List, which ranks mammals according to the extinction threats they face. Drawing on such information for 4000 mammal species, the authors determined what factors, such as small geographic ranges or large body size, put particular species at higher risks of extinction.

The analysis found that for mammals smaller than 3 kilograms, the main risk factors were environmental, such as proximity to agriculture or human populations. Identifying and conserving habitat is likely to be enough to keep these species going, the scientists conclude. But larger animals, such as elephants and pandas, face threats magnified by intrinsic biological constraints, such as small litters and long gestation times. Conservation biologists had suspected that larger mammals face greater extinction risks, but the size of this data set puts the premise on a much stronger footing, Gittleman says.

Mace, Purvis, and their colleagues conclude that the survival of large mammals will likely require a concerted effort tailored to the biology of each species.

–ERIK STOKSTAD

RESEARCH FUNDING

France Hatches 67 California Wannabes

PARIS—France may soon have its own Silicon Valley—or, more likely, 67 miniversions of that icon of American innovation. Last week, Prime Minister Dominique de Villepin announced a list of 67 regional partnerships across the country that his government hopes to nurture into cutting-edge science and technology engines designed to create new jobs and kick-start the economy. But the plan has already run into criticism: Some researchers say industrial strategy shouldn't drive research policy, while others argue that the funds available—some €1.5 billion for the next 3 years—are spread so thin they can't possibly have much impact.

The decision to create "Competitiveness Clusters," as the new regional hubs are called, was taken last year by the previous government, led by Jean-Pierre Raffarin. But it has been embraced by Villepin, who made fighting France's double-digit unemployment his number one priority when he took over last month. Flanked by four cabinet ministers and citing Silicon Valley as a "historic example," Villepin called the plan a "choice for ambition" when he presented it last week.

The clusters—selected from 105 candidates by an interdepartmental panel—consist of a regional collaboration among research institutes, schools, universities, and businesses. Their focus ranges from nanotechnology and secure communications to sports equipment and—in "Cosmetic Valley," a plan backed by companies such as Dior and Yves Saint Laurent—"the science of beauty and well-being." The centers will benefit from tax breaks as well as specific support from funding agencies, including the new National Research Agency. They will also enjoy priority status when the government allocates the 3000 new research jobs it has promised for next year (*Science*, 27 May, p. 1243).

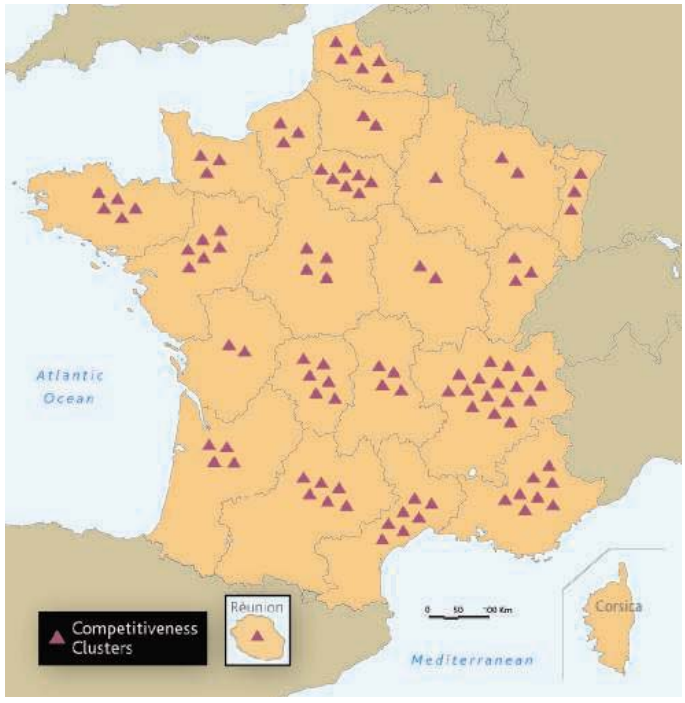

Spreading the wealth. Almost every region in France will be home to several of 67 new Competitiveness Clusters. (The number on this map is greater than 67 because interregional clusters are shown more than once.)

CREDIT: ADAPTED FROM DATAR, OBSERVATOIRE DESTERRITOIRES (JULY 2005)

But some fear that Villepin's version of Silicon Valley may be unattainable. The failure thus far to translate French research into new, profitable technologies stems from a variety of factors, says Alain Trautmann, the spokesperson of Sauvons la Recherche (Let's Save Research), a protest movement—including a less entrepreneurial spirit, timid venture capitalists, and discouraging bankruptcy laws. He doesn't think they can be fixed by scattering extra funds here and there. What's more, Trautmann says, U.S. high-tech hubs arise in areas with excellent basic research, which doesn't "take its orders from industry."

Others have criticized the large number of centers, suggesting that the plan is inspired more by behind-the-scenes lobbying and U.S.-style pork-barrel politics than by a desire to promote excellence. The resulting budget per center (some €7.5 million per year, often shared by dozens of partners) is bound to be ineffective, the opposition Socialist Party said in a statement last week.

But Bruno Goud, a group leader at the Curie Institute—a partner in a health cluster in the Paris region that's on the list—says something is better than nothing. Although it may be "typically French" for the government, rather than market forces, to designate the hot spots of the future, he adds, that doesn't mean it won't work.

–MARTIN ENSERINK

Officials at the U.S. Department of Energy are working to kindle support for a crash program to transform solar energy from a bit player into the world's leading power source

Is It Time to Shoot for the Sun?

Ask most Americans about their energy concerns, and you're likely to get an earful about gasoline prices. Ask Nate Lewis, and you'll hear about terawatts. Lewis, a chemist at the California Institute of Technology in Pasadena, is on a mission to get policymakers to face the need for sources of clean energy. He points out that humans today collectively consume the equivalent of a steady 13 terawatts (TW)—that's 13 trillion watts—of power. Eighty-five percent of that comes from fossil fuels that belch carbon dioxide, the primary greenhouse gas, into the atmosphere. Now, with CO_2 levels at their highest point in 125,000 years, our planet is in the middle of a global experiment.

To slow the buildup of those gases, people will have to replace most, if not all, of those 13 TW with carbon-free energy sources. And that's the easy part. Thanks to global population growth and economic development, most energy experts predict we will need somewhere around an additional 30 TW by 2050. Coming up with that power in a way that doesn't trigger catastrophic changes in Earth's climate, Lewis says, "is unarguably the greatest technological challenge this country will face in the next 50 years."

Clearly, there are no easy answers. But one question Lewis and plenty of other high-profile scientists are asking is whether it's time to launch a major research initiative on solar energy. In April, Lewis and physicist George Crabtree of Argonne National Laboratory in Illinois co-chaired a U.S. Department of Energy (DOE) workshop designed to explore the emerging potential for basic research in solar energy, from novel photovoltaics to systems for using sunlight to generate chemical fuels. Last week, the pair released their report on the Web (www.sc.doe.gov/bes/reports/list.html), and the hard copy is due out soon.

The report outlines research priorities for improving solar power. It doesn't say how much money is needed to reach those goals, but DOE officials have floated funding numbers of about $50 million a year. That's up from the $10 million to $13 million a year now being spent on basic solar energy research. But given the scale of the challenge in transforming the energy landscape, other researchers and politicians are calling for far more.

Fields of gold. Solar power is the most promising renewable energy source.

It is too early to say whether the money or the political support will fall in line. But it is clear that support for a renewed push for solar energy research is building among scientists. Last month, Lewis previewed his upcoming report for members of DOE's Basic Energy Sciences Advisory Committee (BESAC), which regularly must weigh its support for facilities that include x-ray synchrotrons, neutron sources, nanoscience centers, and core research budgets. Despite a painfully lean budget outlook at DOE, support for a solar research program "is nearly unanimous," says Samuel Stupp, a BESAC member and chemist at Northwestern University in Evanston, Illinois.

Why? Terawatts. Even if a cheap, abundant, carbon-free energy source were to appear overnight, Lewis and others point out, it would still be a Herculean task to install the new systems fast enough just to keep up with rising energy demand—let alone to replace oil, natural gas, and coal. Generating 10 TW of energy—about 1/3 of the projected new demand by 2050—would require 10,000 nuclear power plants, each capable of churning out a gigawatt of power, enough to light a small city. "That means opening one nuclear reactor every other day for the next 50 years," Lewis says. Mind you, there hasn't been a new nuclear plant built in the United States since 1973, and concerns about high up-front capital costs, waste disposal, corporate liability, nuclear proliferation, and terrorism make it unlikely that will change in any meaningful way soon.

Other energy alternatives have their drawbacks as well. Fusion reactors have the theoretical potential to provide massive amounts of cheap power—but not soon. Last month, Japan, Europe, China, Russia, South Korea, and the United States agreed to build a new experimental fusion reactor in France at a projected cost of $5 billion (*Science*, 1 July, p. 28). But even if the facility meets proponents' grandest expectations, it will still provide a sustained fusion reaction for at most 500 seconds, a far cry from the continuous operation needed to yield large amounts of power. "Will it work? We don't know. But we think it's worth the investment," says Ray Orbach, who directs DOE's Office of Science.

There is, of course, a grab bag of renewable energy options as well. Chief among them is wind energy. The technology already produces electricity for $0.05 a kilowatt-hour, making it cheaper than all but natural gas and coal plants. Still, scale is a problem. If wind turbines were installed wherever wind is plentiful and the costs reasonable, they still would generate only 2 to 6 TW of power, according to recent estimates from the Intergovernmental Panel on Climate Change and the European Wind Energy Association. (A new estimate from researchers at Stanford University ups the figure to 72 TW, a much

CREDITS (TOP TO BOTTOM): MARTIN BOND/PETER ARNOLD INC.; ARGUS/PETER ARNOLD INC.

higher number based on wind potential at 80 meters off the ground—the height of modern wind turbine hubs—where wind speeds are typically stronger. But that estimate extrapolates global wind potential from point measurements, Lewis says.) In any case, it's clear that wind energy is a critical renewable resource that will be pursued. But if the earlier predictions of wind energy potential are correct, it's no panacea.

Biomass, geothermal, and energy from ocean waves also have potential. But biomass's potential is limited by the need to use arable land to grow food; geothermal energy's potential is limited by high drilling costs; and ocean power has been stalled in part by high construction costs. Shunting CO_2 from power plants underground before it can escape into the atmosphere holds vast promise (*Science*, 13 August 2004, p. 962). But large-scale demonstrations have only recently begun and haven't confirmed that CO_2 will remain underground for hundreds to thousands of years without leaking out. "We absolutely need to be doing this. But it may not technically work," Lewis says. Finally, conservation programs have the potential to squeeze a lot more mileage out of existing energy sources. But by themselves they don't solve the CO_2 problem.

So what is the world to do? Right now the solution is clear: The United States is currently opening natural gas plants at the rate of about one every 3.5 days. A stroll through Beijing makes it clear that China is pursuing coal just as fast. Fossil fuel use shows no signs of slowing (see figure, p. 550).

Handwringing geologists have been warning for years that worldwide oil production is likely to peak sometime between now and 2040, driving oil prices through the roof. The critical issue for climate, however, is not when production of a fossil fuel peaks, but its global capacity. At the 1998 level of energy use, there is still at least an estimated half a century worth of oil available, 2 centuries of natural gas, and a whopping 2 millennia worth of coal. The upshot is that we will run into serious climate problems long before we run out of fossil fuels.

What's left? Solar. Photovoltaic panels currently turn sunlight into 3 gigawatts of electricity. The business is growing at 40% a year and is already a $7.5 billion industry. But impressive as it is, that's still a drop in the bucket of humanity's total energy use. "You have to use a logarithmic scale to see it" graphed next to fossil fuels, Lewis says.

What solar does have going for it is, well, the sun. Our star puts out 3.8×10^{23} kilowatt-hours of energy every hour. Of that, 170,000 TW strike Earth every moment,

CREDIT: KONARKA TECHNOLOGIES INC.

Solar Report Sets the Agenda

If they are ever to supply a major part of the world's energy needs, solar cells must become both much cheaper and more efficient at converting sunlight to electricity. Meeting those somewhat contradictory goals will not be easy. But recent trends in the industry offer hope.

In fact, the efficiency of solar cells has risen steadily over the past 4 decades. And as manufacturing levels have risen, the price of installed solar panels has dropped dramatically—particularly in Japan, where increasing sales slashed solar power prices an average of 7% a year between 1992 and 2003, according to the International Energy Agency. Still, prices must drop another 10- to 100-fold to make solar not just competitive with other electric sources but cheap enough to be used to generate transportation fuel and home heating. In hopes of bringing about those and related changes, the new Department of Energy report identifies 13 priorities for solar energy research. Among them:

Flex time. Reel-to-reel manufacturing could slash the cost of plastic cells.

Revolutionary photovoltaic designs
Standard solar panels can turn at most one-third of the energy in the photons that strike them into electric current. Some of those photons have too little energy to excite electrons in the solar cells, and others have extra energy that just generates heat. Recent lab studies indicate that it may be possible to capture some of the high-energy strays using nano-sized lead-based particles that generate more than one electron from an incoming photon. But the technique has yet to be demonstrated in a working solar cell.

"Plastic" cells
Solar cells made from organic materials, including cheap high-volume polymers, have the potential to drastically reduce the cost of solar electricity. But current versions suffer from low efficiency, as most convert less than 2% of solar energy into electricity. New materials and device designs could change that equation.

Nanotechnology
Although crystalline solar cells can reach efficiencies of about 30%, producing the crystalline silicon in the first place is energy intensive and expensive. Solar cell makers have begun using cheap chemical manufacturing techniques to create nano-sized semiconductor crystals and incorporating these into solar cells. These cells are typically far cheaper to make, but for now the efficiency is stuck at about 10% or less. Researchers might be able to boost that efficiency if they can find ways to organize those nanoparticles to ferry excited electrons out of the cells.

From air and water to fuel
Sunlight can be used to split water molecules into oxygen and hydrogen gas, which can be stored, transported through pipelines, and used either to fuel vehicles or to generate electricity. But here too efficiency is a problem. The catalysts used to split water absorb only a couple of percent of the energy in sunlight that hits them, and in many cases they are unstable in practical settings. That could change if researchers could find new high-efficiency, stable catalysts to do the job. Equally promising is to find high-efficiency catalysts capable of using solar energy to convert carbon dioxide from the air into energy-rich hydrocarbon fuels.

Solar concentrators
Large banks of reflectors that concentrate large amounts of sunlight on a single photovoltaic already produce the lowest-cost solar electricity. Researchers are also looking at related designs to split water to create hydrogen gas, or to strip hydrogen gas from fossil fuels, while sequestering the carbon. To be most efficient, such reactors must concentrate enough sunlight to reach 2000 kelvin. But such high temperatures cause heat shocks that break down the ceramic materials in the chemical reactors. New heat-resistant ceramics could help lower the cost of sunlight-derived fuels. **–R.F.S.**

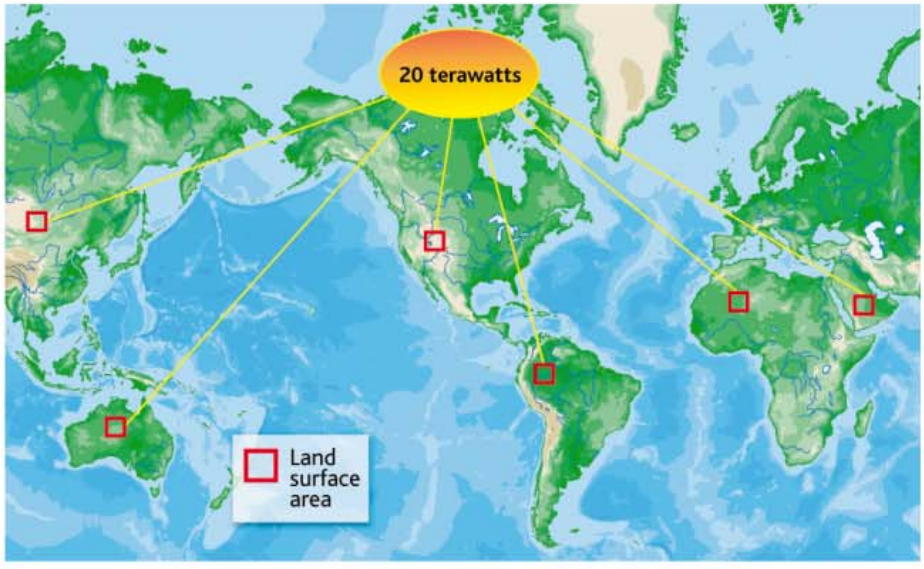

Global need. This map shows the amount of land needed to generate 20 TW with 10% efficient solar cells.

nearly one-third of which are reflected back into space. The bottom line is that every hour, Earth's surface receives more energy from the sun than humans use in a year.

Collecting even a tiny fraction of that energy won't be easy. To harvest 20 TW with solar panels that are 10% efficient at turning sunlight to electricity—a number well within the range of current technology—would require covering about 0.16% of Earth's land surface with solar panels. Covering all 70 million detached homes in the United States with solar panels would produce only 0.25 TW of electricity, just 1/10 of the electric power consumed in the country in the year 2000. That means land will need to be dedicated for solar farms, setting up land use battles that will likely raise environmental concerns, such as destroying habitat for species where the farms are sited.

Solar energy advocates acknowledge that a global solar energy grid would face plenty of other challenges as well. Chief among them: transporting and storing the energy. If massive solar farms are plunked down in the middle of deserts and other sparsely populated areas, governments will have to build an electrical infrastructure to transport the power to urban centers. That is certainly doable, but expensive.

A tougher knot is storing energy from the sun. Because electricity cannot be stored directly, it must be converted to some other form of potential energy for storage, such as the electrochemical energy of a battery or the kinetic energy of a flywheel. The massive scale of global electric use makes both of those forms of energy storage unlikely. Another possibility is using the electricity to pump water uphill to reservoirs, where it can later be released to regenerate electricity. Electricity can also be used to generate hydrogen gas or other chemical fuels, which can then be delivered via pipelines to where they are needed or used directly as transportation fuels. But that too requires building a new expensive infrastructure that isn't incorporated in solar energy's already high cost.

The issue of cost may be solar energy's biggest hurdle. Even without the extra infrastructure, harvesting power from the sun remains one of the most expensive renewable technologies on the market and far more expensive than the competition. In his BESAC presentation last month, Lewis noted that electricity derived from photovoltaics typically costs $0.25 to $0.50 per kilowatt-hour. By contrast, wind power costs $0.05 to $0.07, natural gas costs $0.025 to $0.05, and coal $0.01 to $0.04. What is more, electricity makes up only about 10% of the world's energy use. Globally, most energy goes toward heating homes, something that can usually be done more cheaply than with electricity generated from fossil fuels. As a result, says Lewis, "solar energy needs to be 50-fold lower in cost than fossil fuel electricity to make electric heat cheap enough to compete."

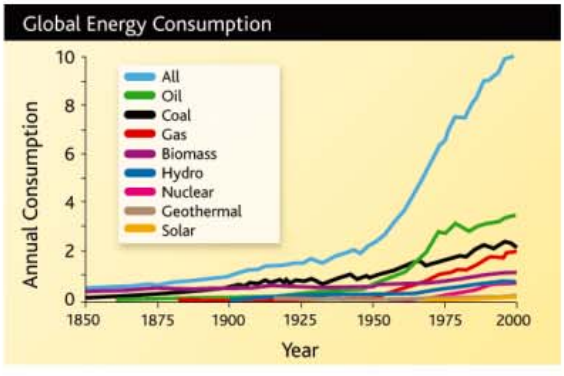

If all this has a familiar ring to it, that's because many of the same arguments and alternatives have been discussed before. In the wake of the oil shocks of the 1970s, the Carter Administration directed billions of dollars to alternative energy research. The big differences now are the threat of climate change and the current huge budget deficits in the United States. Some of the cost numbers have changed, but the gap between solar energy's potential and what is needed for it to be practical on a massive scale remains wide. The April DOE meeting explored many ideas to bridge that gap, including creating plastic solar cells and making use of advances in nanotechnology (see sidebar, p. 549).

That wealth of potentially new technologies makes this "an excellent time to put a lot of emphasis on solar energy research," says Walter Kohn, a BESAC member and chemist at the University of California, Santa Barbara. Some of these ideas do currently receive modest funding, enough to support a handful of individual investigator-driven labs. But Richard Smalley, a chemist at Rice University in Houston, Texas, who advocates renewed support for alternative-energy research, notes that unless research progresses far more rapidly to solve the current energy conundrum by 2020, there is essentially no way to have large amounts of clean-energy technology in place by 2050. "That means the basic enabling breakthroughs have to be made now," Smalley says.

Of course a major sticking point is money. At the April meeting, DOE officials started talking about funding a new solar energy research initiative at about $50 million a year, according to Mary Gress, who manages DOE's photochemistry and radiation research. Lewis is reluctant to say how much money is needed but asks rhetorically whether $50 million a year is enough to transform the biggest industry in the world. Clearly, others don't think so. "I don't see any answer that will change it short of an Apollo-level program," Smalley says.

For the past few years, Smalley has been advocating a $0.05-a-gallon gasoline tax to fund $10 billion a year in alternative energy research, which encompasses more than just solar research. A few members of Congress have recently pushed for that level of funding for alternative energy R&D. But so far such measures have failed to win broad support. Even coming up with $50 million a year in new money will be difficult, given growing pressure to reduce the current $333-billion-a-year deficit. "With the budget outlook the way it is, it'll be pretty hard," says Patricia Dehmer, associate director of science in DOE's Office of Basic Energy Sciences. Asked whether a solar

SOURCES (TOP TO BOTTOM): N. LEWIS/CIT; INTERNATIONAL ENERGY AGENCY

energy research initiative has a shot at receiving backing by the Administration, Joel Parriott, who helps the White House Office of Management and Budget oversee the budget for DOE's Office of Science, says that "it's too early to tell." He adds that the Administration has already set its energy policy priorities as increasing oil drilling in Alaska's Arctic National Wildlife Refuge, clean coal, and hydrogen. However, he says, "that doesn't mean there isn't room for new things."

With Congress close to passing an energy bill that focuses on tax breaks for oil exploration and hybrid cars, it doesn't look as if a big push on solar energy will be one of those "new things" anytime soon. But Dehmer notes that progress on energy issues happens slowly. "I'm trying to lay the groundwork for a commitment on the scale of a major scientific user facility," she says.

At least compared with DOE's earlier push for progress in hydrogen technology, many researchers expect that a push on solar energy research will be a far easier sell. "With hydrogen it was a lot more controversial," Stupp says. "There are scientific issues that are really serious [in getting hydrogen technology to work]. With solar, it's an idea that makes sense in a practical way and is a great source of discovery." If that research and discovery doesn't happen, Lewis says he's worried about what the alternative will bring: "Is this something at which we can afford to fail?"

–ROBERT F. SERVICE

Reproductive Biology

A Powerful First *KiSS-1*

Puberty researchers are finding that the protein kisspeptin and its receptor are central to this sexual maturation

Both anticipated and dreaded, puberty is rarely fun. From swelling breasts and sprouting hair to cracking voices and unexpected urges, this transition is almost always awkward, especially if puberty comes earlier or later than normal. It is a rare teenager who has not wondered, "Why is this happening to me?"

The body's awakening into sexual maturity is no less puzzling for developmental biologists and endocrinologists. And they have an equally straightforward question: How does the body know when, exactly, to unleash the cascade of hormones that change face, voice, height, bone structure, and sexual organs into those of a fertile adult? The emerging answer, it seems, could have come from a teenage romance novel: Puberty starts with a kind of kiss.

Are you ready? A protein called kisspeptin helps trigger the flood of hormones that marks puberty.

Recent studies have shown that a protein called kisspeptin is a key trigger of the complex chain of physiological reactions that readies the body for sexual maturity. Without this signal, people, as well as mice and other mammals, stay in a preteen limbo and never fully grow up. Discovering the involvement of kisspeptin and its receptor, a protein called GPR54, in puberty "is a major breakthrough in reproductive physiology," says Manuel Tena-Sempere of the University of Cordoba in Spain. Indeed, the duo was one of the most-discussed topics at a recent meeting on the control and onset of puberty.*

Scientists hope the two proteins might help them solve long-standing puzzles about the start of puberty, such as how the body revives the hormone production that is prevalent in fetal and newborn development but then mysteriously disappears during childhood, and how puberty might be influenced by nutrition and other metabolic factors. Preliminary evidence suggests, moreover, that the protein pair may even play a lifelong role in regulating sex hormones and reproduction.

The topic is more than academic. For some children, puberty doesn't happen at the right time: Girls who start to develop breasts and pubic hair as young as 6 years old, and boys at 17 who still sing soprano often end up at the pediatrician's office looking for answers. Although the physical consequences of being an early or late bloomer remain unclear, the social consequences can be significant. Boys who develop late may face brutal taunting because of their small stature and underdeveloped muscles. And early-developing girls "have higher rates of depression, substance abuse, and teenage pregnancies," Pierre-André Michaud, a specialist in adolescent medicine at the University of Lausanne in Switzerland, said at the meeting. Consequently, physicians are eager to understand how puberty is controlled and whether they can, or should, safely delay or accelerate it in certain cases.

KiSS-1-ng partner

It was GPR54, not kisspeptin, that appeared first as a player in puberty. The initial clue was a 20-year-old man in Paris who had undeveloped testes, sparse pubic hair, and the bone maturity of a 15-year-old; such lack of sexual development is called idiopathic hypogonadotropic hypogonadism (IHH). Doctors soon discovered that the man was not the only one in his family to fail to complete puberty: Three of his four brothers were similarly affected, and one of his two sisters had experienced only a single menstrual period in her life—at age 16. All had abnormally low levels of sex hormones.

It turned out that the parents of this family were first cousins and, as a team led by Nicolas de Roux of INSERM in Paris reported in 2003, both mother and father carried a mutation in one copy of their *GPR54* gene. The affected children had all inherited two mutated copies of the gene. Other researchers had shown that GPR54 acts as a receptor for kisspeptin, so de Roux and his colleagues suggested that the molecular embrace between the two proteins might be a player in the first steps of puberty.

* 6th Puberty Conference, Evian, France, 26–28 May.

CREDIT: GETTY IMAGES

A month after de Roux's paper was published, that suggestion got a major boost. Stephanie Seminara, Yousef Bo-Abbas, and William Crowley of Harvard Medical School in Boston and their colleagues reported that six members of a large Saudi Arabian family, all diagnosed with IHH, also had mutations in their *GPR54* genes. They also found that an unrelated patient with IHH carried mutations in both his copies of the gene. In the same paper, researchers from Paradigm Therapeutics in Cambridge, U.K., reported that mice lacking the *GPR54* gene also failed to go through the rodent version of puberty.

Scientists at the time knew very little about GPR54. They knew its gene was expressed in the brain and the placenta, and they knew the protein was a receptor for kisspeptin, which is encoded by a gene called *KiSS-1*. *KiSS-1*, on the other hand, was fairly well known, but not among endocrinologists. The gene was discovered by cancer researchers at Pennsylvania State College of Medicine in Hershey, Pennsylvania, who noticed that it played a role in the ability of tumor cells to move and metastasize. (The romantic connection to puberty is accidental: The researchers named the gene for the famous Hershey chocolate drops.)

Because of *KiSS-1*'s known role in cell motility, scientists initially thought that the kisspeptin-GPR54 pairing might influence puberty by directing so-called GnRH neurons to the correct part of the brain. GnRH neurons were identified more than 3 decades ago as the source of gonadotropin-releasing hormone (GnRH), a brain chemical that prompts the pituitary gland to produce follicle stimulating hormone and luteinizing hormone (LH). Those signals in turn stimulate production of sex hormones such as estrogen and testosterone in the ovaries and testes.

Kallmann syndrome, another condition in which patients fail to go through puberty, is caused by the improper migration of GnRH neurons during fetal development, so researchers wondered whether a similar problem affected IHH patients with *GPR54* mutations. But subsequent studies have since shown that GnRH neurons are present in the correct place and quantity in the *GPR54*-knockout mice.

Instead, the mutations may prevent the release of GnRH; GnRH neurons express GPR54 receptors, and their activation by kisspeptin prompts the cells to release their hormonal signal. In cell-based assays, kisspeptin "is one of the most powerful activators of GnRH neurons ever seen," says Robert Steiner of the University of Washington, Seattle. And in February, endocrinologist Tony Plant of the University of Pittsburgh in Pennsylvania reported in the *Proceedings of the National Academy of Sciences* that within 30 minutes of injecting juvenile male rhesus monkeys with kisspeptin, the animals' levels of LH increased 25-fold.

Leading lights. The neurons that express the *KiSS-1* gene (white dots) cluster in a region of the hypothalamus known to respond to sex hormones.

CREDIT: R. STEINER/UNIVERSITY OF WASHINGTON

Puberty's puzzles

Those results solidify the fundamental role of kisspeptin and GPR54 in puberty's onset, but it is not the whole story. "I'm not sure this is the discovery of the Holy Grail for puberty," Steiner says. "You need to have this circuit operating for sure, but the conclusion that this is the ultimate switch for puberty is probably premature."

A missing link, for example, is what turns the circuit on. Steiner and neuroendocrinologist Allan Herbison of the University of Otago in Dunedin, New Zealand, are studying the neurons that produce the protein to find out what signals influence them. One of the most intriguing ideas is that kisspeptin might be connected to the hormone leptin: Steiner said at the meeting that he has preliminary evidence that at least half of the neurons that express *KiSS-1* also carry receptors for leptin.

A few years ago, many scientists thought that leptin, which is produced by fat cells, was the key puberty trigger, providing a way for the body to delay sexual maturation until it has enough stored energy to support reproduction. Women who become too thin, for example, become infertile and stop having periods. And people and mice with mutations in the genes coding for leptin or its receptor are infertile, apparently because of a failure to go through puberty. But further research failed to turn up direct connections between leptin and GnRH neurons.

There's early evidence that kisspeptin may help mediate such a connection. In the June issue of *Endocrinology*, Tena-Sempere reports that rats kept on a restrictive diet produce less messenger RNA (mRNA) from *KiSS-1*, consistent with the idea that the gene responds to leptin and other hormones that signal the body's nutritional status. They also found that administering kisspeptin to underfed juvenile rats could jump-start their delayed puberty, perhaps bypassing the need for leptin to reach some puberty threshold.

The *KiSS-1* neurons, Steiner says, may integrate signals from a wide variety of body systems, such as how much food is available and even circadian clues such as time of day and season of year. The connection may sound surprising, but researchers have long known that GnRH and other sex hormones follow a daily rhythm and that the first hormone surges of puberty tend to occur at night. Steiner says he and his colleagues are looking for connections between *KiSS-1* neurons and the brain's circadian clock to see if they might link the circadian and reproductive systems. But such work is still speculative. "The *KiSS-1* neuron is far from characterized," de Roux cautions.

There is also evidence that the kisspeptin-GPR54 signal helps regulate reproduction long past the first stirrings of puberty. Steiner and his colleagues reported online in the 26 May issue of *Endocrinology* that *KiSS-1* neurons in the mouse brain carry estrogen receptors and that levels of *KiSS-1* mRNA in the brains of adult mice are modulated by injections of the hormone. And a group led by Keiichiro Maeda of Nagoya University in Japan reported online 23 June in *Endocrinology* that when they used antibodies to block the kisspeptin-GPR54 signal in adult female rats, the LH surge that triggers ovulation didn't occur. "It is not just a switch that is activated once," Tena-Sempere says. It seems that, like the best kisses, *KiSS-1* has long-lasting consequences.

–GRETCHEN VOGEL

Europe Joins Forces in Push for Monster Scope Project

European astronomers want to leapfrog current technology to make a telescope 10 times as wide as today's largest. But do they have the know-how or the unity?

DWINGELOO, THE NETHERLANDS—The European Union wants its scientific enterprise to be second to none. At a meeting* here earlier this month, E.U. officials joined a chorus of researchers who want Europe's disparate national astronomy communities to work together in continent-wide organizations. As an example of what could be gained, researchers reported on their grand vision: a gargantuan telescope sporting a mirror 50 to 100 meters across that could be gazing skyward in 10 years. At the meeting, researchers presented a study that lays out the scientific case for the European Extremely Large Telescope (ELT), an effort supported in part by the E.U., and over the next 3 years they will carry out a detailed design study, again with E.U. help.

"Europe is already a world leader" in ground-based optical and infrared astronomy, says Gerry Gilmore of Cambridge University in the U.K. "We aim to stay there." The continent owes its status partly to one pan-European success story: the European Southern Observatory (ESO), which operates several top-rank scopes in Chile. But some astronomers think the Europeans may be overreaching themselves with the ELT; U.S. astronomers will first move from today's 10-meter scopes to something around 20 or 30 meters. "Understandably, Europe doesn't want to be left behind," says Richard Ellis, director of the Caltech Optical Observatories in Pasadena, "but they could avoid that by building a second 30-meter telescope instead."

Ever since Galileo observed the heavens through his home-built spyglass some 4 centuries ago, telescope sizes have doubled every 50 years or so. The current record holders are the two 10-meter Keck telescopes at Mauna Kea, Hawaii. But the ELT's Science Working Group, chaired by Isobel Hook of the University of Oxford, U.K., described plans to break the trend by making the most dramatic leap in the history of telescopic astronomy. If built, the ELT's segmented mirror will be larger than all previous professional telescope mirrors combined.

Roberto Gilmozzi of ESO in Garching, Germany, who will coordinate the ELT design study, says detector technology has improved so rapidly over the past decade that "we now need bigger telescopes" to take full advantage of it. A 100-meter "Overwhelmingly Large Telescope," with adaptive optics to compensate for atmospheric turbulence, could detect stars 5 trillion times fainter than the naked eye can see. It would also have a resolving power of a milli–arc second—enough to discern a dime 3500 kilometers away.

According to Hook's 140-page report laying out the science behind the project, the ELT's main targets will be exoplanets, galactic evolution, and cosmology. The telescope could detect Earth-like planets circling other stars out to a distance of 75 light-years, says Gilmozzi. Spectroscopic studies of such planets might find possible signs of life such as atmospheric oxygen. Current telescopes can't distinguish individual stars in distant galaxies. But the ELT will be able to, and logging millions of them from many galaxies would provide information on the origin and evolution of these vast stellar assemblies. The monster telescope should also be able to look far enough into space, and hence back in time, to learn more about the universe's first light and the mysterious dark energy that is accelerating cosmic expansion.

U.S. astronomers and telescope builders are keeping a close eye on European plans. They themselves are designing and building several telescopes up to 30 meters wide. "Fifty to 100 meters is pretty gutsy and could lead to unfortunate technical choices because of lack of experience at intermediate size," says Roger Angel of the University of Arizona's Mirror Laboratory in Tucson, where the first mirror is currently being cast for the 21-meter Giant Magellan Telescope. Ellis agrees. "It's a big leap," he says.

To orchestrate the effort, in 2004 the E.U. funded the creation of OPTICON (Optical Infrared Coordination Network for Astronomy). The network now consists of 47 groups in 19 countries. Representatives of several similar nascent pan-European collaborations also attended the Dwingeloo meeting. E.U. Research Commissioner Janez Potočnik told them that the new research infrastructures are key to Europe's research future. "They will bring us even closer to answering some of the most fundamental questions that mankind has ever asked," he says. Potočnik acknowledges that the currently stalled negotiations over the E.U. budget mean that "Europe is in crisis" (*Science*, 10 June, p. 1530), but he stresses that building a knowledge society is essential for the future of the continent. "We need these decisions now," he says. Even if a diminished budget scuppers the E.U.'s grand plans, astronomers seem confident that the ELT will be built. "ESO alone would be able to finance a 40- to 60-meter telescope," says Gilmozzi.

In the end, budget considerations may force astronomers on both sides of the Atlantic to work together. According to Ellis, the United States would be very interested in becoming a partner in a global effort to construct a 50- to 100-meter telescope, provided 30-meter instruments are built first. But right now, European bravado makes this scenario seem unlikely. "We'll certainly not go back to 30 meters," says Gilmozzi.

–GOVERT SCHILLING

Govert Schilling is an astronomy writer in Amersfoort, the Netherlands.

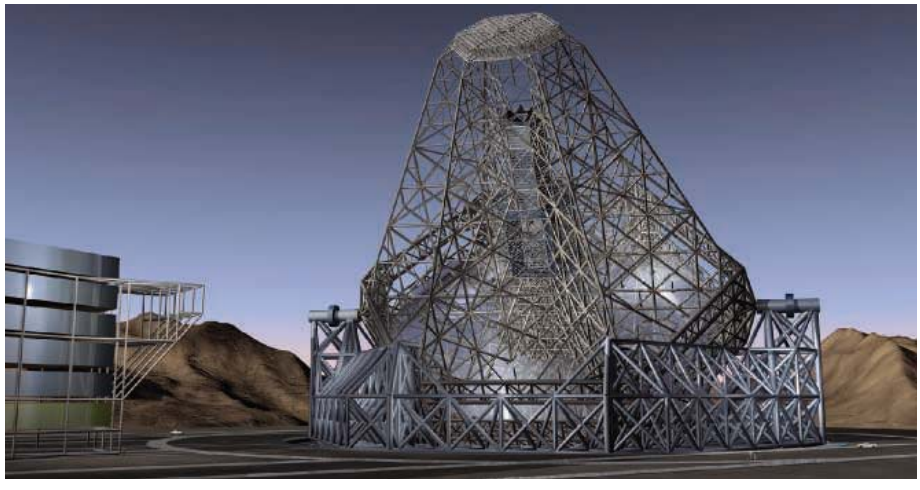

CREDIT: ESO

Giant leap. The proposed Overwhelmingly Large Telescope would boast a 100-meter mirror.

* Astronomy Looks Into the Future—The Role of European Infrastructures, Dwingeloo, the Netherlands, 7 July 2005.

Random Samples

Edited by Constance Holden

Music of the Clouds

Technological wizardry will transform the changing shapes of clouds into live music, in a new version of the "cloud harp" to be unveiled in Montreal, Canada, next year.

An earlier version of the cloud harp, installed last year in Pittsburgh and Montreal, received a lot of attention, says its creator, architect Nicolas Reeves of the University of Quebec. In that version, clouds triggered prerecorded sounds. The new instrument, "Nomadic Cloud Harp," will be more advanced, translating the shapes of clouds directly into sound as they pass over.

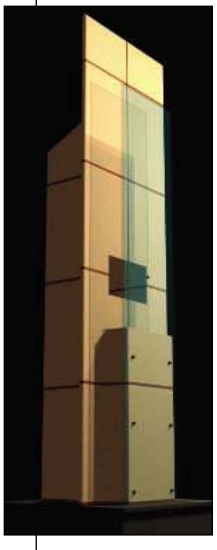

A cloud harp works "like a giant CD player turned upside down," Reeves says. In a CD player, a laser beam reads and converts holes on the surface of a disc into music; the new cloud harp will shoot a big laser beam up 8000 meters to read cloud surfaces. A computer program converts the shapes into an acoustic wave, which is then amplified by the harp. "The sound is modulated by the height and density of the clouds," with higher clouds creating a higher pitch. Denser clouds make for louder music, Reeves explains. He hopes the harp—made of wood and standing 3.5 meters tall—will look "like a precious musical instrument." He says listeners may be able to tune in to it at www.cloudharp.org by September.

TV and Schoolwork Don't Mix

The longer children spend in front of the television, the less likely they are to get through college. So concludes the first long-term study to investigate the educational impacts of childhood viewing habits.

Researchers led by Robert Hancox of Otago University in Dunedin, New Zealand, have followed almost 1000 5-year-old New Zealanders to the age of 26. Those who completed university averaged about 50 minutes less time in front of the television per weekday between the ages of 5 and 15 than did high school dropouts, according to parental and self reports.

Decades of research on whether childhood TV viewing affects educational performance have produced conflicting results. The authors acknowledge that their data do not prove causality. However, they say the association between TV viewing and lower achievement persisted even after controlling for the children's IQs, behavioral problems, and socioeconomic status.

The study, published in the July *Archives of Pediatrics and Adolescent Medicine*, is based on one of the best longitudinal samples in the world, says Anita Thapar, a child and adolescent psychiatrist at Cardiff University in the United Kingdom. So it may be sensible to cut back children's TV viewing "even if the mechanisms ... are not well understood."

The study has been criticized for failing to take into account the content of programs watched. Co-author Barry Milne of University College London counters that "the type of TV that kids *do* watch doesn't seem to do them any good."

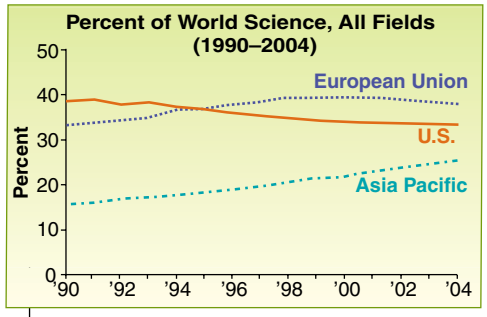

Pacific Progress

The U.S. share of scientific publications has steadily decreased as Asian contributions have steadily risen over the past 15 years, according to the July-August issue of *Science Watch*, published by the Institute for Scientific Information in Philadelphia, Pennsylvania. U.S. scientists still lead by a wide margin in the impact of their papers, as measured by citation analysis.

Europe's Immigration Problem

Europe is being colonized by non-native plant species that are using the highway system to get around, according to researchers from Technical University Berlin, who have done the first systematic study showing the extent of the phenomenon.

A team led by ecologist Moritz von der Lippe set up collection traps for seeds in highway tunnels leading into and out of the city. They found a surprising diversity of seeds, including non-European species such as Australian goosefoot, which presumably arrived with imported sheep wool, and South American gooseberry, probably coming from berries crushed on the tires or beds of trucks. Their study, announced in a 14 July press release, is currently under review for publication.

"This is one more example of how human transportation is homogenizing the distribution of species across the landscape," says Bernd Blossey, director of the program on invasive plants at Cornell University. Although some invasion-wary countries such as New Zealand require the tires of imported used cars to be cleaned on arrival, Europe has no such laws. Von der Lippe notes that one concern the survey raises is that the American locust trees planted along German highways may be sending their seeds out far and wide, displacing native species.

Boring tunnel is a gold mine for ecologists.

CREDITS (TOP TO BOTTOM): THOMSON SCIENTIFIC NATIONAL SCIENCE INDICATORS; NICOLAS REEVES; M. VON DER LIPPE/TU BERLIN

PEOPLE

Edited by Yudhijit Bhattacharjee

JOBS

Familiar shores. Marine ecologist Anson Hines is the new director of the Smithsonian Environmental Research Center (SERC) in Edgewater, Maryland. He succeeds Ross Simon, who is retiring after 8 years at the helm.

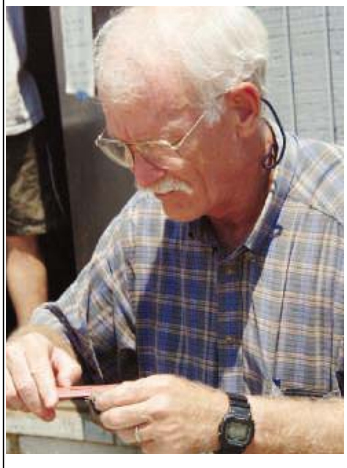

Hines has spent 26 years in SERC's Fish and Invertebrate Ecology Lab studying topics from sea otters and kelp forest ecology to long-term changes in the Chesapeake Bay. The center's 17 senior scientists and 180 researchers focus on coastal ecology.

As assistant director for the past 17 years, Hines also has worked on a program to conserve 1200 hectares of the Rhode River watershed and shoreline. As director, he plans to step up efforts to make the center's "research results accessible to policymakers and environmental resource managers to improve stewardship of the coastal environment."

MIT provost. A microelectronics engineer who has spent a quarter-century on the faculty of the Massachusetts Institute of Technology (MIT) in Cambridge has been named its provost.

Venezuelan-born L. Rafael Reif is a former director of MIT's Microsystems Technology Laboratories and current chair of the department of computer science and electrical engineering. As provost, he will oversee academic and research programs as well as Lincoln Laboratory in Lexington, a defense research facility.

Reif, 54, replaces Robert Brown, who has been named president of Boston University (*Science*, 17 June, p. 1739).

Nerve center. The American Academy of Neurology (AAN) has asked a former congressional staffer to help raise its profile in Washington.

Michael Amery, a lawyer who worked for former Senator Rod Grams (R–MN) before joining AAN's headquarters in St. Paul 5 years ago, has moved back to Washington to run the academy's new D.C. office.

Amery will push for more funding for research on neurological disorders and provide a stronger voice for the academy's concerns about Medicare reimbursement and medical malpractice reform. The academy has 16,000 U.S. members.

Got any tips for this page? E-mail people@aaas.org

AWARDS

Mainstream recognition. It took decades for fisheries biologist Daniel Pauly to win broad support for his predictions that overfishing could lead to a collapse of fisheries worldwide. This week, one of the world's biggest fishing nations joined the bandwagon, with Japan's Expo '90 Foundation awarding Pauly its $350,000 Cosmos Prize.

The 59-year-old Pauly, director of the Fisheries Centre at the University of British Columbia in Vancouver, Canada, has focused on the sustainable management of marine resources (*Science*, 19 April 2002, p. 458). An outspoken critic of modern fishing practices, he once suggested that future generations might be reduced to eating jellyfish.

"I think it's very important that a major Japanese prize would go to someone who has worked fearlessly on the problem of overfishing," says Nancy Knowlton, a marine biologist at the University of California, San Diego, and a member of the screening committee.

DATA POINT

Farewell to arms. Uncertainty about pensions has triggered a surge of retirements this year at the Department of Energy's (DOE's) Los Alamos National Laboratory (LANL), say lab officials. Anticipating that the upcoming management competition would be unsettling (*Science*, 27 May, p. 1244), DOE and LANL laid out clear options for pensions, extended the University of California's current contract by 8 months, and promised employees a window in which to claim their UC benefits after the new contract is in place. But those measures failed to prevent the percentage of retirements from climbing to 5.4%—nearly double the average rate of 2.8% over the past 5 years.

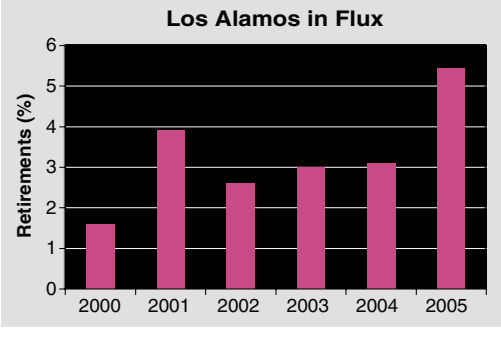

CREDITS (TOP TO BOTTOM): COSMOS PRIZE EXPO '90 FOUNDATION; SMITHSONIAN ENVIRONMENTAL RESEARCH CENTER; DONNA COVENEY/MIT; MIKE AMERY; LANL

LETTERS

The Origins of Olmec Civilization

IN THEIR RESEARCH ARTICLE "OLMEC POTTERY production and export in ancient Mexico determined through elemental analysis" (18 Feb., p. 1068), J. P. Blomster *et al.* report that "all nonlocally produced Olmec-style gray pottery samples found outside the Gulf Coast" and all Conejo Orange-on-White and San Lorenzo White vessels were produced in San Lorenzo. This evidence, they argue, indicates that "the San Lorenzo Olmec played a central role in synthesizing a distinct style and associated iconography, disseminating it across Mesoamerica" during the Early Formative period (circa 1200 to 850 B.C.E). They speculate that "[e]xchange of these symbols formed an important component of communication and negotiation between communities on both intra- and interregional levels" (p. 1071), but do not suggest what information was transmitted. R. A. Diehl poses this question in his accompanying Perspective "Patterns of cultural primacy" (18 Feb., p. 1055) in the discussion of an Olmec stone figure (shown here) displaying several "defining" motifs. He asks, "what goods and other things did they seek?"

Like most other Mesoamericanists, the authors do not mention the striking resemblance between Olmec iconography and Shang writing, which has been demonstrated most recently by Mike Xu with the collaboration of numerous Shang specialists in China (*1*). The three-pronged symbols on the headdress of the statue shown in Diehl's Perspective and here are the Shang symbol for rain, and the cross on the chest represents the Shang sun god (*2*). Translation of the symbols on three of the small "celts" (ungrooved axes) from the famous cache at La Venta, based on Shang counterparts, produces phrases compatible with Shang ritual offerings (*2*), and many other Olmec innovations have Shang antecedents (*3*).

The invention of writing revolutionized Chinese society by facilitating communication among speakers of 60 mutually unintelligible languages and resulted in increased commercial interaction and social intergration. The rapid diffusion of Olmec iconography and associated cultural elaboration suggests it had the same impact across multilingual Mesoamerica. The demise of the Shang Empire circa 1500 B.C.E. coincides with the emergence of Olmec civilization. Rather than speculate in a vacuum on the intangible character of Olmec society, it would seem profitable to compare the archaeological remains with the detailed record of the impact of writing on the development of Chinese civilization. What do we have to lose?

BETTY J. MEGGERS

National Museum of Natural History, Smithsonian Institution, Washington, DC 20560, USA.

References

1. M. Xu, *J. Wash. Acad. Sci.* **88**, 1 (2002).
2. M. Xu, *Origin of the Olmec Civilization* (Univ. of Central Oklahoma Press, Edmond, OK, 1996), figs. 19, 24.
3. B. J. Meggers, *Am. Anthropol.* **77**, 1 (1975).

Response

I THANK MEGGERS FOR HER COMMENTARY. Meggers criticizes our failure to allude to what she considers to be the striking resemblance between Olmec iconography and Shang writing. Although I acknowledge her long-standing interest in this subject (*1*), our Research Article focused on the role of the Gulf Coast Olmec in synthesizing and disseminating the first unified iconographic system in Mesoamerica, rather than the actual origins of Olmec civilization.

The scholar Meggers refers to, Mike Xu, suggests Shang origins for the Olmec, invoking a transcontinental migration (*2*). Ongoing excavations by Ann Cyphers (*3*), as well as previous research (*4*), at the first Olmec center, San Lorenzo, document that

A statue of a water deity from San Lorenzo monument 52.

Olmec culture developed in situ. Precedents to ceramic forms and many sculptural types have been identified at San Lorenzo before the crystallization of Olmec civilization by 1200 B.C.E. (uncalibrated). The origins of Olmec civilization most likely lie in the dynamic social competition and negotiation of agents and factions at San Lorenzo, strategies expressed in both communal and individualistic stone monuments (*5*). No direct evidence of Shang influence on the Olmec—or that of other Old World cultures—has been documented by any of the archaeologists currently working on the Gulf Coast.

The most frequently cited example of "Shang influence" comes from the incised celts found in La Venta Offering 4, which serve as the backdrop for a series of 16 jadeite figurines arranged in a ritual scene. These celts were deposited in Complex A at La Venta between 800 and 700 B.C.E. (*6*), long after the demise of the Shang empire. Xu translates the incisions on the Offering 4 celts based on Shang characters (*2*); these celts, however, were recarved from a larger engraved celt or plaque, so that the incisions represent fragments of a larger original scene and are not individual characters (*6*).

Meggers is quite right to suggest that different possibilities for the rise of the Olmec should be considered, and as scholars we have nothing to lose by maintaining an open mind. There is also much value in Meggers' suggestion of comparing the spread of Olmec iconography across Mesoamerica with the way the invention of Shang writing revolutionized Chinese society by allowing communication across broad regions. Cross-cultural comparisons can be most illuminating, and I thank her for presenting this idea.

JEFFREY P. BLOMSTER

Department of Anthropology, George Washington University, Washington, DC 20052, USA.

References

1. B. J. Meggers, *Am. Anthropol.* **77**, 1 (1975).
2. M. Xu, *J. Wash. Acad. Sci.* **88**, 1 (2002).
3. A. Cyphers, in *Población, Subsistencia y Medio Ambiente en San Lorenzo Tenochtitlán*, A. Cyphers, Ed. (Universidad Nacional Autónoma de México, Mexico City, 1997), pp. 255–274.
4. M. D. Coe, R. A. Diehl, *In the Land of the Olmec*, vol. 1, *The Archaeology of San Lorenzo Tenochtitlán* (Univ. of Texas Press, Austin, TX, 1980).
5. B. Stark, in *Olmec Art and Archaeology in Mesoamerica*, J. Clark, M. Pye, Eds. (National Gallery of Art, Washington, DC, 2000), pp. 31–53.
6. R. A. Diehl, *The Olmecs: America's First Civilization* (Thames & Hudson, London, 2004).

"Intelligent" Design versus Evolution

DONALD KENNEDY'S EDITORIAL ("TWILIGHT for the enlightement?", 8 Apr., p. 165) highlights how ineffective the scientific community has been in the battle for the minds of the American public. Arguing details of scientific facts before this audience has been largely unproductive. Perhaps it is time to take a lesson from recent political campaigns: Instead of defending your position, attack a weakness of the opposition and repeat (again and again), with a modicum of humor. The following script has been effective in dealing verbally with creationists/intelligent design adherents.

"You have a philosophic choice between evolution or belief in ID, so called intelligent design. But even a first-year engineering student would be embarrassed to have

CREDIT: FELIPE DÁVALOS

designed your lower back with the extreme bend that allows you to stand erect even though your pelvis slants forward for knuckle-dragging like all our near relatives. You probably have had braces or wisdom teeth extracted because there are too many teeth for the size of your mouth. Then there are your sinuses, with a flawed drainage system that would provoke laughter from a plumber. Yet evolution provides a ready and rational explanation for all these design failures: by progressive changes into an erect posture, by shortening of a mammalian muzzle into a face, and by expansion of our large brains to crowd the facial bones. So take your choice: Do you prefer evolution or an ID whose letters may as well stand for Incompetent Design?"

After a bit of flustering, the ID adherent usually mumbles something about our inability to know the mind of God. The reply: "Indeed, ID is not science but religion and should be taught as such."

These simple facts need little explanation, bring evolution to a personal level, and leave the ID adherent on the defensive, all with a bit of humor. Others may wish to try it.

DONALD U. WISE
Department of Geosciences, University of Massachusetts, Amherst, MA 01003, USA.

Issues in Indian Science

I AGREE WHOLEHEARTEDLY WITH R. A. Mashelkar's contention that India will emerge as a very strong R&D force on the world stage in a few decades ("India's R&D: reaching for the top," Essay, 4 Mar., p. 1415). The process of scientific repatriation to India could be made more effective if there is a concomitant restructuring in scientific establishments and institutions in India with regard to the selection of personnel and recognition of professional excellence. In most cases, the selection policy is not transparent and dynamic enough and leaves room for favors to be bestowed on less deserving candidates. The case of Nobel Laureate Hargobind Khorana is a grim reminder of such a systemic failure to retain and nourish world-class talent. Khorana returned to India in 1950 after doctoral studies at the University of Liverpool and a brief research stint at the Eidgenössische Technische Hochschule in Zurich, Switzerland (*1*). He applied for several jobs in India, but owing to the lack of any interest in his applications and research proposals, he decided to take up a job as postdoctoral researcher in Cambridge, UK. He won the Nobel Prize in 1968 (Medicine), and 12 years later, the Indian government finally woke up and awarded him with the nation's highest civilian award—the Bharat Ratna (1980).

Another issue relates to giving due recognition for research work. Awarding first authorship of publications to the major contibutor is not the official policy in all Indian research labs. Such a system creates an atmosphere in which credit can be usurped by less deserving people who are better placed in the hierarchy. If research institutions employ better guidelines and actively implement better policies in managing human resources, scientific repatriation to India would increase by a greater magnitude and the cause of science in India would be better served.

VINAYAK SINHA
Max Planck Institute for Chemistry, Joh-J-Becherweg 27, Mainz, Germany. E-mail: vsinha@mpch-mainz.mpg.de

Reference
1. H. G. Khorana, *Science* **287**, 810 (2000).

THE ESSAY "INDIA'S R&D: REACHING FOR THE top" (4 Mar., p. 1415) by R. A. Mashelkar is remarkable not for what it says, but for the issues it sidesteps. The Essay appeared just before the Indian Parliament debated the Patents Bill, which will no longer allow the production of generic drugs for use by people in India and around the world. Pressure from international and domestic pharmaceutical companies has produced legislation that, if passed, will create a situation where sick people will end up paying much more than they now do for desperately needed medicines. Glorifying the pharmaceutical industry and its enormous potential and reach while ignoring the ramifications of the Patent Bill is either disingenuous or, at the very least, implies that Mashelkar is wearing dangerous blinders.

> "The scientific community in India has been serving the needs of the... middle class."
>
> –BYRAVAN

The scientific community in India has been serving the needs of the roughly 3 million middle class. However, 450 million Indians earn less than $1 a day. Rising above one's impoverished background, as Mashelkar has done, is commendable, but science in India is not serving its poorest members. Surely, it is ironic that the country whose cost of intellectual capital is one of the lowest in the world will end up producing drugs that most of its own people will not be able to afford.

SUJATHA BYRAVAN
Executive Director, Council for Responsible Genetics, 5 Upland Road, Suite 3, Cambridge, MA 02140, USA.

Response

SINHA RAISES A FUNDAMENTAL ISSUE RELATing to India's failure to retain world-class talent; he asserts that India's hiring policies are not proactive and transparent enough. He cites the case of Nobel Laureate Hargobind Khorana's quest for a possible job in India. Paradoxically, the Khorana incident led to government initiatives that induced me to return to India.

Indira Gandhi was then the Prime Minister of India. She asked Y. Nayudamma, who was the then Director General of Council of Scientific & Industrial Research (the position that I occupy today) to go abroad, meet the best and the brightest of young scientists, and offer them jobs on the spot. I met Nayudamma in 1974, and after a 30-minute conversation, he offered me a job.

> "The current Indian laws protect the interests of the poor."
>
> –MASHELKAR

I did not go through a formal interview. Unfortunately, what Nayudamma could do for Mashelkar is something that Mashelkar has not been able to do for another Mashelkar in recent times. There is certain amount of opacity that has crept into the system, which is unfortunate, and the case that Sinha makes about transparency is perfectly valid.

His concern about the first authorship of publications is a valid ethical issue; one cannot defend those cases in which such ethical norms are flouted. The Society for Scientific Values in India does take up cases of blatant violations. On the whole, I agree that we need to do better.

Byravan is critical of the fact that India has changed its patent laws to meet its international obligations. The current Indian laws protect the interests of the poor. Our provisions include compulsory licenses as well as measures to avoid "ever greening," which is a tactic often used to extend the life of the patent by filing new patent claims, which show only marginal improvements of no significant consequence. In fact, there are special provisions in the law to ensure that poor countries who do not have manufacturing capacity will be able to benefit from the supply of affordable drugs by Indian companies under special circumstances.

Byravan's concern that Indian science and technology should work for the poor is absolutely right. That is precisely what Indian institutions have been doing. Our achievements include providing cheaper vaccines and drugs for the poor, bullock-driven reverse osmosis plants, and wireless local loop technologies for rural areas. I would like to quote from my Zuckerman lecture, which I delivered at the Royal Society, London (*1*): "Our real challenge seems to be to get the best minds around the world to engage themselves in providing solutions to the problems that can make a difference to the humanity." That is the crux of the matter.

RAGHUNATH A. MASHELKAR
Director General, Council of Scientific and Industrial Research, Anusandhan Bhawan, 2 Rafi Marg, New Delhi 110001, India.

Reference

1. R. A. Mashelkar, *Innovation Strategy Today* **1** (no. 1), 19 (2005) (www.biodevelopments.org).

CORRECTIONS AND CLARIFICATIONS

This Week in Science: "Aging and death" (15 July, p. 352). The image that appears with this item should instead have appeared with the item below it, Reversing neurodegenerative change."

News of the Week: "A new skirmish in the Yanomamö wars" by C. C. Mann (8 July, p. 227). In the photo credit, the photographer's name was misspelled. It should be Antonio Mari.

Special section: 125 Questions: What don't we know?" (1 July, p. 102). In the short item about the Riemann zeta function, the expression "a + bi" should have read "1/2 + bi."

Letters: "Evangelical biologists and evolution" by J. C. Sutherland (1 July, p. 51). The author's e-mail address was incorrect. It should be johsut@elkhorn.net

News Focus: "The ins and outs of exosomes" by J. Couzin (24 June, p. 1862). The story incorrectly identified Mark Marsh of University College London as Michael Marsh.

TECHNICAL COMMENT ABSTRACTS

COMMENT ON "Nervy Links Protein Kinase A to Plexin-Mediated Semaphorin Repulsion"

Ryan J. Ice, Jill Wildonger, Richard S. Mann, Scott W. Hiebert

Terman and Kolodkin (Reports, 20 Feb. 2004, p. 1204) used an antibody directed against the mammalian ortholog of *Drosophila* Nervy (Nvy), ETO/MTG8, to localize Nvy to axonal plasma membranes and show that it associates with Plexin A. We show that this antibody does not recognize Nvy and that a newly generated anti-Nvy antibody labels the nuclei, and not the plasma membranes, of neurons.

Full text at www.sciencemag.org/cg/content/full/309/5734/558b

RESPONSE TO COMMENT ON "Nervy Links Protein Kinase A to Plexin-Mediated Semaphorin Repulsion"

Jonathan R. Terman and Alex L. Kolodkin

Ice *et al*. challenge our observations using results obtained with newly generated anti-Nvy antibody. However, molecular genetic, in situ hybridization, and immunoprecipitation experiments support our original conclusions that Nvy can be found in axons, associates with the axon guidance receptor Plexin A, and links protein kinase A to Plexin A–mediated axon guidance signaling.

Full text at www.sciencemag.org/cg/content/full/309/5734/558c

Letters to the Editor

Letters (~300 words) discuss material published in *Science* in the previous 6 months or issues of general interest. They can be submitted through the Web (www.submit2science.org) or by regular mail (1200 New York Ave., NW, Washington, DC 20005, USA). Letters are not acknowledged upon receipt, nor are authors generally consulted before publication. Whether published in full or in part, letters are subject to editing for clarity and space.

EVOLUTION

Of Whale Knuckles and Placental Trees

Christian de Muizon

Cetaceans are probably the most extraordinary mammals. They are highly adapted to life in water and strictly dependent on their aquatic environment. As a consequence, their anatomy and physiology have been strongly modified and do not resemble those of other mammals. Because cetaceans are so drastically transformed from their terrestrial ancestors, their affinities with other mammals have long been debated. Although researchers agreed that cetaceans had their origin in some group of land mammals that lived during the early Tertiary, there was no consensus on the identity of the group that subsequently evolved into whales and dolphins. Whales have been seen as closely related to seals, creodonts (hyaenodonts), ungulates, and mesonychid condylarths (large carnivorous to omnivorous archaic ungulates). In the absence of a better candidate, the mesonychids were on the verge of becoming accepted when molecular biologists claimed that cetaceans were most closely related to artiodactyls (even-toed ungulates)—specifically to hippos. A few years later, paleontologists discovered postcranial remains of early Eocene cetaceans that demonstrated the presence of a double-pulleyed astragalus (like the sheep ankle bones that the Romans used to play at knucklebones), a characteristic of all artiodactyls and exclusively found in that order. This discovery, among the most important paleontological finds of the past hundred years, led to an immediate consensus on cetacean ancestry. It also demonstrated a remarkable complementarity of two different approaches to the study of the evolution and phylogeny of mammals.

Such interplay between anatomical and paleontological studies, on the one hand, and molecular investigations, on the other, forms a central theme of *The Rise of Placental Mammals*, edited by Kenneth Rose and David Archibald. The volume grew out of a symposium (at the 2002 meeting of the Society of Vertebrate Paleontology) commemorating the centenary of George Gaylord Simpson's birth. The authors offer an extremely useful consideration of current thoughts on the early evolution and phylogenetic relationships of the 18 extant placental orders.

The Rise of Placental Mammals
Origins and Relationships of the Major Extant Clades
Kenneth D. Rose and J. David Archibald, Eds.
Johns Hopkins University Press, Baltimore, MD, 2005. 271 pp. $95, £63.50. ISBN 0-8018-8022-X.

The volume begins with the editors' introduction and a short chapter that recounts Simpson's contributions to the study of placental mammals. These are followed by two chapters that provide broad morphological and molecular perspectives on the clade's origin and diversification. John Wible, Guillermo Rougier, and Michael Novacek use dental, cranial, and postcranial anatomical data to characterize placentals, more basal eutherians, and more distant outgroups. They also discuss relations among Cretaceous eutherians and possible relations to extant placental clades. Mark Springer, William Murphy, Eduardo Eizirik, and Stephen O'Brien review the molecular evidence for superordinal clades. Whereas Wible *et al.* place the origin and diversification of the extant orders after the Cretaceous-Tertiary boundary, Springer *et al.* find support for a Cretaceous interordinal radiation.

Each of the remaining 11 chapters appraises phylogenetic relationships within an order or superordinal clade through a careful examination of the morphological and molecular data. The authors provide thorough discussions of the fossil relatives of the extant orders. Because only anatomical data can be used to compare fossil and recent taxa, the considerations of morphological characters are especially detailed and abundant. The phylogenetic conclusions drawn from morphology and molecules do not always agree so well as in the case of the cetaceans. Nor do the authors always express their personal interpretation of conflicting results. But at least the reader is provided with the data and references, which offer an excellent starting point for more detailed research on the evolution of individual orders. The volume's clear and well-organized presentation demonstrates the editors' success in the difficult task of coordinating a work that covers several highly debated issues.

One such issue, an important problem in recent debates on mammalian systematics that is addressed in several chapters, is the supraordinal taxon Afrotheria: a major group, possibly a clade, of mammals originally endemic to Africa. This taxon was first proposed on the basis of molecular data (*1*) but is not fully corroborated by morphological characters. Molecular phylogenies of placental mammals place the Afrotheria in a basal position; they diverge before the Xenarthra (sloths, anteaters, and armadillos), which have generally been considered the basal group. Afrotheria comprises seven orders of extant African mammals: proboscideans, sirenians (manatees and dugongs), hyracoids (dassies), tubulidentates (aardvarks), macroscelids (elephant shrews), chrysochlorids (golden moles), and tenrecs. That the first three of these orders form a monophyletic group, the paenungulates, is now commonly accepted. Although morphological data leave the phylogenetic position of aardvarks and elephant shrews unclear, "most of the morphological hypotheses are not in conflict with the molecular analyses." On the basis of morphological features, the tenrecs and golden moles are not obviously related to the other Afrotheria; however, a total-evidence tree (using 196 morphological characters, 19

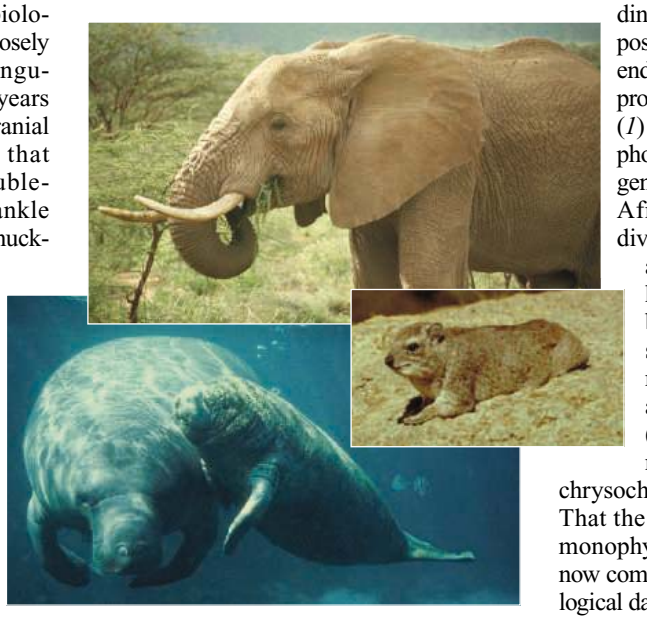

Accepted group. The monophyly of paenungulates—comprising three extant orders, here represented by African elephant (*Loxodonta africana*), rock hyrax (*Procavia capensis*), and West Indian manatee (*Trichechus manatus*)—is now commonly accepted, while debates continue over Afrotheria.

The reviewer is at the Département Histoire de la Terre, Muséum National d'Histoire Naturelle, 57 Rue Cuvier, 75005 Paris, France. E-mail: muizon@mnhn.fr

nuclear genes, and 3 mitochondrial genes) presented by Robert Asher includes them in the Afrotheria. Although the paenungulates are relatively well documented in the fossil record, that is apparently not the case for the four remaining afrotherian orders. This lack of knowledge of the early members of these orders may explain why their molecular affinities are so difficult to corroborate with morphological data; it certainly demonstrates the desirability of finding early Tertiary fossils from these groups. Whether or not the Afrotheria represent a clade, Rose and Archibald's volume clearly sets the problem posed by the group and indicates its importance for mammalian paleontology.

Among the other important phylogenetic questions discussed in the book are the relationship between the Xenarthra and the pangolins, and their affinities with other placentals; the relationship between paenungulates and perissodactyles; the relationships of primates to tupaids ("tree shrews") and dermopterans ("flying lemurs"), and their affinities with bats; the complex problem of identifying the phylogenetic positions of the various groups traditionally placed in the "insectivores"; and the links between Cretaceous placentals and the extant orders.

The Rise of Placental Mammals addresses most current issues in placental phylogeny and systematics. The contributors provide the pros and cons of conflicting interpretations of the data. Although the authors do not always clearly state their personal points of view, the presentation of the arguments allows readers to reach their own conclusions. The volume should be welcome bedside reading for all mammal systematicists and anyone interested in the evolution of mammals. It complements a recent comprehensive examination of Mesozoic mammals (*2*), and I look forward to similar volumes covering other mammals such as marsupials, monotremes, and the many higher taxa known exclusively from Cenozoic fossils (*2*).

References

1. M. J. Stanhope *et al.*, *Proc. Natl. Acad. Sci. U.S.A.* **95**, 9967 (1998).
2. Z. Kielan-Jaworowska, R. L. Cifelli, Z.-X. Luo, *Mammals from the Age of Dinosaurs: Origins, Evolution, and Structure* (Columbia Univ. Press, New York, 2004).

10.1126/science.1112246

EVOLUTION AND RELIGION

Seeing Similarities

Sahotra Sarkar

In this timely book, Michael Ruse interprets the last 200 years of conflict between biology and religion as a struggle between evolutionism and creationism. Evolutionism is not merely an endorsement of the scientific theory of evolution. It consists of "the whole metaphysical or ideological picture built around or on evolution," including a belief in progress and attempts to reduce cultural and ethical values to evolutionary biology. As such, it constitutes a "secular religion." Thus, for Ruse (a philosopher of science at Florida State University), the debate over creationism is more a conflict between two religions than one between religion and science.

The Evolution-Creation Struggle
by Michael Ruse
Harvard University Press, Cambridge, MA, 2005. 310 pp. $25.95, £16.95, €24. ISBN 0-674-01687-4.

The book covers the period from the end of the Enlightenment (roughly the end of the 18th century) to the present. Religious history and that of evolutionary ideas receive equal time. Ruse's account of religion is restricted to Christianity and almost entirely limited to Britain and the United States. He sees the origins of the conflict over evolution in a crisis of religious faith induced by the Enlightenment's emphasis on reason and science and its rejection of text-based established religions. The Enlightenment offered a vision of progress based on human effort. The emerging pre-Darwinian views of evolution (such as those of Erasmus Darwin, Jean-Baptiste de Lamarck, and Robert Chambers), although hardly professional science, co-opted this vision in their accounts of organic change.

Charles Darwin, in contrast, attempted to convert evolution into science by elaborating a material mechanism for it—natural selection. Darwin was at best ambivalent about the ideology of progress. (Alfred Russel Wallace was more convinced of its reality—strangely, he receives scant attention in Ruse's story.) Moreover, natural selection acting on blind variation was antithetical to the idea of progress with its implied directionality. In spite of Darwin's efforts, Ruse argues, evolution did not become established as a professional science in the 19th century or even during the first two decades of the 20th. Instead, it remained popular science. Given the generally accepted ideology of progress, natural selection was often abandoned in favor of directional mechanisms of organic change. According to Ruse, during this period, almost all of those who endorsed evolution also endorsed evolutionism. The social Darwinism of the late 19th century only exemplifies the worst excesses of such an evolutionism.

Religious belief also underwent significant changes during this period. Established denominations of Christianity were often reluctant to feud with science. They rejected evolutionism but typically tried to forge an interpretation of evolution that could coexist with nonliteral interpretations of biblical texts. However, the older sects (such as Presbyterianism, Congregationalism, and Quakerism) gradually saw their constituencies shift to evangelicals and fundamentalists, particularly in the United States after the American Revolution disrupted the established social order. Among fundamentalists, any thought of evolution was anathema because it conflicted with their literal interpretation of Genesis. In the mid-20th century, "young Earth" creationism, which still holds that Earth is less than 10,000 years old, emerged from fundamentalism. It continues to have its devoted adherents but has largely become intellectually irrelevant in the United States since a Supreme Court decision specifically precluded the introduction of religion in science classes.

On Ruse's account, evolution became a professional science following the modern synthesis of the late 1920s and 1930s. Ruse argues, though not very convincingly, that the architects of the synthesis continued to uphold an ideology of progress and endorse evolutionism. He ignores the fact that, with the exception of R. A. Fisher, these architects largely rejected attempts to deploy evolution in the political arena. (Some, such as J. B. S. Haldane, whom Ruse ignores, often explicitly rejected progress.) Ruse's sketch of contemporary evolutionary theory is also idiosyncratic, with sociobiology presented as that theory's most significant achievement. Because the sociobiologists W. D. Hamilton and Edward O. Wilson are the heroes of this story, Ruse claims that contemporary evolutionary biology endorses evolutionism and not merely evolution.

The final chapters of *The Evolution-Creation Struggle* turn all too briefly to the contemporary debates over creationism. Ruse offers a short and cogent critique of intelligent design that concentrates on its failure to spawn any serious scientific research. But the book ends with an unfortunate whimper: we are told that we should try to understand the other side; we are not told how Ruse's understanding of that side will help us prevent the reintroduction of religion in our science classes.

10.1126/science.1115782

The reviewer is in the Section of Integrative Biology and the Department of Philosophy, University of Texas at Austin, Austin, TX 78712, USA. E-mail: sarkar@mail.utexas.edu

ECOLOGY

North Atlantic Right Whales in Crisis

Scott D. Kraus,[1]* Moira W. Brown,[1] Hal Caswell,[2] Christopher W. Clark,[3] Masami Fujiwara,[4] Philip K. Hamilton,[1] Robert D. Kenney,[5] Amy R. Knowlton,[1] Scott Landry,[6] Charles A. Mayo,[6] William A. McLellan,[7] Michael J. Moore,[2] Douglas P. Nowacek,[8] D. Ann Pabst,[7] Andrew J. Read,[9] Rosalind M. Rolland[1]

Despite international protection from commercial whaling since 1935, the North Atlantic right whale (*Eubalaena glacialis*) remains one of the most endangered whales in the world (*1*). Whaling for almost 1000 years brought this species close to extinction in the early 20th century (*2*). Right whales range in the coastal waters of eastern North America from Florida to the Canadian Maritimes, regions that are heavily used by the shipping and fishing industries and by the military. A low reproductive rate and recently declining survival probabilities (*1*, *3*), particularly for breeding females (*4*), appear to have prevented this population from recovering over the last 25 years (*5*). Most right whale mortalities are due to collisions with ships and entanglements in fishing gear (*5*). The right whale population growth rate has declined since 1980, and the total population now appears to be diminishing in size (*4*). This is in stark contrast to southern hemisphere right whales (*Eubalaena australis*), whose population is estimated to be over 10,000 animals and appears to be increasing at 7.2% per year (*6*).

Enhanced online at www.sciencemag.org/cgi/content/full/309/5734/561

Recent mortalities demonstrate the serious problem facing the North Atlantic right whale. In the past 16 months, there have been eight recorded deaths, including six adult females (three were carrying near-term fetuses). Four of these whales were killed by human activities (three by ships and one by fishing gear), a fifth whale was probably killed by a ship, two whales were offshore and could not be retrieved for examination, and a young calf died on the beach in Florida. The loss of this number of whales, and particularly this number of reproductive females, in such a short period, is unprecedented in 25 years of study of this species (*7*). Four of these females were just starting to bear calves, and since the average lifetime calf production is 5.25 calves (*4*), the deaths of these females represent a lost reproductive potential of as many as 21 animals.

The most recently published estimates of right whale survival (*4*, *8*) suggest that the mortality rate increased between 1980 and 1998 to a level of 4 (±1%). From recent population estimates of 350 right whales (*1*), a 4% mortality rate implies 14 animals dying per year. In the last 20 years, an average of 2.4 dead whales has been reported each year, representing a detection rate of 17%. The eight deaths reported in the last 16 months is 2.9 times the average annual rate. Calculations based on demographic data through 1999 (*4*) show that this increase in mortality would reduce population growth by 3.5 to 12% per year. (The range reflects different choices in the details of model selection; the best model implies a reduction in population growth rate of 10% per year.) This dramatic increase in reported deaths may be partly due to improved sighting efforts and reporting awareness but is not a natural variation in mortality. If the 17% mortality detection rate from the last 20 years has remained constant, as many as 47 right whales could have died in the last 16 months.

Of the 50 dead right whales reported since 1986, at least 19 were killed by vessel collisions, and at least six were killed by fishing gear entanglements (*7*). Also during this period, there were 61 confirmed cases of whales carrying fishing gear, including the mortalities. Outcomes of the remaining cases and the fate of individual whales varied. Death is suspected in 12 cases, because of an animal's subsequent disappearance and/or the extremely poor health condition observed at the time of last sighting. Another eight animals are still entangled; their fate is uncertain. Thirty-three animals either shed the gear or were disentangled, and the remaining cases involved unidentifiable individuals. Chronically entangled whales lose weight, so they sink after death, unlike healthy animals that float if killed. Thus, right whale mortality from fishing gear is probably underestimated to a greater degree than ship kills (*5*).

Calf production has increased recently, raising doubts in some quarters about the urgency of the mortality problem. Annual calf production averaged 12 calves up until 2000 (*1*), but totaled 31, 21, 19, 16, and 28 in 2001 to 2005, respectively. However, the increase in the birth rate will have a small positive impact on population growth rate, as a hypothetical doubling of the per capita birth rate would increase population growth rate by at most 1.6% per year. The population is estimated to have been declining at about 2% per year before 2000 (*3*, *4*, *8*). Thus, the effects of recent increases in birth rate are too small to overcome this decline.

Federal managers in the National Oceanic and Atmospheric Administration (NOAA) Fisheries are charged by the Endangered Species Act and the Marine Mammal Protection Act to ensure that there is no human-induced mortality of right whales. There have been efforts to minimize the risk of ship strikes with mandatory ship location reporting, extensive aerial survey efforts, and mariner education. But without requiring changes in the operation of ships within right whale habitats and migratory corridors, this increased awareness has not

[1]Edgerton Research Laboratory, New England Aquarium, Boston, MA 02110–3399, USA. [2]Biology Department, Woods Hole Oceanographic Institution, Woods Hole, MA 02543–1049, USA. [3]Cornell Laboratory of Ornithology, Cornell University, Ithaca, NY 14850–1923, USA. [4]Department of Ecology, Evolution and Marine Biology, University of California, Santa Barbara, CA 93106–9610, USA. [5]Graduate School of Oceanography, University of Rhode Island, Narragansett, RI 02882–1197, USA. [6]Provincetown Center for Coastal Studies, Provincetown, MA, 02657–1911, USA. [7]Biological Sciences, University of North Carolina Wilmington, Wilmington, NC 28403–3201, USA. [8]Oceanography Department, Florida State University, Tallahassee, FL 32306–4320, USA. [9]Marine Laboratory, Duke University, Beaufort, NC 28516–8648, USA.
*Author for correspondence. E-mail: skraus@neaq.org

led to a reduction in ship strike mortalities. The risk of fishing gear entanglement has been addressed by selective area closures and gear modifications (*9*). These closures do not adequately encompass the seasonal movements of right whales, and gear modifications implemented thus far have not reduced entanglement rates. Eight dead right whales in the past 16 months provide clear evidence that management efforts have been woefully inadequate, and much stronger measures are needed to reverse the right whale's decline.

Accordingly, we urge immediate changes to the management of right whales, focusing on reducing human-induced mortality. Some of the following recommendations will also benefit other marine species that face similar threats, such as the endangered leatherback sea turtle (*Dermochelys coriacea*) (*10*). First, emergency measures should be implemented to reduce speeds and reroute commercial and military ships as recommended in the NOAA Fisheries Advanced Notice of Proposed Rule-Making (*11*). Second, the amount of fixed fishing gear in the water column should be eliminated or minimized. There are many steps that could be taken to do this, including (i) mandating changes in the pot-fishing industry (lobster, crab, hagfish, etc.) that will reduce gear in the water; (ii) requiring use of alternative rope types (e.g., sinking ground lines) to minimize entanglement deaths; (iii) developing and implementing fishing methods that do not use vertical lines attached to surface buoys; and (iv) developing a fast-track process for permitting and experimenting with conservation-focused fishing gear modifications and implementation. This means streamlining the current rule-making and National Environmental Policy Act (NEPA) process for right whale research and gear modifications, which now takes years.

Given the slow speed of the regulatory process, interim emergency measures to reduce shipping and fishing mortality in right whales should be implemented immediately. Delays in implementation would be ignoring both scientific and legal mandates and could consign North Atlantic right whales to extinction.

References and Notes

1. S. D. Kraus, P. K. Hamilton, R. D. Kenney, A. R. Knowlton, C. K. Slay, *J. Cetacean Res. Manage. Spec. Issue* **2**, 231 (2001).
2. R. R. Reeves, *J. Cetacean Res. Manage. Spec. Issue* **2,** 187 (2001).
3. H. Caswell, M. Fujiwara, S. Brault, *Proc. Natl. Acad. Sci. U.S.A.* **96**, 3308 (1999).
4. M. Fujiwara, H. Caswell, *Nature* **414**, 537 (2001).
5. A. R. Knowlton, S. D. Kraus, *J. Cetacean Res. Manage. Special Issue* **2**, 193 (2001).
6. P. Best, A. Brandao, D. Butterworth, *J. Cetacean Res. Manage. Spec. Issue* **2**, 161 (2001).
7. M. J. Moore, A. R. Knowlton, S. D. Kraus, W. A. McLellan, R. K. Bonde, *J. Cetacean Res. Manage.* **6** (3), 199 (2005); available at www.whoi.edu/hpb/viewPage.do?id=1432.
8. M. Fujiwara, dissertation, Massachusetts Institute of Technology–Woods Hole Oceanographic Institution (2002).
9. U.S. Code of Federal Regulation (C.F.R.) **50**, Part 229.32
10. M. C. James, C. A Ottensmeyer, R. A. Myers, *Ecol. Lett.* **8**, 195 (2005).
11. *Fed. Regist.* **69** (105), 30857 (1 June 2004).

10.1126/science.1111200

SUSTAINABILITY

Millennium Assessment of Human Behavior

Paul R. Ehrlich* and Donald Kennedy

A growing scientific consensus says that global society is under increasing threat from the impact of human activities: Climate change, loss of biological diversity and ecosystem services, and changes in patterns of land use and land cover are among the more troublesome problems (*1*–*3*). Some of these problems require attention from governments and other social institutions. But it is the collective actions of individuals that lie at the heart of the dilemma. Analysis of individual motives and values should be critical to a solution. Yet society has no prominent international forum in which such issues (like how we should treat our environment and each other) are publicly discussed.

In some countries, quite different views have surfaced recently about the ethics of governmental restrictions on the rights of landowners designed to protect endangered species and about legal provisions that permit "open space" set-asides of long duration. Even in nations with cultures as similar as those of the United States and the United Kingdom, issues of land care, debates over related subsidies, and the responsibilities of private citizens versus their governments can take very different shapes. In approaching sustainability, one needs to determine how the rights of people in the current generation to consume natural capital should be balanced against the rights of future generations. Preservation of animal life and the ethics of various kinds of human interference with "natural" systems are viewed differently by those whose cultural traditions differ. The steps that most members of the relevant scientific community believe are necessary (e.g., reduction of human-caused greenhouse gas emissions, establishment of marine reserves, limiting human population growth and per capita consumption) are disconnected from those measures the rest of society, and especially politicians, are willing to undertake.

We propose to promote the establishment of an ongoing global discussion of key ethical issues related to the human predicament—a Millennium Assessment of Human Behavior (MAHB). The time seems ripe, with the experience gained from the Intergovernmental Panel on Climate Change (IPCC) and the Millennium Ecosystem Assessment (MEA), to start discussing what to do. In the IPCC and the MEA, sociopolitical issues and policy changes that might lessen the chances of catastrophic consequences are considered. But we need an institution to conduct an ongoing examination and public airing of what is known about how human cultures (especially their ethics) evolve, and about what kinds of changes might permit transition to an ecologically sustainable, peaceful, and equitable global society.

Such a process could begin by asking behavioral scientists and laypeople to explore how their own values relate to environmental sustainability and to ask themselves whether their values, if shared by 6.4 billion people, would really lead to the sort of world they want for their descendents. Citizens of the rich nations should ask themselves whether their "way of life" should really be, as the first President Bush once said to Americans, "not negotiable" (*4*). They need to discuss possible lifestyle changes in a framework not limited merely to what is possible for citizens of powerful nations, but enlarged to evaluate what is ethical with respect to a more global view of needs and opportunities.

The MAHB could consist of an ongoing series of open, transparent forums. The MAHB could be modeled on the IPCC but would be focused mainly in the social sciences. It would include a deeper consideration of the ethical dimensions of how we treat each other and our life-support systems. It would also involve broader participation than the IPCC, encourage the involvement of politicians, and focus on public outreach at

P. R. Ehrlich is in the Department of Biological Sciences, D. Kennedy is at the Institute for International Studies, Stanford University, Stanford, CA 94305, USA.*Author for correspondence. E-mail: pre@stanford.edu

nontechnical levels. Because knowledge of public opinions and attitudes will be essential, such communication devices as deliberative polling (*5*) would be built in from the start. What we are asking for is a cultural change; we know that cultures evolve, and our hope is that the very process of debate will speed that process and encourage change in a positive direction.

The MAHB will need to establish working groups to cover particular segments of the broad agenda. They could include exploration of (i) what social scientists and others know about mechanisms of cultural evolution and how changes in direction might be steered democratically; (ii) how scarce and unevenly distributed nonrenewable resources are used and some of the ethical connections between distribution, economic opportunity, and access; (iii) ethical issues related to the world trade system; (iv) conflicts between individual reproductive desires and environmental goals; and (v) economic, racial, and gender inequity as contributors to environmental deterioration.

War, national and international governance, and health maintenance and care are other topics that would clearly require intensive discussion. Certainly many such topics have been under consideration in various forums, including the World Bank and the United Nations. But they have not been addressed in the context of the entire spectrum of the human predicament in a "broadened IPCC" kind of effort.

One central task would be to integrate the results of the working groups on a continuous basis and to make recommendations for action. The MAHB might, for example, help generate public support for mechanisms to constrain corporate power under certain circumstances. Large-scale private activity may be part of the solution, but many analysts think that some limitation is crucial (*6*, *7*).

That open forums and face-to-face negotiation in working groups can produce positive change is clear from many examples. The Montreal Ozone Protocol was put together through the cooperation of representatives of the academic scientific community, government laboratories, and industry (*8*), interacting with corporate decision-makers and politicians. The resulting agreements marked a major change in attitude on the part of governments and even of the manufacturers of ozone-depleting substances. There are other examples on a somewhat smaller scale. In the United States these include establishment of marine protected areas (*9*); development of the Sierra Forest Plan (*10*, *11*); the Forest Stewardship Council's negotiations with timber companies that led to more sustainable harvesting (*12*); and the negotiations resulting in Habitat Conservation Plans in which environmental advocates and developers have reached accord (*13*). The literature on mediation and alternative dispute resolution should also be explored.

Diamond (*14*) has listed several possible causes of "collapse" of past societies. He cites cases in which decisions were rooted in maladaptive cultural tradition or an unwillingness to count the clearly measurable costs of their actions. However, other peoples have created stable, sustainable societies under equally unfavorable conditions (*15*). Modern literature (*16*) has revised the discouraging message of the "Tragedy of the Commons" by demonstrating how even primitive societies can organize fair and sustainable rules for extracting common-pool resources.

"...our hope is that the very process of debate will ... encourage change in a positive direction."

Much of the MAHB program will have to focus on the way in which people make decisions about resource allocation and risk. The discipline of "rational-choice" economics, in which people are expected to make choices in ways predicted by the mathematics of self-interest, has been challenged by data demonstrating anomalies and contradictions (*17*, *18*). We also need more information about the circumstances under which groups come together to form alliances and develop loyalty to them. The growing literature on religious organizations, clubs, and associations [for example (*19*, *20*)] suggests that changing social circumstances influence the degree to which individuals make common cause.

There is much more to learn about behaviors, relationships between individual and societal goals, and institutional arrangements that lead to success or to failure. That will require active participation from groups with different traditions that often do not communicate. The professional societies and community of ecologists are already doing more than most, and we hope that other academic disciplines will do more. Part of the problem is that the disciplines have been historically segregated in universities, and only a few institutions are encouraging interdisciplinary engagement. The MAHB could help by stimulating regular symposia and panel discussions that link different specialties. One subject would be the ethics of time and task allocation by scholars in a world facing increasingly serious problems.

This effort will require support from a variety of sectors. Once an idea gathers interest, the natural starting-points for implementation are the major elements of civic society—in particular, nongovernmental organizations (including scientific and other professional societies), foundations, and other philanthropic entities. The growing international network of funders and civic organizations will need to be involved in the first phase. The United Nations, the World Bank, and other international transgovernment institutions would be natural candidates. Eventually, governments will have to be the decision-makers.

In this and other respects, the MAHB courts criticism for naïveté. But that charge, often levied against new ideas, has been overcome in the past. The goal is too important to be set aside as politically infeasible.

References and Notes

1. "World scientists' warning to humanity" (Union of Concerned Scientists, Cambridge, MA, 1993).
2. "Population Summit of the World's Scientific Academies: A joint statement by 58 of the world's scientific academies," New Delhi, India, 24 to 27 October 1993 (National Academy Press, Washington, DC, 1993).
3. P. R. Ehrlich, A. H. Ehrlich, *One with Nineveh: Politics, Consumption, and the Human Future* (Island Press, Washington, DC, 2004).
4. G. H. W. Bush, speech at 1992 Earth Summit, Rio de Janeiro, Argentina.
5. H. E. Brady, J. F. Fishkin, R. C. Lufkin, *Brookings Rev.* **21**, 16 (summer 2003).
6. M. Kelly, *The Divine Right of Capital: Dethroning the Corporate Aristocracy* (Berrett-Koehler, San Francisco, CA, 2001).
7. D. C. Korten, *When Corporations Rule the World, Second Edition* (Kumarian Press, Bloomfield, CT, and Berrett-Koehler Publishers, San Francisco, CA, 2001).
8. R. E. Benedick, *Ozone Diplomacy: New Directions in Safeguarding the Planet* (Harvard Univ. Press, Cambridge, MA, 1991).
9. National Research Council, *Marine Protected Areas: Tools for Sustaining Ocean Ecosystems* (National Academies Press, Washington, DC, 2001).
10. "Sierra Nevada Forest Plan Amendment, Final Environmental Impact Statement" (Pacific Southwest Region, USDA Forest Service, Vallejo, CA 2001).
11. Also (*10*), further amended in 2004.
12. See www.fscus.org.
13. "Habitat Conservation Planning Handbook" (U.S. Fish and Wildlife Service/National Marine Fisheries Service, Washington, DC, 2000).
14. J. Diamond, *Collapse: How Societies Choose to Fail or Succeed* (Viking, New York, 2005).
15. P. V. Kirch, *Am. Anthropol.* **99**, 30 (1997).
16. For example, see E. Ostrom, *Governing the Commons: The Evolution of Institutions for Collective Action* (Cambridge Univ. Press, Cambridge, 1990).
17. D. Kahneman, P. Slovic, A. Tversky, Eds. *Judgment Under Uncertainty: Heuristics and Biases* (Cambridge Univ. Press, London, 1982).
18. D. Kahneman, A. Tversky, *Am. Psychol.* **39**, 341 (1984).
19. R. Putnam, *Making Democracy Work* (Princeton Univ. Press, Princeton, NJ, 1993).
20. R. Putnam, *Bowling Alone: The Collapse and Revival of American Community* (Simon & Schuster, New York, 2000).

21. We thank P. Brest, G. Daily, R. Dirzo, A. Ehrlich, J. Koseff, P. Matson, H. Mooney, B. Simoni, B. Thompson, and P. Vitousek for helpful comments.

10.1126/science.1113028

ASTRONOMY

Mapping the Large-Scale Structure of the Universe

David H. Weinberg

In a large-scale view of the universe, galaxies are the basic unit of structure. A typical bright galaxy may contain 100 billion stars and span tens of thousands of light-years, but the empty expanses between the galaxies are much larger still. Galaxies are not randomly distributed in space, but instead reside in groups and clusters, which are themselves arranged in an intricate lattice of filaments and walls, threaded by tunnels and pocked with bubbles. Two ambitious new surveys, the Two-Degree Field Galaxy Redshift Survey (2dFGRS) and the Sloan Digital Sky Survey (SDSS), have mapped the three-dimensional distribution of galaxies over an unprecedented range of scales (*1*, *2*). Astronomers are using these maps to learn about conditions in the early universe, the matter and energy contents of the cosmos, and the physics of galaxy formation.

Galaxies and large-scale structure form as a result of the gravitational amplification of tiny primordial fluctuations in the density of matter. The inflation hypothesis ascribes the origin of these fluctuations to quantum processes during a period of exponential expansion that occupied the first millionth-of-a-billionth-of-a-trillionth of a second of cosmic history. Experiments over the last decade have revealed the imprint of these fluctuations as part-in-100,000 intensity modulations of the cosmic microwave background (CMB), which records the small inhomogeneities present in the universe half a million years after the big bang. Although the visible components of galaxies are made of "normal" baryonic matter (mostly hydrogen and helium), the gravitational forces that drive the growth of structure come mainly from dark matter, which is immune to electromagnetic interactions.

By combining precise, quantitative measurements of present-day galaxy clustering with CMB data and other cosmological observations, astronomers hope to test the inflation hypothesis, to pin down the physical mechanisms of inflation, to measure the amounts of baryonic and dark matter in the cosmos, and to probe the nature of the mysterious "dark energy" that has caused the expansion of the universe to accelerate over the last 5 billion years. The 2dFGRS, completed in 2003, measured distances to 220,000 galaxies, and the SDSS is now 80% of the way to its goal of 800,000 galaxies (see the figure). The key challenge in interpreting the observed clustering is the uncertain relation between the distribution of galaxies and the underlying distribution of dark matter. If the galaxy maps are smoothed over tens of millions of light-years, this relation is expected to be fairly simple: Variations in galaxy density are constant multiples of the variations in dark matter density. Quantitative analysis in this regime has focused on the spatial power spectrum, which characterizes the strength of clustering on different size scales (*3*, *4*). The power spectrum describes the way that large, intermediate, and small structures—like the mountain ranges, isolated peaks, and rolling hills of a landscape—combine to produce the observed galaxy distribution. The shape of the dark matter power spectrum is a diagnostic of the inflation model, which predicts the input spectrum from the early universe, and of the average dark matter density, which controls the subsequent gravitational growth. Recent analyses have also detected subtle modulations of the power spectrum caused by baryonic matter, which undergoes acoustic oscillations in the early universe because of its interaction with photons (*4*, *5*).

To go further, one would like to know the precise amplitude of dark matter clustering, not just the variation of clustering

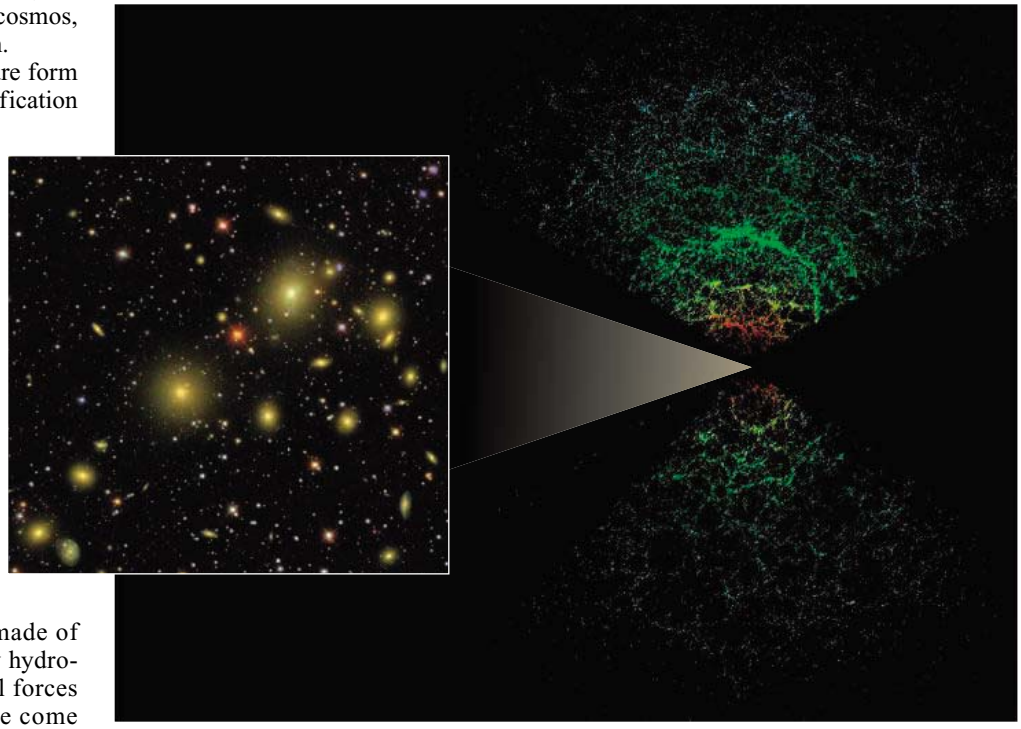

The big picture. Large-scale structure in the SDSS. The SDSS uses a mosaic charge-coupled device camera to image regions of the sky and a fiber-fed spectrograph to measure distances of galaxies selected from these images. The main panel shows the SDSS map of 67,000 galaxies that lie within 5° of the equatorial plane; the region of sky obscured by the Milky Way is not mapped. Each wedge is 2 billion light-years in extent. Galaxies are color-coded by luminosity, and more luminous galaxies can be seen to greater distances. (**Inset**) SDSS image of a cluster of galaxies, showing a region roughly 1 million light-years on a side.

CREDIT: IMAGES COURTESY OF THE SLOAN DIGITAL SKY SURVEY COLLABORATION

The author is in the Department of Astronomy, Ohio State University, 140 West 18th Avenue, Columbus, OH 43210, USA E-mail: dhw@astronomy.ohio-state.edu

with scale. Unfortunately, the factor relating galaxy and dark matter densities depends on aspects of galaxy formation that are difficult to model theoretically. One observational approach to isolating dark matter clustering uses weak gravitational lensing, in which the dark matter surrounding nearby galaxies subtly distorts the apparent shapes of the distant galaxies behind them. Another approach uses the relative probabilities of different triangular configurations of galaxy triples, picking out the characteristic filamentary geometry produced by anisotropic gravitational collapse. Applications of these two methods to the SDSS and the 2dFGRS, respectively, imply that the clustering strength of bright, Milky Way–type galaxies is similar to that of the underlying dark matter (*6*, *7*).

On smaller scales, the relation between galaxies and dark matter becomes more complex, and it is different for different types of galaxies. Redder galaxies composed of older stars reside primarily in clusters, the dense urban cores of the galaxy distribution. Younger, bluer galaxies populate the sprawling, filamentary suburbs. Current efforts to model galaxy clustering in this regime focus on the "halo occupation distribution," a statistical description of the galaxy populations of gravitationally bound "halos" of dark matter. Depending on its mass, an individual dark halo may play host to a single bright galaxy, a small group of galaxies, or a rich cluster.

By combining theoretical predictions for the masses and clustering of halos with precise measurements of the clustering of galaxies, one can infer the halo occupation distribution for different classes of galaxies empirically. Theoretical models of galaxy formation predict a strong dependence of halo occupation on galaxy luminosity and color, and the initial results from the 2dFGRS and the SDSS show good qualitative agreement with these predictions (*8*, *9*). Increased precision and measurements for more galaxy classes will test the predictions in much greater detail, and they will sharpen our understanding of the physical processes that produce visible galaxies in the first place and determine their observable properties. By deriving the relation between galaxies and dark matter from the clustering data themselves, halo occupation methods also allow new cosmological model tests that take advantage of precise measurements on small and intermediate scales.

The large-scale clustering results from the 2dFGRS and the SDSS, in combination with CMB measurements and other cosmological data, support the predictions of a simple inflation model in a universe that contains 5% normal matter, 25% dark matter, and 70% dark energy (*10*). However, several analyses that incorporate smaller scale clustering suggest that either the matter density or the matter clustering amplitude is lower than this "concordance" model predicts, by 30 to 50% (*11*–*13*). This tension could reflect systematic errors in the measurements or the modeling, but it could also signal some departure from the simplest models of primordial fluctuations or dark energy. For example, if inflation produces gravity waves that contribute to observed CMB fluctuations, then naïve extrapolation of these fluctuations would overpredict the level of matter clustering today. Alternatively, evolution of the dark energy component can affect the amount of growth since the CMB epoch. As the SDSS moves toward completion, improved clustering measurements and analyses may restore the consensus on a "vanilla" cosmological model, or they may provide sharper evidence that our theoretical recipe for the universe is still missing a key ingredient.

References and Notes

1. M. Colless *et al.*, *Mon. Not. R. Astron. Soc.* **328**, 1039 (2001).
2. D. G. York *et al.*, *Astron. J.* **120**, 1579 (2000).
3. M. Tegmark *et al.*, *Astrophys. J.* **606**, 702 (2004).
4. S. Cole *et al.*, http://arxiv.org/abs/astro-ph/0501174.
5. D. J. Eisenstein *et al.*, http://arxiv.org/abs/astro-ph/0501171.
6. E. Sheldon *et al.*, *Astron. J.* **127**, 2544 (2004).
7. L. Verde *et al.*, *Mon. Not. R. Astron. Soc.* **335**, 432 (2002).
8. F. C. van den Bosch, X. Yang, H. J. Mo, *Mon. Not. R. Astron. Soc.* **340**, 771 (2003).
9. I. Zehavi *et al.*, http://arxiv.org/abs/astro-ph/0408569.
10. Convergence on this model from several independent lines of evidence was the 2003 *Science* "Breakthrough of the Year," C. Seife, *Science* **302**, 2038 (2003).
11. F. C. van den Bosch, H. J. Mo, X. Yang, *Mon. Not. R. Astron. Soc.* **345**, 923 (2003).
12. N. A. Bahcall *et al.*, *Astrophys. J.* **585**, 182 (2003).
13. J. L. Tinker, D. H. Weinberg, Z. Zheng, I. Zehavi, *Astrophys. J.*, in press; preprint available at http://arxiv.org/abs/astro-ph/0411777.
14. I thank the National Science Foundation for support.

10.1126/science.1115128

PHYSICS

Fingerprinting Spin Qubits

J. Carlos Egues

In addition to mass and charge, every electron also has a property called the magnetic moment. This magnetic moment is directly related to the intrinsic electron spin states up (↑) and down (↓) and, roughly speaking, it defines how electrons interact with magnetic fields. But individual spins can combine to form new states as well. In the case of a two-electron system such as the helium atom, the total spin is either 0 (up and down) or 1 (two ups or two downs). However, quantum mechanics tells us that there are actually four possible spin states with two distinct "parities": $\uparrow\downarrow + \downarrow\uparrow$ and $\uparrow\downarrow - \downarrow\uparrow$ with $p = 0$, and $\uparrow\uparrow$ and $\downarrow\downarrow$ with $p = 1$ (where the parity p is the total spin component of the pair). Interestingly, distinct parities play the role of "spinprints" (that is, fingerprints) for the electron pairs: $p = 0$ uniquely identifies opposite-spin pairs and $p = 1$ uniquely labels parallel-spin pairs. Now, given an electron pair with unknown spin parity, can we "spinprint" it with 100% certainty and nondestructively? That is, can we measure the spin parity of the electron pair exactly, still maintaining its quantum integrity afterward? In such a measurement, the electron pair is initially in a quantum superposition of all four states above, and so a single-shot measurement of the parity yields either $p = 0$ or $p = 1$, thus "projecting" the initial quantum superposition into the respective subset of spin states with a definite parity. The hypothetical apparatus just described could be called a "spin parity meter" that performs projective measurements.

On page 586 of this issue, Engel and Loss (*1*) propose a novel protocol and a realistic physical implementation—achievable with existing state-of-the-art nanoengineering—of just such a spin-parity meter for performing nondestructive projective measurements on electron pairs in artificial atoms or quantum dots (see the figure). This proposal is a concrete step toward the actual implementation of a solid-state quantum computer, as it should enable efficient and fully deterministic measurement-based quantum computation without interactions between the spin quantum bits (*2*).

Quantum computers are machines whose elementary storage unit of information is a quantum mechanical state or a quantum bit (qubit) (*3*). Unlike the classical bits of ordinary digital computers, which can store either 0 or 1 at a time, qubits can store a superposition of the bits 0 and 1—that is, a qubit can hold both 0 and 1 at the same time. In addition, two qubits can be entangled in a very peculiar quantum superposition of states—for instance, "01 + 10," in which both qubits share the 0 and 1 configurations (this is similar to the spin state of the $1s^2$

The author is in the Department of Physics and Informatics, Institute of Physics of São Carlos, University of São Paulo, São Carlos 13560-970, Brazil. E-mail: egues@if.sc.usp.br

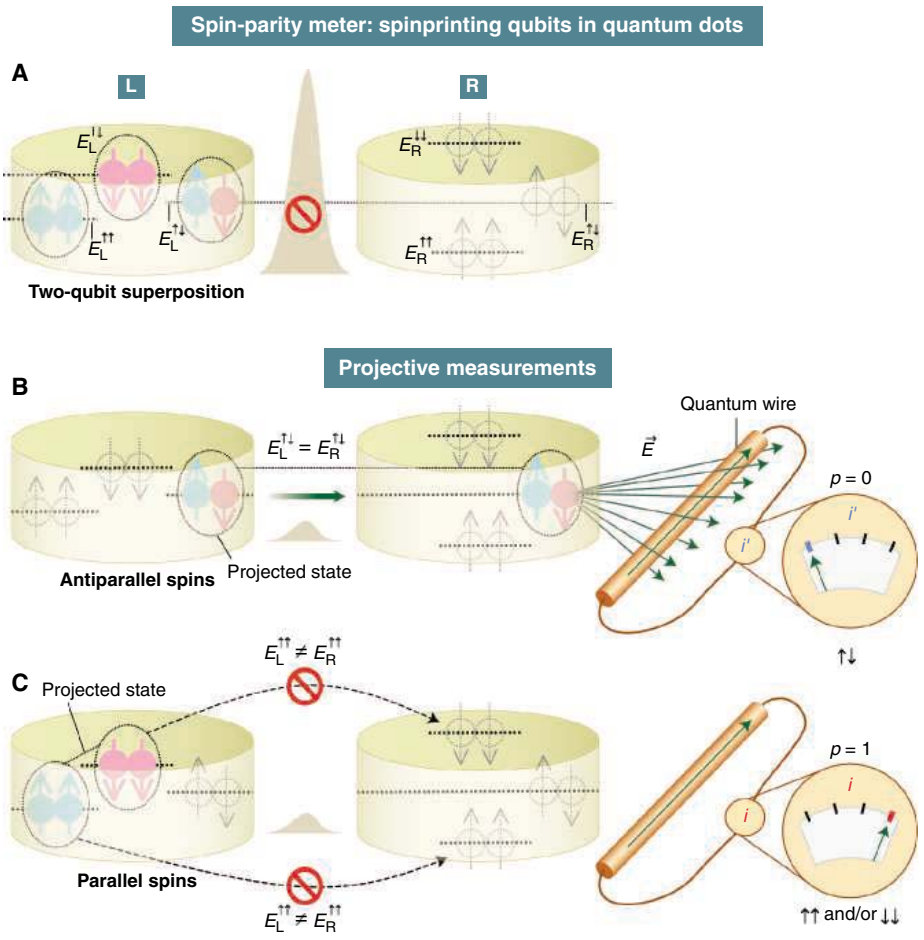

Dusting for spinprints. Spin-parity meter operation based on spin-to-charge conversion and charge detection and its projective-measurement capability for a single-shot measurement. (**A**) Two-spin qubits in an arbitrary superposition of distinct spin parities are loaded into the left dot (initially isolated from the right dot). When the barrier is lowered, either (**B**) a two-qubit pair leaks into the right dot, the charge detector registers its presence there, and a projective measurement takes place—the readout current $i' = i + \Delta i$ ($p = 0$, where i is the current in the wire when the right dot is empty and Δi is the current variation arising when the right dot has electrons) indicates the presence of the two-qubit state $\uparrow\downarrow$ in the right dot; or (**C**) no tunneling occurs, but the detector still registers the absence of the pair in the right dot and a projective measurement also takes place—the readout i ($p = 1$) indicates the presence of the state $\uparrow\uparrow + \downarrow\downarrow$ in the left dot. Ideally, the parity meter always yields readouts with 100% accuracy.

electron configuration of helium). Quantum processing occurs by the manipulation of the encoded information on the qubits via quantum logic gates—controlled unitary operations (or quantum evolution) of the quantum states representing the qubits. For some specific tasks (such as Shor's prime factorization, relevant for cryptography), a quantum computer outperforms its classical counterpart. Essentially, the simultaneous manipulation of many qubits in a superposition allows a quantum computer to execute a quantum algorithm more efficiently.

Qubit-qubit interactions have been a crucial ingredient for quantum computation; most of the early proposals [and experiments (*3*)] relied on controlled qubit-qubit interactions to implement universal two-qubit gates, which, together with single-qubit operations, suffice to perform any quantum computation. In quantum optics with qubits encoded in photon polarization states, the need for qubit-qubit interactions represents a major drawback because photons do not ordinarily interact; nonlinear optical media can mediate photon-photon interaction, but these are not readily available (*4*). The seminal work of Knill *et al.* (*4*) shows the feasibility of efficient quantum computation with free photons, thus obviating the need for photon-photon interaction. Free-photon quantum computation schemes, however, are so far only nearly deterministic (in other words, the quantum gates operate with less than 100% success).

Loss and DiVincenzo (*5*) opened up the field of spin-based solid-state quantum computation by proposing the spin of an electron trapped in a quantum dot as the qubit. This proposal is very promising, as it can benefit from the remarkable advances in the field of semiconductor spintronics (*6*)—in particular, the discovery of exceedingly long spin-diffusion lengths in semiconductors (*7*) and the subsequent successful realization of spin injection with magnetic semiconductors (*8*–*10*). Spin-based quantum computation also relies on qubit-qubit interactions to implement two-qubit gates where the charged spin qubits can interact with each other via the Coulomb exchange interaction. The judicious control of the interaction between the spin qubits (via pulsed electrodes) poses an additional technological challenge for the implementation of spin-based quantum computing.

In a perceptive paper, Beenakker *et al.* (*2*) have shown that projective measurements together with single spin rotations on electron spin qubits can yield efficient (that is, an exponential speedup relative to an ordinary computer) and deterministic quantum computation; no qubit-qubit interaction is needed, and thus free-electron quantum computation is possible. To overcome a theorem (*11*) that seemed to preclude efficient quantum computation with free electrons, these authors used the fact that charge measurements do not affect the spin qubit. However, no experimentally feasible projective-measurement schemes had been proposed for spin qubits until now [the spin-polarizing beam-splitter of Beenakker *et al.* (*2*) is not yet available].

The Engel and Loss proposal (*1*) provides such a scheme. Their spin parity meter is conceptually very simple. It consists of a double-dot system (see the figure, A) where the dots have distinct Zeeman energies in the presence of a magnetic field and are engineered so that (i) the energies of the antiparallel spin states $p = 0$ are equal for both dots, $E_L^{\uparrow\downarrow} = E_R^{\uparrow\downarrow}$, and (ii) the energies of the parallel spin states $p = 1$ are all different, $E_L^{\uparrow\uparrow} \neq E_L^{\downarrow\downarrow} \neq E_R^{\uparrow\uparrow} \neq E_R^{\downarrow\downarrow}$. Hence, when the dots are allowed to communicate (by slowly lowering the potential barrier between them via a gate electrode), only antiparallel spin qubits with parity $p = 0$ can resonantly tunnel from the left to the right dot (see the figure, B). The parallel spin qubits cannot elastically tunnel into the right dot (see the figure, C) because of the energy mismatch [inelastic tunneling is negligible (*1*)]. The partial spin-parity measurement is carried out by probing the charge distribution on the right dot via a quantum wire acting as a charge detector near the right dot. Much like an electromagnetic waveguide, a quantum wire or electron waveguide has a discrete number of available propagating modes (or conducting channels) that determine its conductance. The number of available channels is very sensitive to the electric fields around the wire. By tuning the voltage across the wire

so that only a single channel is conducting (*12*, *13*), the researchers can detect small changes in the electrostatic environment. Hence, when an antiparallel spin-qubit pair tunnels into the right dot, the quantum wire can detect its presence there.

The remarkable recent experimental realizations involving the control, manipulation, and detection of spins in quantum dots (*14*–*18*) are breathtaking; they definitely pave the way to an actual implementation of the spin-parity meter of Loss and Engel. A successful realization of spin-based quantum computing depends on a detailed experimental investigation of the decoherence of the spin qubits (that is, the loss of their quantum mechanical integrity due to interactions with the environment). With a spin-parity meter in hand (together with spin-qubit rotations, perhaps via pulsed magnetic fields) and with decoherence under control, spin-based quantum computation may be closer at hand.

References and Notes

1. H. A. Engel, D. Loss, *Science* **309**, 586 (2005).
2. C. W. J. Beenakker *et al.*, *Phys. Rev. Lett.* **93**, 020501 (2004).
3. M. A. Nielsen, I. L. Chuang, *Quantum Computation and Quantum Information* (Cambridge Univ. Press, New York, 2000).
4. E. Knill *et al.*, *Nature* **409**, 46 (2001).
5. D. Loss, D. P. DiVincenzo, *Phys. Rev.* A **57**, 120 (1998).
6. D. D. Awschalom, D. Loss, N. Samarth, Eds., *Semiconductor Spintronics and Quantum Computation* (Springer, Berlin, 2002).
7. J. M. Kikkawa, D. D. Awschalom, *Nature* **397**, 139 (1999).
8. R. Fiederling *et al.*, *Nature* **402**, 787 (1999).
9. Y. Ohno *et al.*, *Nature* **402**, 790 (1999).
10. For quantum spin filtering with spin-dependent "magnetic" barriers, see J. C. Egues, *Phys. Rev. Lett.* **80**, 4578 (1998).
11. B. M. Terhal, D. P. DiVincenzo, *Phys. Rev. A* **65**, 032325 (2002).
12. M. Field *et al.*, *Phys. Rev. Lett.* **70**, 1311 (1993).
13. J. M. Elzerman *et al.*, *Phys. Rev. B* **67**, R161308 (2003).
14. J. A. Folk, R. M. Potok, C. M. Marcus, V. Umansky, *Science* **299**, 679 (2003).
15. T. Hayashi *et al.*, *Phys. Rev. Lett.* **91**, 226804 (2003).
16. J. M. Elzerman *et al.*, *Nature* **430**, 431 (2004).
17. M. Kroutvar *et al.*, *Nature* **432**, 81 (2004).
18. For a review of spin-based quantum computing and a detailed account of recent experimental accomplishments on charge and spin control in dots, see V. Cerletti, W. A. Coish, O. Gywat, D. Loss, *Nanotechnology* **16**, R27 (2005).

10.1126/science.1115256

ECOLOGY

Population Dynamics: Growing to Extremes

John D. Reynolds and Robert P. Freckleton

We have all heard about the hypothetical pair of houseflies that could cover the Earth with their offspring in a matter of months if all of their descendants survived to reproduce. This hasn't happened yet because as populations grow, their numbers become limited by a lack of resources or by increases in predators and parasites. But how quickly do such limiting factors come into play and how do they affect dynamics of different species? Ecologists have been obsessed with these questions and cracking the underlying mechanisms that explain them because the answers go to the heart of understanding ecology. On page 607 of this issue, Sibly *et al.* (*1*) undertake the most ambitious analyses yet of this problem by examining growth rates of 1780 populations of birds, mammals, bony fishes, and insects. They uncover some interesting patterns, which could contribute fundamentally to our understanding of population dynamics.

The data analyzed by Sibly *et al.* (*1*) were derived from the Global Population Dynamics Database (*2*), which contains nearly 5000 time series of population estimates for a wide variety of plant and animal species. This is an important repository for data that often remain concealed in obscure journals and reports but, if carefully screened, can support powerful statistical analyses to search for broad patterns. After excluding data that covered short time periods or were unsuitable in other ways, the authors were left with 1780 time series for 674 species.

It may seem straightforward to simply plot population growth rates against population size and then assess the relationship by asking whether the shape of the curve is concave, linear, or convex (see the figure). But a large amount of statistical gymnastics is required to fit an appropriate mathematical model to measure the shape. Consider the logistic model, which is arguably the best-known model in ecology, used in hundreds of modeling and statistical studies. This model has only two parameters: r, the maximal rate of population increase from low density, and K, the carrying capacity of the given environment (also called equilibrium). This model makes the restrictive assumption that the relationship between population growth rate and density is linear. But it doesn't have to be, and indeed, that is what the authors were trying to find out. So they used a modified logistic model that contains an extra parameter, θ, which allows the shape of the relationship to be convex ($\theta > 1$), linear ($\theta = 1$), or concave ($\theta < 1$).

Different values of θ may reflect fundamental differences in the nature of density dependence among populations. The linear logistic model ($\theta = 1$) assumes that the absolute negative effect of each additional individual on population growth is the same. This implies scramble competition, whereby each individual requires a fixed amount of resource to survive and reproduce (*3*). A convex ($\theta > 1$) relationship implies that a population can grow almost unchecked until it approaches equilibrium,

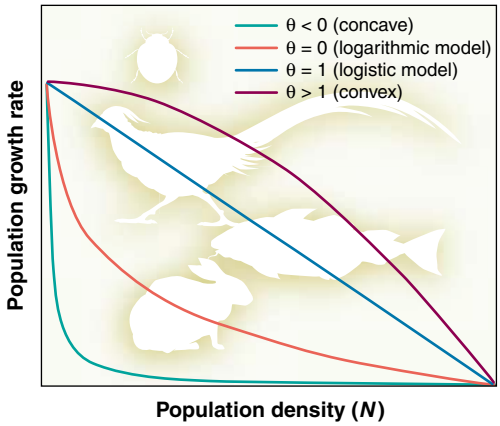

Different shapes for the relationship between population growth rate and density. The shapes of the curves reflect the way a population changes with time, as described in the text. The growth rate–density relationship can be modeled by the θ-logistic equation $pgr = r_1[1 - (N/K)^{\theta}]$: r_1 is the rate of population growth at density 1 [$r_1 = r_0/(1 - K^{-\theta})$, where r_0 is the maximal rate of population growth from low density]; K is the carrying capacity of the environment, or equilibrium; θ controls the shape of the relationship and depends on the ways that members of a population interact at different densities. Sibly *et al.* (*1*) find that mammals, birds, fish, and insects do not generally grow exponentially to carrying capacity, as had been widely thought. Instead, population growth decelerates well before carrying capacity is achieved, as illustrated by the concave curve.

J. D. Reynolds is in the Centre for Ecology, Evolution and Conservation, School of Biological Sciences, University of East Anglia, Norwich NR4 7TJ, UK. E-mail: reynolds@uea.ac.uk R. P. Freckleton is in the Department of Zoology, University of Oxford, South Parks Road, Oxford OX1 3PS, UK. E-mail: robert.freckleton@zoology.oxford.ac.uk

when it stops abruptly as it suddenly runs out of resources or is halted by disease or predators. A weakly concave relationship, where θ is between 0 and 1, implies that the net reduction in population growth per individual is greater at low densities than at high densities; this effect becomes especially pronounced when θ is less than zero.

There is an important caveat in using this analytical approach. The time series use estimates rather than exact counts of populations, and they therefore contain measurement errors. Such errors can substantially bias estimates of the strength of density dependence and make density-independent time series appear as if they were generated from a density-dependent model (*4*). From simulations, Sibly *et al*. claim that the effects of measurement error should not bias estimates of θ toward particularly large positive or negative values. A pure error model, in which all meaningful variation in population size is swamped by measurement error, should yield a value of $\theta = 0$. However, it is not yet clear what happens to estimates of θ in the presence of measurement error if density dependence is weak or absent, and how this may be distinguished from true density dependence.

This caveat notwithstanding, the analyses have turned up a major surprise. The values of θ tend to be negative more often than not, which means that plots of population growth rate against population size are concave. This implies that populations experience strong density dependence early in their growth, with a weaker effect as they approach and exceed their carrying capacity. Why might this be the case? One possibility is that the logistic model ignores the age, size, and developmental-stage dependence of population structure. For example, density dependence may act most strongly at just one particular stage such as during the period of juvenile survival. Population growth rate usually includes all individuals in the population, not just those affected most strongly by density dependence. If the whole population exceeds its carrying capacity, there will be an immediate reduction in the recruitment of juveniles due to density dependence. However, as adults are better competitors, their numbers might respond only slowly, or not at all. Therefore, at high densities the population would not reduce rapidly to equilibrium. Conversely, at low densities, juvenile recruitment will be high, and they will grow rapidly into the adult class and swell the population's number. The net effect of this differential behavior above and below equilibrium is to generate a concave density response. However, this is pure speculation and the issue clearly requires a great deal more thought.

The findings of Sibly *et al*. have some general implications. First, their finding that values of θ tend to be much less than 1 violates a key assumption of the classical logistic equation, whereby growth rate should reduce linearly with density. Although this may not be news to most ecologists, the logistic model is still widely used by theoreticians and is a staple of textbooks. Second, the authors comment that as a consequence of concave density responses, many populations appear to live at densities above the carrying capacity of their environments. Another way of putting this is that rates of population decline will be slower than rates of return, perhaps for the reasons suggested above. It might therefore appear that we can reduce populations substantially before impairing their productivity. However, it would be very risky to manage populations on this basis, for example, when attempting to obtain sustainable yields in hunting or fishing. That is because parameters of the population growth curve will change as populations are exploited. This may change the shapes of the density responses. Furthermore, we still have much to learn about how measurement error affects parameter estimates in such models, and hence the shapes of these relationships. Research on these fronts should prove rewarding for further understanding the ways in which populations change with time and for facilitating better wildlife management and conservation.

References

1. R. M. Sibly *et al*., *Science* **309**, 607 (2005).
2. NERC Centre for Population Biology, Imperial College London, *The Global Population Dynamics Database* (1999), www.sw.ic.ac.uk/cpb/cpb/gpdd.html.
3. T. Royama, *Analytical Population Dynamics* (Chapman & Hall, London, 1992).
4. T. M. Shenk, G. C. White, K. P. Burnham, *Ecol. Monogr.* **68**, 445 (1998).

10.1126/science.1116268

NEUROSCIENCE

Similar Is Different in Hippocampal Networks

György Buzsáki

When driving your car to work on two alternate but familiar routes, different combinations of neurons in the hippocampal region of the brain assist you in the navigation process. This is because ensembles of hippocampal "place cells" form a map-like representation of the environment (*1*). In addition to spatial cues such as shopping malls and other salient landmarks, hippocampal neurons respond to other features during the drive, including speed changes and local information (such as the type of transmission and the shape and size of the car's interior). So how will the hippocampal map representation be affected if you are driving your spouse's Jaguar instead of your two-seater Lotus on the same routes? According to Leutgeb *et al*. on page 619 of this issue (*2*), local information regarding each car as well as either route you may choose to take will be faithfully encoded in the hippocampus and there will be no interference between the two types of representations.

Instead of cars, routes, and human drivers, Leutgeb *et al*. studied rats under two sets of conditions and monitored the firing patterns, or activity, of their hippocampal neurons. In one condition, the rats were tested in each of two different recording chambers (differing in shape) but the chambers were always in the same part of the same room. In the second condition, recordings were made from rats that were placed in each of two different rooms but in the same recording chamber located in the same part of each room. Collection of data began after the rats had at least 1 week of experience in either scenario. In the second condition, both the spatial positions of activated place cells (representing "place fields" in the chambers) and their discharge rates were statistically independent (a phenomenon known as "remapping"), as expected from previous studies. However, in the first condition, virtually all the activated hippocampal neurons remained anchored to the same Cartesian coordinates, even though the firing rate of the individual neurons varied more than an order of magnitude in the different chambers. This finding led the authors to conclude that local information is coded by rate, independently of the ensemble-coded place.

The most basic functions attributed to neuronal networks are the segregation and integration of patterns of activity. Such function is most pertinent in the hippocampus, often con-

The author is at the Center for Molecular and Behavioral Neuroscience, Rutgers University, Newark, NJ 07102, USA. E-mail: buzsaki@axon.rutgers.edu

sidered a single giant cortical module with rich recursive excitatory connections. However, in networks consisting of excitatory neurons only, separation of neuronal assemblies representing different environments is not possible. Inhibitory neuronal connections can provide a high degree of autonomy for individual pyramidal neurons, the principal cell type in the hippocampal cortex ("place cells" are active pyramidal cells). With the help of the inhibitory neurons, excitatory signals can be rerouted within the entire hippocampal network (*3*). Thus, by properly managing the inhibitory networks, minor changes in input excitatory activity can cause instantaneous and large shifts in the assembly behavior of hippocampal neurons. Using the dichotomy of "local" versus "distant" information that is suggested by the authors, a relatively simple circuit can be constructed that can account for their observations (see the figure). The conclusion is that a given environmental context can select the neuronal assembly, whereas gain control (provided by local cues, locomotor speed of the animal, and other factors) can adjust the firing rate of the assembly members.

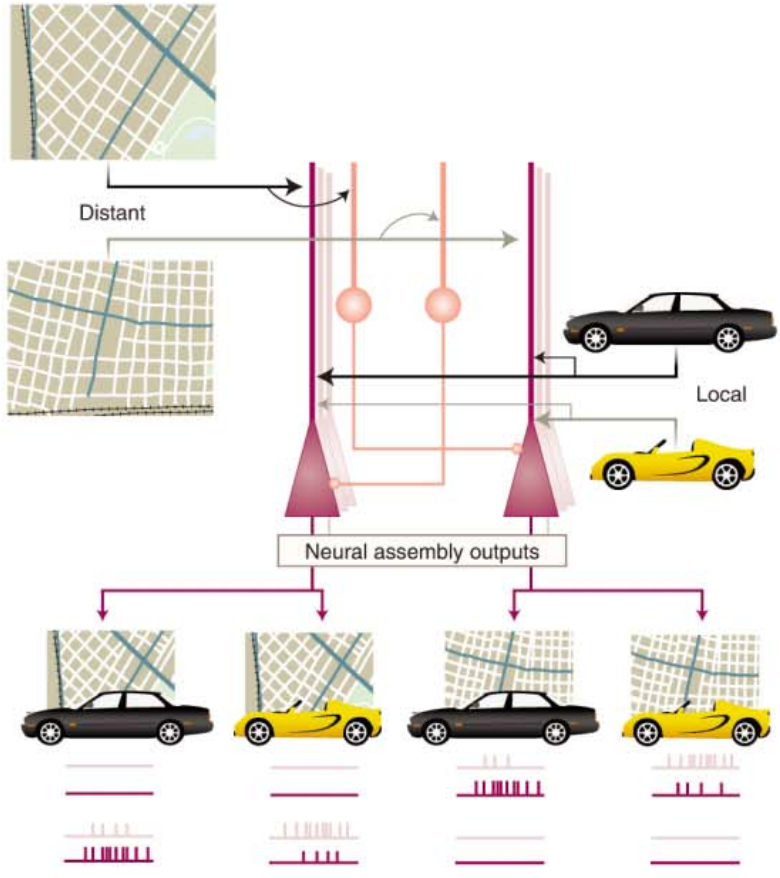

Interneurons allow for pattern separation in cortical networks of the hippocampus. Information from distant cues of one environment (e.g., a city or a given room in the Leutgeb *et al.* study) activates a set of principal neurons (purple). The same input information also activates a single set of interneurons (light red) that prevents the activity of neuronal assemblies that represent other distant environments. Variations in local cues (from a car or the recording chamber in the Leutgeb et al. study) selectively adjust the activity level of the chosen assembly members. This results in distinct patterns of neuronal activity associated with the distant and local cues (shown as line plot patterns).

The observations by Leutgeb *et al.* are backed up by large numbers of neurons and impressive quantitative analysis. However, the hypothesized dual coding scheme of local versus distant inputs is harder to accept. This dichotomy brings to mind our frequent desire to identify the neuronal mechanisms that distinguish numerous qualities: figure and background, context and content, segregated and integrated, separated and completed, aggregated and differentiated, autonomous and dependent, stochastic and deterministic, homogeneous and inhomogeneous, or (in general) the similar and the different. The problem is that nothing in the physical world indicates whether something is near or far. The judgment of local versus distant cues depends solely on the observer, determined largely by the history between those cues and the individual. Past experience may determine which cues will have priority access to the hypothetical assembly-selecting interneurons so that either local or distant cues may cause global remapping in hippocampal representation. In general, one person's judgment of "similar" may be judged as markedly "different" by someone else with more experience, and this may not be so different with rats.

Against this background, it may not be surprising that two recent studies with aims similar to those of the Leutgeb *et al.* study generated different outcomes. In one report, ensembles of place cells abruptly and simultaneously switched as rats experienced either square or cylindrical chambers in the same part of the same room (*4*). In another study, changing the position of objects in the testing apparatus altered most place fields near the objects and caused remapping or cessation of neuronal activity (*5*). Perhaps the most exciting aspect of these and related studies (*6*, *7*) is the consistency of findings within the same laboratories and differences across laboratories. In light of the nonlinear response properties of hippocampal networks, large differences in network behavior are expected even with minor variation of the initial conditions, such as the extent of training and familiarity with the testing conditions.

Leutgeb *et al.* also found remarkable differences between two populations of hippocampal neurons: the CA3 pyramidal cells and CA1 neurons that receive CA3 signals. The firing rate differences observed between chambers in the same room were greater by a factor of 4 in CA3 cells relative to CA1 cells. The differences in the two-room comparison were even greater. This implies a very distinct computation by the CA3 and CA1 neurons. Simultaneous recordings from ensembles of neurons in different stages of information processing, as done by Leutgeb *et al.*, will be required to answer questions regarding the separation and integration of information processing. Such data might explain the inconsistencies between laboratories.

Another important issue is the link between the present findings and episodic memory that is established in the hippocampus. A key feature of episodic memories is their temporal context. In contrast, the representation of a place is assumed to be a temporally independent process (*1*). A fundamental organizational aspect of the hippocampal system is the periodic renewal process of neuron activity by oscillations in their excitation (*8*). Understanding how these oscillations assist in sequential selection of assemblies may pave the way to building a bridge between spatial navigation and episodic memories.

References

1. J. O'Keefe, L. Nadel, *The Hippocampus as a Cognitive Map* (Clarendon, Oxford, 1978).
2. S. Leutgeb *et al.*, *Science* **309**, 619 (2005).
3. T. Freund, G. Buzsáki, *Hippocampus* **6**, 347 (1996).
4. T. J. Wills, C. Lever, F. Cacucci, N. Burgess, J. O'Keefe, *Science* **308**, 873 (2005).
5. P. P. Lenck-Santini *et al.*, *Hippocampus* **15**, 356 (2005).
6. K. M. Gothard *et al.*, *J. Neurosci.* **16**, 823 (1996).
7. W. E. Skaggs, B. L. McNaughton, *J. Neurosci.* **18**, 8455 (1998).
8. G. Buzsáki, A. Draguhn, *Science* **304**, 1926 (2004).

10.1126/science.1116376

Global Consequences of Land Use

Jonathan A. Foley,[1]* Ruth DeFries,[2] Gregory P. Asner,[3] Carol Barford,[1] Gordon Bonan,[4] Stephen R. Carpenter,[5] F. Stuart Chapin,[6] Michael T. Coe,[1]† Gretchen C. Daily,[7] Holly K. Gibbs,[1] Joseph H. Helkowski,[1] Tracey Holloway,[1] Erica A. Howard,[1] Christopher J. Kucharik,[1] Chad Monfreda,[1] Jonathan A. Patz,[1] I. Colin Prentice,[8] Navin Ramankutty,[1] Peter K. Snyder[9]

Land use has generally been considered a local environmental issue, but it is becoming a force of global importance. Worldwide changes to forests, farmlands, waterways, and air are being driven by the need to provide food, fiber, water, and shelter to more than six billion people. Global croplands, pastures, plantations, and urban areas have expanded in recent decades, accompanied by large increases in energy, water, and fertilizer consumption, along with considerable losses of biodiversity. Such changes in land use have enabled humans to appropriate an increasing share of the planet's resources, but they also potentially undermine the capacity of ecosystems to sustain food production, maintain freshwater and forest resources, regulate climate and air quality, and ameliorate infectious diseases. We face the challenge of managing trade-offs between immediate human needs and maintaining the capacity of the biosphere to provide goods and services in the long term.

Land-use activities—whether converting natural landscapes for human use or changing management practices on human-dominated lands—have transformed a large proportion of the planet's land surface. By clearing tropical forests, practicing subsistence agriculture, intensifying farmland production, or expanding urban centers, human actions are changing the world's landscapes in pervasive ways (*1*, *2*) (Fig. 1, fig. S1, and table S1). Although land-use practices vary greatly across the world, their ultimate outcome is generally the same: the acquisition of natural resources for immediate human needs, often at the expense of degrading environmental conditions.

Several decades of research have revealed the environmental impacts of land use throughout the globe, ranging from changes in atmospheric composition to the extensive modification of Earth's ecosystems (*3*–*6*). For example, land-use practices have played a role in changing the global carbon cycle and, possibly, the global climate: Since 1850, roughly 35% of anthropogenic CO_2 emissions resulted directly from land use (*7*). Land-cover changes also affect regional climates through changes in surface energy and water balance (*8*, *9*). Humans have also transformed the hydrologic cycle to provide freshwater for irrigation, industry, and domestic consumption (*10*, *11*). Furthermore, anthropogenic nutrient inputs to the biosphere from fertilizers and atmospheric pollutants now exceed natural sources and have widespread effects on water quality and coastal and freshwater ecosystems (*4*, *12*). Land use has also caused declines in biodiversity through the loss, modification, and fragmentation of habitats; degradation of soil and water; and overexploitation of native species (*13*) (SOM Text S1).

Ironically, just as our collective land-use practices are degrading ecological conditions across the globe, humanity has become dependent on an ever-increasing share of the biosphere's resources. Human activities now appropriate nearly one-third to one-half of global ecosystem production (*14*), and as development and population pressures continue to mount, so could the pressures on the biosphere. As a result, the scientific community is increasingly concerned about the condition of global ecosystems and "ecosystem services" (*15*, *16*) (SOM Text S2).

Land use thus presents us with a dilemma. On one hand, many land-use practices are absolutely essential for humanity, because they provide critical natural resources and ecosystem services, such as food, fiber, shelter, and freshwater. On the other hand, some forms of land use are degrading the ecosystems and services upon which we depend, so a natural question arises: Are land-use activities degrading the global environment in ways that may ultimately undermine ecosystem services, human welfare, and the long-term sustainability of human societies? Here, we examine this question and focus on a subset of global ecosystem conditions we consider most affected by land use. We also consider the challenge of reducing the negative environmental impacts of land use while maintaining economic and social benefits.

Food Production

Together, croplands and pastures have become one of the largest terrestrial biomes on the planet, rivaling forest cover in extent and occupying ~40% of the land surface (*17*, *18*) (Fig. 2). Changing land-use practices have enabled world grain harvests to double in the past four decades, so they now exceed ~2 billion tons per year (*19*). Some of this increase can be attributed to a ~12% increase in world cropland area, but most of these production gains resulted from "Green Revolution" technologies, including high-yielding cultivars, chemical fertilizers and pesticides, and mechanization and irrigation (*4*, *20*) (fig. S2A). During the past 40 years, there has been a ~700% increase in global fertilizer use (*4*, *5*) and a ~70% increase in irrigated cropland area (*21*, *22*).

Although modern agriculture has been successful in increasing food production, it has also caused extensive environmental damage. For example, increasing fertilizer use has led to the degradation of water quality in many regions (*4*, *12*, *13*) (fig. S2B). In addition, some irrigated lands have become heavily salinized, causing the worldwide loss of ~1.5 million hectares of arable land per year, along with an estimated $11 billion in lost production (*20*). Up to ~40% of global croplands may also be experiencing some degree of soil erosion, reduced fertility, or overgrazing (*20*). The loss of native habitats also affects agricultural production by degrading the services of pollinators, especially bees (*23*, *24*). In short, modern agricultural land-use practices may be trading short-term increases in food production for long-term losses

[1]Center for Sustainability and the Global Environment (SAGE), University of Wisconsin, 1710 University Avenue, Madison, WI 53726, USA. [2]Department of Geography and Earth System Science Interdisciplinary Center, University of Maryland, College Park, College Park, MD 20742, USA. [3]Department of Global Ecology, Carnegie Institution of Washington, Stanford, CA 94305, USA. [4]National Center for Atmospheric Research (NCAR), Post Office Box 3000, Boulder, CO 80307–3000, USA. [5]Center for Limnology, University of Wisconsin, 680 North Park Street, Madison, WI 53706, USA. [6]Institute of Arctic Biology, University of Alaska, Fairbanks, AK 99775, USA. [7]Center for Conservation Biology, Department of Biological Sciences, 371 Serra Mall, Stanford University, Stanford, CA 94305, USA. [8]QUEST, Department of Earth Sciences, University of Bristol, Wills Memorial Building, Bristol BS8 1RJ, UK. [9]Department of Atmospheric Sciences, University of Illinois, 105 South Gregory Street, Urbana, IL 61801, USA.

*To whom correspondence should be addressed: jfoley@wisc.edu

†Present address: Woods Hole Research Center, Woods Hole, MA 02543, USA.

in ecosystem services, including many that are important to agriculture.

Freshwater Resources

Land use can disrupt the surface water balance and the partitioning of precipitation into evapotranspiration, runoff, and groundwater flow. Surface runoff and river discharge generally increase when natural vegetation (especially forest) is cleared (*25*, *26*). For instance, the Tocantins River basin in Brazil showed a ~25% increase in river discharge between 1960 and 1995, coincident with expanding agriculture but no major change in precipitation (*26*).

Water demands associated with land-use practices, especially irrigation, directly affect freshwater supplies through water withdrawals and diversions. Global water withdrawals now total ~3900 km^3 yr^{-1}, or ~10% of the total global renewable resource, and the consumptive use of water (not returned to the watershed) is estimated to be ~1800 to 2300 km^3 yr^{-1} (*22*, *27*) (fig. S3A). Agriculture alone accounts for ~85% of global consumptive use (*22*). As a result, many large rivers, especially in semiarid regions, have greatly reduced flows, and some routinely dry up (*21*, *28*). In addition, the extraction of groundwater reserves is almost universally unsustainable and has resulted in declining water tables in many regions (*21*, *28*) (fig. S2, B and C).

Water quality is often degraded by land use. Intensive agriculture increases erosion and sediment load, and leaches nutrients and agricultural chemicals to groundwater, streams, and rivers. In fact, agriculture has become the largest source of excess nitrogen and phosphorus to waterways and coastal zones (*12*, *29*). Urbanization also substantially degrades water quality, especially where wastewater treatment is absent. The resulting degradation of inland and coastal waters impairs water supplies, causes oxygen depletion and fish kills, increases blooms of cyanobacteria (including toxic varieties), and contributes to waterborne disease (*12*, *30*).

Forest Resources

Land-use activities, primarily for agricultural expansion and timber extraction, have caused a net loss of ~7 to 11 million km^2 of forest in the past 300 years (*17*, *32*, *33*). Highly managed forests, such as timber plantations in North America and oil-palm plantations in Southeast Asia, have also replaced many natural forests and now cover 1.9 million km^2 worldwide (*31*).

Many land-use practices (e.g., fuel-wood collection, forest grazing, and road expansion) can degrade forest ecosystem conditions—in terms of productivity, biomass, stand structure, and species composition—even without changing forest area. Land use can also degrade forest conditions indirectly by introducing pests and pathogens, changing fire-fuel loads, changing patterns and frequency of ignition sources, and changing local meteorological conditions (*34*).

In many parts of the world, especially in East Asian countries, reforestation and afforestation are increasing the area of forested lands (*35*). Furthermore, forest management in many regions is acting to improve forest conditions. For example, inadvertent nitrogen fertilization, peatland drainage, and direct management efforts increased the standing biomass of European forests by ~40% between 1950 and 1990, while their area remained largely unchanged (*36*, *37*). These forests have become a substantial sink of atmospheric carbon (~0.14 Pg C yr^{-1} in the 1990s) (*37*), although other ecosystem services (including those provided by peatlands) and biodiversity are likely diminished.

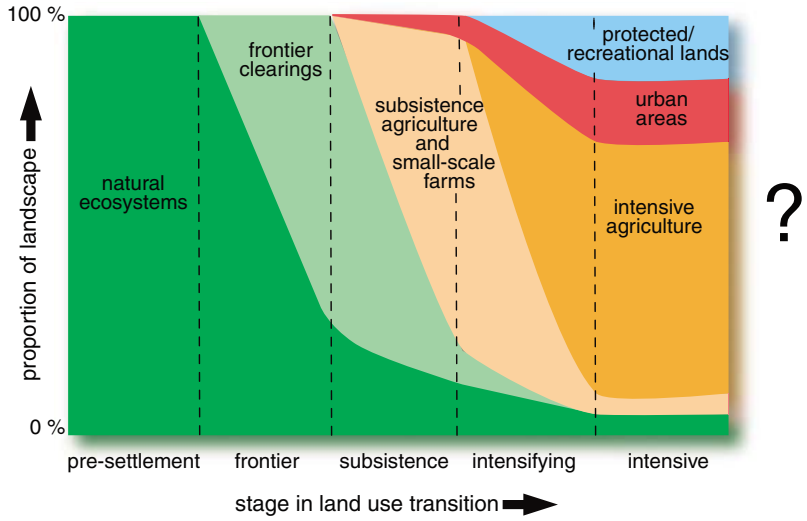

Fig. 1. Land-use transitions. Transitions in land-use activities that may be experienced within a given region over time. As with demographic and economic transitions, societies appear also to follow a sequence of different land-use regimes: from presettlement natural vegetation to frontier clearing, then to subsistence agriculture and small-scale farms, and finally to intensive agriculture, urban areas, and protected recreational lands. Different parts of the world are in different transition stages, depending on their history, social and economic conditions, and ecological context. Furthermore, not all parts of the world move linearly through these transitions. Rather, some places remain in one stage for a long period of time, while others move rapidly between stages. [Adapted from (*1*) and (*2*)]

Regional Climate and Air Quality

Land conversion can alter regional climates through its effects on net radiation, the division of energy into sensible and latent heat, and the partitioning of precipitation into soil water, evapotranspiration, and runoff. Modeling studies demonstrate that land-cover changes in the tropics affect climate largely through water-balance changes, but changes in temperate and boreal vegetation influence climate primarily through changes in the surface radiation balance (*38*). Large-scale clearing of tropical forests may create a warmer, drier climate (*39*), whereas clearing temperate and boreal forest is generally thought to cool the climate, primarily through increased albedo (*40*) (table S2, A and B).

Urban "heat islands" are an extreme case of how land use modifies regional climate. The reduced vegetation cover, impervious surface area, and morphology of buildings in cityscapes combine to lower evaporative cooling, store heat, and warm the surface air (*41*). A recent analysis of climate records in the United States suggests that a major portion of the temperature increase during the last several decades resulted from urbanization and other land-use changes (*9*). Land-cover change has also been implicated in changing the regional climate in China; recent analyses suggest that the daily diurnal temperature range has decreased as a result of urbanization (*42*).

Land-use practices also change air quality by altering emissions and changing the atmospheric conditions that affect reaction rates, transport, and deposition. For example, tropospheric ozone (O_3) is particularly sensitive to changes in vegetation cover and biogenic emissions. Land-use practices often determine dust sources, biomass burning, vehicle emission patterns, and other air pollution sources. Furthermore, the effects of land use on local meteorological conditions, primarily in urban heat islands, also affect air quality: Higher urban temperatures generally cause O_3 to increase (*43*).

Infectious Disease

Habitat modification, road and dam construction, irrigation, increased proximity of people and livestock, and the concentration or expansion of urban environments all modify the transmission of infectious disease and can lead to outbreaks and emergence episodes (*44*). For example, increasing tropical deforestation coincides with an upsurge of malaria

and/or its vectors in Africa, Asia, and Latin America, even after accounting for the effects of changing population density (*44*, *45*).

Disturbing wildlife habitat is also of particular concern, because ~75% of human diseases have links to wildlife or domestic animals (*44*). Land use has been associated with the emergence of bat-borne Nipah virus in Malaysia (*46*), cryptosporidiosis in Europe and North America, and a range of foodborne illnesses globally (*47*). In addition, road building is linked to increased bushmeat hunting, which may have played a key role in the emergence of human immunodeficiency virus types 1 and 2; simian foamy virus was recently documented in hunters, confirming this mechanism of cross-species transfer (*48*).

The combined effects of land use and extreme climatic events can also have serious impacts, both on direct health outcomes (e.g., heat mortality, injury, fatalities) and on ecologically mediated diseases. For example, Hurricane Mitch, which hit Central America in 1998, exhibited these combined effects: 9,600 people perished, widespread water- and vector-borne diseases ensued, and one million people were left homeless (*49*). Areas with extensive deforestation and settlements on degraded hillsides or floodplains suffered the greatest morbidity and mortality (*50*).

Confronting the Effects of Land Use

Current trends in land use allow humans to appropriate an ever-larger fraction of the biosphere's goods and services while simultaneously diminishing the capacity of global ecosystems to sustain food production, maintain freshwater and forest resources, regulate climate and air quality, and mediate infectious diseases. This assertion is supported across a broad range of environmental conditions worldwide, although some (e.g., alpine and marine areas) were not considered here. Nevertheless, the conclusion is clear: Modern land-use practices, while increasing the short-term supplies of material goods, may undermine many ecosystem services in the long run, even on regional and global scales.

Confronting the global environmental challenges of land use will require assessing and managing inherent trade-offs between meeting immediate human needs and maintaining the capacity of ecosystems to provide goods and services in the future (Fig. 3) (*2*, *16*). Assessments of trade-offs must recognize that land use provides crucial social and economic benefits, even while leading to possible long-term declines in human welfare through altered ecosystem functioning (*2*).

Sustainable land-use policies must also assess and enhance the resilience of different land-use practices. Managed ecosystems, and the services they provide, are often vulnerable to diseases, climatic extremes, invasive species, toxic releases, and the like (*51*–*53*). Increasing the resilience of managed landscapes requires practices that are more robust to disturbance and can recover from unanticipated ''surprises.''

There is an increasing need for decision-making and policy actions across multiple geographic scales and multiple ecological dimensions. The very nature of the issue requires it: Land use occurs in local places, with real-world social and economic benefits, while potentially causing ecological degradation across local, regional, and global scales. Society faces the challenge of developing strategies that reduce the negative environmental impacts of land use across multiple services and scales while maintaining social and economic benefits.

What strategies can ameliorate the detrimental effects of land use? Examples of land-management strategies with environmental, social, and economic benefits include increasing agricultural production per unit land area, per unit fertilizer input, and per unit water consumed (*19*, *21*, *54*, *55*); maintaining and increasing soil organic matter in croplands, which is a key to water-holding capacity, nutrient availability, and carbon sequestration

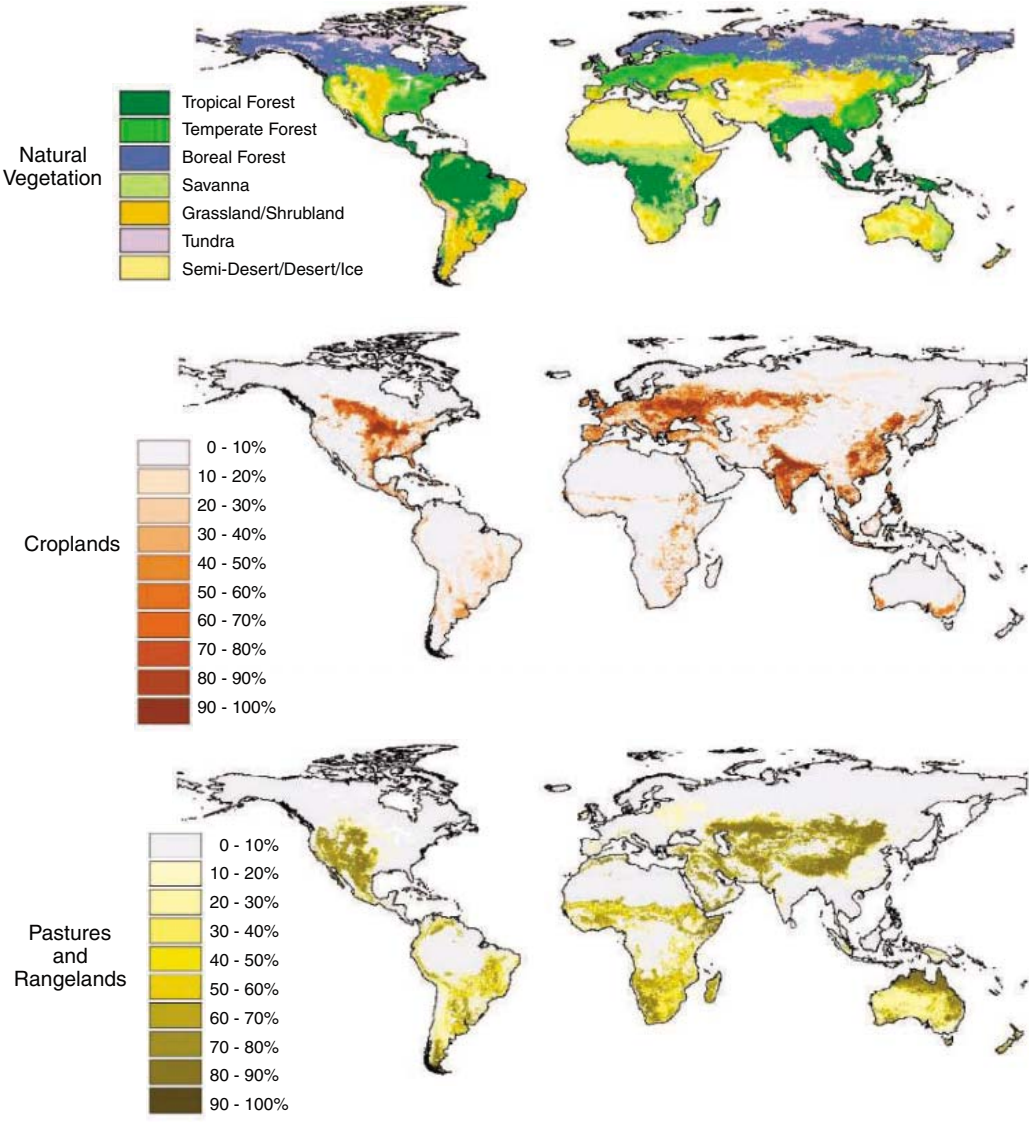

Fig. 2. Worldwide extent of human land-use and land-cover change. These maps illustrate the geographic distribution of "potential vegetation" (top), vegetation that would most likely exist in the absence of human land use, and the extent of agricultural land cover (including croplands and pastures) (middle and bottom) across the world during the 1990s. [Adapted from (*17*) and (*18*)]

(*56–58*); increasing green space in urban areas, thereby reducing runoff and "heat island" effects; employing agroforestry practices that provide food and fiber yet maintain habitats for threatened species; and maintaining local biodiversity and associated ecosystem services such as pollination and pest control. Many of these strategies involve management of landscape structure through the strategic placement of managed and natural ecosystems, so the services of natural ecosystems (e.g., pest control by natural predators, pollination by wild bees, reduced erosion with hedgerows, or filtration of runoff by buffer strips) are available across the landscape mosaic.

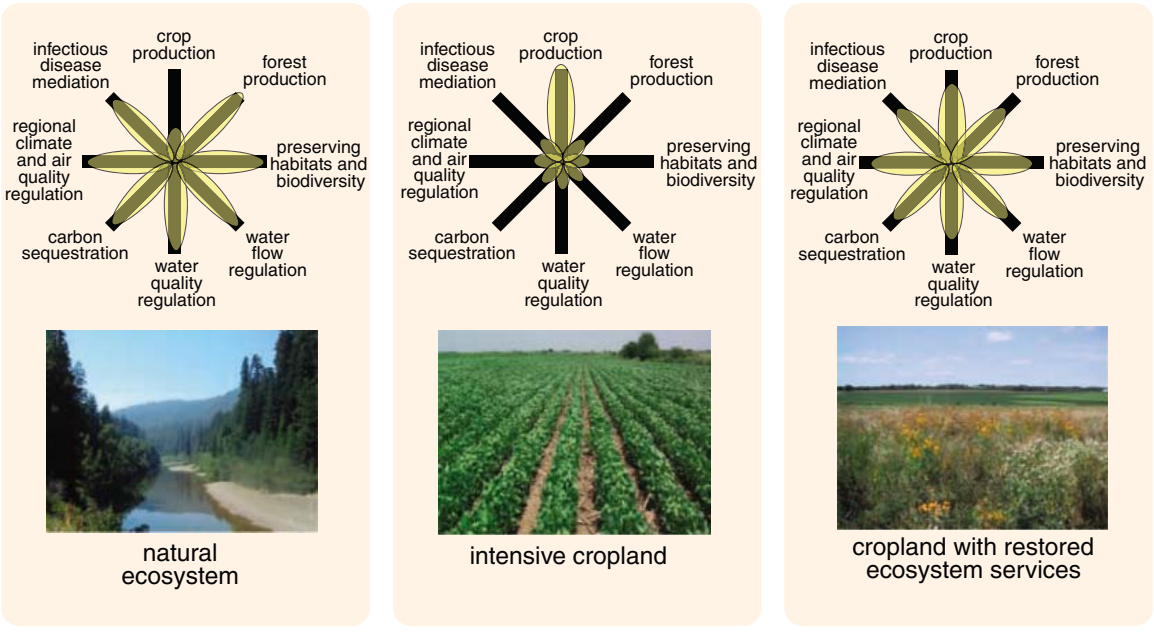

Fig. 3. Conceptual framework for comparing land use and trade-offs of ecosystem services. The provisioning of multiple ecosystem services under different land-use regimes can be illustrated with these simple "flower" diagrams, in which the condition of each ecosystem service is indicated along each axis. (In this qualitative illustration, the axes are not labeled or normalized with common units.) For purposes of illustration, we compare three hypothetical landscapes: a natural ecosystem (left), an intensively managed cropland (middle), and a cropland with restored ecosystem services (right). The natural ecosystems are able to support many ecosystem services at high levels, but not food production. The intensively managed cropland, however, is able to produce food in abundance (at least in the short run), at the cost of diminishing other ecosystem services. However, a middle ground—a cropland that is explicitly managed to maintain other ecosystem services—may be able to support a broader portfolio of ecosystem services.

Local-scale case studies, drawn from a set of worldwide examples, illustrate how land-use practices can offer "win-win-win" environmental, social, and economic benefits:

(i) New York City purchased development rights in watersheds of the Catskill Mountains, which provide water purification services, for ~US$1 billion, instead of building a filtration plant for ~US$6 billion to $8 billion plus annual operating costs of ~US$300 million (*59*).

(ii) Forests in the Yangtze watershed help moderate the discharge of river water, decreasing wet-season flow and enhancing dry-season flow. As a result, the Gezhouba hydroelectric plant produces an additional 40 million kilowatt-hours per year, worth ~US$610,000 per year, or the equivalent of ~40% of the forestry income from the region (*60*).

(iii) Coffee farms within ~1 km of forest benefit from wild pollinators, which can increase coffee yields by ~20% and reduce the frequency of small misshapen coffee beans by ~27% (*24*).

(iv) *Parus major*, a cavity-nesting bird of Europe, reduces the abundance of harmful caterpillars in apple orchards by as much as 50 to 99%. In the Netherlands, the foraging of *P. major* increased apple yields by ~4.7 to 7.8 kg per tree (*61*).

(v) Reflective roofing, green space, and increased shade reduce the effect of urban heat islands, with associated reductions in smog, heat-related mortality, and electricity demands from air conditioning. With such measures, a city like Sacramento, California, could lower its energy costs by ~US$26 million per year and reduce peak ozone concentrations by ~6.5% (*62*).

(vi) Integrated pest management for malaria control (e.g., using larvivorous fish) can reduce the need for chemical pesticides while increasing food supplies. In China, for example, stocking rice paddies with edible fish reduced malaria cases and simultaneously enhanced protein nutrition (*63*).

Developing and implementing regional land-use strategies that recognize both short- and long-term needs, balance a full portfolio of ecosystem services, and increase the resilience of managed landscapes will require much more cross-disciplinary research on human-dominated ecosystems (*16*). However, it will also benefit from closer collaboration between scientists and practitioners—linking, for example, ecologists and land-use planners, hydrologists and farmers, climatologists and architects, and entomologists and physicians. A wide array of skills will be needed to better manage our planet's landscapes and balance human needs, the integrity of ecological infrastructure, the continued flow of ecosystem services, and the long-term health of people and the biosphere.

References and Notes

1. R. DeFries, G. Asner, R. Houghton, Eds., *Ecosystems and Land Use Change*. (American Geophysical Union, Geophysical Monograph Series, Vol. 153, Washington, DC, 2004).
2. R. S. DeFries, J. A. Foley, G. P. Asner, *Front. Ecol. Environ.* **2**, 249 (2004).
3. P. M. Vitousek, H. A. Mooney, J. Lubchenco, J. M. Melillo, *Science* **277**, 494 (1997).
4. P. A. Matson, W. J. Parton, A. G. Power, M. J. Swift, *Science* **277**, 504 (1997).
5. D. Tilman *et al.*, *Science* **292**, 281 (2001).
6. M. Wackernagel *et al.*, *Proc. Natl. Acad. Sci. U.S.A.* **99**, 9266 (2002).
7. R. A. Houghton, J. L. Hackler, ORNL/CDIAC-131, NDP-050/R1 (Oak Ridge National Laboratory, Oak Ridge, TN, 2001).
8. R. A. Pielke Sr. *et al.*, *Philos. Trans. R. Soc. London Ser. B* **360**, 1705 (2002).
9. E. Kalnay, M. Cai, *Nature* **423**, 528 (2003).
10. S. L. Postel, G. C. Daily, P. R. Ehrlich, *Science* **271**, 785 (1996).
11. C. J. Vörösmarty, P. Green, J. Salisbury, R. B. Lammers, *Science* **289**, 284 (2000).
12. E. M. Bennett, S. R. Carpenter, N. F. Caraco, *Bioscience* **51**, 227 (2001).
13. S. L. Pimm, P. Raven, *Nature* **403**, 843 (2000).
14. P. M. Vitousek, P. R. Ehrlich, A. H. Ehrlich, P. A. Matson, *Bioscience* **36**, 368 (1986).
15. G. C. Daily, *Nature's Services: Societal Dependence on Natural Ecosystems* (Island Press, Washington, DC, 1997).
16. Millennium Ecosystem Assessment, *Ecosystems and Human Wellbeing: A Framework for Assessment* (Island Press, Washington, DC, 2003).
17. N. Ramankutty, J. A. Foley, *Global Biogeochem. Cycles* **13**, 997 (1999).
18. G. P. Asner *et al.*, *Annu. Rev. Environ. Resour.* **29** (2004).
19. C. C. Mann, *Science* **283**, 310 (1999).
20. S. Wood, K. Sebastian, S. J. Scherr, *Pilot Analysis of Global Ecosystems: Agroecosystems* (International Food Policy Research Institute and World Resources Institute, Washington, DC, 2000).

21. M. W. Rosegrant, X. Cai, S. A. Cline, *World Water and Food to 2025* (International Food Policy Research Institute, Washington, DC, 2002).
22. P. H. Gleick, *Annu. Rev. Environ. Resourc.* **28**, 275 (2003).
23. C. Kremen, N. M. Williams, R. W. Thorp, *Proc. Natl. Acad. Sci. U.S.A.* **99**, 16812 (2002).
24. T. H. Ricketts, G. C. Daily, P. R. Ehrlich, C. Michener, *Proc. Natl. Acad. Sci. U.S.A.*, in press.
25. V. Sahin, M. J. Hall, *J. Hydrol.* **178**, 293 (1996).
26. M. H. Costa, A. Botta, J. A. Cardille, *J. Hydrol.* **283**, 206 (2003).
27. I. A. Shiklomanov, *UN Comprehensive Assessment of the Freshwater Resources of the World* (State Hydrol. Inst., St. Petersburg, Russia, 1998).
28. S. L. Postel, *Pillar of Sand: Can the Miracle Last?* (W.W. Norton, New York, 1999).
29. S. R. Carpenter *et al.*, *Ecol. Appl.* **8**, 559 (1998).
30. A. R. Townsend *et al.*, *Front. Ecol. Environ.* **1**, 240 (2003).
31. M. Williams, in *The Earth as Transformed by Human Action*, B. L. Turner *et al.*, Eds. (Cambridge Univ. Press, New York, 1990), pp. 179–201.
32. Food and Agriculture Organization, FAOSTAT Forestry Database (2004); http://faostat.fao.org.
33. H. K. Gibbs, thesis, Ohio State University, Columbus, OH (2001).
34. D. C. Nepstad *et al.*, *Nature* **398**, 505 (1999).
35. Fang *et al.*, *Science* **292**, 2320 (2001).
36. P. E. Kauppi *et al.*, *Science* **256**, 70 (1992).
37. G. J. Nabuurs *et al.*, *Global Biogeochem. Cycles* **9**, 152 (2003).
38. P. K. Snyder, C. Delire, J. A. Foley, *Clim. Dyn.* **23**, 279 (2004).
39. M. H. Costa, J. A. Foley, *J. Clim.* **13**, 18 (2000).
40. G. B. Bonan, D. Pollard, S. L. Thompson, *Nature* **359**, 716 (1992).
41. G. B. Bonan, *Ecological Climatology* (Cambridge Univ. Press, Cambridge, 2002).
42. Zhou *et al.*, *Proc. Natl. Acad. Sci. U.S.A.* **101**, 9540 (2004).
43. S. Sillman, F. J. Samson, *J. Geophys. Res.* **100**, 11497 (1995).
44. J. A. Patz *et al.*, *Environ. Health Perspect.* **112**, 1092 (2004).
45. A. Y. Vittor *et al.*, *J. Am. Trop. Med. Hyg.*, in press.
46. K. B. Chua *et al.*, *Lancet* **354**, 1257 (1999).
47. J. B. Rose *et al.*, *Environ. Health Perspect.* **109**, 211 (2001).
48. N. D. Wolfe *et al.*, *Lancet* **363**, 932 (2004).
49. Editorial Staff, *Environ. Health Perspect.* **107**, 139 (1999).
50. A. Cockburn, J. St Clair, K. Silverstein, *Int. J. Health Serv.* **29**, 459 (1999).
51. M. Scheffer *et al.*, *Nature* **413**, 591 (2001).
52. R. Costanza *et al.*, *Bioscience* **50**, 149 (2000).
53. B. L. Turner II *et al.*, *Proc. Natl. Acad. Sci. U.S.A.* **100**, 8074 (2003).
54. C. R. Frink *et al.*, *Proc. Natl. Acad. Sci. U.S.A.* **96**, 1175 (1999).
55. K. G. Cassman, A. Dobermann, D. T. Walters, *Ambio* **31**, 132 (2002).
56. D. Tilman, *Nature* **396**, 211 (1998).
57. N. J. Rosenberg, R. C. Izaurralde, *Clim. Change* **51**, 1 (2001).
58. R. Lal, *Clim. Change* **51**, 35 (2001).
59. President's Committee of Advisors on Science and Technology, Panel on Biodiversity and Ecosystems (Office of Science and Technology Policy, Washington, DC, 1998).
60. Z. Guo, X. Xiangming, L. Dianmo, *Ecol. Appl.* **10**, 925 (2000).
61. C. M. M. Mols, M. E. Visser, *J. Appl. Ecol.* **39**, 888 (2002).
62. U.S. Environmental Protection Agency, Heat Island Effect, http://yosemite.epa.gov/oar/globalwarming.nsf/content/ActionsLocalHeatIslandEffect.html (2003).
63. N. Wu *et al.*, *SE Asian J Trop Med Public Health* **22**, 436 (1991).

64. We acknowledge the important contributions of both the American Geophysical Union Chapman Conference on Ecosystems and Land Use Change and the Millennium Ecosystem Assessment in spurring these ideas. We also wish to thank S. Donner, D. Foley, and anonymous reviewers for their constructive comments on earlier versions of the manuscript. We are grateful to M. Sternitzky and N. Olejniczak for the maps and illustrations and to K. Flick and C. Webb for help with the references. The authors declare that they have no competing financial interests.

Supporting Online Material

www.sciencemag.org/cgi/content/full/309/5734/570/DC1
SOM Text
Figs. S1 to S3
Tables S1 and S2
References

10.1126/science.1111772

Web-Spinning Caterpillar Stalks Snails

Daniel Rubinoff* and William P. Haines

The Hawaiian archipelago is the most isolated landmass on Earth, and this isolation appears to have allowed for feeding strategies that occur nowhere else, particularly for invertebrates. Among the novelties discovered in Hawaii are ambush predator caterpillars (*1*), damselflies with terrestrial nymphs (*2*), and spiders that impale their prey in flight (*3*). Web-spinning caterpillars that feed on snails are an equally unusual addition to this list of Hawaiian anomalies.

The order Lepidoptera consists overwhelmingly of herbivorous species: Of ~150,000 described species of moths and butterflies worldwide (*4*), only ~200 species (0.13%) are known to be obligate predators or parasites (*5*). Of these, most feed on soft-bodied scale insects or ant brood and belong to a few species-rich lineages (*5*), suggesting that predatory lifestyles have evolved only a few times in moths and butterflies. Here we report a Hawaiian predatory caterpillar specializing on snails. No other Lepidoptera have been reported to feed on mollusks.

The caterpillars of the newly described species *Hyposmocoma molluscivora* (Cosmopterigidae) (supporting online text) are small (~8 mm in length) case-bearers that lumber along leaves of various plants in mesic forests. The caterpillars do not eat plant foliage, even when starving. Because a snail's shell presents a unique challenge to predators, *H. molluscivora* has evolved a specialized strategy. Although all caterpillars have silk glands, this predatory caterpillar uses silk in a spiderlike fashion to capture and immobilize prey. When they encounter a resting snail of the native genus *Tornatellides*, they immediately begin to spin silk webbing attaching the snail shell to the leaf on which it rests, apparently to prevent the snail from sealing itself against the leaf or dropping to the ground once the larva attacks the soft tissue of the living snail (Fig. 1). The larva then wedges its case next to or inside the snail shell and stretches much of its body out of its silk case, pursuing the retreating snail to the end of the shell from which there is no escape. We observed 18 attacks by 10 different larvae following this sequence.

Hyposmocoma is an endemic Hawaiian genus of small moths containing 350 recognized species (*2*), making it second only to Hawaiian *Drosophila* in numbers of endemic species. The diversity of ecological niches occupied by *Hyposmocoma* spp. far exceeds that of *Drosophila* spp., with different species of the moths specializing on most native plants, dead wood, lichens, algae (both aquatic and terrestrial), or detritus. Land snails are unusual prey even in a Lepidopteran genus with such a broad range of phytophagous species. The native genus of *Tornatellides* snails may represent a specific food source, because the caterpillars are always found in close association with the snails and often have small snail shells attached to their cases.

Other anomalous associations may exist for other *Hyposmocoma*, as the larval habits of most species are unknown. The moths have representatives in habitats as diverse as new lava flows and primary forest and ranging from sea level to alpine scrub at elevations of more than 3300 m. The widespread destruction of lowland habitats and the extinction of large numbers of endemic Hawaiian plant species suggest that *Hyposmocoma* diversity has also suffered greatly, especially as the moths show a very high degree of local endemism, with greater than 90% of the species endemic to a single island (*2*). The nature preserves where these snail-eaters are found contain some of the last vestiges of mesic forest in the archipelago. It is imperative that remaining native habitat be preserved to maintain other, as yet undiscovered, evolutionary novelties that are uniquely Hawaiian. Research on how such unusual evolutionary phenomena arose in Hawaii may help to explain their rarity in the rest of the world.

In addition to *H. molluscivora* from Maui (figs. S1 to S5), another, undescribed species with snail-eating caterpillars has been collected from the island of Molokai, and there are similar reports from other islands, suggesting a radiation of predatory moths with caterpillars that have unique tastes and unorthodox hunting methods.

Caterpillars and terrestrial snails co-occur widely on all the continents where they are present, but only in Hawaii have caterpillars evolved to hunt snails. Specialized predatory behavior by lepidopteran larvae, an extremely rare phenomenon worldwide, has independently arisen at least twice in Hawaii, both in ambush predator geometrid caterpillars (*1*) and in the *Hyposmocoma* caterpillars, providing fresh evidence of the importance of isolation in the evolution of novel traits.

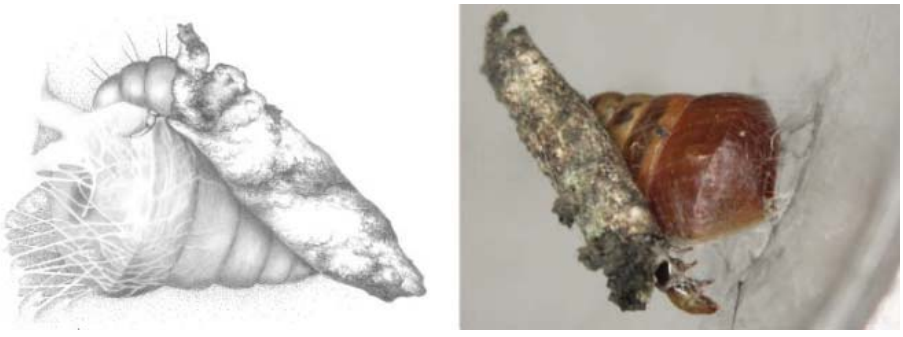

Fig. 1. The case-bearing caterpillar of *H. molluscivora* binds its snail prey to a leaf with silk restraints.

References and Notes

1. S. L. Montgomery, *Entomol. Gen.* **8**, 27 (1982).
2. E. C. Zimmerman, *Insects of Hawaii* (Univ. of Hawaii Press, Honolulu, HI, 1948 and 1978), vols. 2 and 9.
3. R. G. Gillespie, *Nature* **355**, 212 (1992).
4. N. P. Kristensen, A. W. Skalski, in *Lepidoptera: Moths and Butterflies*, N. P. Kristensen, Ed. (Walter de Gruyter, Berlin, 1999), chap. 2.
5. N. E. Pierce, *J. Lepid. Soc.* **49**, 412 (1995).

6. We thank M. Bryce, S. Montgomery, F. Starr, and K. Starr for bringing specimens to our attention; B. Holland and R. Cowie of the University of Hawaii for identifying snail specimens; F. Duvall for access to the Makawao Forest Reserve; and T. Lau of The Nature Conservancy Hawaii for access to the Kamakou Preserve. Figure 1A was drawn by J. Winhall-Rice.

Supporting Online Material

www.sciencemag.org/cgi/content/full/309/5734/575/DC1
SOM Text
Figs. S1 to S5
References and Notes

28 January 2005; accepted 15 April 2005
10.1126/science.1110397

310 Gilmore Hall, Department of Plant and Environmental Protection Sciences, 3050 Maile Way, University of Hawaii, Honolulu, HI 96822, USA.

*To whom correspondence should be addressed. E-mail: rubinoff@hawaii.edu

^{142}Nd Evidence for Early (>4.53 Ga) Global Differentiation of the Silicate Earth

M. Boyet* and R. W. Carlson

New high-precision samarium-neodymium isotopic data for chondritic meteorites show that their ^{142}Nd/^{144}Nd ratio is 20 parts per million lower than that of most terrestrial rocks. This difference indicates that most (70 to 95%) of Earth's mantle is compositionally similar to the incompatible element–depleted source of mid-ocean ridge basalts, possibly as a result of a global differentiation 4.53 billion years ago (Ga), within 30 million years of Earth's formation. The complementary enriched reservoir has never been sampled and is probably located at the base of the mantle. These data influence models of Earth's compositional structure and require revision of the timing of global differentiation on Earth's Moon and Mars.

Radiogenic isotope tracers are often used to understand the chemical evolution of planetary bodies. In one system, Sm decays to Nd via two radioactive decay schemes: ^{146}Sm-^{142}Nd [half-life $T_{1/2}$ = 103 million years (My)] and ^{147}Sm-^{143}Nd [$T_{1/2}$ = 106 billion years (Gy)]). Both Sm and Nd are refractory lithophile (prefer silicates over metal) elements, whose relative abundances should not be affected by either volatile loss or core formation. The long-lived ^{147}Sm-^{143}Nd system has been widely used to trace planetary-scale processes such as the evolution of the bulk silicate Earth (BSE, defined as all the Earth except for its metallic core) and its chemical differentiation into crust and mantle over Earth's history. The early epic of Earth's differentiation is better investigated with the short-lived chronometer ^{146}Sm-^{142}Nd, because of the lack of available samples from Earth's first 500 My of existence and the sensitivity of most long-lived radioactive systems to resetting by events occurring later in Earth's history. Recent studies have reported small ^{142}Nd/^{144}Nd excesses in a small number of samples from 3.8 Ga from the Isua Supracrustal Belt, Greenland (*1*, *2*), which is the first evidence for differentiation of the silicate portion of Earth that must have occurred close in time to the well-documented early differentiation of the Moon (*3*) and Mars (*4*, *5*). The standard assumption in using this radiometric system to model the geochemical evolution of Earth is that the BSE has Sm/Nd, ^{143}Nd/^{144}Nd, and ^{142}Nd/^{144}Nd ratios approximately equal to those of chondritic meteorites, the building blocks of the planet. Chondritic meteorites show a relatively limited range in Sm/Nd (^{147}Sm/^{144}Nd from 0.1932 to 0.2000), with corresponding ^{143}Nd/^{144}Nd from 0.512525 to 0.512722, when fractionation is corrected to ^{146}Nd/^{144}Nd = 0.7219 (*6*–*8*), and the average chondritic values of 0.1966 and 0.512638 (*6*) have been used to represent the BSE model values for 25 years. Here we present Sm-Nd data from chondrites that overlap previous Sm/Nd and ^{143}Nd/^{144}Nd ratio determinations but indicate a measurable difference of ^{142}Nd/^{144}Nd ratios between chondrites and all terrestrial samples. If the BSE has an Sm/Nd ratio within the range measured for chondrites, the higher-than-chondritic ^{142}Nd/^{144}Nd ratio of terrestrial materials requires that the silicate Earth experienced a global chemical differentiation during the lifetime of ^{146}Sm, resulting in high and complementary low Sm/Nd ratio reservoirs that have remained separate over all of Earth's history.

Terrestrial Sm-Nd evolution. The most active volcanic system on Earth, the global ocean ridge system, erupts magmas with ^{143}Nd/^{144}Nd ratios considerably higher than any value measured for bulk chondritic meteorites. This value reflects the high Sm/Nd ratio and the general depletion of the oceanic mantle in those elements that selectively partition into melts (the so-called incompatible elements), because Nd is more incompatible than Sm. The incompatible element depletion of the mid-ocean ridge basalt (MORB) source generally is modeled as resulting from the extraction of the incompatible element–rich continental crust over Earth's history. To explain the high Sm/Nd in the MORB source purely by continental crust extraction from a mantle that initially had chondritic Sm/Nd, only roughly one-third to one-half of the mantle can be as incompatible element–depleted as the MORB source (*9*–*11*). The rest of the mantle has typically been assumed to have remained primitive, with a chondritic Sm/Nd ratio. However, some observations are difficult to reconcile with this model (*12*, *13*). For example, recent seismic imaging of the mantle suggests that convective motion may stir at least the upper three-quarters of the mantle (*14*), if not most of it. Also, the oldest crustal rocks on Earth (dating to 4 Ga) have superchondritic ^{143}Nd/^{144}Nd ratios, requiring an episode of even earlier crustal extraction, although only volumetrically insignificant amounts of this pre–4-Ga crust survive at Earth's surface today (*15*, *16*). Other evidence that the incompatible element depletion that now characterizes the MORB source mantle is an old feature, not related to the formation of the current continental crust, is the presence of excess ^{129}Xe (derived from the decay of 17-My–half-life ^{129}I) and Pu-fission Xe in the MORB, which indicate that the source must have been outgassed within 50 My of Earth's formation (*17*, *18*).

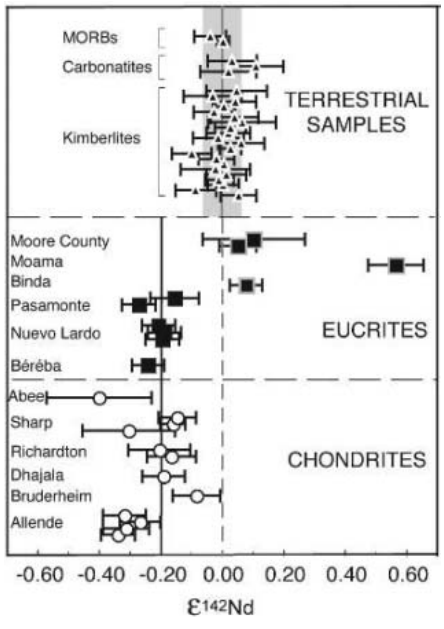

Fig. 1. ^{142}Nd/^{144}Nd ratios measured for chondrites and eucrites compared to the La Jolla terrestrial Nd standard (ε^{142}Nd). All chondrites and basaltic eucrites have negative ε^{142}Nd values outside the external analytical error of ± 0.07 ε units (2σ) (shaded area). Cumulate eucrites have positive ε^{142}Nd values in agreement with their high Sm/Nd, resulting from igneous processes on their parent body. The error bars correspond to the internal precision ($2\sigma_{mean}$). Terrestrial samples (MORBs, kimberlites, and carbonatites of different ages and collected in diverse locations) measured using the same procedure (*27*) have been added to demonstrate the significant excess of 0.2 ε units in all the terrestrial material (samples and standard) relative to the mean chondritic value. All terrestrial samples were measured several times using the same procedures as were used for the chondrites. The uncertainties reported on the mean are 2σ.

Department of Terrestrial Magnetism, Carnegie Institution of Washington, 5241 Broad Branch Road, N.W., Washington, DC 20015, USA.

*To whom correspondence should be addressed. E-mail: boyet@dtm.ciw.edu

Chondritic $^{142}Nd/^{144}Nd$. Because of the small variations in $^{142}Nd/^{144}Nd$, ^{142}Nd studies generally use a terrestrial Nd standard to express the ^{142}Nd anomalies in samples by direct comparison between the two measurements $\{\varepsilon^{142}Nd = [(^{142}Nd/^{144}Nd)_{sample} / (^{142}Nd/^{144}Nd)_{standard} - 1] \times 10^4\}$ on the assumption that the terrestrial standard has chondritic $^{142}Nd/^{144}Nd$. This assumption was derived from measurements that showed no resolvable difference between the $^{142}Nd/^{144}Nd$ of chondrites and that of the laboratory standard. For example, works by Jacobsen and Wasserburg (*6*, *7*), which are the only published measurements of bulk chondrites that include $^{142}Nd/^{144}Nd$ data, reported an average $\varepsilon^{142}Nd$ of –0.04 ± 0.54 (2σ of the population) with a range from –0.5 ± 0.4 to +0.4 ± 0.4. Amelin and Rotenberg (*19*) reported measurements of individual chondrules and phosphates separated from a variety of chondrites that provide a ^{146}Sm-^{142}Nd isochron and would yield a present-day value of $\varepsilon^{142}Nd$ = 0.01 ± 0.83 for a $^{147}Sm/^{144}Nd$ of 0.1966. The relatively large errors reflect that these data were either obtained on an older generation of mass spectrometer; measured NdO^+ instead of Nd^+, thus requiring an additional correction for oxygen isotopic composition and further complicating correction for Ce, Pr, and Sm interference; or were run on small samples. Today, a precision of a few parts per million (ppm) on Nd isotope ratios can be obtained with the new generation of thermal ionization mass spectrometer (*2*, *20*).

We measured the isotopic composition of Sm and Nd on a Thermo-Finnigan Triton thermal ionization mass spectrometer using the Nd^+ ion beam on samples passed repeatedly through ion-exchange chemistry, in order to reduce Ce and Sm interferences to negligible levels. Details of the analytical procedures and all the raw isotopic data measured on these samples are provided in the supporting online material (*21*). All of the analyzed chondrites and basaltic eucrites have $^{142}Nd/^{144}Nd$ ratios lower than the La Jolla Nd standard by between –40 and –8 ppm (Table 1). The deviations compared with the terrestrial reference are clearly significant because the external precision (2σ) measured on repeated runs is lower than 7 ppm for both samples and standards (Fig. 1 and Table 1). Both the $^{142}Nd/^{144}Nd$ and $^{143}Nd/^{144}Nd$ ratios of the chondrites and basaltic eucrites are positively correlated with their $^{147}Sm/^{144}Nd$ ratios, but the very small spread in $^{147}Sm/^{144}Nd$ ratios does not allow for precise isochrons to be constructed (Fig. 2). The mean values of $^{147}Sm/^{144}Nd$, $^{143}Nd/^{144}Nd$, and $^{142}Nd/^{144}Nd$ for the chondrites we measured are 0.1948 ± 0.0018, 0.512611 ± 0.000048, and –0.20 ± 0.14 ε units, respectively ($^{142}Nd/^{144}Nd$ expressed relative to the average for La Jolla Nd). The data for the enstatite (E)-chondrite, Abee, were excluded from this average because of the relatively poor-quality data for this sample. The averages of the basaltic eucrites measured here are indistinguishable within error from these chondrite averages. The chondrite average Sm/Nd ratio is slightly lower than the average of previous chondrite determinations, but our data scatter along a 4.567-Ga ^{147}Sm-^{143}Nd isochron (Fig. 2A), overlapping other recent chondrite results (*8*). Increasing the measured Sm/Nd for the samples reported here by 0.2% to account for our low measured Sm/Nd for the California Institute of Technology n(Sm/Nd)β standard, compared with that reported by Patchett *et al*. (*8*), would increase the degree of overlap of these data. Earlier chondrite Sm-Nd results (*6*, *7*) are offset to slightly higher $^{147}Sm/^{144}Nd$ for a given $^{143}Nd/^{144}Nd$. This offset may be because these earlier results were measured as NdO^+ and a linear instead of exponential relationship was applied, normalizing to $^{150}Nd/^{142}Nd$ or $^{146}Nd/^{142}Nd$ for mass fractionation correction, all of which complicate data comparison at this level of precision.

Early terrestrial differentiation. The homogeneity of the $^{142}Nd/^{144}Nd$ ratio among terrestrial samples has been widely demonstrated, especially with studies on Archean samples, but also in MORBs, ocean island basalts, kimberlites, and carbonatites, where $^{142}Nd/^{144}Nd$ excesses of a few parts per million (5 to 30) have been measured only in 3.8-Ga samples from Isua (*1*, *2*, *22*–*28*). However, all of these $^{142}Nd/^{144}Nd$ values were always compared to the measured value for the terrestrial Nd standard. Thus, the difference between all measured terrestrial values and the $^{142}Nd/^{144}Nd$ ratio of chondrites was not evident. Our new chondrite data show that ^{142}Nd anomalies in terrestrial samples relative

Table 1. Sm-Nd isotope and concentration data for chondrite and eucrite samples. Sm and Nd concentrations were determined by isotope dilution on a spiked aliquot taken after dissolution. $^{143}Nd/^{144}Nd$ ratios are normalized to 0.511860 for the La Jolla Nd standard. $^{142}Nd/^{144}Nd$ ratios are expressed in epsilon notation relative to La Jolla Nd (*21*). For Nuevo Laredo, Pasamonte, and one Sharp, Nd isotopic measurements were made on the same aliquot (only one dissolution) but loaded on separate filaments run in different barrels. The analytical uncertainties correspond to internal within-run precision (2σm). The external reproducibility on the $^{142}Nd/^{144}Nd$ ratio is about 7 ppm, except for Pasamonte. The lower precision reported for one measurement of Sharp and for Abee is explained by the small Nd signal. Dissolution in steel-jacket Teflon bombs or closed beakers on a hot plate produced no difference in results. The $\varepsilon^{149}Sm$ of 0 [$^{149}Sm/^{152}Sm$ ratios relative to the mean of the Sm standard (n = 7 samples)] measured for different samples signifies that isotopic ratios have not been significantly affected by neutron fluence effects. The internal precision on $\varepsilon^{149}Sm$ is lower than 0.3 ε units. Bas. Euc., basaltic eucrite; Cum. Euc., cumulate eucrite.

Meteorite name	Class	Sm	Nd	$^{147}Sm/^{144}Nd$	$^{143}Nd/^{144}Nd$ ± 2σm	$\varepsilon^{142}Nd$ ± 2σm	$\varepsilon^{149}Sm$
Allende*	CV3	0.3147	0.9858	0.1930	0.512573 ± 0.000003	–0.26 ± 0.07	–0.47
Allende	CV3	0.3238	1.010	0.1938	0.512563 ± 0.000002	–0.34 ± 0.05	–0.55
Allende	CV3	0.3128	0.9802	0.1929	0.512558 ± 0.000003	–0.31 ± 0.07	–0.64
Allende	CV3				0.512560 ± 0.000003	–0.32 ± 0.07	–0.25
Bruderheim	L6	0.1746	0.5399	0.1955	0.512620 ± 0.000003	–0.08 ± 0.08	0.19
Dhajala	H3.8	0.2012	0.6225	0.1954	0.512621 ± 0.000003	–0.19 ± 0.07	–0.58
Richardton*	H5	0.1912	0.5952	0.1942	0.512622 ± 0.000003	–0.16 ± 0.08	–2.17
Richardton	H5				0.512632 ± 0.000004	–0.20 ± 0.10	–2.60
Sharp	H3.4	0.1855	0.5722	0.1959	0.512624 ± 0.000006	–0.30 ± 0.15	–1.61
Sharp	H3.4	0.1901	0.5920	0.1951	0.512622 ± 0.000002	–0.16 ± 0.04	
					0.512627 ± 0.000003	–0.14 ± 0.06	
Abee	EH4	0.1460	0.4640	0.1903	0.512586 ± 0.000008	–0.40 ± 0.17	–0.20
Béréba	Bas. Euc.	1.699	5.284	0.1944	0.512597 ± 0.000002	–0.24 ± 0.05	0.09
Nuevo Laredo	Bas. Euc.	2.661	8.283	0.1942	0.512602 ± 0.000003	–0.19 ± 0.06	–0.34
					0.512601 ± 0.000002	–0.19 ± 0.05	
					0.512599 ± 0.000002	–0.21 ± 0.05	
Pasamonte	Bas. Euc.	2.293	7.126	0.1945	0.512598 ± 0.000002	–0.27 ± 0.05	–0.25
					0.512599 ± 0.000003	–0.15 ± 0.08	
Binda	Cum. Euc.	0.3566	0.9857	0.2187	0.513319 ± 0.000002	0.08 ± 0.05	0.60
Moama	Cum. Euc.	0.1575	0.3772	0.2523	0.514397 ± 0.000004	0.57 ± 0.09	–0.54
Moore County	Cum. Euc.	0.7071	2.082	0.2053	0.512996 ± 0.000003	0.05 ± 0.06	–0.36
					0.512988 ± 0.000007	0.10 ± 0.17	

*Dissolution in steel-jacket Teflon bomb.

to chondrites are not scarce; they are ubiquitous. Two explanations can account for this observation: (i) the BSE actually has an Sm/Nd ratio higher than that measured for chondrites, or (ii) all terrestrial rocks derive from a mantle reservoir with a high Sm/Nd ratio formed during the short lifetime of ^{146}Sm, that is, in the first 300 My of solar-system history. Given the refractory lithophile nature of both Sm and Nd and the small range of Sm/Nd ratios measured in different types of chondrites, there is no obvious reason to expect the BSE to have a higher-than-chondritic Sm/Nd ratio, but this option is not impossible. Regardless of whether the high ^{142}Nd/^{144}Nd ratios of terrestrial rocks reflect a nonchondritic Sm/Nd ratio in the BSE or an early differentiation event, the result requires major revision of models of the evolution and structure of Earth's interior.

The evolution of the 20-ppm excess in the ^{142}Nd/^{144}Nd ratios observed in terrestrial rocks requires a superchondritic Sm/Nd ratio, the magnitude of which depends on when the high Sm/Nd ratio was formed. The later the high Sm/Nd reservoir formed, the higher its Sm/Nd ratio must be to evolve the observed excess in ^{142}Nd/^{144}Nd value compared with that of chondrites. Because the Sm/Nd ratio also affects evolution of the ^{143}Nd/^{144}Nd value, any formation time for this reservoir more than 30 My after solar system formation would require an Sm/Nd ratio so high that the reservoir would evolve a ^{143}Nd/^{144}Nd value higher than that measured in MORBs (Fig. 3). For formation times of 4.562 and 4.537 Ga, the ^{147}Sm/^{144}Nd ratios needed to evolve a 20-ppm excess in ^{142}Nd/^{144}Nd value over the average chondrite value in our data are 0.209 and 0.212, respectively, which translate into present-day ^{143}Nd/^{144}Nd ratios of 0.513041 (ε^{143}Nd = +8.4) and 0.513129 (ε^{143}Nd = +10.1). These values overlap the range of Nd isotopic compositions measured in MORBs and also pass through the data for Archean samples (Fig. 4A).

Size and composition of early terrestrial reservoirs. Because all terrestrial rocks analyzed so far have ^{142}Nd/^{144}Nd values higher than our chondritic values, including the Isua samples, which are higher still, the early-formed high Sm/Nd reservoir inside Earth must have been the primary source for crust formation throughout at least the last 4 Gy of Earth's history. Constraints on the size and composition of the high Sm/Nd reservoir (termed here the "early depleted reservoir" or EDR), and its low Sm/Nd complement (termed the "early enriched reservoir" or EER) can be derived by considering the effect that the continental crust extraction would have on the composition of the mantle from which it was derived. Models relating depletion of the MORB mantle to extraction of the continental crust (*9–11*) use the mass balance equation of elements between continental crust and depleted mantle

$$[x]_{CC} \times M_{CC} + [x]_{MORBs} \times M_{MORBs} = [x]_{BSE} \times M_{BSE} \quad (1)$$

where $[x]$ represents the concentration of element x in the continental crust (CC), MORB source mantle (MORBs), and BSE, and M is the mass of these reservoirs. Given estimates for the average composition of continental crust (*29*), the depleted mantle (*30*), the BSE (*31*), and the known mass of the continental crust, this equation can be solved, providing the one-third to one-half value mentioned earlier (*9–11*). However, the nonchondritic ^{142}Nd/^{144}Nd of all terrestrial rocks requires a new mass balance equation

$$[x]_{CC} \times M_{CC} + [x]_{MORBs} \times M_{MORBs} = [x]_{EDR} \times M_{EDR} \quad (2)$$

The Sm/Nd ratio needed to evolve the superchondritic terrestrial ^{142}Nd/^{144}Nd results in a present-day ^{143}Nd/^{144}Nd value close to the value measured for the MORB. Therefore, the extraction of continental crust from this already-depleted reservoir (the EDR) cannot have greatly increased the Sm/Nd ratio of the MORB source; otherwise its ^{143}Nd/^{144}Nd value would have evolved to higher values than those observed for any terrestrial rock.

In order to minimize the effect of continent extraction on the degree of compositional fractionation of the residual mantle, the volume of mantle from which the continental crust was extracted must be large. For example, if the EDR was formed at 4.53 Ga, the ^{147}Sm/^{144}Nd ratio of 0.213 that is needed to evolve the terrestrial ^{142}Nd/^{144}Nd value is well matched by adding continental crust (*29*) to mantle with MORB source composition (*30*), only if the volume of mantle is as large as the whole mantle overlying the D″ layer. In other words, roughly 96% of the mantle must be as incompatible element–depleted as the MORB source, if the continents formed from an EDR with an Sm/Nd ratio high enough to explain the terrestrial ^{142}Nd/^{144}Nd value. Sufficient uncertainty exists in the crustal and MORB source compositions to allow a slightly smaller EDR, but the overriding result is that mantle that is compositionally similar to the MORB source must occupy most of the mantle.

The nonchondritic ^{142}Nd/^{144}Nd value of terrestrial rocks diminishes the importance of a chondritic, or BSE, composition source in the interpretation of the chemical and isotope systematics of Earth. The observation that the Nd-Hf isotope correlation displayed by oceanic basalts does not simultaneously pass through chondritic Hf and Nd isotopic composition is a problem that has led to debate (*32*). But there is no reason why this correlation should pass through chondritic composition if these reservoirs were derived from an EDR instead of the BSE. Similarly, the correlation between Nd and Sr isotopic composition defined by oceanic basalts has been used to estimate the BSE values of Sr isotopic composition, and hence Rb/Sr ratio, on the as-

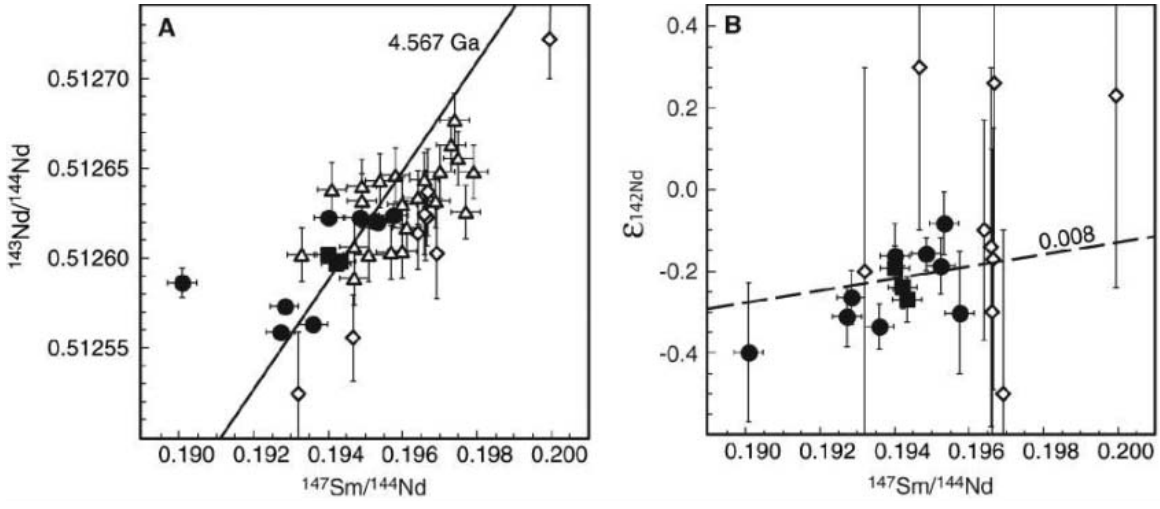

Fig. 2. (**A**) ^{147}Sm-^{143}Nd isochron diagram for chondrites (solid circles) and basaltic eucrites (solid squares) measured in this work. Our data and all previous chondrite measurements (open symbols) scatter along a 4.567-Ga isochron (*44*). Diamonds are from (*6*, *7*) and triangles are from (*8*). Errors bars correspond to the internal precision (2σ). (**B**) ^{146}Sm-^{142}Nd evolution diagram plots as ε^{142}Nd versus ^{147}Sm/^{144}Nd. The symbols are the same as in (A). Shown for reference is a line corresponding to ^{142}Nd/^{144}Nd evolution with the estimated solar system initial ^{146}Sm/^{144}Nd of ~0.008 (*45–48*).

sumption that Earth should have a chondritic Sm/Nd ratio. This assumption is no longer valid, at least for the portion of the mantle that has participated in crust formation. Thus, the BSE concentration of elements such as Rb and Pb, whose volatility and/or siderophile (metallic phase) nature make it unlikely that they are present in chondritic relative abundances in the BSE, depends strongly on the composition of the complementary enriched reservoir produced during early terrestrial differentiation.

A missing reservoir? The lack of terrestrial samples with subchondritic $^{142}Nd/^{144}Nd$ values indicates either that the BSE has a superchondritic Sm/Nd ratio or that the EER that is complementary to the early-formed EDR has never substantially participated in surface volcanism; thus, its composition is poorly constrained. An estimate of the composition of the EER can be obtained from a similar mass-balance approach on the assumption that EDR + EER = BSE, approximating the EDR composition by using that estimated for the MORB source mantle (*30*). This approach depends on the accuracy of the BSE composition, which, for the reasons described above, is now robust only for refractory lithophile elements, and on whether the MORB source is an adequate representation of the composition of the EDR. As shown in Fig. 5, if the EER is small, for example, the size of the D″ layer, then it must be quite enriched in incompatible elements to explain the magnitude of incompatible element depletion in the EDR. If the EER is as large as the mantle beneath 1600 km (*14*), then it will be considerably less enriched than a D″ EER, but still enriched by about a factor of 2 in most incompatible elements as compared with the BSE. The EER, regardless of its size, would thus contain about 43% of Earth's U, Th, and K, leading to ~9 TW of heat production. The lack of a signature of any low $^{142}Nd/^{144}Nd$ reservoir in crustal rocks suggests that the EER could reside at the base of the mantle and has not participated in producing rocks sampled at Earth's surface. As such, there is no compelling reason to assume that mantle convection is layered at mid-mantle depths based on the Sm-Nd data, but that there is a convective boundary at great depth in the mantle that has effectively isolated the small EER part of the mantle, unless the BSE has a nonchondritic composition. A similar model for a deep enriched reservoir and its implications for high heat production and for the rare gas evolution of Earth has recently been presented (*18*). In these models, the EER could serve both as a heat source for plume formation (*33*) and as a warm blanket to keep the outer core molten throughout Earth history and provide the energy needed to drive the geodynamo (*34*).

How the EER formed is suggested by the smooth BSE-normalized incompatible-element patterns calculated here for the EER. Most of the elements shown in Fig. 5 are refractory

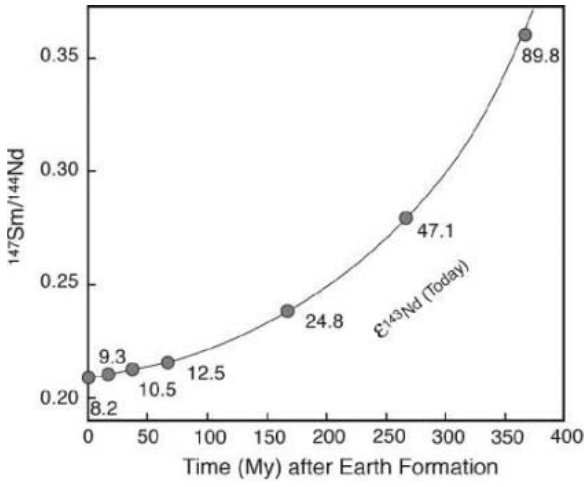

Fig. 3. Sm/Nd ratios needed to produce a 20-ppm excess in $^{142}Nd/^{144}Nd$ ratios, depending on when the Sm/Nd ratio is increased from the average chondritic value. The later the fractionation event, the higher the Sm/Nd ratio must be in the second stage to evolve the observed terrestrial excess in $^{142}Nd/^{144}Nd$ as compared to chondrites. The corresponding present-day $^{143}Nd/^{144}Nd$ ratios [expressed as $\varepsilon^{143}Nd$ relative to the average chondrite values of (*6*)] for these Sm/Nd ratios are shown for a few points along the curve. High Sm/Nd reservoirs formed during the first 30 My of Earth's history would be characterized today by an $\varepsilon^{143}Nd$ value lower than +10 ($^{147}Sm/^{144}Nd \sim 0.21$).

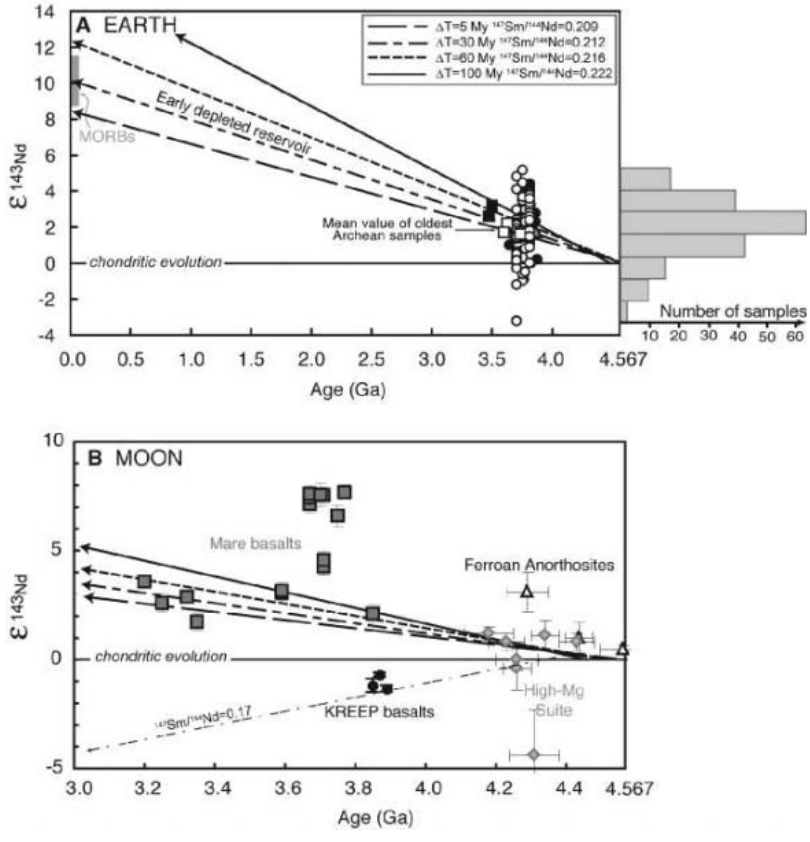

Fig. 4. (**A**) $\varepsilon^{143}Nd$ evolution of the early depleted reservoir on Earth as a function of the time of its formation. The different evolution lines were calculated considering an excess of 20 ppm for the $^{142}Nd/^{144}Nd$ ratio in Earth's mantle relative to chondrites. Each evolution line is defined by a specific slope dependent on the magnitude of the Sm/Nd fractionation and the age of the differentiation event (ΔT). A solar system initial $^{146}Sm/^{144}Sm$ of 0.008 (*45*, *46*) at 4.567 Gy (*44*) was used for these calculations, and we consider the mean values determined in this study for the chondritic reservoir. The geochemical data [i.e., the radiogenic $^{143}Nd/^{144}Nd$ ratios measured in most of the Archean samples (*49*–*53*)] (mean of +2 $\varepsilon^{143}Nd$), and the range of MORB values (+9 to +12), are best fit if the differentiation event occurred during the first 30 My of Earth's history. (**B**) Nd isotopic evolution for lunar samples [see (*54*) for recent review]. The superchondritic $^{142}Nd/^{144}Nd$ of the lunar samples (*12*) and the similarity to terrestrial values suggest that the Moon formed by a giant impact with Earth after Earth had undergone global differentiation. A superchondritic Sm/Nd in the bulk Moon is in agreement with the radiogenic $\varepsilon^{143}Nd$ reported for the oldest lunar samples (High-Mg suite samples and ferroan anorthosites). The lunar $^{142}Nd/^{144}Nd$ evolution is complicated by a second stage, the crystallization of the lunar magma ocean. The age of the second fractionation corresponds to the intersection of the lunar mantle evolution with the KREEP line ($^{147}Sm/^{144}Nd = 0.17$) at 4.42 Gy, implying that the lunar magma ocean required about 120 My to crystallize. Error bars are 2σ.

lithophile elements, and this observation is unlikely to be affected by revisions in BSE concentrations, except for elements such as Rb and Pb. The order of elements on the *x* axis is based on the relative incompatibility of these elements during shallow melting of the mantle (*11*), and thus depends primarily on the partition coefficients of clinopyroxene, a phase stable only in the upper few hundred kilometers of the mantle. The smooth patterns for the EER thus suggest that this reservoir was not formed by fractionation of some high-pressure phase such as perovskite, particularly given the distribution coefficients of trace elements recently measured for both Ca- and Mg-perovskite (*35*). Instead, a better analog for the EER may be the KREEP (basalts rich in K, rare earth elements, and P) component of the Moon, which is a highly incompatible element–enriched residual liquid believed to have formed at low pressure by near-complete crystallization of a lunar magma ocean (*36*). If the terrestrial EER also formed at shallow depth, its lack of contribution to surface volcanism suggests that it now must reside in the deep mantle. The sinking of a dense, Fe- and Ti-rich residual liquid like KREEP through the lunar mantle has been modeled (*37*). A similar event may have happened to a shallow terrestrial EER, taking it from near Earth's surface to the base of the mantle. Such a dense layer could be stable at great depth and remain poorly mixed with the rest of the mantle over the age of Earth (*33*). The small deficit in ^{142}Nd (–10 ppm relative to the terrestrial standards) recently reported in a few flood basalts from the Deccan Province (*38*) could indicate some mixing of the enriched deep material with depleted overlying mantle.

Implications for Mars and Earth's Moon. The new chondritic ^{142}Nd/^{144}Nd value also requires a revision of the interpretation of the early evolution of other planetary bodies, in particular the Moon and Mars. Martian rocks (as sampled by the SNC meteorites) span a wide range of ^{142}Nd/^{144}Nd values [from +90 ppm to –20 ppm, relative to the terrestrial standard (*4*)]. Compared with the terrestrial ^{142}Nd/^{144}Nd values, martian ^{146}Sm-^{142}Nd systematics allow the differentiation of the silicate portion of Mars to have occurred as late as 40 My after solar system formation (*5*). Using instead the new chondritic value for the ^{142}Nd/^{144}Nd ratio requires that this time interval be shortened. Martian core formation dated with ^{182}Hf-^{182}W and mantle differentiation could have occurred simultaneously at ~12 My after solar system formation (*5*, *39*).

Most lunar samples have ^{142}Nd/^{144}Nd values close to terrestrial values, with the exception of some high-Ti basalts, which have values that are 20 ppm higher (*3*). The new chondrite values mean that all lunar samples, like Earth's, have superchondritic ^{142}Nd/^{144}Nd ratios. This suggests that the Moon formed from a giant impact into an already-differentiated Earth, sampling the depleted reservoir that also has been the source of terrestrial crustal rocks. Numerical simulations of a giant impact origin for the Moon suggest that at least two-thirds of the material that makes up the Moon is derived from the impactor, not from Earth (*40*). This expectation is difficult to reconcile with the similar nonchondritic lunar and terrestrial ^{142}Nd/^{144}Nd ratios, unless the impactor had a similar history of silicate differentiation as did the early Earth. Nevertheless, the superchondritic lunar ^{142}Nd/^{144}Nd value is consistent with the superchondritic initial ^{143}Nd/^{144}Nd value measured for the oldest lunar crustal samples (Fig. 4B) (*41*–*43*).

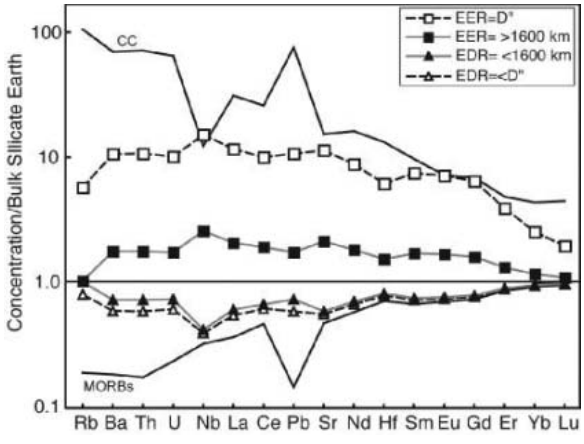

Fig. 5. BSE (*31*) normalized trace element abundances for early-differentiated reservoirs of different sizes. These curves are calculated by assuming that the ^{147}Sm/^{144}Nd of the EDR is 0.21, needed to evolve the 20-ppm terrestrial excess in ^{142}Nd/^{144}Nd for a reservoir formation age of 30 My after Earth formation. The remaining elemental compositions of the EDR are then calculated by adding average continental crust (*29*) to average MORB source mantle (*30*) until this Sm/Nd is achieved. The composition of the EER is then calculated on the assumption that the composition of the EER and EDR sum to BSE (*31*) for the various assumed mass ratios of EER and EDR shown in the figure.

References and Notes

1. M. Boyet *et al.*, *Earth Planet. Sci. Lett.* **214**, 427 (2003).
2. G. Caro, B. Bourdon, J.-L. Birck, S. Moorbath, *Nature* **423**, 428 (2003).
3. L. E. Nyquist *et al.*, *Geochim. Cosmochim. Acta* **59**, 2817 (1995).
4. C. L. Harper Jr., L. E. Nyquist, B. Bansal, H. Wiesmann, C.-Y. Shih, *Science* **267**, 213 (1995).
5. C. N. Foley *et al.*, *Geochim. Cosmochim. Acta*, in press.
6. S. B. Jacobsen, G. J. Wasserburg, *Earth Planet. Sci. Lett.* **50**, 139 (1980).
7. S. B. Jacobsen, G. J. Wasserburg, *Earth Planet. Sci. Lett.* **67**, 137 (1984).
8. P. J. Patchett, J. D. Vervoort, U. Söderlund, *Earth Planet. Sci. Lett.* **222**, 29 (2004).
9. S. B. Jacobsen, G. J. Wasserburg, *J. Geophys. Res.* **84**, 7411 (1979).
10. C. J. Allègre, S. R. Hart, J.-F. Minster, *Earth Planet. Sci. Lett.* **66**, 191 (1983).
11. A. W. Hofmann, *Earth Planet. Sci. Lett.* **90**, 297 (1988).
12. F. Albarède, R. D. Van der Hilst, *Philos. Trans. R. Soc. London Ser. A* **360**, 2569 (2002).
13. P. E. van Keken, E. H. Hauri, C. J. Ballentine, *Annu. Rev. Earth Planet. Sci.* **30**, 493 (2002).
14. L. H. Kellogg, B. H. Hager, R. D. Van der Hilst, *Science* **283**, 1881 (1999).
15. V. C. Bennett, in *Treatise on Geochemistry, Volume 2—The Mantle and Core*, H. D. Holland, K. K. Turekian, R. W. Carlson, Eds. (Elsevier, Oxford, 2003), pp. 493–520.
16. S. A. Wilde, J. W. Valley, W. H. Peck, C. M. Graham, *Nature* **409**, 175 (2001).
17. C. J. Allègre, T. Staudacher, P. Sarda, M. Kurz, *Nature* **303**, 762 (1983).
18. I. Tolstikhin, A. W. Hofmann, *Phys. Earth Planet. Int.* **148**, 109 (2005).
19. Y. Amelin, E. Rotenberg, *Earth Planet. Sci. Lett.* **223**, 267 (2004).
20. M. Sharma, C. Chen, *Precamb. Res.* **135**, 315 (2004).
21. Materials and methods are available as supporting material on *Science* Online.
22. V. C. Bennett, M. T. McCulloch, *Trans. Am. Geophys. Union* **73**, 621 (1992).
23. S. J. G. Galer, S. L. Goldstein, *Trans. Am. Geophys. Union* **73**, 622 (1992).
24. C. L. Harper, S. B. Jacobsen, *Nature* **360**, 728 (1992).
25. M. Regelous, K. D. Collerson, *Geochim. Cosmochim. Acta* **60**, 3513 (1996).
26. M. Sharma, D. A. Papanastassiou, G. J. Wasserburg, R. F. Dymek, *Geochim. Cosmochim. Acta* **60**, 2037 (1996).
27. M. Boyet, R. W. Carlson, *EoS* **85**, abstract U41A-0723 (2004).
28. M. Boyet, M. O. Garcia, R. Pik, F. Albarède, *Geophys. Res. Lett.* **32**, L04306 (2005).
29. R. L. Rudnick, S. Gao, in *Treatise on Geochemistry, Volume 3—The Crust*, H. D. Holland, K. K. Turekian, Eds. (Elsevier-Pergamon, Oxford, 2003), pp. 1–64.
30. V. J. M. Salters, A. Stracke, *Geochem. Geophys. Geosyst.* **5**, 10.1029/2003GC000597 (2004).
31. W. F. McDonough, S.-s. Sun, *Chem. Geol.* **120**, 223 (1995).
32. J. Blichert-Toft, F. Albarède, *Earth Planet. Sci. Lett.* **148**, 243 (1997).
33. H. Samuel, C. G. Farnetani, *Earth Planet. Sci. Lett.* **207**, 39 (2003).
34. B. A. Buffett, *Science* **299**, 1675 (2003).
35. A. Corgne, C. Liebske, B. J. Wood, D. C. Rubie, D. J. Frost, *Geochim. Cosmochim. Acta* **69**, 485 (2005).
36. P. H. Warren, J. T. Wasson, *Rev. Geophys. Space Phys.* **17**, 73 (1979).
37. E. M. Parmentier, S. Zhong, M. T. Zuber, *Earth Planet. Sci. Lett.* **201**, 473 (2002).
38. R. Andreasen, K. V. Subbarao, M. Sharma, *Geochim. Cosmochim. Acta* **68**, A747 (2004).
39. T. Kleine, C. Münker, K. Mezger, H. Palme, *Nature* **418**, 952 (2002).
40. R. M. Canup, *Icarus* **168**, 433 (2004).
41. R. W. Carlson, G. W. Lugmair, *Earth Planet. Sci. Lett.* **90**, 119 (1988).
42. C. Alibert, M. D. Norman, M. T. McCulloch, *Geochim. Cosmochim. Acta* **58**, 2921 (1994).
43. L. E. Borg *et al.*, *Geochim. Cosmochim. Acta* **63**, 2679 (1999).
44. Y. Amelin, A. N. Krot, I. D. Hutcheon, A. A. Ulyanov, *Science* **297**, 1678 (2002).
45. G. W. Lugmair, J. G. Galer, *Geochim. Cosmochim. Acta* **56**, 1673 (1992).
46. A. Prinzhofer, D. A. Papanastassiou, G. J. Wasserburg, *Geochim. Cosmochim. Acta* **56**, 797 (1992).
47. L. E. Nyquist, B. Bansal, H. Wiesmann, C.-Y. Shih, *Meteoritics* **29**, 872 (1994).
48. B. W. Stewart, D. A. Papanastassiou, G. J. Wasserburg, *Geochim. Cosmochim. Acta* **58**, 3487 (1994).
49. B. M. Jahn *et al.*, *Precamb. Res.* **34**, 311 (1987).
50. S. B. Jacobsen, R. F. Dymek, *J. Geophys. Res.* **93**, 338 (1988).
51. G. Gruau, M. Rosing, D. Bridgwater, R. C. O. Gill, *Chem. Geol.* **133**, 225 (1996).
52. V. C. Bennett, A. P. Nutman, M. T. McCulloch, *Earth Planet. Sci. Lett.* **119**, 299 (1993).
53. J. D. Vervoort, J. Blichert-Toft, *Geochim. Cosmochim. Acta* **63**, 533 (1999).

54. G. A. Snyder, L. E. Borg, L. E. Nyquist, L. A. Taylor, in *Origin of the Earth and Moon*, R. M. Canup, K. Righter, Eds. (Univ. of Arizona Press, Tucson, AZ, 2000), pp. 361–395.

55. Acquisition of our Triton mass spectrometer was made possible by NSF grant EAR-0320589 and a matching contribution from the Carnegie Institution of Washington. We thank G. Tilton for generously donating his meteorite collection to D.T.M., which facilitated this project. Abee and Allende are from the Smithsonian (United States National Museum nos. 6581 and 3329, respectively), provided by T. McCoy. We thank M. Horan and T. Mock for analytical support and S. Shirey and two anonymous reviewers for their constructive comments that greatly benefited the paper.

Supporting Online Material
www.sciencemag.org/cgi/content/full/1113634/DC1
Materials and Methods
Fig. S1
Table S1
References

15 April 2005; accepted 8 June 2005
Published online 16 June 2005;
10.1126/science.1113634
Include this information when citing this paper.

Crystal Structure of Human Toll-Like Receptor 3 (TLR3) Ectodomain

Jungwoo Choe, Matthew S. Kelker, Ian A. Wilson*

Toll-like receptors (TLRs) play key roles in activating immune responses during infection. The human TLR3 ectodomain structure at 2.1 angstroms reveals a large horseshoe-shaped solenoid assembled from 23 leucine-rich repeats (LRRs). Asparagines conserved in the 24-residue LRR motif contribute extensive hydrogen-bonding networks for solenoid stabilization. TLR3 is largely masked by carbohydrate, but one face is glycosylation-free, which suggests its potential role in ligand binding and oligomerization. Highly conserved surface residues and a TLR3-specific LRR insertion form a homodimer interface in the crystal, whereas two patches of positively charged residues and a second insertion would provide an appropriate binding site for double-stranded RNA.

Innate immunity is based on an ancient and ubiquitous system of cells and molecules that defend the host against infection. This system can recognize virtually all microbes, using a limited repertoire of germ-line–encoded receptors that recognize broadly conserved components of bacterial and fungal cell walls or genetic material, such as double-stranded viral RNA (*1*, *2*).

The Toll-like receptors (TLRs) are among the most important sensors of the innate immune system (*3*). The ten known human Toll-like receptors recognize pathogen-associated molecules, such as lipoteichoic acid (recognized by TLR2), lipopolysaccharide (TLR4), flagellin (TLR5), and unmethylated CpG DNA motifs (TLR9). Binding of these ligands to TLRs initiates a series of signaling processes that stimulate and orchestrate the innate and adaptive immune responses (*4*, *5*). Human TLRs are implicated in a number of diseases and, hence, constitute potential therapeutic targets (*6*, *7*).

TLRs are integral membrane proteins located either on the cell surface or in intracellular compartments. Their extracellular or ectodomains (ECDs) are responsible for ligand binding and contain 19 to 25 leucine-rich repeat (LRR) motifs that are also found in a number of other proteins with diverse cellular functions (*8*). The intracellular domain, known as the Toll/interleukin-1 receptor homology (TIR) domain, recruits adaptor molecules, such as MyD88, TRIF, and TIRAP, to initiate the signaling process (*4*, *9*).

Human TLR3 is activated by double-stranded RNA (dsRNA) associated with viral infection (*10*), endogeneous cellular mRNA (*11*), and sequence-independent small interfering RNAs (*12*). TLR3 is distinct from other TLRs in that it is not dependent on MyD88 but rather on TRIF for signaling (*13*). Other key features of TLR3 signaling include a requirement for phosphorylation of tyrosine residues in the TIR domain (*14*) and the involvement of phosphatidylinositol-3 kinase (*15*). In turn, TLR3 activates genes for secreted antiviral cytokines, such as interferon (IFN-β), and those that encode intracellular, viral, stress-inducible proteins (*16*).

Overall structure. The complete ectodomain of human TLR3 without the N-terminal signal sequence (residues 27 to 700) was expressed using a baculovirus system and purified by Ni-nitrilotriacetic acid (NTA) affinity, ion-exchange, and size-exclusion chromatography

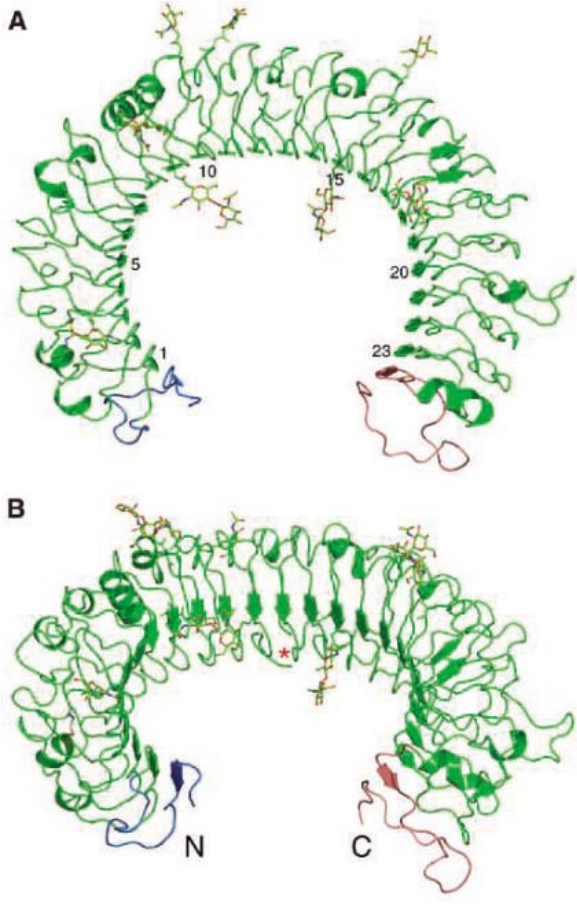

Fig. 1. Overall architecture of TLR3 ECD in a ribbon representation. The N-terminal cap region is colored blue; the 23 canonical LRRs are in green; and the C-terminal region is in pink. N-linked sugars (N-acetylglucosamines) that are observed in the electron density maps are shown in ball-and-stick representation, attached to their respective Asn residues. The disulfide bond linking LRRs 2 and 3 is drawn in orange, adjacent to the glycosylation site. **(A)** Side view of TLR3 with the convex face pointing outwards, the concave face inwards, and the heavily glycosylated side face pointing toward the viewer. **(B)** View rotated 45° from (A) that highlights the continuous β sheet that forms the concave surface. The position of the large insertion in LRR12 that extends toward the glycosylation-free face is marked with an asterisk.

Department of Molecular Biology and The Skaggs Institute for Chemical Biology, The Scripps Research Institute (TSRI), 10550 North Torrey Pines Road, La Jolla, CA 92037, USA.

*To whom correspondence should be addressed. E-mail: wilson@scripps.edu

(*17*). TLR3 native crystals diffracted to 2.1 Å, and a 3.1 Å multiwavelength anomalous diffraction (MAD) data set from a K_2OsO_4 derivative was used for the initial phase calculation (*18*). The three-dimensional structure of human TLR3 (ECD) reveals a large, horseshoe-shaped assembly consisting of 23 LRRs that adopt a right-handed solenoid structure (Fig. 1). Human TLR3 (ECD) contains 23 canonical and two irregular LRRs, which is the largest number yet observed among LRR-containing proteins with known structures. The inner and the outer radii of the TLR3 horseshoe are ~26 Å and 40 Å, respectively, which is substantially larger than that of ribonuclease inhibitor (inner radius, 18 Å) (fig. S3) (*19*). The concave (inner) surface is formed from 25 parallel β strands, 23 from LRRs and one each from the N- and C-terminal cap regions, that assemble into a highly curved, continuous β sheet that spans 270° of arc. The convex (outer) surface contains more diverse secondary structure elements, including a variety of different length of loops, four α helices, seven 3_{10} helices, and two β strands. The superposition of 23 LRRs shows that the residues that compose the inner β strands overlap extraordinarily closely with each other, with root mean square deviations (RMSDs) ranging only from 0.3 to 0.8 Å (Fig. 2A). In contrast, the rest of the motif is more diverse, with RMSDs of 1.0 to 2.5 Å when equivalent C_α atoms are used in the superposition. One disulfide bond was observed between Cys^{95} and Cys^{122}, linking LRR2 and LRR3 (Fig. 1).

Leucine-rich repeats. The LRRs of TLR3 (ECD) follow the typical consensus motif of a 24-residue repeat, consisting of $xL^2xxL^5xL^7xxN^{10}xL^{12}xxL^{15}xxxxF^{20}xxL^{23}x$, where L represents obligate hydrophobic residues, which for TLR3 include leucine (most prevalent), isoleucine, valine, methionine, and phenylalanine; F is a conserved phenylalanine; and N is a conserved asparagine (*20*) (fig. S1). The seven conserved hydrophobic residues of the LRRs (at positions 2, 5, 7, 12, 15, 20, and 23) (fig. S1) point inward into the solenoid and form a tightly packed hydrophobic core (Fig. 2, A and B) that provides lateral stability to the repeating LRR motifs. The parallel β sheet that forms the inner concave surface is fairly typical for LRR proteins, except that, at either end, the carbonyl groups form additional bifurcated hydrogen bonds with main-chain amides (Fig. 2C). The side chains of the conserved asparagines (position 10) at the end of type VI β-turn regions also make extensive bridging interactions, including three hydrogen bonds to the amide and carbonyl groups from the previous LRR motif and one to the carbonyl group of residue 7 from the same LRR repeat, that further stabilize the solenoid structure (Fig. 2D). Seventeen of the 23 human TLR3 LRRs have the canonical 24-residue motif, and only LRR12 and LRR20 have insertions longer than 5 residues (fig. S1). LRR12 is composed of 33 residues with a 10-residue insertion after position 11 that points toward the glycosylation-free side face (marked with an asterisk in Fig. 1B) (*21*); however, six of these inserted residues are disordered and are not included in the refined structure. LRR20 has 32 residues with an 11-residue insertion after position 13, which points toward the outer convex surface.

N-terminal and C-terminal caps. Most proteins with LRR motifs contain flanking regions at their N- and C-termini that cap the exposed edges of the hydrophobic core of the solenoid structure formed by the canonical LRRs. In TLR3, the N-terminal capping region consists of residues 27 to 51, in which Val^{34} to Ser^{36} initiate a modified LRR repeat that extends the continuous β sheet. Residues Ala^{35}, Leu^{40}, Leu^{42}, Val^{45}, and Leu^{49} point toward the hydrophobic core of LRR1, whereas the remaining residues are mainly hydrophilic and form a lid over one end of the hydrophobic core (fig. S2). The C-terminal region of human TLR3 spans from Asn^{636} to Ala^{700}, but a large part of this domain is disordered in the crystal and only Asn^{636} to Thr^{664} are included in the refined structure. As with the N-terminal cap, a modified LRR is found where Glu^{639} to Leu^{641} form a β strand that extends the continuous β sheet (*22*), and Leu^{637}, Leu^{640}, Met^{642}, and Phe^{647} contact the other edge of the hydrophobic core at LRR23 (fig. S2). Although the C-terminal region contains the characteristic four cysteine motif ($CxCx_nCx_nC$), no disulfide bonds were observed due to disorder in the C-terminal residues.

Glycosylation. Fifteen potential N-linked glycosylation sites are located in the extracellular domain of human TLR3 (*23*). Electron density for one or two N-acetylglucosamines of each carbohydrate moiety was observed at eight of these locations, corresponding to Asn^{124}, Asn^{252}, Asn^{265}, Asn^{275}, Asn^{291}, Asn^{398}, Asn^{413}, and Asn^{507} (Fig. 1). When fully glycosylated sugars, which in insect cells are mainly oligomannans such as $Man_9GlcNAc_2$, are modeled onto the 15 predicted N-glycosylation sites, most of the TLR3 surface is masked by carbohydrate, including the inner concave and outer convex surfaces and one of the two major faces of the horseshoe-shaped structure (Fig. 3). Importantly, one face is completely

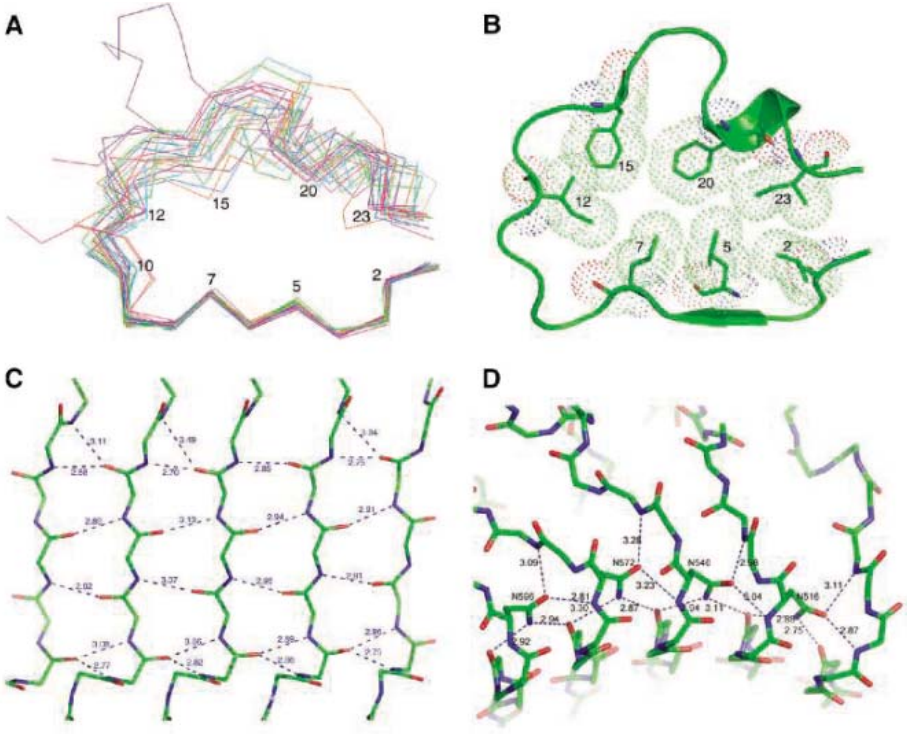

Fig. 2. Structural features of the LRR motifs in TLR3. (**A**) The 23 canonical LRR motifs of TLR3 are superimposed with the C_α atoms of the eight residues that form the concave surface of the repeating β strands. The positions of the two major insertions in LRR12 and LRR20 can readily be visualized, as well as the loops and helices that connect each LRR motif. (**B**) The conformation of the LRR motif (LRR7) highlights the tight packing of the conserved hydrophobic residues with their van der Waals' radii outlined in dots. The residues are numbered by their position in the 24-residue consensus motif (fig. S1). (**C**) A portion of the continuous β sheet that highlights additional main-chain bifurcated hydrogen bonds formed at both ends of the β strands. Hydrogen bond interactions with distances less than 3.5 Å are indicated. (**D**) The intricate hydrogen bond network formed by the conserved asparagines (position 10) that stabilize the assembly of repeating LRR motifs.

devoid of any glycosylation (Fig. 3). When the locations of the predicted N-glycosylation sites of the other nine human TLRs are examined, the concave surface, which is formed from LRR residues 2 to 9 (fig. S1), usually contains glycosylation sites and suggests that glycosylation of the inner concave surface is not unique to TLR3. This result is unexpected because the concave surface was predicted to contain the ligand-binding site of TLRs, including that for dsRNA in TLR3 (*20*).

Electrostatic surface potential. When the surface electrostatic potential of TLR3 was calculated with GRASP (*24*), the concave surface was largely negatively charged (Fig. 4) and again inconsistent with its predicted interaction with dsRNA. Considering that dsRNA is acidic, we then searched for positively charged regions on the TLR3 surface. Such a patch was found on one sector of the glycosylation-free face and is formed from Lys^{331}, Lys^{335}, Arg^{394}, Lys^{416}, Lys^{418}, Lys^{467}, Arg^{489}, and Lys^{493} (Fig. 4C). The convex surface close to the N terminus contains another patch of positively charged residues, including Arg^{65}, Lys^{89}, Lys^{117}, Lys^{137}, Lys^{139}, Lys^{145}, Lys^{147}, and Lys^{163}. Thus, either of these two regions could correspond to potential RNA binding sites, but the former is also adjacent to a TLR3-specific insertion that would further suggest some functional significance.

Comparison with other LRR proteins. The concave surface of human TLR3 (ECD) corresponds to the β sheet of the solenoid and is composed of 25 β strands, 23 from LRRs and one each from the N- and C-terminal capping regions. The radius of the concave surface defined by the inner β strand is ~26 Å, and the overall rotation angle of the 25 β strands is ~270°, which corresponds to 11.3° per repeating LRR unit. Comparison with other LRR proteins, including pRI (*25*), hGPIbα (*26*), ypYopM (*27*), hNogo (*28*), and mCD14 (*29*), indicates that the overall architectural characteristics of the repeating LRR motifs of human TLR3 are most similar to the hNogo receptor, which also has typical 24-residue LRR motifs (fig. S3). Human TLR3 exhibits the largest difference in curvature with pRI, because the outer surface of pRI is composed of repeating α helices rather than loops, as for human TLR3 (fig. S3) (*30*). The overall shape and dimensions of a tail-to-tail CD14 dimer observed in its crystal structure (*29*) roughly matches the overall dimensions of TLR3 (fig. S3). Although it is not clear that this CD14 dimer has any biological relevance, it provides some clues as to possible heterodimeric interactions with TLR4, which is predicted to have 21 LRRs.

dsRNA binding site and mode of signaling. One of the unexpected findings from the TLR3 (ECD) structure was the location of four potential glycosylation sites in the inner concave surface. Electron density for two N-acetylglucosamines was observed at Asn^{252} and Asn^{413}. Although the inner diameter of the concave surface is ~52 Å, which is large enough to hold a double-stranded A-form RNA with a diameter of ~26 Å, fully glycosylated sugars (*31*) would severely hamper binding of dsRNA (Fig. 3). Considering that human TLR3 (ECD) appears to reside in the endosome (*32*), these glycosylation sites would be expected to be fully substituted, although the exact nature of glycoforms that are present on TLR3 in mammalian cells has not yet been determined. Notwithstanding, whether high mannose or complex sugars, these potential glycosylation sites of TLR3 (ECD) are not evenly distributed on the TLR3 surface and map to the concave (four sugars) and convex (four) surfaces, as well as to one of the two major side faces (seven). The other major side face is completely glycosylation-free, which leaves it accessible for interaction

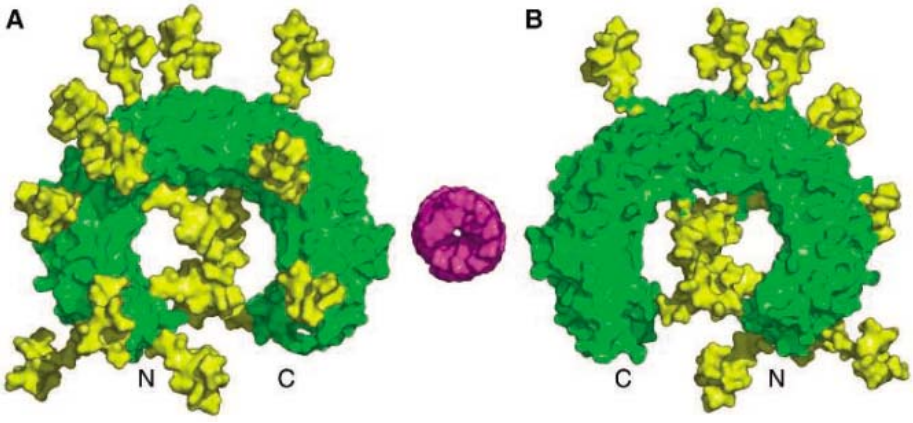

Fig. 3. N-linked glycosylation of TLR3. (**A**) Oligomannose-type sugars, as found predominantly in insect cells (up to nine mannoses and two N-acetylglucosamines), are modeled onto the 15 predicted N-linked glycosylation sites to give a representation of the potential extent of the TLR3 surface masked by carbohydrate (same view as Fig. 1A). The TLR3 surface is represented in green and the sugars in yellow. An end view of an A-form dsRNA is also shown in pink for comparison. The exact nature of the carbohydrate, whether complex or high mannose, is not the issue here, only that glycosylation covers a large part of the TLR3 surface. (**B**) View rotated 180° from (A) showing the glycosylation-free face.

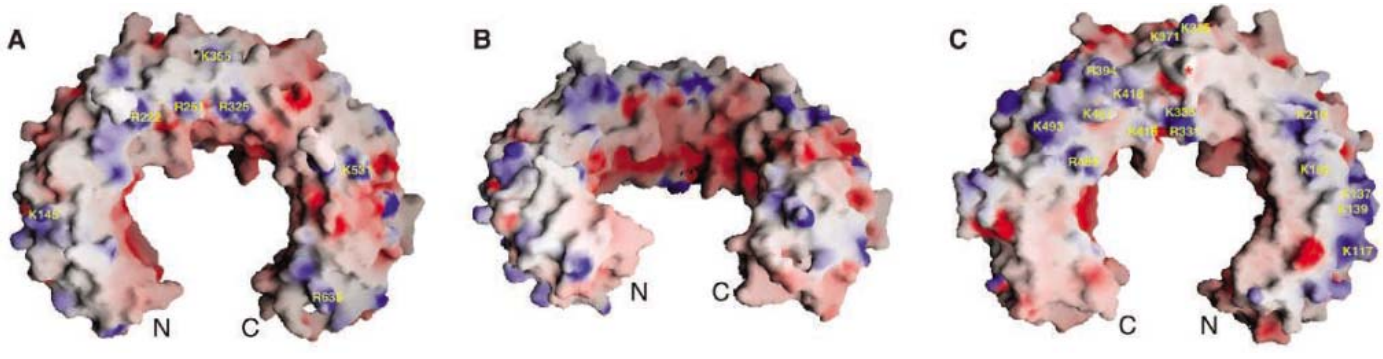

Fig. 4. Surface representation of TLR3, with the surface colored according to the electrostatic potential calculated by GRASP. Red surfaces indicate negative potential and blue positive (±15 kT/e). (**A**) The glycosylated side face with some of the positively charged residues labeled. (**B**) The concave surface showing its predominantly negative electrostatic potential. (**C**) The glycosylation-free face that highlights two clusters of positively charged residues (upper left and lower right) that might interact with the ligand dsRNA. The position of the large insertion in LRR12 is close to the major positive patch (upper left) and is marked with an asterisk; it is also consistent with the proposed location of the ligand binding site. Although these patches are not absolutely conserved in all known TLR3 sequences, they do partially overlap with conserved patches when homologous amino acid substitutions are allowed. K, lysine; R, arginine.

with ligands, including any potential accessory molecules, or for formation of self- or other oligomeric assemblies.

The combined presence of glycosylation sites and the predominant negative charge of concave surface make it an unlikely site for binding double-stranded RNA. This conclusion is contrary to the assumed binding mechanism for LRR-containing proteins that use the concave surface for interacting with their binding partners (*20*). However, analysis of several LRR proteins indicates that other regions can also act as binding sites. For example, ribonuclease inhibitor binds ribonuclease A on its concave surface, as well as on the side face proximal to the C terminus (*33*). Glycoprotein Ibα also binds its ligand, the von Willebrand factor A1 domain, on the concave surface, but with major contributions from a β finger from the N terminus and a β switch region from the C terminus (*34*). Other examples include RanGAP, which binds Ran on the side of the LRR domain (*35*), and the lipopolysaccharide-binding protein CD14, where the binding site is predicted to be located in a surface pocket close to the N terminus (*29*).

Examination of the symmetry-related interactions of TLR3 molecules in the crystal shows a dimer that could be of biological relevance (Fig. 5A). The homodimer interface is close to the C terminus on the glycosylation-free face (Fig. 5C). Although its buried surface area is relatively small (640 Å^2), this region contains the densest cluster of conserved, surface-exposed residues, when five different TLR3 sequences were aligned (Fig. 5B and fig. S4). Interactions at this dimer interface were mostly hydrophilic, including ionic interactions (Glu^{442}–Lys^{467} and Lys^{547}–Asp^{575}), hydrogen bonds between side chains, and water-mediated hydrogen bonds (fig. S5). A limited number of hydrophobic interactions were observed. Three residues involved in this hydrophobic interaction (Lys^{547}, Ala^{549}, and Pro^{551}) come from the TLR3-specific insertion in LRR20 and significantly increase the contact area in the dimer interface. Although the human TLR3 ECD exists as a monomer in solution according to our size-exclusion chromatographic results, TLR3 is an integral membrane protein and could readily form a stable or transient dimer when embedded in the membrane and subject only to lateral diffusion. In fact, certain TLRs are known to form functional oligomers in vivo. For ex-

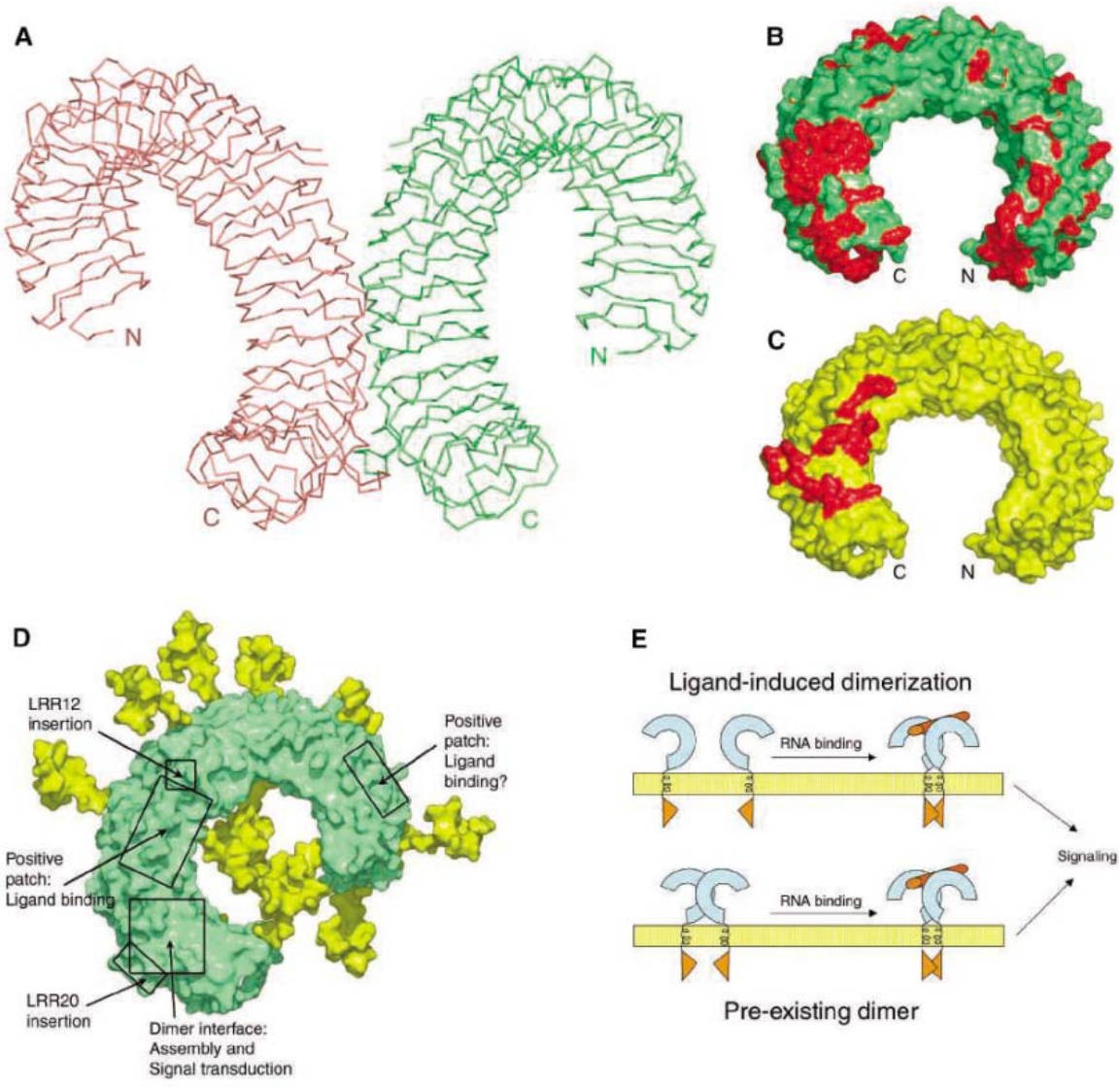

Fig. 5. Possible mode of TLR3 dimerization and a model for dsRNA binding and mode of signaling. (**A**) A homodimer observed in the crystal is shown with one monomer in green and the other in pink. One monomer points away from and the other toward the viewer. No other interactions between monomers in the crystal have sufficient buried surface area to warrant consideration as physiologically relevant oligomers. (**B**) Surface representation of TLR3 (green) highlights sequence conservation on the TLR3 surface (red). The largest conserved patch is on the glycosylation-free face (same view as Fig. 3B). The five TLR3 sequences used in the alignment are *Homo sapiens* (BC059372), *Pan troglodytes* (XP_526756), *Bos taurus* (NP_001008664), *Rattus norvegicus* (NM_198791), and *Takifugu rubripes* (AC156436). (**C**) The dimer interface of TLR3 also maps to the glycosylation-free face. The residues involved in the dimerization are colored in red. The large patch of conserved surface residues of TLR3 (panel B) map to this dimer interface region. (**D**) Potential functional sites on the TLR3 surface. The positions of positive patches and one of the two large insertions in the LRR motifs that are implicated for ligand binding on the glycosylation-free surface are indicated. Similarly, the conserved buried surface and the other large TLR3 LRR insertion maps to this dimerization interface region. Oligomannose-type sugars are drawn in yellow. (**E**) Binding of a dsRNA, either itself or with an accessory protein, could either induce dimerization or changes in a pre-existing dimeric assembly and trigger signal transduction in mechanism similar to those seen for other cell-surface receptors, such as cytokine receptors.

ample, TLR2 makes functional heterodimers with TLR1 and TLR6 (*36*), and TLR4 assembles into a homodimer for signaling (*37*). However, the physiological significance of the dimer observed in the crystal is still speculative and awaits further confirmation by mutagenesis and other biophysical methods. Clearly, if not involved in dimerization, this surface would also be a strong candidate for a ligand binding site.

We propose then that the putative ligand binding site for dsRNA is also located on the glycosylation-free face of TLR3 because it contains the densest cluster of basic residues on the entire TLR3 surface (Fig. 5D). Examination of other dsRNA binding proteins indicates that a strong positively charged region, though sometimes present, is not a necessary condition for RNA binding (*38–40*). Importantly, the 10-residue insertion in LRR12 is also on this same face and only ~15 Å from the positive patch. Although 7 out of 10 residues in this insertion are disordered and not seen in our current structure, they could potentially interact with the major groove of dsRNA through their six hydrophilic residues in the loop. Furthermore, as 36 residues at the C terminus are also disordered, the possibility of this region forming an extended binding site, as in glycoprotein Ibα, cannot be excluded.

If direct binding of dsRNA to TLR3 actually triggers signaling, binding to only one face of the receptor would appear to be a reasonable solution, because binding to the concave surface, like a ring on a finger, may induce uncontrolled oligomerization of TLR3 depending on the length of dsRNA. By binding to dsRNA using only one face of TLR3, two TLR3 monomers could potentially sandwich dsRNA in a ternary complex of two TLR3s and one dsRNA. This possible mode of dimerization would position the positive patches and the 10-residue insertion in LRR12 on either side of the dsRNA (fig. S6). Furthermore, binding of dsRNA in this fashion may either strengthen the dimerization or induce conformational changes in a pre-existing dimer that could trigger changes in the disposition of the intracellular C-terminal TIR domains to bring them closer for signal transduction (Fig. 5E). Thus, a ligand-induced change in a pre-existing dimer assembly, as observed in the erythropoietin receptor (*41*), or a ligand-induced dimerization, as for other cytokine receptors (*42*), would assist formation of the active complex for signaling.

However, although abundant experimental data have been accumulated that strongly support the proposition that dsRNA or RNA analogs induce immune activation by signaling through TLR3 (*10–12*, *16*, *43*), no direct experimental evidence has yet been provided for the physical association of dsRNA with TLR3. Nevertheless, in our gel-shift assay, poly(I:C), a ligand widely used to activate TLR3 in vivo (*10*), binds to TLR3 ECD and changes its migration pattern (fig. S7) (*44*). Considering that some TLRs recognize their ligands in cooperation with co-receptor proteins (*45–47*), it is still possible that TLR3 could recognize dsRNA in conjunction with a not-yet-identified accessory protein(s). However, the TLR3 structure would still suggest that any such ligand interaction would be made on the glycosylation-free face and induce dimer assembly or reorganization. The TLR3 structure now provides a framework to design experiments to characterize TLR's ligand specificity and define its mode of signaling.

References and Notes

1. C. A. Janeway Jr., R. Medzhitov, *Annu. Rev. Immunol.* **20**, 197 (2002).
2. B. Beutler, *Mol. Immunol.* **40**, 845 (2004).
3. K. Takeda, S. Akira, *Int. Immunol.* **17**, 1 (2005).
4. S. Akira, K. Takeda, *Nat. Rev. Immunol.* **4**, 499 (2004).
5. A. Iwasaki, R. Medzhitov, *Nat. Immunol.* **5**, 987 (2004).
6. R. J. Ulevitch, *Nat. Rev. Immunol.* **4**, 512 (2004).
7. C. Zuany-Amorim, J. Hastewell, C. Walker, *Nat. Rev. Drug Discov.* **1**, 797 (2002).
8. B. Kobe, A. V. Kajava, *Curr. Opin. Struct. Biol.* **11**, 725 (2001).
9. L. A. O'Neill, K. A. Fitzgerald, A. G. Bowie, *Trends Immunol.* **24**, 286 (2003).
10. L. Alexopoulou, A. C. Holt, R. Medzhitov, R. A. Flavell, *Nature* **413**, 732 (2001).
11. K. Karikó, H. Ni, J. Capodici, M. Lamphier, D. Weissman, *J. Biol. Chem.* **279**, 12542 (2004).
12. K. Karikó, P. Bhuyan, J. Capodici, D. Weissman, *J. Immunol.* **172**, 6545 (2004).
13. M. Yamamoto *et al.*, *Science* **301**, 640 (2003).
14. S. N. Sarkar, H. L. Smith, T. M. Rowe, G. C. Sen, *J. Biol. Chem.* **278**, 4393 (2003).
15. S. N. Sarkar *et al.*, *Nat. Struct. Mol. Biol.* **11**, 1060 (2004).
16. G. C. Sen, S. N. Sarkar, *Cytokine Growth Factor Rev.* **16**, 1 (2005).
17. The extracellular domain of TLR3 from residues 27 to 700 with an engineered C-terminal His_6-tag was cloned into pAcGP67A vector. The protein was expressed with Hi5 cells and a baculovirus expression system. We infected the cells with baculovirus using a multiplicity of infection of 3, and protein was harvested from the media after 4 days. We purified the protein using Ni-NTA, ion-exchange (MonoQ, Pharmacia), and size-exclusion chromatography (Superdex 200, Pharmacia). The purified protein was concentrated to 15 mg/ml in 10 mM TrisHCl at pH 7.5, 100 mM NaCl, 2 mM EDTA, and 5 mM DTT.
18. TLR3 crystals were initially obtained from 15% PEG 4000 and 0.2 M $(NH_4)_2SO_4$, pH 7.5, and diffraction quality crystals were grown from 23% PEG 2000 and 0.4 M $(NH_4)_2SO_4$, pH 7.5. We prepared the derivative crystal for MAD phasing by soaking a crystal in 10 mM K_2OsO_4 for 12 hours. The native data set was collected at Advanced Light Source beamline 8.2.1 to 2.1 Å resolution, and a three-wavelength MAD data set with K_2OsO_4 derivative was collected at Stanford Synchrotron Radiation Laboratory beamline 11-1 to 3.1 Å. Phases to 3.1 Å were obtained from the MAD data set with the program SOLVE, and density modification was performed by RESOLVE (*48*). At this stage, the electron density clearly illustrated the complete structure of the horseshoe-shaped TLR3. Phases were extended with the native data set (2.1 Å) with the program DM (*49*). Although the density clearly showed the main chain and some of the side-chain features, automatic model building trials with Arp/Warp (*50*) and RESOLVE (*48*) were not satisfactory. A poly-alanine model was built manually from the phase-extended map. With this poly-alanine model, Arp/Warp (*50*) then successfully built over 90% of the model with side chains. The resulting model was refined with Refmac5 (*49*), and manual model fitting was carried out using the program O. The final model consists of 629 TLR3 residues (30 to 336 and 343 to 664), 362 waters, 11 N-acetylglucosamines, 6 glycerols, and 2 SO_4^{2-} molecules. Data collection and refinement statistics are summarized in table S1.
19. Ribonuclease inhibitor was the first LRR structure and is the most similar to TLR3, in that it forms an almost complete horseshoe but with different dimensions and a different number of repeats.
20. J. K. Bell *et al.*, *Trends Immunol.* **24**, 528 (2003).
21. The point of insertion at position 11 was determined by comparison with neighboring LRR motif structures. It is often referred to as an insertion at position 15 from previous sequence comparisons.
22. The first 12 residues of the C-cap region corresponding to the consensus LRR motif of TLR3 form a modified, incomplete LRR structure.
23. N. Blom, T. Sicheritz-Ponten, R. Gupta, S. Gammeltoft, S. Brunak, *Proteomics* **4**, 1633 (2004).
24. A. Nicholls, K. A. Sharp, B. Honig, *Proteins* **11**, 281 (1991).
25. B. Kobe, J. Deisenhofer, *Nature* **366**, 751 (1993).
26. S. Uff, J. M. Clemetson, T. Harrison, K. J. Clemetson, J. Emsley, *J. Biol. Chem.* **277**, 35657 (2002).
27. A. G. Evdokimov, D. E. Anderson, K. M. Routzahn, D. S. Waugh, *J. Mol. Biol.* **312**, 807 (2001).
28. X. L. He *et al.*, *Neuron* **38**, 177 (2003).
29. J. I. Kim *et al.*, *J. Biol. Chem.* **280**, 11347 (2005).
30. P. Enkhbayar, M. Kamiya, M. Osaki, T. Matsumoto, N. Matsushima, *Proteins* **54**, 394 (2004).
31. The sugars are modeled here as oligomannans, which predominate in insect cells as in our construct, with up to nine mannoses and two N-acetylglucosamines.
32. M. Matsumoto *et al.*, *J. Immunol.* **171**, 3154 (2003).
33. B. Kobe, J. Deisenhofer, *J. Mol. Biol.* **264**, 1028 (1996).
34. E. G. Huizinga *et al.*, *Science* **297**, 1176 (2002).
35. M. J. Seewald, C. Korner, A. Wittinghofer, I. R. Vetter, *Nature* **415**, 662 (2002).
36. A. M. Hajjar *et al.*, *J. Immunol.* **166**, 15 (2001).
37. H. Lee, S. Dunzendorfer, P. S. Tobias, *J. Biol. Chem.* **279**, 10564 (2004).
38. J. B. Ma *et al.*, *Nature* **434**, 666 (2005).
39. J. M. Ryter, S. C. Schultz, *EMBO J.* **17**, 7505 (1998).
40. B. Tian, P. C. Bevilacqua, A. Diegelman-Parente, M. B. Mathews, *Nat. Rev. Mol. Cell Biol.* **5**, 1013 (2004).
41. O. Livnah *et al.*, *Science* **283**, 987 (1999).
42. A. M. de Vos, M. Ultsch, A. A. Kossiakoff, *Science* **255**, 306 (1992).
43. Z. Jiang *et al.*, *J. Biol. Chem.* **278**, 16713 (2003).
44. The poly(I:C) was purchased from InvivoGen, San Diego. For experimental details, see fig. S7.
45. Y. Nagai *et al.*, *Nat. Immunol.* **3**, 667 (2002).
46. Q. Jiang, S. Akashi, K. Miyake, H. R. Petty, *J. Immunol.* **165**, 3541 (2000).
47. K. Hoebe *et al.*, *Nature* **433**, 523 (2005).
48. T. C. Terwilliger, *Methods Enzymol.* **374**, 22 (2003).
49. Collaborative Computation Project, number 4, *Acta Crystallogr. D Biol. Crystallogr.* **50**, 760 (1994).
50. A. Perrakis, R. Morris, V. S. Lamzin, *Nat. Struct. Biol.* **6**, 458 (1999).

51. We thank R. Ulevitch for kindly providing template TLR3 DNA; X. Dai and R. Stanfield for help with data collection; staff members at the Stanford Synchrotron Radiation Laboratory beamline 11-1 and Advanced Light Source 8.2.1; and B. Beutler and R. Ulevitch for helpful comments and suggestions. Supported by NIH grant nos. AI-42266 and CA-58896 (I.A.W.); a Skaggs Institute post-doctoral fellowship (J.C.); and NIH postdoctoral training grant no. T32 AI077606, a TSRI Skaggs predoctoral fellowship, and a TSRI Jairo H. Arévelo fellowship (M.S.K.). This is manuscript number 17439-MB from the Scripps Research Institute. Structure factors and the coordinates are deposited in the Protein Data Bank under accession code 1ZIW.

Supporting Online Material

www.sciencemag.org/cgi/content/full/1115253/DC1
Figs. S1 to S7
Table S1

24 May 2005; accepted 8 June 2005
Published online 16 June 2005;
10.1126/science.1115253
Include this information when citing this paper.

Fermionic Bell-State Analyzer for Spin Qubits

Hans-Andreas Engel[1,2] and Daniel Loss[2]

We propose a protocol and physical implementation for partial Bell-state measurements of Fermionic qubits, allowing for deterministic quantum computing in solid-state systems without the need for two-qubit gates. Our scheme consists of two spin qubits in a double quantum dot where the two dots have different Zeeman splittings and resonant tunneling between the dots is only allowed when the spins are antiparallel. This converts spin parity into charge information by means of a projective measurement and can be implemented with established technologies. This measurement-based qubit scheme greatly simplifies the experimental realization of scalable quantum computers in electronic nanostructures.

Recent theoretical work has shown that quantum computation with photons is possible using only linear optics (*1*). Partial measurements (*2*) of these optical quantum states are sufficient and, remarkably, gates coupling qubits with each other are no longer required. The extension of this paradigm to other types of qubits, particularly systems based on Fermions, has been a highly desirable (but elusive) goal, because it would eliminate the need to control the strength and pulsing of the interaction between the qubits with extremely high precision. For measurement-based quantum computation, we replaced this requirement with projective measurements, which do not require precise control of the coupling strength to the measurement apparatus. In principle, either full Bell-state measurements (in which all four Bell states are differentiated) in combination with some initial source of entanglement (*3*) or partial Bell-state measurements (in which only the parity subspace is determined) (*4*) are sufficient for universal quantum computing. Still, the most crucial element—the physical implementation of such measurements for Fermions—has not been found so far. We propose a solution to this fundamental problem by considering electrons confined to quantum dots in which the spin represents the qubit. Such spin qubits promise scalable quantum computing (*5*), and single-qubit readout has recently been demonstrated (*6*, *7*). We consider partial and full Bell-state measurements on two spin qubits and demonstrate that it can be performed with available technologies such as spin-to-charge conversion and charge detection. This may open up the possibility for quantum computing in solid-state systems without the need for two-qubit gates.

[1]Lyman Laboratory, Department of Physics, Harvard University, Cambridge, MA 02138, USA. [2]Department of Physics and Astronomy, University of Basel, Klingelbergstrasse 82, CH-4056 Basel, Switzerland.

The spin degree of freedom of the electron promises many applications in the field of spintronics (*8*, *9*). Moreover, single electrons can be controlled through their charge, confining them in quantum dot structures in the Coulomb blockade regime (*10*). The spin-qubit proposal (*5*) combines these two fields of research and uses the spin of electrons confined to quantum dots as qubits for quantum computation, where the spin-½ state of each electron encodes exactly one qubit. The proposal includes two-qubit quantum gates that rely on the exchange interaction of coupled quantum dots and comprises spin-to-charge conversion for efficient readout schemes, satisfying all theoretical requirements for quantum computing (*8*). However, if a partial Bell-state measurement can be implemented, these two-qubit gates would no longer be required, simplifying the realization of a scalable quantum computer. To take such a measurement, one must determine the parity of the two qubit spins by differentiating the spin states with antiparallel spins, $|T_0\rangle, |S\rangle = (|\uparrow\downarrow\rangle \pm |\downarrow\uparrow\rangle)/\sqrt{2}$, from the states with parallel spins, $|T_+\rangle = |\uparrow\uparrow\rangle$ and $|T_-\rangle = |\downarrow\downarrow\rangle$. The measurement must be "nondestructive" with respect to these two subspaces, which requires that a superposition such as the Bell state $|\Psi_2\rangle = (|\uparrow\uparrow\rangle + |\downarrow\downarrow\rangle)/\sqrt{2}$ remain unchanged. Using two such parity measurements, one can construct a controlled NOT (CNOT) gate on two qubits with the use of an additional ancilla qubit, a single-qubit measurement, and the application of single-qubit operations depending on the measurement outcomes (*4*). Because the CNOT gate is a universal quantum gate, partial Bell-state measurements and single-qubit operations are sufficient to build a universal quantum computer. [Conversely, if CNOT gates are available, nondestructive parity measurements can be performed (*11*).] Alternatively, one can use full Bell-state measurements, but this requires preparation of initial entanglement as a resource (*3*).

When reading out single spin qubits, it is most convenient to convert the qubit information from spin to charge (*5*), as demonstrated in recent experiments (*6*). We propose a partial Bell-state (parity) measurement of two qubits that relies on spin-to-charge conversion. The qubits are defined by two electron spins on two coupled quantum dots (Fig. 1). Gate voltages can be tuned such that in the ground state there is a single electron on each dot (*12*). Furthermore, both electrons can be moved to the left dot or to the right dot and we assume that these two states, $|LL\rangle$ and $|RR\rangle$, are degenerate. The energy difference $U = E_{LL} - E_{LR}$ to the ground state $|LR\rangle$ is given by the sum of the charging energies of each dot, reduced by the capacitative coupling between the two dots (*13*).

Let us turn now to the spin states and describe the procedure for the partial Bell measurement, first qualitatively and then quantitatively. We assume that the dots have different Zeeman splittings, Δ_z^L and Δ_z^R (*14*). This can be achieved, for example, with locally different magnetic fields, or with an inhomogeneous g factor resulting from different materials or nuclear polarizations for each dot. This configuration converts spin parity into charge, because tunneling is only resonant for antiparallel spins. Finally, the charge distribution can be measured with a charge detector, such as a quantum point contact (QPC) (*15*). With a time-resolved measurement, the individual tunneling events can be identified (*16*, *17*). (In our case, a time-averaged measurement was already sufficient to perform the partial Bell measurement, because for parallel spins the electrons always remain on the left dot). To check if this scheme works for a realistic experimental setup, we developed a microscopic modeling which allowed us to give a quantitative description of the readout process. Furthermore, we showed that the proposed scheme is robust (within defined limits) against nonideal processes.

We modeled our readout setup by considering only the lowest orbital energy states of the dots for a given charge and spin configuration (*18*, *19*). [We discuss excited states in the supporting online material (SOM) text.] We then needed to consider the 12 states in which two electrons with spins σ, σ' are both on the left dot, $|\sigma_L\sigma'_L\rangle$ the right dot, $|\sigma_R\sigma'_R\rangle$, or different dots, $|\sigma_L\sigma'_R\rangle$. When both electrons are on the same dot, the spin state can be in the singlet (S) or triplet (T_0) configuration, with energy separation $J = E_{T_0LL} - E_{SLL}$. It is well known that this singlet-triplet splitting can be tuned to zero by means of magnetic fields (*18*). We describe the coupling between the left and right dot with the tunneling amplitudes t_S and t_T for singlet and triplet states, respectively. We first consider the symmetric case $J = 0$ and $t_S = t_T$ and then address the general case.

Next, we found the transition rates for the tunneling between the charge states LL and RR, as a function of the level detuning ε. For this, we consider the charge states {|LR⟩, |LL⟩, and |RR⟩} and define a Hamiltonian by the eigenenergies $E_{LR} = 0$ and $E_{LL,RR} = U \pm \varepsilon/2$ (in the absence of tunneling) and the tunneling $H_T = t_d\,|LL\rangle\langle LR| + t_d\,|RR\rangle\langle LR| + \text{H.c.}$ with tunneling amplitude t_d and where H.c. is the Hermitian conjugate. We then describe the double-dot state with the reduced density matrix ρ(*t*) and determine its time evolution with a Bloch-Redfield master equation (*20*). The diagonal elements, ρ_n, describe the probabilities of a given charge state $|n\rangle$ of the double dot. The off-diagonal elements, ρ_{nm}, describe a superposition of dot states $|n\rangle$ and $|m\rangle$. We need to consider these off-diagonal elements because at short time scales the tunneling is coherent and superpositions of charge states are formed. However, such superpositions decay rapidly, with a typical charge dephasing rate $\Gamma_d = (1\text{ ns})^{-1}$ (*21*). Generally, there are different dephasing rates, Γ_{d1} for superpositions of |LR⟩ and |LL⟩ (or |RR⟩) and a rate Γ_{d2} for a superposition of $|LL\rangle$ and $|RR\rangle$. We are interested in time scales for which the charge distribution on the double dot can be measured—i.e., in times longer than $1/\Gamma_d$—allowing us to set $\dot{\rho}_{nm} = 0$. By doing so, we can simplify the master equation to a classical rate equation and identify the following effective tunneling rates. First, the tunneling of both charges from left to right, LL↔RR, is given by

$$W_{L\leftrightarrow R} = \frac{2t_d^4}{U^2}\,\frac{\Gamma_{d2}}{\varepsilon^2 + \Gamma_{d2}^2} \qquad (1)$$

This corresponds to a resonant process and the effective rate is maximal when the detuning ε vanishes. The width of the rate is given by the dephasing rate Γ_{d2}. In particular, for $\varepsilon > \Gamma_{d2}$ the tunneling is suppressed. Furthermore, there is an effective rate describing the relaxation to the ground state, such as LL→LR,

$$W_{relax} = \frac{2t_d^2\Gamma_{d1}}{U^2} \qquad (2)$$

This rate is consistent with transport experiments through double dots (*22*), which indicate relaxation on a time scale of ≥1 μs for $t_d = 10$ μeV and $U = 1$ meV. Furthermore, we can include an intrinsic rate Γ_r to describe additional inelastic tunneling processes (e.g., in which a phonon is emitted and the dot relaxes to the ground state). The experimental data (*21*, *22*) indicate that $\Gamma_r \ll \Gamma_d$, suggesting that adjustments of the off-diagonal rates due to Γ_r are not relevant.

With this model, we can estimate the required range for the relevant parameters. There are two main criteria to be met. (i) Our readout should be efficient: The parity of the spin state should be detected with a high probability. Thus, within a given time, tunneling of an antiparallel spin state should be observed, although a parallel spin state should not tunnel. Comparing tunneling rates (Eq. 1) at resonance and for detuning due to antiparallel spins, we found the requirement $4(\Delta_z^R - \Delta_z^L)^2 > \Gamma_{d2}^2$. This can be satisfied for typical GaAs quantum dots, such as a magnetic field of $B = 1$ T and a difference in g factors of $\Delta g = 0.01$. (ii) The relaxation to the ground state |LR⟩ must be slow compared with the resonant tunneling of parallel spins; otherwise the charge state relaxes before the spin state has been measured. [Moreover, this decay to the ground state leads possibly to decoherence of the spin state (*19*).] According to Eqs. 1 and 2, we need $t_d > \Gamma_d$, which can be satisfied with typical experimental parameters (*23*). In Fig. 2, we give an explicit numerical example, proving that partial Bell measurements are feasible.

Let us now consider whether this scheme reaches the quantum limit of measurement efficiency. A single-qubit readout and our parity measurement must distinguish between two states and subspaces $i = 1,2$. When the detected signal is Gaussian distributed with mean μ_i and standard deviation σ_i, the infidelity α is the probability of obtaining the wrong measurement result and is given by $z_{1-\alpha} = |\mu_2 - \mu_1|/(\sigma_1 + \sigma_2)$, where $z_{1-\alpha}$ is the quantile of the standard normal distribution, i.e., $1 - \alpha = \frac{1}{2}\left[1 + \text{erf}(z_{1-\alpha}/\sqrt{2})\right]$. One common assumption is to set $z_{1-\alpha} = \sqrt{2}$ (*24*, *25*); that is, one implicitly considers measurements with infidelity $\alpha = 7.9\%$. With this choice of α, the quantum limit of measurement is defined such that the measurement rate Γ_{meas} (the inverse

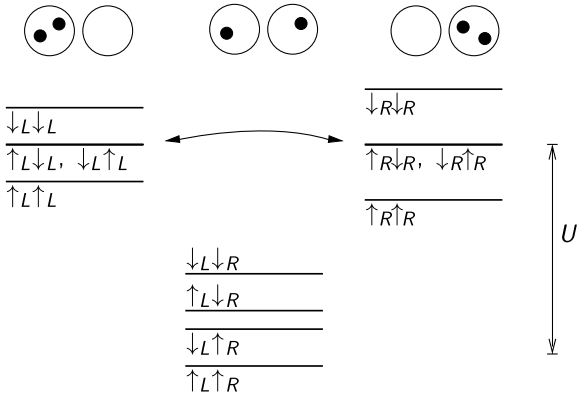

Fig. 1. Energy spectrum of a double quantum dot with two electrons. The charge state of the double dot is shown schematically on top, where each electron can be in a different dot or where both electrons are in the left (L) or right (R) dot. To apply our measurement scheme, first a state |LL⟩ is prepared, e.g., by starting with one electron on dot L and adiabatically adding in another "input" electron from a third dot [ideally with the same Zeeman splitting as dot L and with equal tunneling amplitudes for singlet and triplet (*19*)]. Then, the gate voltages are swept to the configuration shown in this figure, where |LL⟩ is an excited state. For a better control during preparation, the coupling of dots L and R can be switched off temporarily (*26*). Both electrons can elastically tunnel onto the right dot, LL↔RR. The transition to the ground state (i.e., LL→LR) only occurs inelastically, typically with an emission of a phonon. For the spins, we assume different Zeeman splittings on the left and right dot, $\Delta_z^L < \Delta_z^R$. The partial Bell-state (parity) measurement proceeds as follows. If the spins are antiparallel, the states |LL⟩ and |RR⟩ are in resonance (indicated by horizontal arrow) and tunneling occurs through the intermediate state |LR⟩ with one electron on each dot. However, if the spins are parallel, the states on the right dot are detuned by $\varepsilon = \pm 2(\Delta_z^R - \Delta_z^L)$ and tunneling is suppressed. The resulting charge distribution thus depends on spin parity and can be detected subsequently by a charge detector.

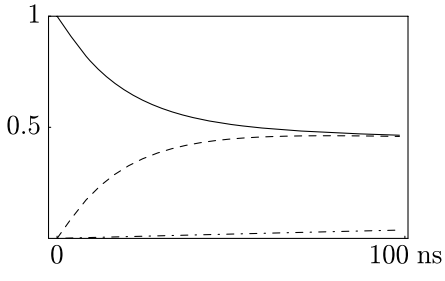

Fig. 2. Example of partial Bell measurement, with simulation of time evolution for the initial state $|\Psi_0\rangle = |SLL\rangle = (|\uparrow_L\downarrow_L\rangle - |\downarrow_L\uparrow_L\rangle)/\sqrt{2}$. We take the parameters $t_d = 10$ μeV, $U = 1$ meV, $1/\Gamma_{d2} = 1$ ns, $B = 1$ T, and $\Delta g = 0.05$. For antiparallel spin (e.g., $|\Psi_0\rangle$), tunneling LL↔RR occurs on a time scale of $1/W_{L\leftrightarrow R}(\varepsilon = 0) \approx 20$ ns. On this time scale, the state on the double dot will relax to a mixture with both electrons either on the left dot or on the right dot. This mixture can then be detected by the QPC current. However, it must be distinguished from the case of parallel spins, where tunneling is strongly suppressed and only occurs on the time scale of 2 μs, defining the required time resolution of the QPC signal. (This does not impose a fundamental requirement of fast charge readout, because this time can be increased by using larger *B* or Δ*g*. However, a fundamental limit is set by inelastic charge relaxation.) To analyze the full dynamics, we performed a simulation and took the back-action of the QPC (including dephasing) into account microscopically (SOM text). We first diagonalized the dynamics of the double dot (*14*) and then evaluated the coupling to the QPC in lowest order. Because the *z* component of the total spin is conserved, it is sufficient to consider a 6×6-density matrix. We obtained the explicit master equation for this density matrix, but because this analytical result is lengthy, it is presented as SOM text. We consider an initial state $|\Psi_0\rangle$ and plot the singlet populations of the left state ρ_{SLL} (solid line), the right state ρ_{SRR} (dashed line), and the ground state ρ_S (dashed-dotted line). The singlet population remains 1 at the end of the measurement; i.e., there is no admixture of the triplet state $|T_0\rangle$. [It is well known that relaxation processes to the other triplet states are also suppressed (*27*).] This implies that superpositions like |↑↓⟩-|↓↑⟩ remain unaffected in that our measurement scheme does not destroy coherence within the parity subspaces.

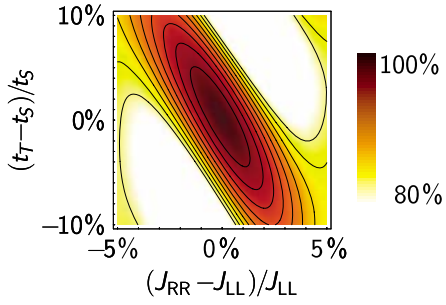

Fig. 3. Measurement fidelity for imperfect measurement parameters. We consider the initial state $(1/\sqrt{2})|\uparrow_L\downarrow_L\rangle + \frac{1}{2}|\uparrow_L\uparrow_L\rangle + \frac{1}{2}|\downarrow_L\downarrow_L\rangle$ and simulate its time evolution, including all states of our model (144-dimensional Liouville space). We obtain the state of the double dot after 100 ns, described by the density matrix ρ_f of the final state *f*. Ideally, we expect the initial state to decay to state *e* that is a mixture of different parities, ρ_e, where the probability is 50% for having parallel spins on the left dot (we include a dynamical phase $2\Delta_z^L$ due to Zeeman splitting) and the probability is 50% for having two antiparallel spins, both on the left or both on the right dot (we include a dynamical phase *J* between $|S\rangle$ and $|T_0\rangle$ states). By comparing the final state of this simulation with this ideal case, we simultaneously test whether the measurement is efficient and whether the parity subspaces remain coherent. We can quantify the accuracy of the imperfect measurement with the Uhlmann (square-root) fidelity $F = \mathrm{Tr}\sqrt{\rho_f^{1/2}\rho_e\rho_f^{1/2}}$ (*28*), with *F* = 100% in the ideal case. We use the same parameters as in Fig. 2, but now with J_{LL} = 1 μeV, and we plot $F(J_{RR},t_T)$ and show contour lines spaced at 2%.

measurement time that is required to obtain $\alpha = 7.9\%$) is equal to the decoherence rate Γ_φ of the quantum system (*25*). For a partial measurement, the decoherence of a superposition of states with different parity is relevant. To evaluate Γ_{meas} and Γ_φ, we extend our simple 3×3 model to a 6×6 model, with which we consider states that are at resonance (antiparallel spins) or off-resonant (parallel spins). Initially, both electrons are on the left dot, but in superposition of states with different parity. By accounting for tunneling to the right dot and by eliminating the off-diagonal elements with different charge, we obtain the effective measurement rate and the decoherence rate. We find

$$\Gamma_\varphi = \Gamma_{meas} = \frac{1}{2}W_{L\leftrightarrow R} \qquad (3)$$

indicating that our scheme operates in the quantum limit of measurement.

Finally, we assess setups which deviate from the ideal configuration. We consider imperfections due to extra phases that result from the inhomogeneous Zeeman splittings, finite *J*, different tunnel couplings of singlet and triplet, and spin-orbit interaction. Our results are presented in Fig. 3 and in the SOM text. We find that even if the double-dot system cannot be perfectly controlled, partial Bell measurements are still possible. Finally, spin qubits decohere as a result of hyperfine interaction with nuclear spins, leading to computation errors. This could be circumvented by polarizing the nuclei, by using refocusing techniques, or by using materials without nuclear spins such as isotopically pure Si, Ge, nanowires, or carbon nanotubes.

References and Notes

1. E. Knill, R. Laflamme, G. J. Milburn, *Nature* **409**, 46 (2001).
2. M. A. Nielsen, I. L. Chuang, *Quantum Computation and Quantum Information* (Cambridge Univ. Press, New York, 2000).
3. D. Gottesman, I. L. Chuang, *Nature* **402**, 390 (1999).
4. C. W. J. Beenakker, D. P. DiVincenzo, C. Emary, M. Kindermann, *Phys. Rev. Lett.* **93**, 020501 (2004).
5. D. Loss, D. P. DiVincenzo, *Phys. Rev. A.* **57**, 120 (1998).
6. J. M. Elzerman *et al.*, *Nature* **430**, 431 (2004).
7. M. Kroutvar *et al.*, *Nature* **432**, 81 (2004).
8. D. D. Awschalom, D. Loss, N. Samarth, Eds., *Semiconductor Spintronics and Quantum Computation* (Series on Nanoscience and Technology, Springer, Berlin, 2002).
9. S. A. Wolf *et al.*, *Science* **294**, 1488 (2001).
10. L. P. Kouwenhoven, G. Schön, L. L. Sohn, *Mesoscopic Electron Transport, NATO Advanced Study Institute, Series E* (Kluwer Academic Publishers, Dordrecht, Netherlands, 1997), vol. 345.
11. G.-P. Guo, C.-F. Li, G.-C. Guo, *Phys. Lett. A* **286**, 401 (2001).
12. J. M. Elzerman *et al.*, *Phys. Rev. B* **67**, 161308 (2003).
13. W. G. van der Wiel *et al.*, *Rev. Mod. Phys.* **75**, 1 (2003).
14. H.-A. Engel *et al.*, *Phys. Rev. Lett.* **93**, 106804 (2004).
15. M. Field *et al.*, *Phys. Rev. Lett.* **70**, 1311 (1993).
16. W. Lu, Z. Q. Ji, L. Pfeiffer, K. W. West, A. J. Rimberg, *Nature* **423**, 422 (2003).
17. R. Schleser *et al.*, *Appl. Phys. Lett.* **85**, 2005 (2004).
18. L. P. Kouwenhoven, D. G. Austing, S. Tarucha, *Rep. Prog. Phys.* **64**, 701 (2001).
19. Materials and methods are available as supporting material on *Science* Online.
20. K. Blum, *Density Matrix Theory and Applications* (Plenum Press, New York, 1996).
21. T. Hayashi, T. Fujisawa, H.-D. Cheong, Y.-H. Jeong, Y. Hirayama, *Phys. Rev. Lett.* **91**, 226804 (2003).
22. T. Fujisawa *et al.*, *Science* **282**, 932 (1998).
23. L. DiCarlo *et al.*, *Phys. Rev. Lett.* **92**, 226801 (2004).
24. Y. Makhlin, G. Schön, A. Shnirman, *Phys. Rev. Lett.* **85**, 4578 (2000).
25. A. A. Clerk, S. M. Girvin, A. D. Stone, *Phys. Rev. B* **67**, 165324 (2003).
26. A. C. Johnson, C. M. Marcus, M. P. Hanson, A. C. Gossard, *Phys. Rev. B* **71**, 115333 (2005).
27. T. Fujisawa, D. G. Austing, Y. Tokura, Y. Hirayama, S. Tarucha, *Nature* **419**, 278 (2002).
28. A. Uhlmann, *Rep. Math. Phys.* **45**, 407 (2000).

29. We thank D. DiVincenzo, L. I. Glazman, J. Lehmann, A. Kitaev, J. Petta, and J. Schliemann for discussions. We acknowledge support from the Swiss NSF, National Center of Competence in Research on Nanoscale Science at Basel, Defense Advanced Research Projects Agency, and NSF grant DMR-02-33773.

Supporting Online Material

www.sciencemag.org/cgi/content/full/309/5734/586/DC1
SOM Text
Figs. S1 and S2
References

5 April 2005; accepted 20 May 2005
10.1126/science.1113203

Creating, Varying, and Growing Single-Site Molecular Contacts

Mohamed Siaj and Peter H. McBreen*

The known range of chemisorption bonds forms the toolbox for the design of electrical contacts in molecular electronics devices. Double-bond contacts to technologically relevant materials would be attractive for a number of reasons. They are truly single-site, bonding to a single surface atom. They obviate the need for a thiol linkage, and they may be amenable to further modification through olefin-metathesis methodologies. We report olefin-metathesis methods for establishing, varying, and growing thermally stable double-bond contacts to molybdenum carbide, a conducting material.

Establishing efficient electrical contact from metallic surfaces to molecules is a key challenge in the development of molecular electronics devices. These contacts should be both robust and well defined. Most experimental work has focused on contacts to metals such as gold, but transition metal carbides are potentially important for the development of nanoelectronic devices. In particular, Zhang *et al.* reported on the formation of carbide heterojunctions between carbon nanotubes and transition metals (*1*). The latter approach was exploited to prepare highly effective titanium carbide and cobalt carbide ohmic contacts in carbon nanotube devices (*2*, *3*).

Well-defined metal-ligand structures are a feature of organometallic complexes and have long served as a guide to understanding chemisorption bonding. However, one entire area of organometallic chemistry, that of metal-ligand multiple bonds, appears to display very little in common with surface science observations; there are few reports (*4*, *5*) of surface alkylidene, $M{=}CR_1R_2$, species where M is a single metal atom. Metal alkylidenes serve as initiating and propagating sites for olefin metathesis. Although olefin metathesis is a powerful synthetic tool in homogeneous chemistry (*6*), steric hindrance and competing chemisorption of the olefin may inhibit the reaction for alkylidene groups situated directly on an

Département de chimie, Université Laval, Québec, PQ, Canada G1K 7P4

*To whom correspondence should be addressed. E-mail: peter.mcbreen@chm.ulaval.ca

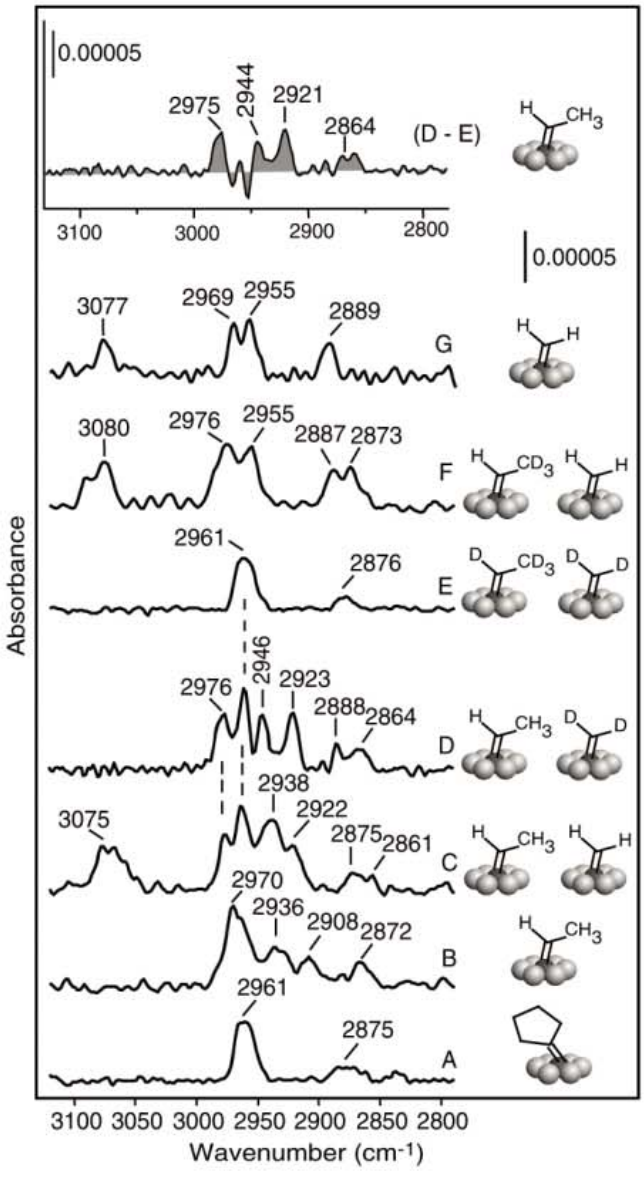

Fig. 1. RAIRS spectra for the interaction of propene and ethene with cyclopentylidene on β-Mo_2C: (**C**) CH_2CHCH_3, (**D**) CD_2CHCH_3, (**E**) CD_2CDCD_3, (**F**) CH_2CHCD_3, and (**G**) C_2H_4. Reference data for cyclopentylidene and ethylidene on β-Mo_2C are included as spectra (**A**) and (**B**), respectively. The top panel displays the difference spectrum [(D) minus (E)]. The observed reactivity is summarized in Scheme 1.

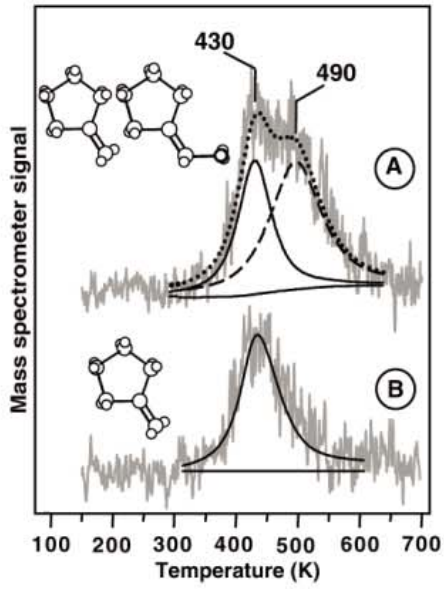

Fig. 2. Temperature-programmed reaction mass spectrometry data (m/e = 67) for the interaction of cyclopentylidene with propene (**A**) and ethene (**B**) on β-Mo_2C. The experiments were performed by heating the alkylidene functionalized carbide at 1 K/s in the presence of 2×10^{-8} Torr olefin. The desorption products are those predicted by the Hérisson-Chauvin mechanism for olefin metathesis (*7*).

extended planar surface. However, we report the spectroscopic observation of facile cross-metathesis reactions between propene and cyclopentylidene on β-Mo_2C leading to the simultaneous isolation of surface methylidene and ethylidene (Scheme 1), the two primary propagator species in the Hérisson-Chauvin mechanism (*7*) for propene metathesis.

Furthermore, we report the observation of ring-opening metathesis polymerization (ROMP) from a surface. The latter method is particularly important in that it involves both a double-bond contact to the surface and chain growth away from the carbide surface.

Surface cyclopentylidene initiator sites were prepared on a clean β-Mo_2C foil under ultrahigh vacuum conditions by the dissociative chemisorption of cyclopentanone in a surface reaction (*8*), which is directly analogous to the oxidative addition of cyclopentanone to the single-atom organometallic complex $WCl_2(PMePh_2)_4$ reported by Bryan and Mayer (*9*).

We used reflection-absorption infrared spectroscopy (RAIRS) to search for alkylidene propagators and ring-opening polymerization products on the surface, and thermal desorption mass spectrometry to search for gas-phase metathesis products. Transalkylidenation between surface cyclopentylidene and simple gas-phase olefins was investigated by annealing the cyclopentylidene functionalized sample from 100 K at a rate of 1 K/s in a background pressure of 2×10^{-8} Torr propene. New surface species formed at 470 K that were identified as methylidene and ethylidene propagators by RAIRS experiments performed using deuterium-labeled propene (Fig. 1). Interaction with CH_2CHCH_3 (Fig. 1, spectrum C) led to new CH stretching bands at 3075, 2976, 2938, 2922, and 2861 cm^{-1}.

The band at ~3075 cm^{-1} is absent for experiments performed using CD_2CDCD_3 (spectrum 1E) and CD_2CHCH_3 (spectrum 1D) but is present for experiments performed with CH_2CHCH_3, CH_2CHCD_3 (spectrum 1F), and C_2H_4 (spectrum 1G). The latter spectrum shows that annealing the cyclopentylidene functionalized surface to 470 K in 2×10^{-8} Torr ethene yields new bands at 3077 and 2955 cm^{-1}, in addition to the two bands that arise from residual unreacted surface cyclopentylidene. Spectrum 1A is the reference spectrum of surface cyclopentylidene. The bands at ~3077 and ~2955 cm^{-1} were also resolved for experiments performed using CH_2CHCD_3 (spectrum 1F) and are attributed to the $\nu_{as}(CH_2)$ and $\nu_s(CH_2)$ vibrations of surface methylidene. This assignment is confirmed by reference to data for matrix-isolated $H_2C{=}Re(O)_2OH$ (*10*). The latter system displays $\nu(CH_2)$ bands at 3080 and 2986 cm^{-1}.

Spectrum 1B is a reference spectrum for ethylidene formed from acetaldehyde on β-Mo_2C (*5*). Comparison of spectra 1B and 1C shows that the new bands at ~2976, 2938, 2922, and 2861 cm^{-1} may be attributed to surface ethylidene. This attribution is confirmed by the difference spectrum (1D − 1E), shown in the top panel of Fig. 1, for experiments performed using CD_2CHCH_3 (spectrum 1E) and CD_2CDCD_3 (spectrum 1D). It is also in agreement with calculated spectra for $Mo{=}CHCH_3$ species (*5*). Hence, we may conclude that chemisorbed methylidene and ethylidene propagators, as predicted by the Hérisson-Chauvin mechanism, are formed by the interaction of propene with surface cyclopentylidene. The primary gas-phase products predicted by the Hérisson-Chauvin mechanism are methylidene cyclopentane and ethylidene cyclopentane.

The mass spectrometry data in Fig. 2 show that both products are detected in desorption experiments performed by annealing the cyclopentylidene functionalized carbide at 1 K/s in the presence of 2×10^{-8} Torr propene. The parent peaks for methylidene cyclopentane and ethylidene cyclopentane appear at 430 and 490 K, respectively. The difference of 60 K in reaction temperature may be attributed to the combined effect of steric 1,2 versus 1,3 substitution (*11*) and adsorption interactions in the Hérisson-Chauvin metallacyclobutane. In particular, the metallacyclobutane leading to methylidene cyclopentane formation will be stabilized by the noncovalent interaction of the methyl group with the surface. Molybdenum carbide is a conducting material, and the noncovalent interaction of the CH_3 group with the surface could reduce the activation energy for metathesis by as much as 6 kJ/mol (*12*).

Having established that transalkylidenation (Scheme 1) can be carried out on β-Mo_2C, we then investigated ring-opening metathesis at alkylidene sites on the carbide surface. ROMP is a particularly powerful method (*13*, *14*) in materials science, and its application to the growth of polymers directly from surface sites would be a major advance. Growth from the surface is a necessary condition to achieve direct molecular contact between a polymer chain and a conducting material. We report that ring-opening metathesis can be carried out at cyclopentylidene initiator sites on the surface of β-Mo_2C. Figure 3 shows data for ring-opening metathesis reactions of cyclopentene and norbornene on the cyclopentylidene functionalized carbide surface. Exposure to gas-phase norbornene at 500 K leads to a gradual replacement of the cyclopentylidene spectrum (spectrum 3A) with bands at 3058, 2953, 2914, and 2877 cm^{-1} through monomer insertion (Fig. 3). Polynorbornene films grown using a Grubbs catalyst tethered to the native oxide layer on Si display a weak band at ~3050 cm^{-1} and three strong bands at 2946, 2910, and 2866 cm^{-1} (*15*). The agreement between the vibrational data confirms that the ROMP reaction occurs on β-Mo_2C and leads to polynorbornene formation. By comparing spectra for norbornene ring-opening (spectra 3C and 3D) with data for cyclopentene (spectrum 3B), the $\nu_s(CH_2)$ vibrational signature of the linear C_3 alkane segment formed from cyclopentene ring-opening is resolved at 2830 cm^{-1}.

Olefin metathesis can be used to manipulate double-bond contacts on the surface of a technologically relevant material. The propensity to form double bonds suggests that the carbide surface behaves as an array of isolated metal atoms leading to the inhibition of bridged chemisorption configurations. The most likely reason alkylidenes are not readily observed on metal surfaces is that adsorbates generally tend to occupy high-coordination surface sites. Thus, for example, although the diradical CH_2 would react with an isolated metal (M) atom to form an $M{=}CH_2$ methylidene species, it would be expected to react with an extended metal surface to form a bridging methylene species (*16*). The latter adsorption geometry is advantageous in that it permits tetravalent coordination of the carbon atom (*17*). In contrast, the truly single-site bonding observed for the surface alkylidene systems implies that identical local bonding will occur at all size scales from a single-atom organometallic complex up to a macroscopic surface. This highly selective bonding to the carbide surface suggests applications such as double-bond contacts to carbided STM tips or double-bond connections between carbide sources and drains. Hence, we anticipate that the demonstrated ability to control and monitor olefin metathesis in chemisorbed layers will play a role in the development of new nanoscale devices.

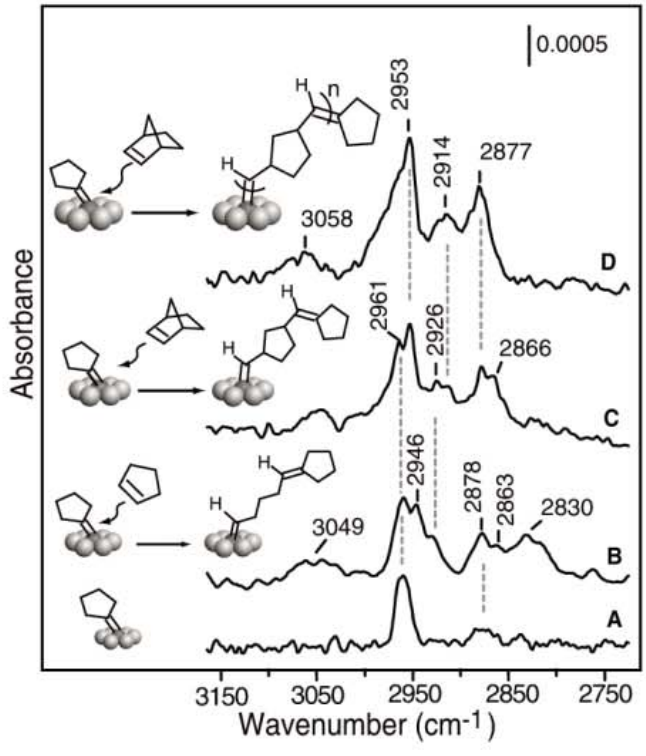

Fig. 3. RAIRS spectra for the ring-opening metathesis reactions of norbornene (**C** and **D**) and cyclopentene (**B**) monomers with cyclopentylidene sites on β-Mo_2C. The reaction with norbornene was carried out by heating from 100 to 500 K in 7×10^{-8} Torr. One heating cycle yielded spectrum (C), and two cycles yielded spectrum (D). The reaction with cyclopentene was carried out at 470 K in 2×10^{-8} Torr. Spectrum (**A**) is included as a reference spectrum for surface cyclopentylidene.

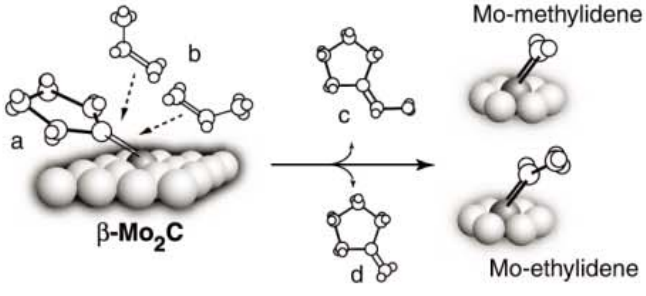

Scheme 1. Observed surface and gas-phase products for cross-metathesis reactions between propene (b) and cyclopentylidene (a) groups on β-Mo_2C: (c) ethylidene cyclopentane; (d) methylidene cyclopentane.

References and Notes

1. Y. Zhang, T. Ichihashi, E. Landree, F. Nihey, S. Iijima, *Science* **285**, 1719 (1999).
2. R. Martel *et al.*, *Phys. Rev. Lett.* **87**, 256805 (2001).
3. J. A. Misewich *et al.*, *Science* **300**, 783 (2003).
4. E. Zahidi, H. Oudghiri-Hassani, P. H. McBreen, *Nature* **409**, 1023 (2001).
5. M. Siaj, C. Reed, S. T. Oyama, S. L. Scott, P. H. McBreen, *J. Am. Chem. Soc.* **126**, 9514 (2004).
6. M. R. Buchmeiser, *Chem. Rev.* **100**, 1565 (2000).
7. J. L. Hérisson, Y. Chauvin, *Makromol. Chem.* **141**, 161 (1971).
8. Details of the preparation and thermal stability of the cyclopentylidene groups on molybdenum carbide are available as supporting material on *Science* Online.
9. J. C. Bryan, J. M. Mayer, *J. Am. Chem. Soc.* **112**, 2298 (1990).
10. L. J. Morris *et al.*, *Organometallics* **20**, 2344 (2001).
11. M. Leconte, J. M. Basset, *J. Am. Chem. Soc.* **101**, 7296 (1979).
12. R. Z. Lei, A. J. Gellman, B. E. Koel, *Surf. Sci.* **554**, 125 (2004).
13. I. M. Rutenberg *et al.*, *J. Am. Chem. Soc.* **126**, 4062 (2004).
14. G. K. Jennings, E. L. Brantley, *Adv. Mat.* **16**, 1983 (2004).
15. N. Y. Kim *et al.*, *Macromolecules* **33**, 2793 (2000).
16. P. M. George *et al.*, *J. Am. Chem. Soc.* **105**, 1393 (1983).
17. M. A. Petersen, S. J. Jenkins, D. A. King, *J. Phys. Chem. B* **108**, 5909 (2004).

18. This work was supported by a Natural Sciences and Engineering Research Council of Canada Discovery Grant and a Fonds québécois de la recherche sur la nature et les technologies grant for the Centre de recherche sur les propriétés des interfaces et la catalyze.

Supporting Online Material

www.sciencemag.org/cgi/content/full/309/5734/588/DC1
Materials and Methods
Figs. S1 and S2
References

18 April 2005; accepted 13 June 2005
10.1126/science.1113667

Formation of Catalytic Metal-Molecule Contacts

George S. Tulevski,[1] Matt B. Myers,[1] Mark S. Hybertsen,[2] Michael L. Steigerwald,[1]* Colin Nuckolls[1]*

We describe a new strategy for the in situ growth of molecular wires predicated on the synthesis of a trifunctional "primed" contact formed from metal-carbon multiple bonds. The ruthenium-carbon π bond provides structural stability to the molecular linkages under ambient conditions, and density functional calculations indicate the formation of an efficient conduit for charge carriers to pass between the metal and the molecule. Moreover, the metal-carbon π bond provides a chemically reactive site from which a conjugated molecular wire can be grown in situ through an olefin metathesis reaction.

For single-molecule electronics, more effort has been invested in the design and synthesis of the molecules and less in the fabrication of the molecule-to-metal contact. A common approach for molecular wires is an extended, conjugated, organic π system bonded to a metal surface (most frequently as a thiol linkage to gold) (*1*). One limitation is that the gold thiol linkage is only structural; it lacks any subsequent chemistry that is useful. Also, because it is difficult to modify the energies and occupations of the sulfur 3*p* orbitals substantially, the metal-thiolate contact lacks an essential orbital conduit for electrons and/or holes.

We present an alternative strategy for the in situ growth of molecular wires predicated on the synthesis of a trifunctional "primed" contact formed from metal-carbon multiple bonds. The primed contact provides static structural stability and a chemically reactive site from which a molecular wire can be grown. It should also create an efficient conduit for charge carriers to pass between the metal and the molecule; the metal-carbon π bond continues the π conjugation from the conjugated molecule directly into the metal. The metal-carbon π bond is active in the olefin metathesis reaction, indicating that the reactivity of such sites can be exploited to grow conjugated molecular wires in situ.

Ruthenium (Ru) is an attractive material for electrodes because it readily forms hard, highly conductive thin films (*2*). It is also a very active catalytic metal; carbene complexes in solution can catalyze the metathesis of olefins (*3*). There are precedents for Ru-surface carbene complexes in ultrahigh vacuum (UHV): one using diazomethane (*4*) and the other diphenyl diazomethane (*5*). In addition, the UHV studies of McBreen and co-workers have shown that surface molecule multiple bonds on metal-carbide surfaces are some of the most thermally stable adlayers (*6*) and are catalytically active (*6*–*8*). We found that a freshly prepared Ru thin film (*9*) reacts at room temperature with either 4-bromophenyldiazomethane (**1**) or trimethylsilyldiazomethane (**2**) to give the derivatized surfaces **1a** and **2a**, respectively (insets to Figs. 1 and 2) (*10*). In each case, the C-N bond cleaves, and the C(H)R (R = 4-bromophenyl or trimethylsilyl, respectively) fragment bonds directly to the metal. Scanning tunneling microscopy images on ruthenium single crystals indicate that a single, dense layer forms (*11*).

[1]Department of Chemistry and the Nanoscience Center, [2]Department of Applied Physics and Applied Mathematics and the Nanoscience Center, Columbia University, New York, NY 10027, USA.

*To whom correspondence should be addressed. E-mail: cn37@columbia.edu (C.N.); mls2064@columbia.edu (M.L.S.)

The photoelastic modulation infrared (IR) reflection-absorption spectrum (*12*) of **1a** (Fig. 1A) contains the C=C symmetric stretching modes at 1610 and 1585 cm^{-1} characteristic of a 1,4-disubstituted phenyl group. Three other major resonances are also present: the C=C asymmetric stretch (1465 cm^{-1}) and the parallel (1370 cm^{-1}) and perpendicular (940 cm^{-1}) in-plane ring stretches (*13*, *14*). We did not observe any stretching modes indicative of the dibromostilbene that would result from the coupling of two carbenes or from a diazo functionality. The x-ray photoelectron spectrum (XPS) (*12*) of **1a** shows the presence of the characteristic Br doublet arising from the $3d_{5/2}$ and $3d_{3/2}$ core levels (*15*, *16*).

For the reaction between a freshly prepared Ru surface and trimethylsilyldiazomethane, **2**, the IR spectrum is dominated by two sets of peaks: one a broad and intense resonance at around 1200 cm^{-1} and the other a cluster of three peaks (2953, 2916, and 2854 cm^{-1}) (fig. S1A) (*12*). The former is well known in methylsilane monolayers (*17*) and arises from the silicon-carbon stretch of the trimethylsilyl (TMS) group. The other three peaks are the asymmetric (2953 cm^{-1}) and symmetric (2916 and 2854 cm^{-1}) stretches indicative of terminal methyl groups (*17*). Again, there was no evidence of a diazo stretch or an alkene stretch. The XPS for **2a** shows the expected transition at about 100.5 eV for the silicon 2*p* core levels

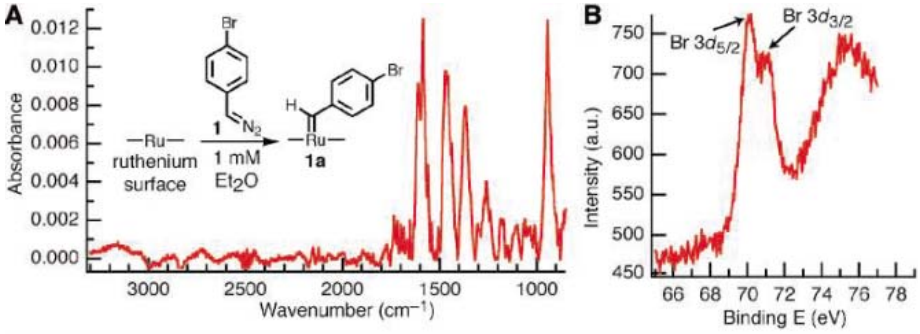

Fig. 1. To form the monolayer **1a**, a fresh ruthenium surface reacted with 4-bromophenyldiazomethane (**1**). (**A**) Surface polarized IR spectrum. (Inset) Reaction of a ruthenium surface with 4-bromophenyldiazomethane to give a derivatized surface. (**B**) XPS showing the presence of bromine atoms. a.u., arbitrary units.

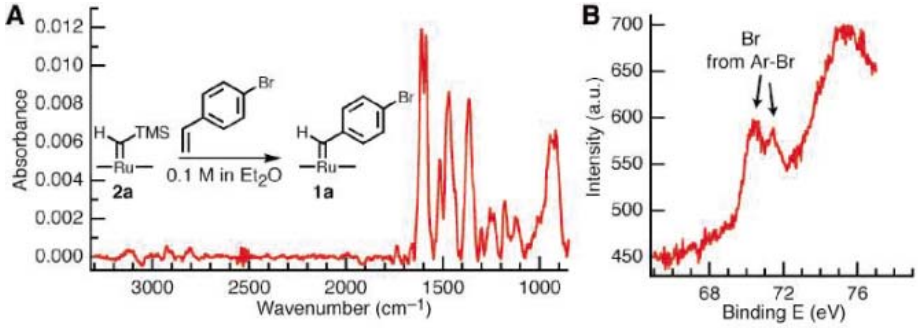

Fig. 2. Conversion of **2a** into **1a** with the use of a 1 mM solution of 4-bromostyrene in ether. (**A**) IR spectrum. (Inset) Reaction of derivatized surface **2a** with 4-bromostyrene to give derivatized surface **1a**. (**B**) XPS from the bromine after reaction. a.u., arbitrary units.

from the TMS group (fig. S1B) (*18*). The only other diagnostic feature in the XPS spectra from either **1a** or **2a** is the presence of well-known ruthenium nitrides (*19*–*21*).

These monolayers on Ru are exceedingly stable. We took no measures to protect the samples from oxygen or moisture, yet the XPS and IR signals from the monolayers remained unchanged when measured intermittently over the course of a few days. When we heated the films to 160°C for several hours the only detectable difference in the spectra was the conversion of the molecular nitride into the atomic nitride—a well-studied process (fig. S2) (*20*, *21*). Similarly, when the monolayers were placed into solvents such as ether, tetrahydrofuran (THF), or dodecane overnight they showed no change.

The IR and XPS data show that diazoalkanes react with a Ru surface, but it is yet to be determined the exact nature of the bonding of the otherwise divalent carbon to the surface of the metal. This C atom may form the carbon-metal double bond to a single surface Ru atom, as deduced from previous UHV studies (*4*, *5*). A second alternative is that the carbon bridges adjacent surface atoms, in either a doubly or triply bridge bonded arrangement. Unfortunately, we cannot observe spectral features assignable to any of these modes, and therefore we cannot distinguish which bonding form occurs in the present samples.

The distinction between the bonding modes may not be as practically important as one might imagine. Even if the carbene carbon bonds in a bridging fashion to two or more Ru atoms, its chemical reactivity should be similar to that of a "mononuclear" metal carbene. In solution, they show qualitatively similar chemistry when the carbene is either bridge-bonded between two ruthenium atoms or when there is an unambiguous carbon-ruthenium double bond (*22*) (although the former is catalytically less active).

In any case, we found that the surface-bound $Ru_nC(H)(R)$ unit can catalyze olefin metathesis and that the Ru-C linkage behaves sufficiently like a multiple bond that it warrants further study as a molecule-to-metal contact. When we treated **2a** (prepared from **2** as above) with a large excess of 4-bromostyrene in diethylether overnight at room temperature, we saw the spectral features characteristic of **2a** disappear and those of **1a** appear (Fig. 2) (*23*). After reaction, the characteristic XPS signature for Br was present (Fig. 2B), but the Si signature from the TMS group at ~100.5 eV was absent (fig. S3). Similarly, the IR spectrum shows the loss of the intense C-Si stretch and appearance of the four resonances characteristic of the parasubstituted phenyl ring of **1a**. The spectra of the surfaces prepared by means of diazoalkanes and by means of metathesis show different ratios of the C-C ring-stretching doublet around 1600 cm^{-1}, an indication of the surface conformation of parasubstituted aromatics, that likely reflects the different density of carbenes on the two surfaces.

The converse reaction, converting monolayer **1a** into a monolayer **2a** using vinyltrimethylsilane (Fig. 3A) also occurs. Under identical conditions to those used above for **2a**, the conversion to **1a** gives a mixture of different carbenes on the surface in approximately 8:5 ratio indicating a 60% conversion (fig. S4). This reaction does not proceed to completion, whereas the reverse reaction does. This difference could be due to the surface **1a** (prepared from **1**) having a higher density of carbenes compared with that of surface **2a** (prepared from **2**) based on the larger cross-sectional area for the bulky trimethylsilyl group, so that it is not possible to fully convert **1a** to **2a** by metathesis.

The data in Fig. 3B obtained with gas chromatography/mass spectrometry (GC/MS) serve as a strong indication that the surface reaction proceeds through a metathesis reaction. To aid in the analysis (by increasing the surface area and therefore the amount of the 4-bromostyrene produced), ruthenium particles were used instead of planar metal films. These Ru particles were allowed to react with **1** and then placed in a solution of vinyltrimethylsilane. Both a 4-bromostyrene standard and the reaction mixture showed a peak in the chromatogram at a retention time of 7.27 min. The mass spectrum of this peak in both cases shows the expected mass and isotope pattern from 4-bromostyrene. The demonstration of a surface-initiated olefin metathesis reaction not only provides evidence of the multiple bond character of the Ru-C link but is also essential to our broader strategy of in situ synthesis of molecular wires starting from a primed metal surface (Fig. 3C).

A carbene precursor such as a diazoalkane is necessary to initiate any of this chemistry. For example, when a fresh Ru surface is treated with either 4-bromostyrene or vinyltrimethylsilane under the conditions that led to metathesis (above), we did not observe bromine or silicon peaks in the XPS. Also, a "carbene metal" such as Ru is necessary; the use of Au instead of Ru in these reactions did not produce a derivatized Au surface. Neither of the diagnostic peaks that result from the reaction of **2** with Ru (i.e., the Si-C stretch at 1236 cm^{-1} nor the Si peak in the XPS at 100.5 eV) was present when we treated a Au film with a solution of **2** in ether (fig. S5).

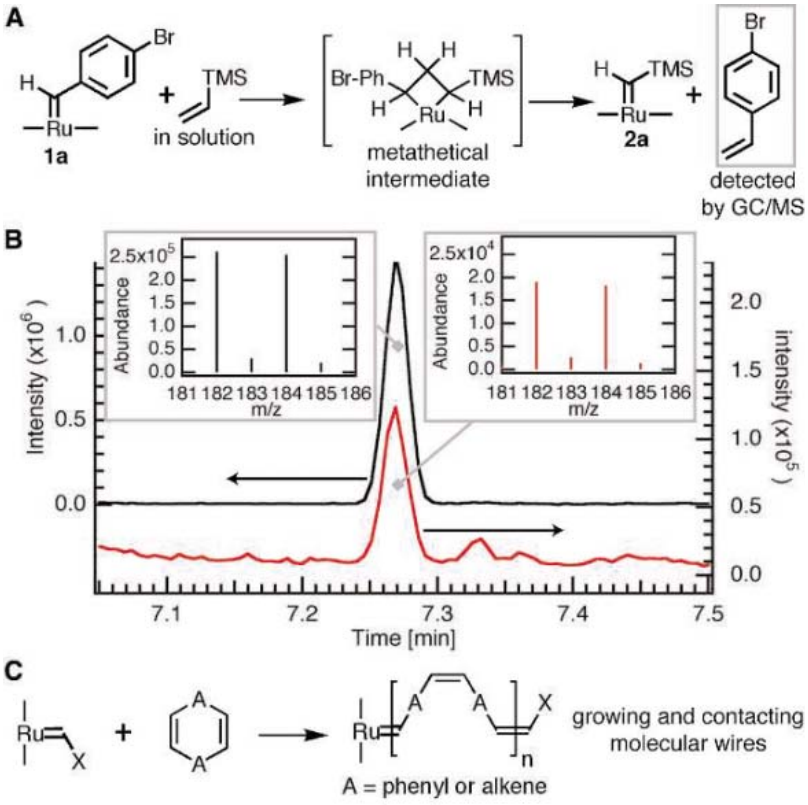

Fig. 3. (**A**) Reaction of **1a** with vinyl-trimethylsilane through a surface metathesis reaction to yield **2a** and 4-bromostyrene. (**B**) The 4-bromostyrene can be detected by GC/MS. The insets show the characteristic mass and isotope pattern for the 4-bromostyrene standard (left inset) and for the reaction mixture (right inset). m/z, mass-to-charge ratio. (**C**) Ring opening metathesis polymerization pathway to conjugated molecular wires in electrical contact with a Ru metal particle or surface.

To understand the bonding of the ruthenium surface carbenes and the character of the electronic states that link to a molecular wire, we conducted a series of density functional theory calculations (*24*, *25*). Both Ru clusters (*26*) and periodic slabs (*27*, *28*) of Ru have been considered, coupled to several different carbenes. In Fig. 4A, we show results obtained for a carbene at the end of a 1,3-pentadienchain, C_5H_6: The conjugated π system forms a short molecular "wire," whereas the terminal divalent carbon forms the carbene link to the metal. The bonding to the atop site on the Ru(0001) surface with the terminal carbene forms a simple double bond, giving a Ru-C bond length of 1.96 Å. The length of the adjacent C-C single bond is similar to that of the corresponding bond in the related hexa-1,3,5-triene (table S1). Figure 4A also shows the frontier π orbital for the RuC_5H_6 molecule. The Ru-to-C π bonding is essentially continuous with the rest of the π system on the molecule. Figure 4B shows the parallel comparison for C_5H_5, a carbyne, bonded in the hexagonally close-packed hollow site of the Ru(0001) surface. Again, the continuity of the π system bonding on the molecule is apparent and the geometry of the C_5H_5 is indistinguishable from the double-bonded organic analog.

The degree of coupling of the π system to the extended states in the metal was monitored by computing the local density of states as a function of energy, projecting on the region of the last two C atoms in the molecule. The results are shown for energies near the Ru metal Fermi energy in Fig. 4C (*29*). The occupied resonance clearly has the character of the highest occupied π state in the organic, with two nodes along the chain. The unoccupied resonance is similarly derived from the first empty π state, with three nodes along the chain (including the link to the surface.) The occupied resonance is quite broad, and the state has the general character of the organic π state throughout. These results indicate that the π bonding on the organic backbone couples smoothly to the *d* orbitals in the Ru metal. This looks very promising as a high conductance link between the Ru metal and the molecule. The π resonance overlaps the metal Fermi energy and is partially empty. This is consistent with the calculated change in the work function upon formation of this 2×2 adlayer (namely ~–0.5 eV).

This study demonstrates that solution-phase chemistry can be used to form stable monolayers between carbenes and ruthenium surfaces. These surface-bound carbenes are able to initiate olefin metathesis. Given the strong electronic coupling between the molecular π states and the conducting states in the metal, these systems form primed contacts with utility in molecular electronics as highly conductive and catalytic sites for in situ wire growth from electrode surfaces.

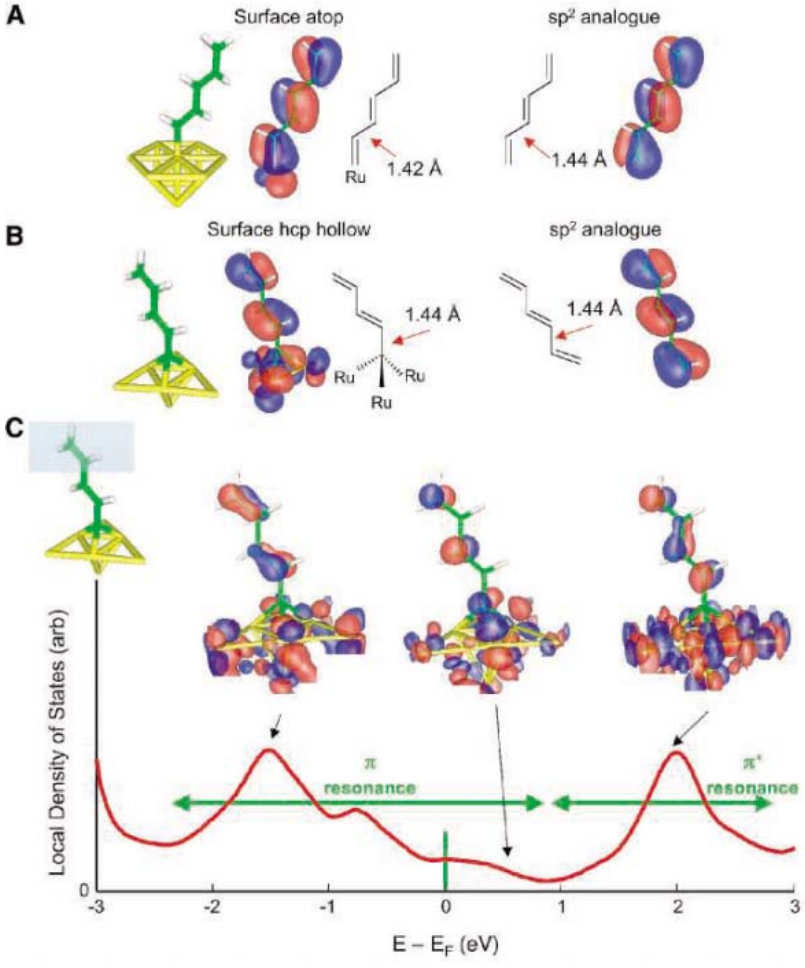

Fig. 4. Two candidate bonding geometries. (**A**) Atop binding of a carbene on the Ru(0001) surface and (**B**) threefold hexagonal close-packed (hcp) hollow site binding of the carbyne on the Ru(0001) surface. Results for the relaxed geometry computed for the 2×2 surface unit cell are compared to those for a C_6H_8 organic analog. The highest occupied π state for the pentadienyl fragments bound to the ruthenium cluster is compared to the analog in an isosurface plot. (**C**) Local density of states for the carbyne bonded to the hcp hollow of the Ru(0001) surface (modeled by a four monolayer slab) for energies near the Ru Fermi energy. The state density is projected on the region of the last two carbon atoms on the chain as indicated. Isosurface plots for selected wave functions are shown. The plots are truncated to the near-surface region. arb, arbitrary units.

References and Notes

1. A. Nitzan, M. A. Ratner, *Science* **300**, 1384 (2003).
2. H. Zhong, G. Heuss, Y.-S. Suh, V. Misra, S.-N. Hong, *J. Electron. Mater.* **30**, 1493 (2001).
3. R. H. Grubbs, *The Handbook of Olefin Metathesis,* R. H. Grubbs, Ed. (Wiley-VCH, Weinheim, ed. 1, 2003).
4. P. M. George, N. R. Avery, W. H. Weinberg, F. N. Tebbe, *J. Am. Chem. Soc.* **105**, 1393 (1983).
5. M. Gunia, P. Jakob, W. Sander, C. Woell, *J. Phys. Chem. B* **108**, 14025 (2004).
6. E. M. Zahidi, H. Oudghiri-Hassani, P. H. McBreen, *Nature* **409**, 1023 (2001).
7. M. Siaj, C. Reed, S. T. Oyama, S. L. Scott, P. H. McBreen, *J. Am. Chem. Soc.* **126**, 9514 (2004).
8. M. Siaj, H. Oudghiri Hassani, E. Zahidi, P. H. McBreen, *Surf. Sci.* **579**, 1 (2005).
9. To form the monolayers **1a** and **2a**: 200 nm of Ru metal (Kurt J. Lesker) was sputtered onto silicon wafers (Silicon Sense) with the use of a home-built sputtering chamber. The native oxide was removed from the samples by hydrogenation (1 atm H_2, 120°C, 1 hour) immediately before use. The metal films were immersed in a solution of either **1** (0.1 mM solution in benzene) or **2** (0.1 mM solution in Et_2O) for 2 hours, and then they were removed, rinsed in copious amounts of fresh solvent, and dried under a stream of nitrogen gas.
10. D. S. Wulfman, S. Yousefian, J. M. White, *Synth. Commun.* **18**, 2349 (1988).
11. G. Flynn, M. Lay, G. S. Tulevski, M. L. Steigerwald, C. Nuckolls, data not shown.
12. Materials and methods are available as supporting material on *Science* Online.
13. Here, parallel and perpendicular refer to the 1,4-phenyl axis.
14. R. Arnold, A. Terfort, C. Woell, *Langmuir* **17**, 4980 (2001).
15. We used **1** and **2** in these studies because they carry marker atoms (i.e., bromine or silicon) that are easily identified with XPS. These marker atoms are necessary because the carbon 1*s* core level cannot be monitored because its x-ray photoelectron energy is coincident with the ruthenium $3d_{5/2}$ core level.
16. Y. Kaga, Y. Abe, H. Yanagisawa, M. Kawamura, K. Sasaki, *Surf. Sci. Spectra* **6**, 68 (1999).
17. J. R. Combes, L. D. White, C. P. Tripp, *Langmuir* **15**, 7870 (1999).
18. S. R. Wasserman, Y. T. Tao, G. M. Whitesides, *Langmuir* **5**, 1074 (1989).
19. T. Birchem, M. Muhler, *Surf. Sci.* **334**, L701 (1995).
20. K. Jacobi, *Phys. Status Solidi A* **177**, 37 (2000).
21. E. Umbach, *Solid State Commun.* **51**, 365 (1984).
22. M. R. Gagne, R. H. Grubbs, J. Feldman, J. W. Ziller, *Organometallics* **11**, 3933 (1992).

23. Conditions for metathesis reaction: **1a** or **2a**, prepared from the corresponding diazoalkanes, was immersed in a solution (0.1 M solution in THF) of the corresponding alkenes for 2 hours. The films were removed, rinsed with fresh THF, and dried under a stream of nitrogen gas.
24. The generalized gradient approximation was used (*12*, *25*).
25. J. P. Perdew, K. Burke, M. Ernzerhof, *Phys. Rev. Lett.* **77**, 3865 (1996).
26. Jaguar 5.0, Schrodinger, L.L.C., Portland, OR (1991–2003).
27. The ABINIT code is a common project of the Université Catholique de Louvain, Corning Incorporated, and other contributors (www.abinit.org).
28. X. Gonze *et al.*, *Comp. Mater. Sci.* **25**, 478 (2002).
29. The substructure of the occupied resonance is due to the size of the slab (4 monolayers). However, there is continuous state density through this energy region, resulting from dispersion of the states in the direction parallel to the surface.
30. We acknowledge primary financial support from the Nanoscale Science and Engineering Initiative of the NSF under NSF award number CHE-0117752 and by the New York State Office of Science, Technology, and Academic Research (NYSTAR). We acknowledge support from the Chemical Sciences, Geosciences and Biosciences Division, Office of Basic Energy Sciences, U.S. Department of Energy (#DE-FG02-01ER15264). C.N. thanks the American Chemical Society Petroleum Research Fund type G (#39263-G7), the Camille Dreyfus Teacher Scholar Program (2004), and the Alfred P. Sloan Fellowship Program (2004). We thank the Materials Research Science and Engineering Center Program of the NSF under award number DMR-0213574 and by the NYSTAR for financial support for M.L.S. and the shared instrument facility.

Supporting Online Material
www.sciencemag.org/cgi/content/full/309/5734/591/DC1
Materials and Methods
Figs. S1 to S5
Table S1
References

25 March 2005; accepted 10 June 2005
10.1126/science.1112767

Martian Surface Paleotemperatures from Thermochronology of Meteorites

David L. Shuster[1]* and Benjamin P. Weiss[2]†

The temporal evolution of past martian surface temperatures is poorly known. We used thermochronology and published noble gas and petrographic data to constrain the temperature histories of the nakhlites and martian meteorite ALH84001. We found that the nakhlites have not been heated to more than 350°C since they formed. Our calculations also suggest that for most of the past 4 billion years, ambient near-surface temperatures on Mars are unlikely to have been much higher than the present cold (<0°C) state.

Daily mean equatorial temperatures on Mars are close to 215 K. Surface geomorphic evidence of the flow of liquids, weathering minerals indicative of liquid/rock interactions, and the enrichment of heavy isotopes of several atmospheric species have led to suggestions that early Mars was significantly warmer, with temperatures possibly remaining above 273 K for extended periods of time (*1*). On the basis of crater counting statistics, the colder, drier conditions are thought to have emerged at ~3.7 billion years ago (Ga), with large (~10^8 to 10^9 years) uncertainties (*2*). The growing geochemical and petrographic data set for martian meteorites (*3*) provides an opportunity to constrain the martian paleoclimate using multiple independent samples. We used noble gas thermochronometry of meteorites as an indicator of the evolution of surface temperatures on Mars.

K/Ar and $^{40}Ar/^{39}Ar$ dating studies have been conducted on all seven known nakhlites (*4*) and on martian meteorite ALH84001 (*5*, *6*). Fifteen K/Ar analyses on the nakhlites all give ages of ~1.3 Ga, which are nearly identical to crystallization ages specified by the Rb/Sr, U/Pb, and Sm/Nd chronometers (*7*) and much older than the 11 million years ago (Ma) age of ejection from Mars, as specified by cosmic ray exposure dating (*8*, *9*). (U-Th)/He dating of the nahklites meteorites Nakhla, Lafayette, and MIL03346 (*10*, *11*) has measured similarly ancient (~0.8 to 1.2 Ga) ages. The coincidence of the K/Ar and (U-Th)/He ages with the other chronometers suggests that the nakhlites have experienced no major heating since they formed. Similarly, the ancient 4 Ga $^{40}Ar/^{39}Ar$ age (*6*) and 4 Ga U/Pb apatite age (*12*) for ALH84001 suggests that this meteorite, which has Rb/Sr and Sm/Nd crystallization ages of 4.5 Ga and a cosmic ray exposure age of 15 Ma (*13*), has not experienced any major heating since 4 Ga. This is generally consistent with (U-Th)/He dating of ALH84001 phosphate, which gives a wide range of ages between 0.1 and 3.5 Ga (*14*). Like the nakhlites, the $^{40}Ar/^{39}Ar$ age of Chassigny is ~1.3 Ga and is close to its Sm/Nd and Rb/Sr crystallization ages (*6*, *13*). $^{40}Ar/^{39}Ar$ ages for most shergottites are ambiguous because of significant abundances of trapped Ar (*6*, *13*).

Using whole-rock ^{39}Ar release data of Swindle and Olson (*15*) and following the methods of (*5*, *16*), we estimated the temperature dependence of the Ar diffusion coefficient $D(T)$ through the feldspar in Nakhla and Lafayette, assuming a spherical diffusion domain geometry (*17*). We first considered Swindle and Olson's Nakhla subsample 1. We assumed that the colinearity observed for the first ~80% of the released ^{39}Ar (Fig. 1) indicates that the diffusion of Ar in Nakhla is thermally activated over this range. We also assumed that the presence of distinct arrays clearly separated by breaks in slope (Fig. 1) indicates that multiple diffusion domains are present. From this, we identified three (or possibly even four) primary arrays from the ^{39}Ar data and adopted the interpretation of (*15*) that the first three domains [the low-retentivity domain (LRD) and the one or two high-retentivity domains, which we will refer to as HRD and HHRD] likely represent iddingsite (LRD) and predominantly potassium feldspar admixed with plagioclase (HRD and HHRD). The final array, composed of the final ~20% of gas released, appears to be from a phase (probably clinopyroxene) implanted with recoiled ^{39}Ar (*15*, *18*).

We characterized the spatial distribution of radiogenic ^{40}Ar ($^{40}Ar^*$) and the Ar diffusion kinetics in the HRD alone. The HRD corresponds to the ~1.3 Ga $^{40}Ar/^{39}Ar$ plateau age identified in (*15*). We calculated a diffusion domain model by assuming that the neutron-induced ^{39}Ar distributions were initially uniform within two distinct domains. Gas was not permitted to exchange between the domains. We derived the following diffusion parameters for the two-domain (LRD and HRD only) model for the HRD of Nakhla: activation energy E_a = 117 ± 5.4 kJ mol^{-1} and $\ln(D_o/a^2)$ = 5.7 ± 0.9 $\ln(s^{-1})$ for diffusivity at infinite temperature D_o and diffusive length scale a. These are in good agreement with diffusion parameters estimated for terrestrial potassium feldspars (*19*). Nearly identical results were obtained for the nakhlite Lafayette and another Nakhla subsample (fig. S1, A and B). Similar [within a factor of ~1.2 and ~2.4 for E_a and $\ln(D_o/a^2)$, respectively] values for the HRD were also obtained for a subset one-domain (HRD only) regression (*20*) and a three-domain (LRD, HRD, and HHRD) model, indicating that the inferred diffusion kinetics are not strongly sensitive to the form of the domain modeling (*21*).

In the following calculations, we assume that this Arrhenius relation and corresponding diffusive length scale a have held for the nakhlites' HRD since 1.3 Ga (*22*). The model

[1]Division of Geological and Planetary Sciences, California Institute of Technology, 100-23, Pasadena, CA 91125, USA. [2]Department of Earth, Atmospheric, and Planetary Sciences, Massachusetts Institute of Technology, 54-724, Cambridge, MA 02139, USA.

*Present address: Berkeley Geochronology Center, 2455 Ridge Road, Berkeley, CA 94709, USA
†To whom correspondence should be addressed. E-mail: bpweiss@mit.edu

LRD diffusion kinetics predict essentially no ^{40}Ar* retention over geologic time, which is consistent with the zero age ^{40}Ar/^{39}Ar in the first ~3% of extracted ^{39}Ar observed by (*15*). With the two-domain model (Fig. 1) and a numerical solution to the radiogenic production/diffusion equation described by (*5*, *23*) using a pre-atmospheric meteorite radius of 0.2 m (*8*), we simulated the expected ^{40}Ar* distributions within the sample after various thermal perturbations. The model ^{40}Ar* distributions were calculated for the HRD and then passed through a simulated degassing experiment to produce a set of ^{40}Ar* release fractions (Fig. 2).

Our calculations demonstrate that only ~1% of the ingrown ^{40}Ar* has been diffusively lost from the HRD of Nakhla and Lafayette since 1.3 Ga. From a similar analysis using the Ar release data of Bogard and Garrison (*6*), we confirm our conclusion (*5*) that less than 8% of the ingrown ^{40}Ar* has been diffusively lost from the HRD of ALH84001 since 4 Ga (figs. S1C and S2C).

Solving for a sample's continuous thermal history from an observed radiometric age and an inferred spatial distribution of the daughter product is an ill-posed problem: A family of thermal limits can be uniquely constrained, although a single solution does not generally exist (*19*). For instance, let us suppose that the nakhlites were heated to some peak temperature during ejection from Mars at 11 Ma. If we assume that the meteorites cooled diffusively and degassed ^{40}Ar* diffusively solely during this ejection event, then following the methods of (*5*), we find that the central temperatures of these meteorites could not have exceeded ~350°C for even short periods of time (no more than a few hours) (Fig. 2). This is a conservative upper limit, because we assume (i) that the diffusion domains are spherical and that during the other 1.3 billion years of history (ii) there was no other diffusive loss of ^{40}Ar* and (iii) no loss of ^{40}Ar* caused by nonthermal mechanisms (such as weathering or shock). These results are consistent with petrographic constraints, which suggest that the nakhlites have been shocked only to peak pressures of 10 to 20 GPa and peak temperatures of –50° to 100°C, respectively [following (*24*, *25*) and using ambient martian surface temperatures between –120° and 0°C]. Given the petrographic similarities linking the nakhlites, it is likely that the conclusions drawn from Nakhla and Lafayette extend to the five other known meteorites in this class.

Because the magnetization of the nakhlites is thought to be dominated by titanomagnetite with a Curie point of ~500° to 550°C (*26*), much of the magnetization measured in the nakhlites is likely to have been a thermoremanence that originated on Mars at 1.3 Ga. However, this remanence is likely to have been modified by shock (*27*).

Our results are consistent with the observed low shock state of nakhlites (*24*, *25*), which implies that they were not heat-sterilized (that is, they were cooler than ~100°C) during ejection from Mars and transfer to Earth. Although ALH84001 also is thought to have experienced only mild heating during its transfer to Earth (*5*, *28*), the case for the nakhlites is stronger because of their substantially lower shock state (*29*). This illustrates the efficiency of mechanisms for ejecting weakly shocked rocks from Mars (*24*, *30*) and underscores the possibility that the terrestrial planets have not been biologically isolated from one another.

Finally, these results highlight the difference in thermal histories between Mars and Earth. The small amounts of ^{40}Ar* degassing observed for the nakhlites and particularly for ALH84001 require that they must have been at low temperatures for nearly their entire histories. Linearly extrapolating the HRD Arrhenius relations (Fig. 1 and fig. S1) to low temperatures, we find that during the past 1.3 billion years, the three nakhlites could not have been at a constant temperature exceeding –8° to –49°C, depending on which Arrhenius model for the HRD is used (Fig. 3A and fig. S3A). A constant temperature of no more than –2° to –43°C lasting for 200 million

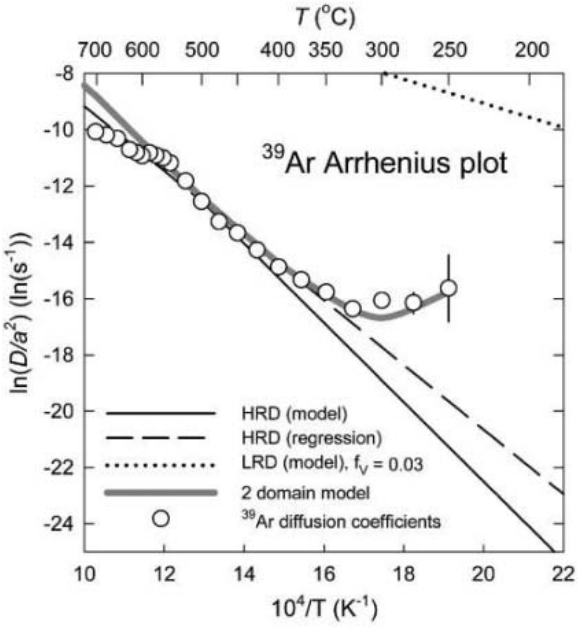

Fig. 1. Diffusivity as a function of temperature (Arrhenius plot) for martian meteorite Nakhla (subsample 1) inferred from ^{39}Ar release data of Swindle and Olson (*15*). Circles are the diffusion coefficients as calculated following (*16*). The bold gray curve shows the best-fit two-domain model, which contains a volume fraction f_v of 3% LRD mixed with 97% HRD. The solid and dotted black lines show model $D(T)/a^2$ for the HRD and LRD, respectively. The dashed black line shows the one-domain model, given by the linear regression fit only to the subset HRD array [it includes the 375° to 675°C steps (*20*)]. Error bars (specified by a vertical line through each point) are smaller than the size of the circle for all but the two lowest temperature steps. Similar results are obtained for both a second Nakhla subsample and for Lafayette (fig. S1).

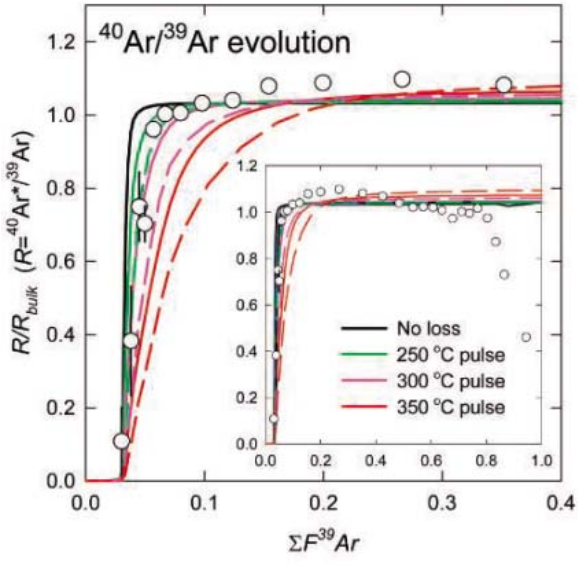

Fig. 2. Measured and modeled ^{40}Ar*/^{39}Ar ratio evolution spectra for martian meteorite Nakhla (subsample 1). These spectra were calculated using the two-domain model in Fig. 1 for various assumed diffusively cooling thermal pulses experienced by the HRD. Following (*19*), we found that it takes several hours for the meteorites to cool to ambient temperatures. The LRD was assumed to contain no radiogenic Ar (^{40}Ar*), and the spatial distribution of ^{40}Ar* within the HRD was assumed to be uniform before ejection. Shown are the calculated ^{40}Ar*/^{39}Ar ratios R (normalized to the bulk ratio R_{bulk}) plotted as a function of the cumulative ^{39}Ar release fraction ΣF^{39}Ar. Circles are the data of (*15*). Solid curves correspond to various peak temperature pulses during ejection from Mars at 11 Ma: black, no diffusive loss experienced by the HRD; green, 250°C; pink, 300°C; red, 350°C. Dashed curves are the same calculations using the one-domain model shown in Fig. 1. Error bars (specified by a vertical line through each point) are smaller than the size of the circle for all but the nine lowest temperature steps. Similar results are obtained for both a second Nakhla subsample and for Lafayette (fig. S2).

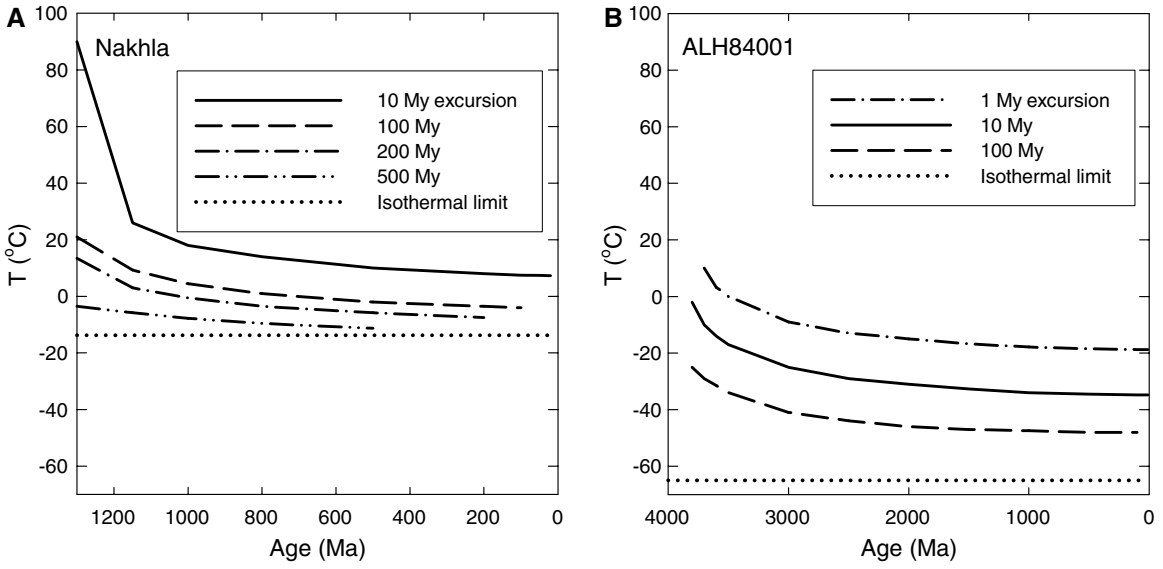

Fig. 3. Long-duration temperature limits for (**A**) Nakhla (subsample 1) and (**B**) ALH84001. Curves depict the maximum temperature that each meteorite could have experienced during a single assumed temperature excursion as a function of the time before the present (age) in martian history when the excursion begins. Each curve corresponds to a particular assumed duration for the excursion. The HRDs of the meteorites are assumed to experience no diffusive loss of ^{40}Ar* at all times other than during the temperature excursion. Each model is constrained to match the deficit gas fraction (the diffusively lost proportion of ^{40}Ar* relative to complete retention) observed in the HRD of each meteorite today (1 and 8% for Nakhla and ALH84001, respectively). These curves were calculated using the two-domain Arrhenius relations in Fig. 1. Figure S3 shows the sensitivity of these time/temperature constraints to the uncertainties in the diffusion kinetics.

years of the past 1 billion years of Nakhla's history is also required. This result is consistent with constraints derived from ALH84001, which suggest that since 4 Ga, it could not have been at a constant temperature exceeding –60° to –70°C, and since 3.5 Ga it could not have been warmer than –7° to +7°C for all but the briefest time period (1 million years) (Fig. 3B and fig. S3B). Given our assumptions, these are conservative upper limits. In all, four subsamples from three rocks taken from two martian meteorite classes with vastly different ages, petrographic textures, compositions, and argon diffusion kinetics give similar constraints on martian temperatures.

Our results may seem surprising given that Mars' obliquity and surface temperatures are thought to have regularly reached high values over the planet's entire history, with dominant frequencies of ~120,000 years and longer (*1*, *31*). However, because temperature changes at the martian surface will be attenuated at depth, deeply buried rocks may not sample these events (*1*, *32*). Although the burial depths of the martian meteorites are largely unknown, it is conceivable that ALH84001 was at more than 1 km depth for the past 4 billion years, whereas the nakhlites likely resided at depths of between a few meters to no more than a few hundred meters (*33*). Therefore, all of the meteorites subjected to the thermochronological calculations described here should not have been subject to diurnal or annual thermal variations. ALH84001 may not have sampled even the longest-period obliquity-induced thermal waves. However, the nakhlites formed at such shallow depths that they almost certainly experienced elevated temperatures associated with the full frequency range of obliquity changes since 1.3 Ga.

Our calculations imply that during the past 4 billion years, average temperatures within the top few kilometers of the martian crust were not significantly warmer than the present cold (subzero) conditions and therefore that pure liquid water was not likely to have been stable at the martian surface for extended periods of time. This is consistent with suggestions (*34*) that the secondary minerals only observed in these meteorites are the products of brief (less than a few days) interactions with liquid water.

References and Notes

1. M. Carr, *Water on Mars* (Oxford Univ. Press, Oxford, 1996).
2. W. K. Hartmann, G. Neukum, *Space Sci. Rev.* **96**, 165 (2001).
3. C. Meyer, *Mars Meteorite Compendium—2003* (NASA Johnson Space Center, Houston, TX, 2003), www-curator.jsc.nasa.gov/curator/antmet/mmc/mmc.htm.
4. Additional details about ^{40}Ar/^{39}Ar dating of nakhlites and our thermochronology methods are available as supporting material on *Science* Online.
5. B. P. Weiss, D. L. Shuster, S. T. Stewart, *Earth Planet. Sci. Lett.* **201**, 465 (2002).
6. D. D. Bogard, D. H. Garrison, *Meteorit. Planet. Sci.* **34**, 451 (1999).
7. H. Y. McSween, A. H. Treiman, in *Planetary Materials*, J. J. Papike, Ed. (Mineralogical Association of America, Washington, DC, 1998), pp. 6-1 to 6-53.
8. O. Eugster, H. Busemann, S. Lorenzetti, D. Terrebilini, *Meteorit. Planet. Sci.* **37**, 1345 (2002).
9. K. Marti, K. J. Mathew, *Antarct. Meteorite Res.* **17**, 117 (2004).
10. R. Ganapathy, E. Anders, *Geochim. Cosmochim. Acta* **33**, 775 (1969).
11. S. V. S. Murty, R. R. Mahajan, J. N. Goswami, N. Sinha, *Lunar Planet. Sci.* **XXXVI**, abstract 1280 (2005).
12. K. Terada, T. Monde, Y. Sano, *Meteorit. Planet. Sci.* **38**, 1697 (2003).
13. L. E. Nyquist *et al.*, *Space Sci. Rev.* **96**, 105 (2001).
14. K. Min, P. W. Reiners, *Lunar Planet. Sci.* **XXXVI**, abstract 2214 (2005).
15. T. D. Swindle, E. K. Olson, *Meteorit. Planet. Sci.* **39**, 755 (2004).
16. H. Fechtig, S. Kalbitzer, in *Potassium-Argon Dating*, O. A. Schaeffer, J. Zahringer, Eds. (Springer, Heidelberg, Germany, 1966), pp. 68–106.
17. The four highest temperature steps with ^{40}Ar/^{39}Ar clearly influenced by ^{39}Ar recoil were excluded from the total ^{39}Ar abundance used to calculate ^{39}Ar release fractions. Because these four steps were likely derived from a K-poor phase with higher Ar retentivity than the HRD of interest, they were excluded from the total so as not to bias the calculated diffusion coefficients for the lower-temperature extractions.
18. R. Burgess, G. Holland, V. Fernandes, G. Turner, *J. Conf. Abs.* **5**, 266 (2000).
19. I. McDougall, T. M. Harrison, *Geochronology and Thermochronology by the ^{40}Ar/^{39}Ar Method* (Oxford Univ. Press, New York, ed. 2, 1999).
20. In a sample with multiple and distinct diffusion domains, and for stepwise extractions that sequentially increase in temperature, linear regression through a subset array in a plot of $\ln(D/a^2)$ versus $1/T$ places lower bounds on the activation energy and $\ln(D_o/a^2)$ for the domain that dominates Ar release at those steps. Therefore, this one-domain model places maximum bounds on Ar diffusivity at low-temperature extrapolations. For this regression, the linear subset array was selected for steps between 375° and 675°C.
21. O. M. Lovera, M. Grove, T. M. Harrison, *Geochim. Cosmochim. Acta* **66**, 1237 (2002).
22. Specifically, we assume that the HRD argon diffusion kinetics measured in the laboratory between 250° and 700°C can be extrapolated to the (i) longer time scales, (ii) lower temperatures, and (iii) different pressures encountered in nature. We also assume that the characteristic diffusive length scale *a* of the HRD implied by Fig. 1 has not been modified since the initiation of ^{40}Ar* accumulation. Because the nakhlites were shock-fractured sometime after their formation (*25*), we are implicitly assuming that *a* is smaller than the characteristic distances between cracks and that the diffusion domains are not defined by the bulk geometry of the feldspar fragments.
23. D. L. Shuster, K. A. Farley, *Earth Planet. Sci. Lett.* **217**, 1 (2004).
24. N. Artemieva, B. Ivanov, *Icarus* **171**, 84 (2004).
25. J. Fritz, A. Greshake, D. Stoffler, *Lunar Planet. Sci.* **XXXIV**, abstract 1335 (2003).
26. D. W. Collinson, *Meteorit. Planet. Sci.* **32**, 803 (1997).
27. S. A. Gilder, M. LeGoff, J. C. Chervin, J. Peyronneau, *Geophys. Res. Lett.* **31**, L10612 (2004).
28. B. P. Weiss *et al.*, *Science* **290**, 791 (2000).
29. ALH84001 has been shocked to >40 GPa, but our thermochronological calculations indicate that this occurred at 4 Ga rather than during ejection (*5*). Although paleomagnetic analyses have been used to argue that ALH84001 was cooler than 40°C (*28*), it is

possible that the observed low-temperature paleomagnetic remanence was affected by viscous remagnetization. The thermal histories experienced by shergottites and chassignites are less well known because of the paucity of magnetic analyses and high-resolution $^{40}Ar/^{39}Ar$ age spectra free of trapped Ar for these rocks. (U-Th)/He dating of the shergottite Los Angeles (*35*) found that the meteorite was strongly heated (to probably at least several hundred degrees C) during ejection, but the peak temperature is not well constrained because the diffusivity of helium in Los Angeles merrillite is not currently known.

30. H. J. Melosh, *Nature* **363**, 498 (1993).
31. J. Laskar *et al.*, *Icarus* **170**, 343 (2004).
32. F. P. Fanale, J. R. Salvail, W. B. Banerdt, R. S. Saunders, *Icarus* **50**, 381 (1982).
33. Cosmic ray exposure data (*8*) imply that ALH84001 and most of the nakhlites must have been buried at least a few meters deep for nearly all of their histories. The nakhlites are thought to be cumulate rocks that originated in a shallow intrusion or lava flow. Analyses of iron and magnesium zoning in nakhlite olivines (*36*) suggest that Nakhla and Lafayette formed at depths of 3 to 10 m and >30 m, respectively. These estimates are consistent with but more restrictive than depth estimates inferred from studies of Theo's Flow, which are ultramafic lavas several hundred meters thick thought to be a terrestrial analog for the nakhlite source region (*37*, *38*). ALH84001 probably formed as a cumulate in a deep (several tens of kilometers) intrusion (*7*). However, given our thermal constraints, two observations suggest that it was later excavated to much shallower depths. First, the thermal gradient on Mars, although not well constrained, is thought to be ~10°C/km. Second, ALH84001 was strongly shocked at least twice (once before 4 Ga and then again at 4 Ga) (*5*, *7*, *39*) and then ejected from Mars without experiencing postshock temperatures greater than 350°C. This suggests that by the 15 Ma ejection event, it resided in the spall zone of the impactor. For a 10-km impactor, this would imply a burial depth of no more than a few kilometers (*40*).
34. J. C. Bridges *et al.*, *Space Sci. Rev.* **96**, 365 (2001).
35. K. Min, P. W. Reiners, S. Nicolescu, J. P. Greenwood, *Geology* **32**, 677 (2004).
36. T. Mikouchi, E. Koizumi, A. Monkawa, Y. Ueda, M. Miyamoto, *Antarct. Meteorite Res.* **16**, 34 (2003).
37. R. C. F. Lentz, G. J. Taylor, A. H. Treiman, *Meteorit. Planet. Sci.* **34**, 919 (1999).
38. A. H. Treiman, *Lunar Planet. Sci.* **XVIII**, 1022 (1987).
39. J. P. Greenwood, H. Y. McSween, *Meteorit. Planet. Sci.* **36**, 43 (2001).
40. H. J. Melosh, *Impact Cratering: A Geologic Process* (Oxford Univ. Press, Oxford, 1986).

41. We thank T. Swindle and D. Bogard for generously sharing their Ar data with us and for helpful discussions, along with T. Grove, A. Maloof, and J. Eiler. B.P.W. is supported by the NASA Mars Fundamental Research and NSF Geophysics programs.

Supporting Online Material

www.sciencemag.org/cgi/content/full/309/5734/594/DC1
SOM Text
Figs. S1 to S3
References

4 April 2005; accepted 7 June 2005
10.1126/science.1113077

Genomic Sequencing of Pleistocene Cave Bears

James P. Noonan,[1,2] Michael Hofreiter,[3] Doug Smith,[1] James R. Priest,[2] Nadin Rohland,[3] Gernot Rabeder,[4] Johannes Krause,[3] J. Chris Detter,[1,5] Svante Pääbo,[3] Edward M. Rubin[1,2]*

Despite the greater information content of genomic DNA, ancient DNA studies have largely been limited to the amplification of mitochondrial sequences. Here we describe metagenomic libraries constructed with unamplified DNA extracted from skeletal remains of two 40,000-year-old extinct cave bears. Analysis of ~1 megabase of sequence from each library showed that despite significant microbial contamination, 5.8 and 1.1% of clones contained cave bear inserts, yielding 26,861 base pairs of cave bear genome sequence. Comparison of cave bear and modern bear sequences revealed the evolutionary relationship of these lineages. The metagenomic approach used here establishes the feasibility of ancient DNA genome sequencing programs.

Genomic DNA sequences from extinct species can help reveal the process of molecular evolution that produced modern genomes. However, the recovery of ancient DNA is technologically challenging, because the molecules are degraded and mixed with microbial contaminants, and individual nucleotides are often chemically damaged (*1*, *2*). In addition, ancient remains are invariably contaminated with modern DNA, which amplifies efficiently compared with ancient DNA, and therefore inhibits the detection of ancient genomic sequences (*1*, *2*). These factors have limited most previous studies of ancient DNA sequences to polymerase chain reaction (PCR) amplification of mitochondrial DNA (*3*–*8*). In exceptional cases, small amounts of single-copy nuclear DNA have been recovered from ancient remains less than 20,000 years old obtained from permafrost or desert environments, which are well suited to preserving ancient DNA (*9*–*12*). However, the remains of most ancient animals, including hominids, have not been found in such environments.

To circumvent these challenges, we developed an amplification-independent direct-cloning approach to constructing metagenomic libraries from ancient DNA (Fig. 1). Ancient remains are obtained from natural environments in which they have resided for thousands of years, and their extracted DNA is a mixture of genome fragments from the ancient organism and sequences derived from other organisms in the environment. A metagenomic approach, in which all genome sequences in an environment are anonymously cloned into a single library, may therefore be a powerful alternative to the targeted PCR approaches that have been used to recover ancient DNA molecules. We chose to explore this strategy with the extinct cave bear instead of an extinct hominid, to unambiguously assess the issue of modern human contamination (*1*, *2*). In addition, because of the close evolutionary relationship of bears and dogs, cave bear sequences in these libraries can be identified and classified by comparing them to the available annotated dog genome. The phylogenetic relationship of cave bears and modern bear species has also been inferred from mitochondrial sequences, providing the opportunity to compare the phylogenetic information content of cave bear mitochondrial and genomic DNA (*13*).

We extracted DNA from a cave bear tooth recovered from Ochsenhalt Cave, Austria, and a cave bear bone from Gamssulzen Cave, Austria, dated at 42,290 (error +970/–870) and 44,160 (+1400/–1190) years before the present, respectively, by accelerator mass spectrometry radiocarbon dating (table S1). We used these ancient DNA molecules to construct two metagenomic libraries, designated CB1 and CB2 (Fig. 1) (*14*). These libraries were constructed in a laboratory into which modern carnivore DNA has never been introduced. Ancient DNA molecules were blunt end–repaired before ligation but were otherwise neither enzymatically treated nor amplified. We sequenced 9035 clones [1.06 megabases (Mb)] from library CB1 and 4992 clones (1.03 Mb) from library CB2. The average insert sizes for each library were 118 base pairs (bp) and 207 bp, respectively.

We compared each insert in these libraries to GenBank nucleotide, protein, and environmental sequences, and the July 2004 dog whole genome shotgun assembly, by using Basic Local Alignment Search Tool (BLAST) software with an expect value cutoff of 0.001 and a minimum hit size of 30 bp (*14*–*16*). 1.1% of clones in library CB1 (Fig. 2A) and 5.8% of clones in library CB2 (Fig. 2B) had significant hits to dog genome or modern bear sequences. Our direct-cloning approach produces chimeric inserts, so we defined as candidate cave bear

[1]United States Department of Energy Joint Genome Institute, Walnut Creek, CA 94598, USA. [2]Genomics Division, Lawrence Berkeley National Laboratory, Berkeley, CA 94720, USA. [3]Max Planck Institute for Evolutionary Anthropology, Leipzig, D-04103, Germany. [4]Institute of Paleontology, University of Vienna, Vienna, A-1010 Austria. [5]Biosciences Directorate, Lawrence Livermore National Laboratory, Livermore, CA 94550, USA.

*To whom correspondence should be addressed. E-mail: emrubin@lbl.gov

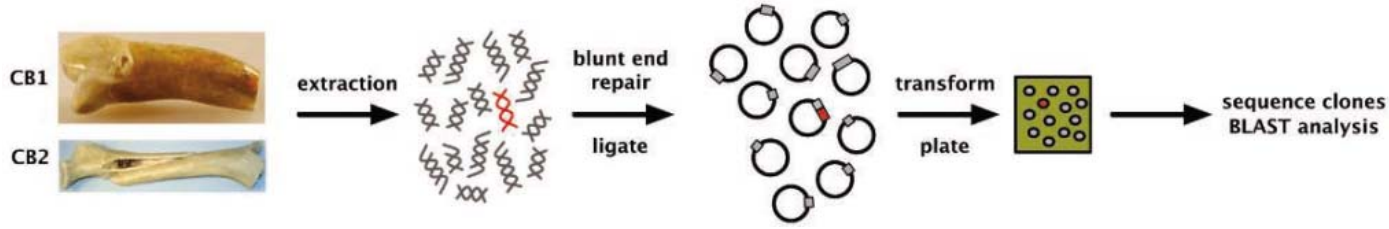

Fig. 1. Schematic illustration of the ancient DNA extraction and library construction process. Extracts prepared from a cave bear tooth (library CB1) and a bone (library CB2) contain cave bear DNA (red) and a mixture of DNA from other organisms (gray).

sequence only that part of the insert that had a hit to dog or bear sequence. The average hit for the 100 clones in library CB1 with significant hits to carnivore sequence was 68 bp long and covered 58% of the insert; whereas the average hit for the 289 clones in library CB2 with significant carnivore hits was 70 bp and covered 49% of the insert. None of these clones showed homology to cave bear mitochondrial DNA sequences, which is consistent with the expected ratio of nuclear versus mitochondrial clones, given the much greater size of the nuclear genome (*14*). Based on the amount of cave bear genomic DNA used to construct library CB2, we estimate that it could yield >10-fold coverage of the cave bear genome if sequenced completely (*14*).

BLAST hits to the dog genome from libraries CB1 and CB2 were on average 92.4 and 92.3% identical to dog, respectively. To confirm that these sequences were indeed those of the cave bear, we designed primers against 124 putative cave bear sequences and successfully amplified and sequenced 116 orthologous sequences from the modern brown bear. All 116 of these modern bear sequences were at least 97% identical to their cave bear orthologs, verifying that all or nearly all of the carnivore sequences in both libraries are genuine cave bear genomic sequences. Only 6 of 14,027 sequenced clones had an insert that was identical to modern human genomic DNA (Fig. 2, A and B). The average BLAST hit length to the human genome for these clones was 116 bp, and the average hit covered 76% of the insert. Although we cannot establish a formal insert length or insert coverage threshold that differentiates between ancient and modern inserts because of the limited number of modern sequences we obtained, these values are significantly greater than the corresponding values for clones with cave bear sequences ($P < 0.05$ for the difference in both average clone length and average insert coverage calculated by two-tailed t test). This result suggests that it may be possible to discriminate between inserts derived from short ancient DNA molecules and inserts containing modern undamaged DNA in ancient DNA libraries. This may have relevance to the application of these methods to ancient hominids, in which the ability to distinguish ancient hominid DNA from modern contamination will be essential.

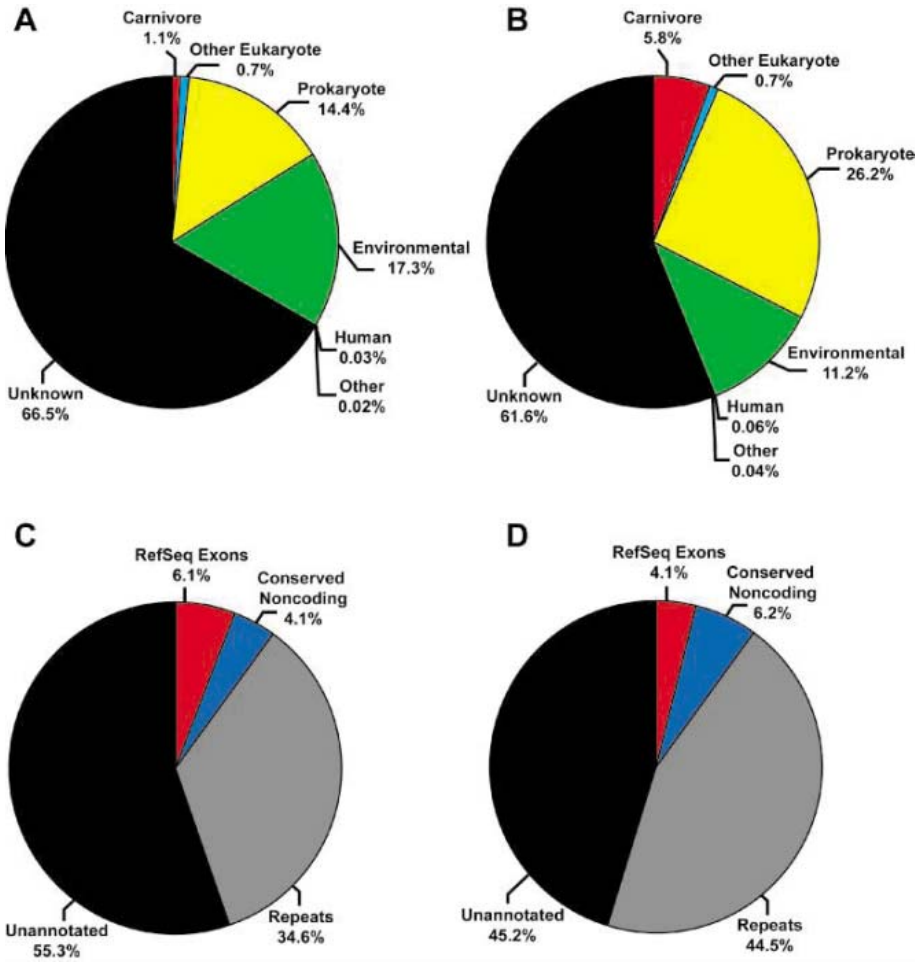

Fig. 2. Characterization of two independent cave bear genomic libraries. Predicted origin of 9035 clones from library CB1 (**A**) and 4992 clones from library CB2 (**B**) are shown, as determined by BLAST comparison to GenBank and environmental sequence databases. Other refers to viral or plasmid-derived DNAs. Distribution of sequence annotation features in 6,775 nucleotides of carnivore sequence from library CB1 (**C**) and 20,086 nucleotides of carnivore sequence from library CB2 (**D**) are shown as determined by alignment to the July 2004 dog genome assembly.

The remaining inserts with BLAST hits to sequences from known taxa were derived from other eukaryotic sources, such as plants or fungi, or from prokaryotic sources (bacteria and archaea), which provided the majority of known sequences in each library. The end-repair reaction performed on each ancient DNA extract is likely biased toward less-damaged ancient DNA fragments and modern DNA, which could contribute to the abundance of prokaryotic sequences relative to cave bear sequences in these libraries. The representation we observe in the libraries thus reflects the proportion of clonable sequences from each source, not the true abundances of such sequences in the original extracts. However, the results from both libraries demonstrate that substantial quantities of genuine cave bear genomic DNA are efficiently end-repaired and cloned, despite this possible bias. A considerable fraction of inserts in each library (17.3% in library CB1 and 11.2% in library CB2; Fig. 2) had hits only to uncharacterized environmental sequences. The majority of these

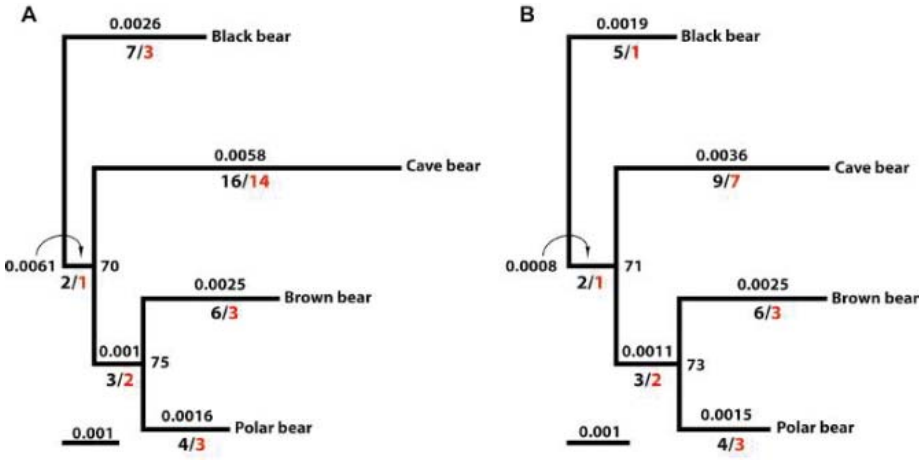

Fig. 3. (**A**) Phylogenetic relationship of cave bear and modern bear sequences obtained by maximum-likelihood estimation using 3201 aligned sites. (**B**) Phylogeny obtained using all sites from (A), excluding cave bear and orthologous modern bear sites corresponding to two heavily damaged cave bear clones (table S3). Substitution rates, total substitutions (black), and GC–AT transitions (red) for each branch are shown. Orthologous dog sequence was used to root the trees. Percent support for internal nodes is also shown.

clones had BLAST hits to GenBank sequences derived from a single soil sample (*17*), consistent with the contamination of each cave bear bone with soil bacteria from the recovery site. As in other metagenomic sequencing studies, most inserts in each library had no similarity to any sequences in the public databases.

To annotate cave bear genomic sequences, we aligned each cave bear sequence to the dog genome assembly using BLAST-like alignment tool (BLAT) (*18*). 6.1% of 6775 cave bear nucleotides from library CB1 and 4.1% of 20,086 cave bear nucleotides from library CB2 aligned to predicted dog RefSeq exons, in a total of 21 genes distributed throughout the dog genome (Fig. 2, C and D, and table S2). 4.1% and 6.2% of cave bear nucleotides, respectively, from library CB1 and library CB2 aligned to constrained nonexonic positions in the dog genome with phastCons conservation scores ≥ 0.8 (conserved noncoding, Fig. 2, C and D) (*14*). The majority of cave bear sequence in each library, however, aligned to dog repeats or regions of the dog genome with no annotated sequence features. These latter sequences are likely fragments of neutrally evolving, nonrepetitive sequence from the cave bear genome. Constrained sequences are slightly overrepresented in our set: Only 1.7% of bases in the dog genome assembly were annotated as RefSeq exons, and ~10% of the cave bear sequences we obtained appear to be constrained overall, whereas 5 to 8% of positions in sequenced mammalian genomes are estimated to be under constraint (*19*). This discrepancy may be caused by our use of BLAST sequence similarity to identify cave bear sequences, an approach that is biased in favor of more-constrained sequences. Nevertheless, coding sequences, conserved noncoding sequences, and repeats appear in both cave bear genomic libraries at frequencies roughly proportional to what has been observed in modern mammalian genomes.

To determine whether the cave bear sequences we obtained contain sufficient information to reconstruct the phylogeny of cave bears and modern bears, we generated and aligned 3201 bp of orthologous sequences from cave bears and modern black, polar, and brown bears and estimated their phylogeny by maximum likelihood (Fig. 3A) (*20*). This phylogeny is topologically equivalent to phylogenies previously obtained using cave bear and modern bear mitochondrial DNA (*13*). This result further indicates that our libraries contain genuine cave bear sequences and demonstrates that we can obtain sufficient ancient sequences from those libraries to estimate the evolutionary relationships between ancient and modern lineages.

The substitution rate we estimated for cave bears is higher than that in any other bear lineage. On the basis of results from PCR-amplified ancient mitochondrial DNA, cytosines in ancient DNA can undergo deamination to uracil, which results in an excess of G-to-A and C-to-T (GC–AT) transitions (*21*). The inflated substitution rate in cave bears is likely caused by an excess of such events, because many of the substitutions assigned to the cave bear lineage are GC–AT transitions (Fig. 3A). These presumably damage-induced substitutions complicate phylogenetic reconstruction and the identification of functional sequence differences between extinct and modern species. However, these substitutions are not randomly distributed among all cave bear sequences but are clustered on a few clones from library CB2. Thus, two clones from library CB2 have three and four GC–AT transitions specific to cave bears, an observation that is extremely unlikely given that the occurrence of true randomly arising substitutions on cave bear clones should follow a Poisson distribution (table S3). When these two clones are excluded from the analysis (Fig. 3B), the apparent substitution rate and the excess of GC–AT transitions in cave bears are reduced, with little impact on estimates of substitution rates in the modern bear lineages. Although we cannot distinguish individual GC–AT substitutions from deamination-induced damage, these observations provide a quantitative means to identify cloned ancient DNA fragments with an excess of cytosine deamination events. It is also likely that heavily degraded ancient DNA fragments are poorly end-repaired and will therefore appear at reduced frequency in ancient DNA genomic libraries.

Although small amounts of genomic sequence have previously been obtained by amplification from <20,000-year-old remains (*12*), the direct cloning strategy employed here has yielded considerably more genomic DNA sequence from much older samples. Based on our results, ancient DNA sequencing programs for extinct Pleistocene species, including hominids, are feasible using a metagenomic approach. By revealing the phylogenomic terrain of recent mammalian evolution, these efforts should help identify the molecular events underlying adaptive differences among modern species.

References and Notes

1. S. Pääbo *et al.*, *Annu. Rev. Genet.* **38**, 645 (2004).
2. M. Hofreiter, D. Serre, H. N. Poinar, M. Kuch, S. Pääbo, *Nat. Rev. Genet.* **2**, 353 (2001).
3. C. Hänni, V. Laudet, D. Stehelin, P. Taberlet, *Proc. Natl. Acad. Sci. U.S.A.* **91**, 12336 (1994).
4. M. Krings *et al.*, *Cell* **90**, 19 (1997).
5. M. Krings, H. Geisert, R. W. Schmitz, H. Krainitzki, S. Pääbo, *Proc. Natl. Acad. Sci. U.S.A.* **96**, 5581 (1999).
6. M. Hofreiter *et al.*, *Mol. Biol. Evol.* **19**, 1244 (2002).
7. D. Serre *et al.*, *PLoS Biol.* **2**, 313 (2004).
8. M. Hofreiter *et al.*, *Proc. Natl. Acad. Sci. U.S.A.* **101**, 12963 (2004).
9. P. Goloubinoff, S. Pääbo, A. C. Wilson, *Proc. Natl. Acad. Sci. U.S.A.* **90**, 1997 (1993).
10. A. D. Greenwood, C. Capelli, G. Possnert, S. Pääbo, *Mol. Biol. Evol.* **16**, 1466 (1999).
11. V. Jaenicke-Després *et al.*, *Science* **302**, 1206 (2003).
12. H. Poinar, M. Kuch, G. McDonald, P. Martin, S. Pääbo, *Curr. Biol.* **13**, 1150 (2003).
13. O. Loreille *et al.*, *Curr. Biol.* **11**, 200 (2001).
14. Materials and methods are available as supporting material on *Science* Online.
15. The dog genome sequence generated by the Broad Institute and Agencourt Biosciences was obtained from the University of California at Santa Cruz Dog Genome Browser (http://genome.ucsc.edu).
16. S. F. Altschul *et al.*, *Nucleic Acids Res.* **25**, 3389 (1997).
17. S. G. Tringe *et al.*, *Science* **308**, 554 (2005).
18. W. J. Kent, *Genome Res.* **12**, 656 (2002).
19. G. M. Cooper *et al.*, *Genome Res.* **14**, 539 (2004).
20. We cannot formally exclude alternative topologies, given the small number of nucleotide sites in the analysis and the limited divergence among these bear species, which also accounts for the low percent support for the internal nodes. Damage-induced substitutions in cave bears also perturb the phylogeny. The topology with the next-best likelihood score has cave bears as the outgroup to the modern bears due to an excess of GC–AT substitutions in several library CB2 sequences.
21. M. Hofreiter, V. Jaenicke, D. Serre, A. von Haeseler, S. Pääbo, *Nucleic Acids Res.* **29**, 4793 (2001).
22. Data have been deposited into GenBank with accession

numbers CZ551658 to CZ552046. We thank members of the Rubin and Pääbo laboratories for insightful discussions and support. This work was performed under the auspices of the U.S. Department of Energy's Office of Science Biological and Environmental Research Program and by the University of California; Lawrence Berkeley National Laboratory; Lawrence Livermore National Laboratory; and Los Alamos National Laboratory under contract numbers DE-AC03-76SF00098, W-7405-Eng-48, and W-7405-ENG-36, respectively, with support from NIH grants U1 HL66681B and T32 HL07279 and at the Max Planck Institute for Evolutionary Anthropology.

Supporting Online Material
www.sciencemag.org/cgi/content/full/1113485/DC1
Materials and Methods
Tables S1 to S3
References

12 April 2005; accepted 26 May 2005
Published online 2 June 2005;
10.1126/science.1113485
Include this information when citing this paper.

Marked Decline in Atmospheric Carbon Dioxide Concentrations During the Paleogene

Mark Pagani,[1] James C. Zachos,[2] Katherine H. Freeman,[3] Brett Tipple,[1] Stephen Bohaty[2]

The relation between the partial pressure of atmospheric carbon dioxide (pCO_2) and Paleogene climate is poorly resolved. We used stable carbon isotopic values of di-unsaturated alkenones extracted from deep sea cores to reconstruct pCO_2 from the middle Eocene to the late Oligocene (~45 to 25 million years ago). Our results demonstrate that pCO_2 ranged between 1000 to 1500 parts per million by volume in the middle to late Eocene, then decreased in several steps during the Oligocene, and reached modern levels by the latest Oligocene. The fall in pCO_2 likely allowed for a critical expansion of ice sheets on Antarctica and promoted conditions that forced the onset of terrestrial C_4 photosynthesis.

The early Eocene [~52 to 55 million years ago (Ma)] climate was the warmest of the past 65 million years. Mean annual continental temperatures were considerably elevated relative to those of today, and high latitudes were ice-free, with polar winter temperatures ~10°C warmer than at present (*1*–*3*). After this climatic optimum, surface- and bottom-water temperatures steadily cooled over ~20 million of years (*4*, *5*), interrupted by at least one major ephemeral warming in the late middle Eocene (*6*). High-latitude cooling eventually sustained small Antarctic ice sheets by the late Eocene (*7*), culminating in a striking climate shift across the Eocene/Oligocene boundary (E/O) at 33.7 Ma. The E/O climate transition, Earth's first clear step into "icehouse" conditions during the Cenozoic, is associated with a rapid expansion of large continental ice sheets on Antarctica (*8*, *9*) in less than ~350,000 years (*10*, *11*).

Changes in the partial pressure of atmospheric carbon dioxide (pCO_2) are largely credited for the evolution of global climates during the Cenozoic (*12*–*14*). However, the relation between pCO_2 and the extraordinary climate history of the Paleogene is poorly constrained. Initial attempts to estimate early Paleogene pCO_2 have provided conflicting results, with both high (*15*) and low (i.e., similar to modern) (*16*) estimates of pCO_2. This deficiency in our understanding of the history of pCO_2 is critical, because the role of CO_2 in forcing long-term climate change during some intervals of Earth's history is equivocal. For example, Miocene pCO_2 records (~25 to 5 Ma) argue for a decoupling between global climate and CO_2 (*15*–*17*). These records suggest that Miocene pCO_2 was rather low and invariant across periods of both inferred global warming and high-latitude cooling (*17*). Clearly, a more complete understanding of the relation between pCO_2 and climate change requires the extension of paleo-pCO_2 records back into periods when Earth was substantially warmer and ice-free.

Paleoatmospheric CO_2 concentrations can be estimated from the stable carbon isotopic compositions of sedimentary organic molecules known as alkenones. Alkenones are long-chained (C_{37}-C_{39}) unsaturated ethyl and methyl ketones produced by a few species of Haptophyte algae in the modern ocean (*18*). Alkenone-based pCO_2 estimates derive from records of the carbon isotopic fractionation that occurred during marine photosynthetic carbon fixation (ε_p). Chemostat experiments conducted under nitrate-limited conditions indicate that alkenone-based ε_p values ($\varepsilon_{p37:2}$) vary as a function of the concentration of aqueous CO_2 ($[CO_{2aq}]$) and specific growth rate (*19*–*21*). These experiments also provide evidence that cell geometry accounts for differences in ε_p among marine microalgae cultured under similar conditions (*21*). In contrast, results from dilute batch cultures conducted under nutrient-replete conditions yield substantially lower $\varepsilon_{p37:2}$ values, a different relation for ε_p versus μ/CO_{2aq} (where μ = algal growth rate), and a minimal response to $[CO_{2aq}]$ (*22*). Thus, comparison of the available culture data suggests that different growth and environmental conditions potentially trigger different carbon uptake pathways and carbon isotopic responses (*23*). A recent evaluation of the efficacy of the alkenone-CO_2 approach, using sedimentary alkenones in the natural environment, supported the capacity of the technique to resolve relatively small differences in water column $[CO_{2aq}]$ across a variety of marine environments when phosphate concentrations and temperatures are constrained (*24*).

In our study, we extended records of the carbon isotopic composition of sedimentary alkenones ($\delta^{13}C_{37:2}$) from the middle Eocene to the late Oligocene and established a record of pCO_2 for the past ~45 million years. Samples from Deep Sea Drilling Project sites 516, 511, 513, and 612 and Ocean Drilling Program site 803 (Fig. 1) were used to reconstruct $\delta^{13}C_{37:2}$ and $\varepsilon_{p37:2}$ records ranging from the middle Eocene to the late Oligocene (~25 to 45 Ma). These sites presumably represent a range of oceanic environments with a variety of surface-water nutrient and algal-growth conditions and thus reflect a set of environmental and physiological factors affecting both $\delta^{13}C_{37:2}$ and $\varepsilon_{p37:2}$ values.

These data are presented as a composite record, in large part because the measurable concentration of di-unsaturated alkenones varied both spatially and temporally. Moreover, continuous alkenone records spanning the entire Eocene and Oligocene from individual sites were not recovered. As a consequence, most of the Oligocene record is represented at site 516, whereas the majority of the Eocene is represented at site 612 (Fig. 2A). Age models for each site were developed by linearly interpolating between biostratigraphic datums (*25*–*31*), calibrated to the Geomagnetic Polarity Time Scale (*32*).

Eocene $\delta^{13}C_{37:2}$ values range from ~–30 to –35 per mil (‰), with the most negative values (sites 511 and 513) occurring near the E/O boundary. $\delta^{13}C_{37:2}$ values increase substantially through the Oligocene with maximum values of ~–27‰ by ~25.5 Ma. This trend is briefly reversed near the end of the Oligocene as $\delta^{13}C_{37:2}$ values become more negative, reaching ~–32‰ by 25 Ma (Fig. 2A). The overall pattern of ^{13}C enrichment continues into the Miocene, establishing a clear secular trend from the middle Eocene to the middle Miocene (Fig. 2B). These isotopic

[1]Department of Geology and Geophysics, Yale University, 210 Whitney Avenue, New Haven, CT 06511, USA. [2]Earth Sciences Department, University of California, 1156 High Street, Santa Cruz, CA 95064, USA. [3]Department of Geosciences, Pennsylvania State University, University Park, PA 16802, USA.

trends do not mirror changes in the $\delta^{13}C$ of dissolved inorganic carbon ($\delta^{13}C_{DIC}$) because $\delta^{13}C$ records of bulk carbonate (*33*) and benthic foraminifera (*10*) indicate small changes in $\delta^{13}C_{DIC}$ for the Eocene to Oligocene relative to the change in $\delta^{13}C_{37:2}$. Nonetheless, interpretations of long-term trends in $\delta^{13}C_{37:2}$ are enhanced when $\delta^{13}C_{37:2}$ values are converted to $\varepsilon_{p37:2}$ (*34*), thus eliminating the influence of $\delta^{13}C_{DIC}$.

The temporal pattern of $\varepsilon_{p37:2}$ is similar to that of $\delta^{13}C_{37:2}$ (Fig. 2, C and D), consistent with other studies (*17*). Higher values of $\varepsilon_{p37:2}$ (~19.5 to 21.5‰) characterize the Eocene and then decrease through the Oligocene. The $\varepsilon_{p37:2}$ values recorded for the Eocene and earliest Oligocene are higher than any recorded for the modern ocean (Fig. 2D). Given our present understanding of the controls on $\varepsilon_{p37:2}$, the decrease in $\varepsilon_{p37:2}$ from the Eocene through the Oligocene could be driven by a consistent change in the cell dimensions of alkenone-producing algae over time, a secular increase in growth rates of alkenone-producing algae, or a long-term decrease in $[CO_{2aq}]$ and/or increased utilization of bicarbonate ($[HCO_3^-]$) as a result of low $[CO_{2aq}]$ (*35*). At present, evolutionary changes in algal cell geometries are poorly constrained. If the long-term decrease in $\varepsilon_{p37:2}$ were driven solely by changes in algal cell dimensions, it would require a pattern of increasing ratios of cell volume to surface area with time. If ε_p scales linearly with the ratio of cell volume to surface area (*21*), the observed change in $\varepsilon_{p37:2}$ values would require an ~60% increase in the cell diameters of alkenone-producing algae from the Eocene to the Miocene (i.e., sites 516 and 612). Further, given that Miocene and Modern $\varepsilon_{p37:2}$ values are similar, Eocene coccolithophores would have to have been ~60% smaller than modern alkenone producers, such as *Emiliania huxleyi*, with cell diameters of ~5 μm (*21*). However, the available data suggest that placoliths from probable alkenone producers, specifically species within the genus *Reticulofenestra*, were substantially larger than modern species and then decreased through the Oligocene and early Miocene (*36*, *37*). If we reasonably assume that placolith geometry scales to cell geometry (*38*), then cell diameters decreased during the late Paleogene. A trend of decreasing cell diameters should lead to an increase in $\varepsilon_{p37:2}$ values (*21*), which is contrary to our measurements. Thus, although a long-term change in cell geometry might have influenced the relative magnitude of Paleogene $\varepsilon_{p37:2}$ values, it was not responsible for the pattern observed in our record.

Alternatively, variations in $\varepsilon_{p37:2}$ could be ascribed to variations in the specific growth rates of alkenone-producing algae (μ_{alk}), with higher μ_{alk} values associated with lower $\varepsilon_{p37:2}$ values. Under this scenario, Eocene and early

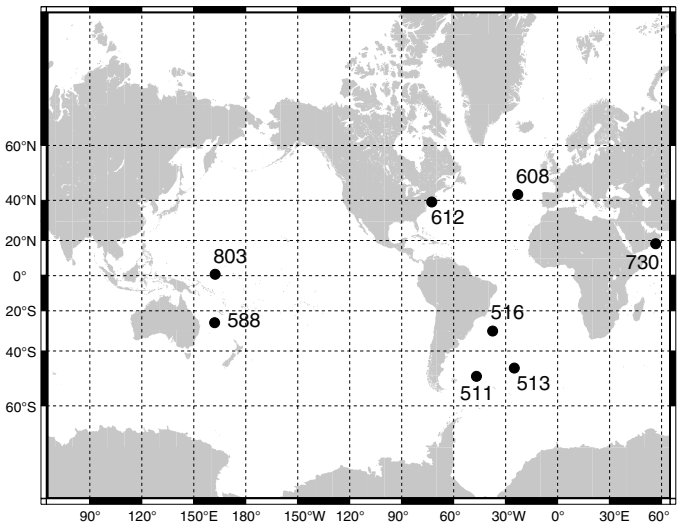

Fig. 1. Site location map. Sites 612, 516, 803, 511, and 513 were used to reconstruct Eocene and Oligocene $\varepsilon_{p37:2}$ values. Sites 588, 608, 730, and 516 were used to reconstruct Miocene $\varepsilon_{p37:2}$ values.

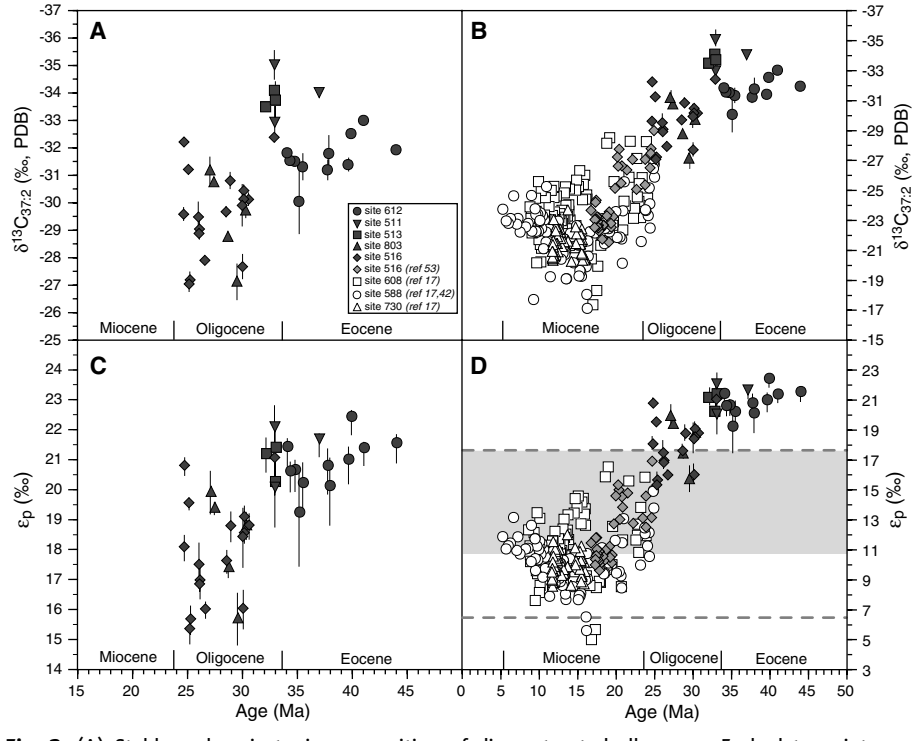

Fig. 2. (**A**) Stable carbon isotopic composition of di-unsaturated alkenones. Each data point represents one measurement or an average of multiple measurements, with error bars bracketing the range of values for each sample. PDB, Pee Dee belemnite standard. (**B**) Compilation of the carbon isotopic composition of di-unsaturated alkenones from this study and Pagani *et al*. (*17*, *42*, *53*). (**C**) Paleogene $\varepsilon_{p37:2}$ values. $\varepsilon_{p37:2}$ is calculated from the $\delta^{13}C$ of di-unsaturated alkenones as follows: $\varepsilon_{p37:2} = [(\delta d + 1000/\delta p + 1000) - 1] \times 10^3$, where δd is the carbon isotopic composition of CO_{2aq} calculated from mixed-layer carbonates and δp is the carbon isotopic composition of haptophyte organic matter enriched by 4.2‰ relative to alkenone $\delta^{13}C$ (*54*). Carbon isotopic compositions of mixed-layer carbonates were used to calculate δd by assuming equilibrium conditions and applying temperature-dependent isotope equations (*55*, *56*). Mixed-layer temperatures were calculated from the $\delta^{18}O$ of planktonic foraminifera (*57*) as follows: site 612, *Acarinina* spp.; site 513, *Subbotina* spp. and *Chiloguembelina cubensis*; and site 511, *Subbotina* spp. Temperatures for sites 516 and 803 were estimated from the $\delta^{18}O$ compositions of the <60-μm carbonate fraction, assuming that the $\delta^{18}O$ composition of seawater changed from –0.75‰ during the Eocene to –0.5‰ during the Oligocene. Error bars reflect the range of $\varepsilon_{p37:2}$ values calculated by applying the maxima and minima of both the measured $\delta^{13}C$ of di-unsaturated alkenones and calculated temperatures. (**D**) Compilation of $\varepsilon_{p37:2}$ values from this study and Pagani *et al*. (*17*, *42*, *53*). Dashed horizontal lines bracket the range of $\varepsilon_{p37:2}$ values from surface waters of modern oceans. In general, higher and lower $\varepsilon_{p37:2}$ values come from oligotrophic and eutrophic environments, respectively. The shaded box represents the range of $\varepsilon_{p37:2}$ values from oligotrophic sites where $[PO_4^{3-}]$ ranges between 0.0 to 0.2 μmol/liter.

Oligocene $\varepsilon_{p37:2}$ values must reflect substantially lower μ_{alk} than modern μ_{alk} found in oligotrophic waters where $[PO_4^{3-}]$ is ~0 μmol/liter (Fig. 2D). That is, algal growth rates during the Paleogene from both eutrophic and oligotrophic environments would have to be lower than the lowest growth rates found in the modern oligotrophic ocean. Further, if growth rates were indeed the first-order control on $\varepsilon_{p37:2}$ values, the lowest Miocene $\varepsilon_{p37:2}$ values would require substantially higher algal growth rates in oligotrophic settings, comparable to those of the highly productive Peru upwelling margin (Fig. 2D). Therefore, we conclude that rather extraordinary changes in μ_{alk} are required to explain the temporal pattern of $\varepsilon_{p37:2}$ values and thus are not the primary cause for the observed long-term trends. Instead, we contend that the Cenozoic evolution of $\varepsilon_{p37:2}$ was forced primarily by changes in $[CO_{2aq}]$ and pCO_2. Accordingly, these records would qualitatively reflect high surface-water $[CO_{2aq}]$ during the middle to late Eocene, a pattern of decreasing $[CO_{2aq}]$ through the Oligocene, and near-modern levels during the Neogene. If the change in $\varepsilon_{p37:2}$ values during the Paleogene was brought about by an increased utilization of HCO_3^- over CO_{2aq}, then it implies that $[CO_{2aq}]$ became increasingly limiting to algal growth in both oligotrophic and eutrophic environments. Although this would compromise quantitative estimates of atmospheric pCO_2, it would still support a scenario of decreasing pCO_2 with time. Until evidence emerges to the contrary, we must assume that the physiological processes responsible for $\varepsilon_{p37:2}$ in the past were similar to those operating in modern surface waters (*19*, *24*) and use these data to estimate both $[CO_{2aq}]$ and pCO_2 over the past 45 million years.

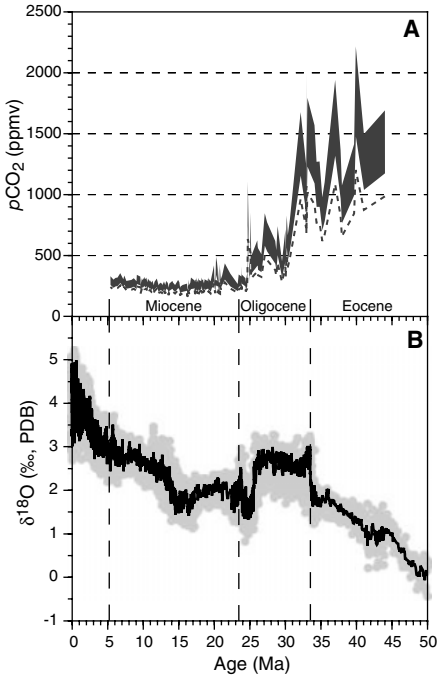

Fig. 3. (**A**) pCO_2 estimates calculated from $\varepsilon_{p37:2}$. $\varepsilon_p = \varepsilon_f - b/[CO_{2aq}]$ (*39*), where $b = \{(118.52[PO_4^{3-}]) + 84.07\}/(25 - \varepsilon_{p37:2})$, calculated from the geometric mean regression of all available data (*19*, *20*, *23*, *58*, *59*). $[CO_{2aq}]$ values were calculated using mean $\varepsilon_{p37:2}$ values and a range of $[PO_4^{3-}]$ values for each site. $[PO_4^{3-}]$ ranges applied for individual sites were as follows: site 612, 0.5 to 0.3 μmol/liter; site 516, 0.4 to 0.2 μmol/liter; sites 511 and 513, 1.10 to 0.8 μmol/liter; site 803, 0.3 to 0.1 μmol/liter; and site 588, 0.3 to 0.2 μmol/liter. Values of CO_{2aq} were converted to pCO_2 by applying Henry's Law (*60*), calculated assuming a salinity of 35 and surface-water temperatures derived from $\delta^{18}O$ of marine carbonates. Maximum pCO_2 estimates were calculated using maximum temperatures (*61*) for each sample and maximum $[PO_4^{3-}]$ for each site. Intermediate and minimum (dashed line) pCO_2 estimates were calculated using intermediate and minimum temperatures for each sample and minimum $[PO_4^{3-}]$ for each site. An analytical treatment of error propagation suggests that relative uncertainties in reconstructed CO_2 values are ~20% for the Miocene data and approach 30 to 40% for Paleogene samples with higher (20 to 24‰) $\varepsilon_{p37:2}$ values (*62*). (**B**) Global compilation of benthic oxygen isotope records (*5*).

The conversion of $\varepsilon_{p37:2}$ values to pCO_2 requires an estimate of surface-water $[PO_4^{3-}]$ (*39*) and temperature for each site. For this study, we assumed that modern surface-water distributions of $[PO_4^{3-}]$ at each site between 0 and 100 m encompassed the probable range at any given time, and we applied temperatures derived from the oxygen isotope composition of coeval carbonates in order to convert estimates of $[CO_{2aq}]$ to pCO_2. This approach assumes relative air-sea equilibrium, which may not be valid for every site. However, although disequilibrium could lead to overestimates of pCO_2, our treatment of the data ultimately yields a range of CO_2 concentrations that reflects the uncertainty associated with this effect. On a broad scale, our results indicate that CO_2 concentrations during the middle to late Eocene ranged between 1000 and 1500 parts per million by volume (ppmv) (*40*) and then rapidly decreased during the Oligocene, reaching modern levels by the latest Oligocene (Fig. 3A). In detail, a trend toward lower CO_2 concentrations is evident from the middle to late Eocene, reaching levels by the E/O boundary that could have triggered the rapid expansion of ice on east Antarctica (*2*). An episode of higher pCO_2 in the latest Oligocene occurs concomitantly with a ~2-million-year low in the mean $\delta^{18}O$ composition of benthic foraminifera (Fig. 3B), indicating that global climate and the carbon cycle were linked from the Eocene to the late Oligocene. This association weakens in the Neogene, when long-term patterns of climate and pCO_2 appear to be decoupled (*17*).

In addition to climate, the change in CO_2 implied by our record would have substantially affected the growth characteristics of terrestrial flora. In particular, the expansion of C_4 grasses has received considerable attention as an indicator of environmental change (*41*, *42*). The C_4 pathway concentrates CO_2 at the site of carboxylation and enhances rates of photosynthesis by eliminating the effects of photorespiration under low CO_2 concentrations (*43*). Moreover, higher rates of carbon assimilation can be maintained under water-stressed conditions. This results in a water-use efficiency (water loss per unit of carbon assimilated) in C_4 plants that is twice that of C_3 plants at ~25°C (*44*). Given our understanding of the environmental parameters affecting C_3 and C_4 plants, a prevalent supposition has emerged that C_4 photosynthesis originated as a response to stresses associated with photorespiration (*41*, *45*). The CO_2 threshold below which C_4 photosynthesis is favored over C_3 flora is estimated at ~500 ppmv (*41*), a level that is breached during the Oligocene. Molecular phylogenies (*46*, *47*) and isotopic data (*48*) place the origin of C_4 grasses before the Miocene between 25 to 32 Ma (*46*, *47*, *49*), the interval when CO_2 concentrations approached modern levels. This confluence strongly suggests that C_4 photosynthesis evolved as a response to increased photorespiration rates forced by a substantial drop in pCO_2 during the Oligocene. Near-global expansion of C_4 ecosystems ensued later in the Miocene (*41*), possibly driven by drier climates and/or changes in patterns of precipitation (*42*).

References and Notes

1. J. C. Zachos, L. D. Stott, K. C. Lohmann, *Paleoceanography* **9**, 353 (1994).
2. K. G. Miller, R. G. Fairbanks, G. S. Mountain, *Paleoceanography* **2**, 1 (1987).
3. L. D. Stott, J. P. Kennett, N. J. Shackleton, *Proc. Ocean Drilling Program Sci. Results* **113**, 849 (1990).
4. N. J. Shackleton, J. P. Kennett, *Init. Rep. Deep Sea Drill. Proj.* **29**, 743 (1975).
5. J. C. Zachos, M. Pagani, L. Sloan, E. Thomas, K. Billups, *Science* **292**, 686 (2001).
6. S. Bohaty, J. C. Zachos, *Geology* **31**, 1017 (2003).
7. J. V. Browning, K. G. Miller, D. K. Pak, *Geology* **24**, 639 (1996).
8. C. Robert, J. P. Kennett, *Geology* **25**, 587 (1997).
9. J. C. Zachos, B. N. Opdyke, C. N. Quinn, C. E. Jones, A. N. Halliday, *Chem. Geol.* **161**, 165 (1999).
10. J. C. Zachos, T. M. Quinn, K. A. Salamy, *Paleoceanography* **11**, 251 (1996).
11. H. K. Coxall, P. A. Wilson, H. Pälike, C. H. Le, *Nature* **433**, 53 (2005).
12. M. E. Raymo, *Geology* **19**, 344 (1991).
13. R. A. Berner, Z. Kothavala, *Am. J. Sci.* **301**, 182 (2001).
14. R. M. DeConto, D. Pollard, *Nature* **421**, 245 (2003).
15. P. N. Pearson, M. R. Palmer, *Nature* **406**, 695 (2000).
16. D. L. Royer *et al.*, *Nature* **292**, 2310 (2001).
17. M. Pagani, M. A. Arthur, K. H. Freeman, *Paleoceanography* **14**, 273 (1999).
18. M. H. Conte, J. K. Volkman, G. Eglinton, in *The Haptophyte Algae*, J. C. Green, B. S. C. Leadbeater, Eds. (Clarendon Press, Oxford, 1994), pp. 351–377.
19. R. R. Bidigare *et al.*, *Global Biogeochem. Cycles* **11**, 279 (1997).
20. R. R. Bidigare *et al.*, *Global Biogeochem. Cycles* **13**, 251 (1999).
21. B. N. Popp *et al.*, *Geochim. Cosmochim. Acta* **62**, 69 (1998).
22. U. Riebesell, A. T. Revill, D. G. Hodsworth, J. K. Volkman, *Geochim. Cosmochim. Acta* **64**, 4179 (2000).
23. E. A. Laws, B. N. Popp, R. R. Bidigare, *Geochem. Geophys. Geosyst.* **2**, 2000GC000057 (2001).

24. M. Pagani, K. H. Freeman, N. Ohkouchi, K. Caldeira, *Paleoceanography* **17**, 1069 (2002).
25. P. Valentine, *Init. Rep. Deep Sea Drill. Proj.* **95**, 359 (1987).
26. K. G. Miller, W. A. Berggren, J. Zhang, J. A. A. Palmer, *Palaios* **6**, 17 (1991).
27. W. Wei, S. W. Wise, *Mar. Micropaleontol.* **14**, 119 (1989).
28. C. Pujol, *Init. Rep. Deep Sea Drill. Proj.* **72**, 623 (1983).
29. R. M. Leckie, C. Farnham, M. G. Schmidt, *Proc. Ocean Drill. Program* **130**, 113 (1993).
30. S. W. Wise Jr., *Init. Rep. Deep Sea Drill. Proj.* **71**, 481 (1983).
31. I. A. Basov, P. F. Ciesielski, V. A. Krasheninnikov, F. M. Weaver, S. W. Wise Jr., *Init. Rep. Deep Sea Drill. Proj.* **71**, 445 (1983).
32. W. A. Berggren, D. V. Kent, C. C. I. Swisher, M. P. Aubry, in *Geochronology, Time Scales and Global Stratigraphic Correlation*, W. A. Berggren, D. V. Kent, M. P. Aubry, J. Hardenbol, Eds. (Special Publication No. 54, Society for Sedimentary Geology, Tulsa, OK, 1995), pp. 129–212.
33. N. J. Shackleton, M. A. Hall, A. Boersma, *Init. Rep. Deep Sea Drill. Proj.* **74**, 599 (1984).
34. Calculation of $\varepsilon_{p37:2}$ requires knowledge of the $\delta^{13}C$ of ambient CO_{2aq}($\delta^{13}C_{CO_{2}aq}$) during alkenone production and of temperature, which can be approximated from the $\delta^{13}C$ of shallow-dwelling foraminifera, assuming isotopic and chemical equilibria among all the aqueous inorganic carbon species and atmospheric CO_2, as well as foraminiferal calcite (*17*). In this study, records of planktonic foraminifera coeval with alkenone measurements were available from sites 511, 513, and 803. Site 612 had well-preserved planktonic and benthic foraminifera, but some samples lacked coeval samples of planktonic foraminifera. In these cases, the isotopic compositions of planktonic foraminifera were modeled by calculating the average difference between benthic and planktonic foraminifera and adding this value to the isotopic compositions of benthic foraminifera. Site 516 had poor carbonate preservation and lacked an adequate foraminiferal record. For this site, surface $\delta^{13}C_{CO_{2}aq}$ and values were modeled from the $\delta^{13}C$ compositions of the <60-μm fine fraction (FF), assuming an isotopic offset between the FF and shallow-dwelling foraminifera of +0.5‰, as indicated by Miocene (*50*) and Eocene (this study) records from this site. Similarly, surface-water temperatures, required in the calculation of both $\delta^{13}C_{CO_{2}aq}$ and pCO_2, were estimated from the $\delta^{18}O$ compositions of shallow-dwelling planktonic foraminifera or modeled from the $\delta^{18}O$ compositions of the <60 μm FF, assuming an isotopic offset between the FF and shallow-dwelling foraminifera of −1.5‰ (*50*).
35. B. Rost, U. Riebesell, S. Burkhardt, *Limnol. Oceanogr.* **48**, 55 (2003).
36. J. Backman, J. O. R. Hermelin, *Palaeogeogr. Palaeoclimatol. Palaeoecol.* **57**, 103 (1986).
37. J. Young, *J. Micropalaeontol.* **9**, 71 (1990).
38. J. Young, personal communication.
39. $\varepsilon_{p37:2}$ is related to [CO_{2aq}] by the expression $\varepsilon_p = \varepsilon_f - b/[CO_{2aq}]$, where ε_f represents the carbon isotope fractionation due to carboxylation. *b* represents the sum of physiological factors, such as growth rate and cell geometry, affecting the total carbon isotope discrimination. In the modern ocean, *b* is highly correlated to surface-water [PO_4^{3-}] (*19*). However, it is unlikely that [PO_4^{3-}] alone is responsible for the variability in growth rate inferred from variation in *b*. Instead, [PO_4^{3-}] may represent a proxy for other growth-limiting nutrients, such as specific trace elements that exhibit phosphate-like distributions.
40. For comparison with our record, middle to late Eocene-age estimates of ocean *p*H using the boron isotopic compositions of foraminifera (*15*) yield early Eocene CO_2 concentrations that are potentially 10 times higher than preindustrial levels (~3500 ppmv), reaching levels as low as ~350 ppmv during the middle to late Eocene. Our Eocene estimates do not support a scenario of low pCO_2 during this time.
41. T. E. Cerling *et al.*, *Nature* **389**, 153 (1997).
42. M. Pagani, K. H. Freeman, M. A. Arthur, *Science* **285**, 876 (1999).
43. R. W. Pearcy, J. Ehleringer, *Plant Popul. Biol.* **7**, 1 (1984).
44. M. D. Hatch, *Biochim. Biophys. Acta* **895**, 81 (1987).
45. J. R. Ehleringer, R. F. Sage, L. B. Flanagan, R. W. Pearcy, *Trends Ecol. Evol.* **6**, 95 (1991).
46. B. S. Gaut, J. F. Doebley, *Proc. Natl. Acad. Sci. U.S.A.* **94**, 6809 (1997).
47. E. A. Kellogg, in *C_4 Plant Biology*, R. F. Sage, R. K. Monson, Eds. (Academic Press, New York, 1999), pp. 313–371.
48. D. L. Fox, P. L. Koch, *Geology* **31**, 809 (2003).
49. R. E. Sage, *New Phytol.* **161**, 341 (2004).
50. A. Ennyu, M. A. Arthur, M. Pagani, *Mar. Micropaleontol.* **46**, 317 (2002).
51. D. P. Schrag, *Chem. Geol.* **161**, 215 (1999).
52. P. N. Pearson *et al.*, *Nature* **413**, 481 (2001).
53. M. Pagani, M. A. Arthur, K. H. Freeman, *Paleoceanography* **15**, 486 (2000).
54. B. N. Popp, F. Kenig, S. G. Wakeham, E. A. Laws, R. R. Bidigare, *Paleoceanography* **13**, 35 (1998).
55. W. G. Mook, J. C. Bommerson, W. H. Staberman, *Earth Planet. Sci. Lett.* **22**, 169 (1974).
56. C. S. Romanek, E. L. Grossman, J. W. Morse, *Geochim. Cosmochim. Acta* **56**, 419 (1992).
57. J. Erez, B. Luz, *Geochim. Cosmochim. Acta* **47**, 1025 (1983).
58. B. N. Popp *et al.*, in *Reconstructing Ocean History: A Window into the Future*, F. Abrantes, A. Mix, Eds. (Plenum, New York, 1999), pp. 381–398.
59. M. E. Eek, M. J. Whiticar, J. K. B. Bishops, C. S. Wong, *Deep-Sea Res. II* **46**, 2863 (1999).
60. R. F. Weiss, *Mar. Chem.* **2**, 203 (1974).
61. All carbonates are assumed to be diagenetically altered to some degree, which acts to increase their $\delta^{18}O$ composition (*51*, *52*), yielding minimum temperatures. In order to compensate for this uncertainty, three temperature estimates were used in the calculation of $\varepsilon_{p37:2}$ and pCO_2, reflecting minimum temperatures calculated directly from the $\delta^{18}O$ value of carbonates ($Temp_{min}$), intermediate temperatures ($Temp_{min}$ + 3°C), and maximum temperatures ($Temp_{min}$ + 6°C).
62. K. H. Freeman, M. Pagani, in *A History of Atmospheric CO_2 and its Effects on Plants, Animals, and Ecosystems*, J. R. Ehleringer, T. E. Cerling, M. D. Dearing, Eds. (Springer, New York, 2005), pp. 35–61.

63. The authors thank two anonymous reviewers who helped improve the quality of the manuscript. We also thank B. Berner and K. Turekian for coffee and animated conversations that helped develop and inspire ideas. This work was funded by a grant from NSF.

21 January 2005; accepted 7 June 2005
Published online 16 June 2005;
10.1126/science.1110063
Include this information when citing this paper.

Global Mammal Conservation: What Must We Manage?

Gerardo Ceballos,[1]* Paul R. Ehrlich,[2] Jorge Soberón,[3]† Irma Salazar,[1] John P. Fay[2]

We present a global conservation analysis for an entire "flagship" taxon, land mammals. A combination of rarity, anthropogenic impacts, and political endemism has put about a quarter of terrestrial mammal species, and a larger fraction of their populations, at risk of extinction. A new global database and complementarity analysis for selecting priority areas for conservation shows that ~11% of Earth's land surface should be managed for conservation to preserve at least 10% of terrestrial mammal geographic ranges. Different approaches, from protection (or establishment) of reserves to countryside biogeographic enhancement of human-dominated landscapes, will be required to approach this minimal goal.

Research on population and species extinctions shows an accelerating decay of contemporary biodiversity. This pressing environmental problem is likely to become even worse in coming decades (*1*–*3*). Although impacts of human activities are global in scope, they are not uniformly distributed. The biota of certain countries and regions can be identified as being most at risk, having both exceptionally high richness and endemism and exceptionally rapid rates of anthropogenic change. Because resources for conservation are limited, ecologists must provide managers and politicians with solid bases for establishing conservation priorities (*4*) to minimize population and species extinctions (*5*), to reduce conservation conflicts (*6*, *7*), and to preserve ecosystem services (*8*).

Even for charismatic taxa, we lack a global view of patterns of species distributions useful for establishing conservation priorities. Such a view would allow evaluation of the effort required, for example, to preserve all species in a given taxon. It would also be relevant to setting global conservation goals such as protecting a certain percentage of Earth's land surface (*9*). More restricted approaches such as identifying hot spots and endemic bird areas have called attention to relatively small areas where large numbers of species might be protected (*10*–*13*). For instance, recently the number of vertebrate species that lack populations within major protected areas was estimated (*12*). But now more comprehensive analyses are possible.

[1]Instituto de Ecología, UNAM, Apdo. Postal 70-275, México D.F. 04510, México. [2]Center for Conservation Biology, Department of Biological Sciences, Stanford University, Stanford, CA 94305–5020, USA. [3]Comisión Nacional de Biodiversidad, Periferico-Insurgentes 4903, Mexico.

*To whom correspondence should be addressed. E-mail: gceballo@miranda.ecologia.unam.mx
†Present address: Natural History Museum, Dyke Hall, University of Kansas, Lawrence, KS 66045, USA.

Here we conduct a global examination of mammal distributions to evaluate conservation priorities based on (i) range size distribution, (ii) global patterns of species richness, (ii) political endemism (i.e., the proportion of species restricted to one country), (iv) the minimum area required to preserve one population or 10% of the range of each species, and (v) conservation conflicts in priority areas.

We created maps for 4795 mammal species, excluding only marine species, from the literature (*14*, *15*). To evaluate the minimum area required for preserving these mammal species, we compared "minimal" and "conservative" preservation criteria. Under the minimal criterion, cells required to have appropriate management to preserve all mammal species in at least one 10,000-km^2 cell were selected. Under the conservative criterion, enough cells were selected to preserve a minimum of 10% of the range of each species. Using a percentage criterion was judged better than selecting a number of cells, because we are only dealing with conservation of species here. The much more difficult and possibly more important issue of population conservation to maintain ecosystem services (*2*) is only partially considered and obviously would require even more extensive management. Our selection of cells includes the complete distribution of many species with a species range (SR) equal to or smaller than 10,000 km^2, and a large percentage of the SR of species with a range smaller than 50,000 km^2. A database of cells and the species found in each was entered into the MARXAN Reserve Design program (version 1.8.2) (*16*) to produce 250 scenarios for both minimal and conservative preservation criteria (*15*). Each scenario was a result of MARXAN's simulated annealing algorithm set to produce an optimal solution based on 10,000 iterations. We used the best solution (the one needing the minimum number of cells) to represent our global conservation management network (*16*). We used a fractional crop cover data set to estimate the proportion of each cell that is occupied by cropland (*17*). Spatially referenced human population data from the Center for International Earth Science Information Network [CIESIN (*18*)] were used to determine the population density for each cell in the global reserve network.

Species with small geographic ranges are more vulnerable to human impacts (and thus to extinction) than are widespread ones, and the number of those restricted-range species is positively related to the number of sites required to preserve global mammalian diversity. Although the geographic distributions of land mammals vary from very small (<10 km^2; one cell) for some island species to very large for species such as the wolf (*Canis lupus*, >49 million km^2; 4900 cells), most (76%) species have a SR smaller than 1 million km^2 (100 cells) (Fig. 1). Rare species (n = 1198), defined here as those comprising the first quartile of the frequency distribution of geographic

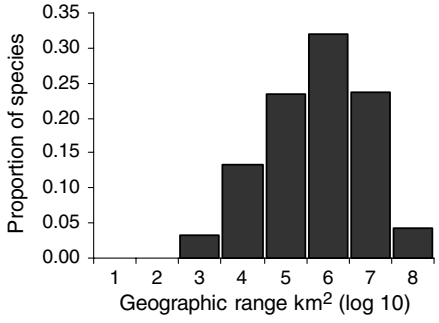

Fig. 1. Most mammal species have relatively small geographic ranges (<400,000 km^2), encompassing 20% or less of the continent where they occur. Such limited geographic ranges tend to make those species relatively prone to extinction.

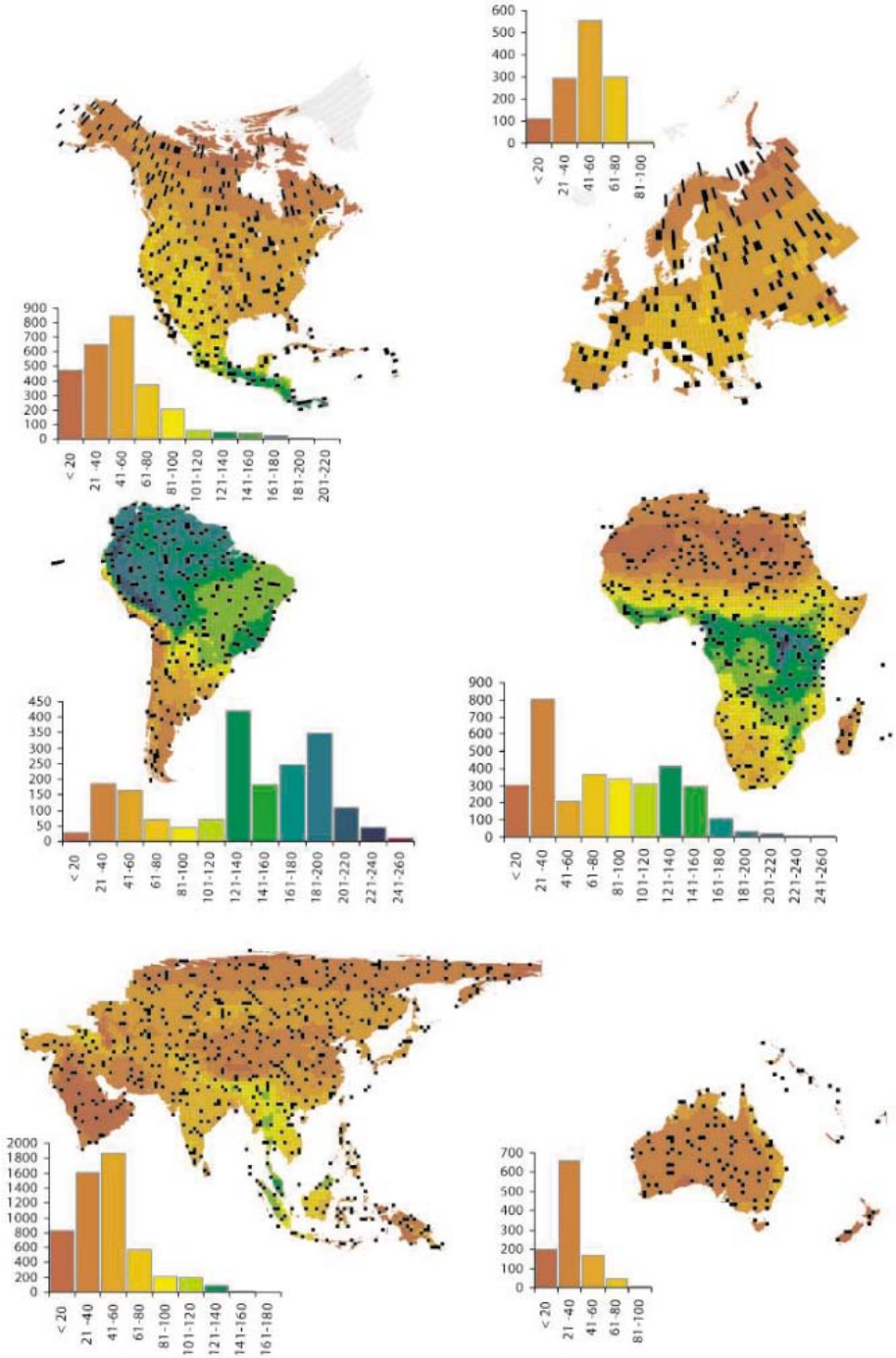

Fig. 2. Patterns of mammal species richness in six major regions of the world. The abscissa shows number of cells, and the ordinate shows species richness. Most diverse regions are found in South America and Africa. Marked cells indicate priority areas for the maintenance of 10% of the geographic ranges of all mammal species.

ranges, have a SR smaller than 24,000 km^2 (less than three cells, roughly half the size of Costa Rica). There are more rare species in Asia, followed by Africa, South America, North America, and Australia. Similarly, 32% (1531) of the species have a SR smaller than 50,000 km^2 (five cells), which is a threshold used with other factors to determine species endangerment by international conservation agencies such as the World Conservation Union (*19*). An unexpected result is that only 8% of mammal species are exclusively found in hot spots [sensu (*11*)], 62% are shared between hot spots and other regions [i.e., "cold spots" sensu (*13*)], and 30% are restricted to cold spots. Similarly, the ranges of 95% of all species intersect with at least one reserve in the 2004 IUCN/UNEP (World Conservation Union/United Nations Environment Programme) World database of protected areas.

As expected on the basis of biogeographic theory and patterns in other taxa, distribution of mammal species richness is very heterogeneous, with regions of low and high diversity on each continent and higher richness at lower latitudes (Fig. 2). As a result, the number of species in a single cell varies from 10 to 257. Most cells throughout the world have relatively few species (<100), especially in large regions in northern Africa and Asia, and nearly all of Europe and Australia. Unexpectedly, only four regions—Central America, the Andes-Amazonia in South America, east-central Africa, and Southeast Asia—have very rich cells, containing 200 or more species. South America has by far more of these cells.

The threat to the almost 40% (1900) of politically endemic (*5*) mammals is at least partially negatively correlated with economic development. Developing nations often lack resources for conservation. Centers of political endemism, with 5% or more of the world's endemic mammals each, are Australia, Indonesia, Mexico, Brazil, the United States, Philippines, Madagascar, China, and Papua New Guinea. Most countries, and most megadiverse countries, are underdeveloped, and endemic species are concentrated in those countries. Some 47% (906) are found in countries like Iran, ranking below the top 100 countries in PPP (Purchase Parity Power; <U.S. $5900); only 18% of mammal species are politically endemic to industrialized countries (PPP > U.S. $11,000) (*20*).

The minimal preservation criterion (all species in at least one 10,000-km^2 cell) requires the management of 668 cells (6,680,000 km^2), ~4.2% of Earth's ice-free land surface. In contrast, the more conservative criterion (cells to represent 10% of the geographic range of all species) requires managing at least 1702 cells (17,020,000 km^2), accounting for 11% of the ice-free land surface. Cells in the conservative scenario were located in Asia (589), Africa (349), North America (299), South America (220), Europe (126), and Australia (119). Many mammal species (3293, 68%) were represented in very few priority cells (<10); 6% (290 species) were found in more than 100 cells, and the range was from 1 to 404 cells (Fig. 3). The total number of species occurrences in these cells, which could be used as a very conservative estimate for the number of populations [Mendelian populations or demographic units (*2*)] of mammals, is 116,103.

Practically, it is important to carry out a sensitivity analysis to determine the degree of substitutability of cells; that is, if one becomes uninhabitable, how readily can a substitute be found. It is highly unlikely that all selected cells will retain high conservation value because human impacts and removing a degraded cell can affect the value of others in MARXAN scenarios. Hence, strategic conservation investment would involve back-up or next-best site sets as well as the priority set. More than 93% (15,057) of cells were selected in at least 1 of 250 scenarios for the 10% preservation criterion, and 135 cells (<1%) were irreplaceable, that is, selected in all scenarios (Fig. 2). Irreplaceable cells were located in all continents; most were in Asia (51, 37%), followed by North America (31, 23%), South America (20, 15%), Africa (19, 14%), Australia (10, 7%), and Europe (4, 4%). This is a favorable outcome, because 95% of the cells can be replaced by other cells without loss of conservation value, which gives the opportunity for strategic conservation planning. On the other hand, 1225 (72%) and 120 (89%) of the 1702 and 135 priority or irreplaceable cells in the best solution, respectively, intersect any one of the IUCN protected area polygons, indicating a relatively good correspondence between priority cells and protected areas.

To evaluate the extent to which a few species are driving the selection of priority cells, we quantified the difference in number of grid cells needed to achieve the conservative goal as compared to the number needed to protect 10% of the range of species endangered according to the IUCN (*21*). Only 48% (814) of cells would be required to represent those species, and those cells are found in North America (32%), Africa (27%), Asia (18%), South America (13%), Australia (8%), and Europe (2%). Similarly, we determined that to represent all mammals except rodents, the most diverse order, required 5% fewer cells. Randomly reducing the number of species to be protected at 10% intervals showed very slow reductions in the number of cells. Dropping 10, 20, 50, and 90% of the species represented a reduction of >1, 2, 7, and 21% of cells in the conservative (10%) representation goal.

Although land area under agriculture and human population density by themselves might seem to be crude estimators of anthropogenic impact, they actually are good indicators of overall biodiversity loss and conservation conflict, defined as the overlap of human activities and priority areas for conservation (*22–26*). We found a positive relation between species richness and human population density within the conservative, 10% criterion cells (Fig. 4A). One alarming result that requires immediate attention is that ~80% of the land area that must be managed under this conservative criterion has been affected to some degree by agriculture (Fig. 4B). Indeed, 20% of such cells have lost from 26 to 100% of their natural vegetation to agriculture, re-

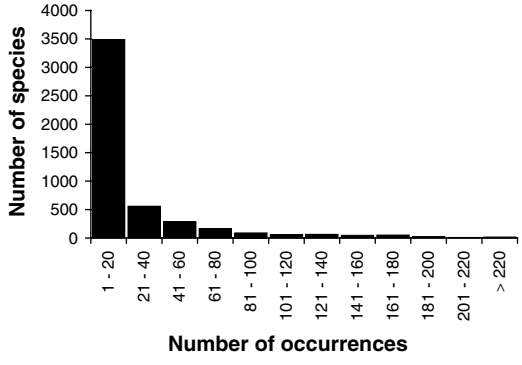

Fig. 3. Frequency distribution of the number of cells occupied by mammal species in the conservative criterion, in which at least 10% of the range area of each species is protected. Most of these species occur in fewer than 40 100-km by 100-km cells, equivalent to the area of California (USA) or three-quarters the area of France.

Table 1. Percentage of each priority cell for conservation covered by cropland (*17*) in six regions of the world. This is a measure of conservation conflict. Many cells have less than 25% conversion to cropland, suggesting opportunities for ameliorating conflict through countryside biogeography.

Cells	Africa	Asia	Australia	Europe	North America	South America	Total
None	20	14	55	6	36	1	20
1–25	70	58	39	35	41	95	59
26–50	6	13	5	29	14	4	11
51–75	4	11	1	22	6	0	7
76–100	0	4	0	8	3	0	3

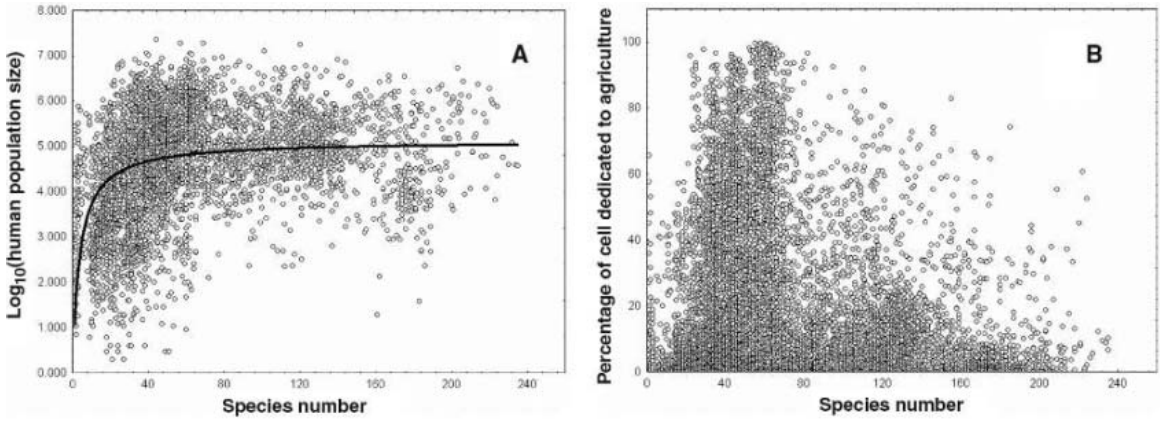

Fig. 4. Conservation conflict as represented by the relation between mammal species richness and human population density (**A**), and agriculture (**B**), in the priority cells. (A) A Michaelis-Menten type of curve was adjusted by a nonlinear method, and the r^2 (proportion of variance accounted for by the model) was calculated for each continent. Human population and number of mammal species are more strongly associated in Europe (r^2 = 0.77), Africa (r^2 = 0.59), and Asia (r^2 = 0.53) than in North America (r^2 = 0.29), South America (r^2 = 0.19), and Australia (r^2 = 0.09). (B) A simple linear fit yields a low value of r^2 (0.09), indicating a lack of relation between agriculture and number of mammal species.

ducing the value of each for conservation (Table 1).

Our results have clear implications for conservation. First, the large number of mammal species with restricted geographic ranges calls forth complex conservation scenarios because those species are intrinsically vulnerable to human impacts and stochastic extinction, and many are politically endemic. The high frequency of restricted ranges reinforces the obvious point that a larger and more dispersed selection of sites is required to preserve global mammalian diversity than would be required if range size distribution were skewed in the other direction. As the human population and its impacts have escalated, being politically endemic with a restricted geographic range in developing nations (e.g., orang-utan, *Pongo pygmeus*, in Indonesia) could, in most cases, considerably increase extinction risk because conservation legislation and resources are lacking. In contrast, the many endemic species in Australia are now subject to the kinds of intense management efforts that only rich nations are able to afford. Further complicating the conservation task is that even a well-known taxon such as mammals is more speciose than previously thought. There are now 10% more mammal species than were estimated a decade ago (*27*), and the total number is certain to be higher.

Second, our study supports previous ones showing that a large fraction of Earth's surface is important for the conservation of species diversity (*9*, *11*, *12*, *25*). This is especially true given that we focus only on mammals—the cells that would be selected for, say, butterflies or freshwater fishes would likely be quite different (*9*). Obviously, it is very important to designate and manage reserves from which human activity is excluded or strongly restricted. Many species and populations such as the mountain gorilla (*Gorilla gorilla*) in Africa could not now survive without effective reserves. Conservation by protected areas, however, although effective and necessary, cannot be the only strategy. Even under optimistic assumptions, managing just 4% of Earth's surface, as in our minimum protection scenario, would be a gigantic task, especially when considering both high levels of conservation conflict throughout the world and gaps in the representation of species in protected areas.

In some places, the required habitat types or resources could be protected without formal reserves, through conservation finance approaches or through other cultural and political mechanisms. This work and related studies throw into sharp relief the importance of areas outside of protected parks and reserves for the maintenance of mammalian diversity. This is the domain of countryside biogeography (*8*). Many species can and do survive in regions with different degrees of human impact. For example, research in the Las Cruces region in southern Costa Rica indicates that a large percentage of the mammals (and other taxa) can survive in a region with ~9% of its original forest cover remaining (*28*). Similar patterns have been found throughout the world, even for populations of very large species such as tigers in India and Nepal (*29*). From the viewpoint of both ecosystem services and biodiversity preservation, we now need to start managing the whole planet better, as Vitousek *et al.* (*30*) point out. In some sense, "we" already manage the whole planet. However, the problem of planetary management, paying careful attention to "priority" grid cells and political endemism for a diverse selection of taxa, is especially daunting because of the great differences in the ability of nations to protect organisms within their borders. That, and the scale of the problem, mean that an unprecedented international effort will be needed—one requiring the development of both new attitudes and institutions (*31*). Developing those in a politically sensitive and cost-effective way is perhaps the major challenge for conservation biology.

References and Notes

1. P. R. Ehrlich, A. Ehrlich, *Extinction: The Causes and Consequences of the Disappearance of Species* (Random House, New York, 1981).
2. J. B. Hughes, G. C. Daily, P. R. Ehrlich, *Science* **278**, 689 (1997).
3. S. Pimm, P. Raven, *Nature* **403**, 843 (2000).
4. C. R. Margules, R. L. Pressey, *Nature* **405**, 243 (2000).
5. G. Ceballos, P. R. Ehrlich, *Science* **296**, 904 (2002).
6. W. G. Luck, G. C. Daily, P. R. Ehrlich, *Trends Ecol. Evol.* **18**, 331 (2003).
7. J. K. McKee, P. W. Sciulli, C. D. Fooce, T. A. Waite, *Biol. Conserv.* **115**, 161 (2004).
8. G. C. Daily, Ed., *Nature's Services* (Island Press, Washington, DC, 1997).
9. T. M. Brooks *et al.*, *Bioscience* **54**, 1081 (2004).
10. A. J. Long, M. J. Crosby, A. J. Stattersfield, D. C. Wege, *Global Ecol. Biogeogr. Lett.* **5**, 281 (1996).
11. N. Myers, R. A. Mittermeier, C. G. Mittermeier, G. A. B. da Fonseca, J. Kent, *Nature* **403**, 853 (2000).
12. A. S. Rodrigues *et al.*, *Nature* **428**, 640 (2004).
13. P. Kareiva, M. Marvier, *Am. Sci.* **91**, 344 (2003).
14. Supporting online material includes additional information on materials and methods, a list of all sources used for obtaining the distribution maps, and the list of species included in this study.
15. The maps are an approximation of the current geographic distributions of these species. Maps for well-known species such as lions are probably more accurate than are those for poorly known species of rodents, shrews, and bats. Maps were digitized and the data analysis was done using ArcView 3.3. Earth's surface was divided into a 10,000-km^2 grid cell network using the Behrmann equal area projection. We defined a species range (SR) as all cells that intersected the species map (*32*). We choose not to have a different threshold for species with tiny ranges, because our selection of 10,000 km^2 priority cells includes all or most of the range of species with a SR equal to or smaller than 10,000 km^2. A similar trend occurs for other species with other small SRs. For example, a single-cell representation of species with a 20,000- or 30,000-km^2 SR likely represents 50 and 33% of its geographic range, and so on.
16. H. I. Possingham, I. Ball, S. Andelman, in *Quantitative Methods for Conservation Biology*, S. Ferson, M. Burgman, Eds. (Springer, New York, 2000), pp. 291–305.
17. N. Ramankutty, J. A. Foley, *Glob. Ecol. Biogeogr.* **8**, 381 (1999).
18. http://sedac.ciesin.columbia.edu/plue/gpw
19. World Conservation Union (IUCN), *The 2003 IUCN Red List of Threatened Species* (IUCN, Gland, Switzerland, 2003).
20. World Bank, *World Development Indicators 2004* (World Bank, Washington, DC, 2004).
21. We considered as "endangered" all species classified by the 2003 IUCN red data list as critically endangered, endangered, and threatened (*19*).
22. J. Liu, G. C. Daily, P. R. Ehrlich, G. W. Luck, *Nature* **421**, 530 (2003).

23. A. Balmford *et al.*, *Science* **291**, 2616 (1991).
24. R. P. Cincotta, J. Wisnewski, R. Engelman, *Nature* **404**, 990 (2000).
25. K. J. Gaston, T. M. Blackburn, K. K. Goldewijk, *Proc. R. Soc. London B. Biol. Sci.* **270**, 1293 (2003).
26. D. Tilman *et al.*, *Science* **292**, 281 (2001).
27. A. Duff, A. Lawson, *Mammals of the World: A Checklist* (A & C Black, London, 2004).
28. G. C. Daily, G. Ceballos, J. Pacheco, G. Suzan, A. Sánchez Azofeifa, *Conserv. Biol.* **17**, 1 (2003).
29. E. Wikramanayake *et al.*, *Conserv. Biol.* **18**, 839 (2004).
30. P. M. Vitousek, H. A. Mooney, J. Lubchenco, J. M. Melillo, *Science* **277**, 494 (1997).
31. P. R. Ehrlich, A. H. Ehrlich, *One with Nineveh: Politics, Consumption, and the Human Future* (Island Press, Washington, DC, 2004).
32. Environmental Systems Research Institute (ESRI), *ESRI Data and Maps 2002* (Environmental Systems Research Institute, Redlands, CA, 2002); see www.esri.com.
33. We thank G. C. Daily, R. A. Medellin, C. Sekercioglu, R. List, and K. M. A. Chan for comments on the manuscript. This study was supported by the National University of Mexico, CONABIO (Mexico), the Center for Conservation Biology–Stanford University, EcoCiencia (Mexico), and the John Simon Guggenheim Memorial Foundation.

Supporting Online Material
www.sciencemag.org/cgi/content/full/309/5734/603/DC1
Materials and Methods
References
Species list

25 April 2005; accepted 17 June 2005
10.1126/science.1114015

On the Regulation of Populations of Mammals, Birds, Fish, and Insects

Richard M. Sibly,[1]* Daniel Barker,[1] Michael C. Denham,[2] Jim Hone,[3] Mark Pagel[1]

A key unresolved question in population ecology concerns the relationship between a population's size and its growth rate. We estimated this relationship for 1780 time series of mammals, birds, fish, and insects. We found that rates of population growth are high at low population densities but, contrary to previous predictions, decline rapidly with increasing population size and then flatten out, for all four taxa. This produces a strongly concave relationship between a population's growth rate and its size. These findings have fundamental implications for our understanding of animals' lives, suggesting in particular that many animals in these taxa will be found living at densities above the carrying capacity of their environments.

The way a population's size changes through time—its dynamics—depends on the way it grows when small and declines when big. More specifically, the dynamics result from the precise relationship between the population's size (N) and its per capita growth rate (pgr), defined as $^{1}/_{N} \times {}^{dN}/_{dt}$, where t is time (Fig. 1). The simplest case is a straight-line relationship, such that pgr declines linearly with increasing N (Fig. 1A, left). Linearity produces the well-known logistic population growth equation $N(t) = \frac{KN_0}{(K-N_0)e^{-r_0 t} + N_0}$, where r_0 is a parameter representing pgr when $N = 0$, N_0 is the size of the population at time = 0, and K is the population's carrying capacity (*1*).

The relationship between pgr and N is generally taken to be monotonic and decreasing and can be either concave or convex (*2*). Convex relationships (Fig. 1B) imply that pgr varies little until population size is near carrying capacity, then drops rapidly. Concavity (Fig. 1C) means that pgr is initially relatively high, so small populations grow quickly, but pgr then declines rapidly as population size increases, later flattening out so that the approach to carrying capacity is relatively slow. In a variant possible in theory and occasionally reported in nature, the slope of the relationship between pgr and N becomes positive in small populations, such that pgr actually increases with N over a narrow range of population sizes, giving an Allee effect (*2–4*).

The way in which pgr declines with population size is conventionally modeled by the theta-logistic equation, given by

$$pgr = r_0[1 - (N/K)^{\theta}] \qquad (1)$$

where r_0 and K are as before, and θ is a parameter describing the curvature of the relationship (*2*). In practice, population density is sometimes used in place of population size, and r_0 is best replaced by r_m, representing pgr when population size N is at a defined low value, corresponding to a population of, for example, one individual (*5*) (Fig. 2). Values of θ greater or less than 1 correspond to convex and concave relationships, respectively (Figs. 1 and 2). Mechanistically, the value of θ must depend on the ways that animals interact at different densities (*6*).

There has been a persistent suggestion that the shape of the pgr-density relationship depends on a species' life history (*5*, *7*, *8*). The widely cited argument (*9–14*) is as follows. Large, long-lived species generally live close to the carrying capacity of their environments, being limited mainly by resources, and are only rarely subject to natural selection for increased performance at low population density. As a consequence, these species' population growth rates are relatively unaffected until populations are nearing carrying capacity, producing the convex curve of $\theta > 1$ seen in Fig. 1. By contrast, species that spend most of their time at densities much lower than carrying capacity are selected for a high maximum rate of increase. As a result, these species are affected even at relatively low densities in their abilities to acquire foods, and so the concave relationship of $\theta < 1$ between pgr and N arises. There are a number of cases of density dependence that together have suggested that pgr-density relationships are convex for large mammals and similar species but concave for species with life histories like those of insects and some fish (*5*, *7*, *15*).

The form of the pgr-density relationship has implications beyond population dynamics, and it is used to make predictions and to analyze management options in areas such as conservation (*16*), pest management (*17*), risk assessment (*18*), and disease epidemiology (*19*). In spite of this, there have been few attempts to establish generalities about how pgr varies with population size (*5*, *15*, *20*). Here we analyze an extensive compilation of time series data from 4926 different populations in the Global Population Dynamics Database (GPDD) (*21*, *22*). The GPDD is a collection of time series of population counts or indices of these, together with other taxonomic details of more than 1400 species.

After exclusion of time series that were very short, did not vary, or contained zeros, the GPDD contained 3766 time series from 1084 species (table S1). We further excluded 469 series (12%) that showed a significant decline in size with time, because unknown factors may have prevented population recovery and biased the form of the estimated pgr-density relationship, and 1% that showed positive density dependence (i.e., pgr increased with density), because these show no evidence of population regulation. We examined the remaining 3269 series for evidence of Allee relationships, but these were rare if present at all: There were only 20 cases in which a quadratic regression of pgr on N fitted better ($P < 0.05$) than a linear regression, with a turning point of the required

[1]School of Animal and Microbial Sciences, University of Reading, Whiteknights, Reading RG6 6AJ, UK. [2]Statistical Sciences Europe, GlaxoSmithKline Research and Development Limited, New Frontiers Science Park, Third Avenue, Harlow, Essex CM19 5AW, UK. [3]Institute for Applied Ecology, University of Canberra, Canberra ACT 2601, Australia.

*To whom correspondence should be addressed. E-mail: r.m.sibly@reading.ac.uk

type and within the range of observed values of N, and in only 5 was the pattern clearly nonmonotonic (*22*). We conclude that there is clear evidence of Allee effects in only a small minority (0.2%) of GPDD data sets. Absence of Allee effects in bird studies has been noted by Saether *et al*. (*23*).

We fitted Eq. 1 to each of the 3269 tractable time series in the GPDD using a nonlinear least-squares procedure and discarded cases yielding relatively imprecise estimates of θ (*22*). The main taxonomic groups represented were birds (150 species), mammals (79), bony fish (64), and insects (381). Figure 3 shows the frequencies of occurrence of fitted values of θ in each of the main taxonomic groups. In each taxon, there are far more instances where $\theta < 1$ (concave) than where $\theta > 1$ (convex). The average proportion of cases where $\theta < 1$ is 0.78. This is higher than the proportion (0.62) found in the only comparable study (*5*), but that was based on only 13 species of birds. The proportion of cases where $\theta < 1$ differs only a little between the major taxonomic groups, though there is a suggestion that the proportion is higher in fish than in mammals, birds, and insects (taking the average value of θ for each species and counting species, $\chi_3^2 = 6.9$, nonsignificant) (Fig. 3).

It is not possible to apply explicit phylogenetic methods to these data because no phylogeny exists to describe them, but we repeated analyses using genus means and then family means as a way of controlling for the lack of independence among species (counting genera, $\chi_3^2 = 8.2$, $P < 0.05$; counting families, $\chi_3^2 = 8.0$, $P < 0.05$). θ was significantly ($P < 0.05$) different from 1 in 613 of the 1780 time series analyzed, being less than 1 in 581 cases and greater than 1 in 32. The reason only 613 estimates were significantly different from 1 is that some of the estimates are imprecise. Our strategy for dealing with imprecision was to remove very imprecise estimates (*22*), but this retained quite a number that still had wide confidence intervals. Among the small proportion (0.22) of cases where $\theta > 1$, there are no obvious taxonomic or other patterns: All major taxonomic groups are represented. Our results suggest that in mammals, birds, fish, and insects, population regulation is generally the result of a concave relationship between a population's growth rate and its size.

The histograms of θ suggest that θ is normally less than 1, but they do not directly test the hypothesis that θ would increase with a species' body size (*7*, *8*, *15*). However, there is no suggestion of such a relationship in any of the four taxonomic groups we analyzed. In mammals, the reverse is the case: The relationship is negative, not positive as predicted [regression with one point per species: $r_{36} = -0.32$, $P < 0.05$ (fig. S2); with one point per family or genus, the relationship is still negative: $r_{11} = -0.253$, nonsignificant, and $r_{28} = -0.291$, nonsignificant, respectively]. Our results, based on a much larger data set than previous analyses, appear to rule out the possibility that the shape of the *pgr*-density relationship is strongly associated with taxonomy or body size.

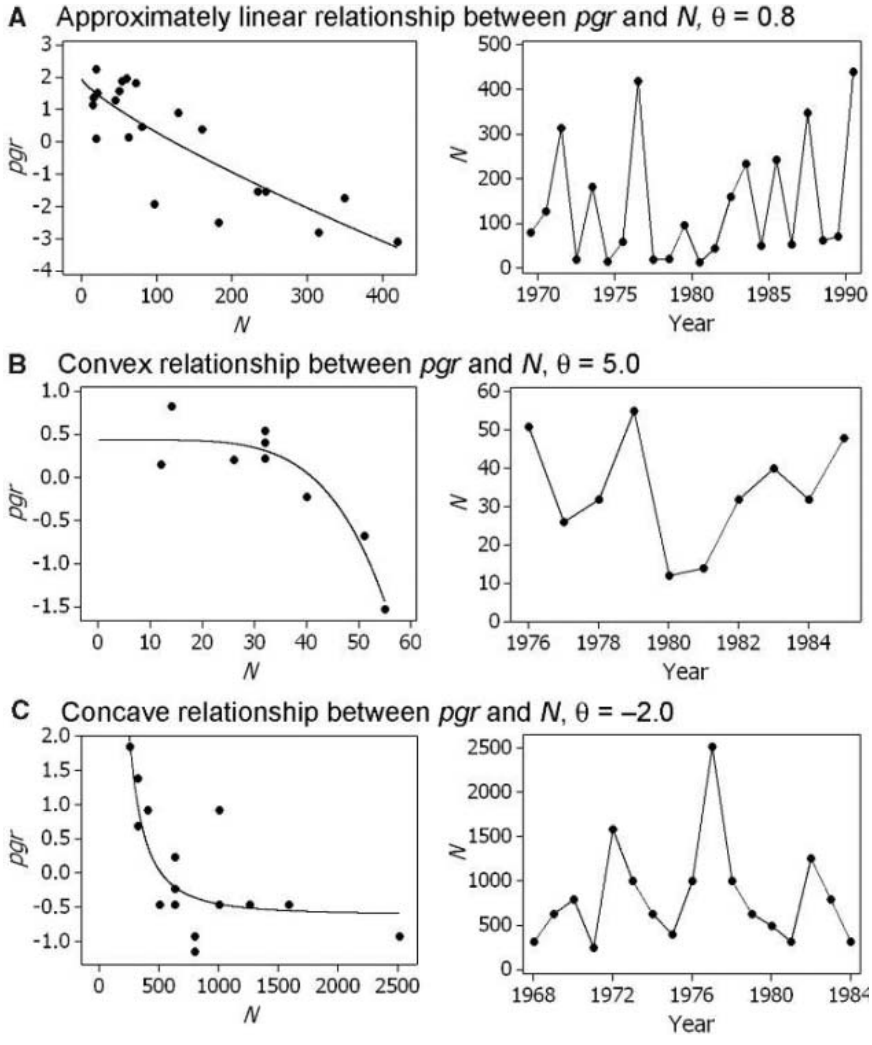

Fig. 1. (**A** to **C**) (Left) The relationships between population growth rates (*pgr*) and size (*N*) with (right) their associated population time series. The observed values on the left are calculated from the time series, and the fitted curves are of the type of Eq. 1. The data come from three insect populations in the GPDD with (A) $\theta \approx 1$ (*Acyrthosiphon pisum*, GPDD main ID 8383), (B) $\theta > 1$ (*Inachis io*, ID 3276), (C) $\theta < 0$ (*Xylena vetusta*, ID 6321). The form of *pgr*-*N* relationships are specific to the time and place in which the data were collected (*32*).

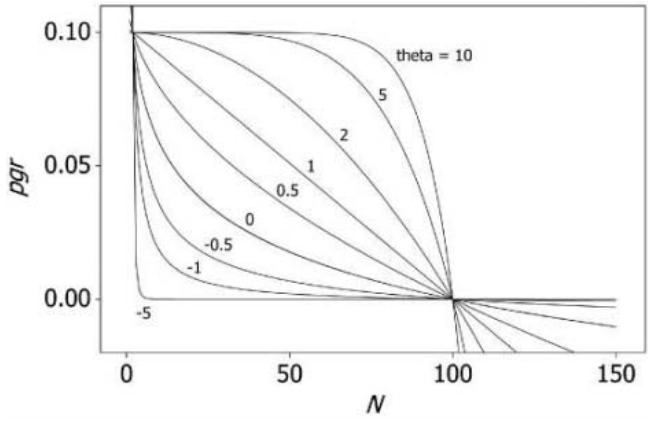

Fig. 2. Illustration of the curves generated by the theta-logistic equation (Eq. 1) for different values of θ. *N* represents population size or density. Each curve is constrained to go through (1, 0.1) and (100, 0); thus, the minimum population size is 1 and $r_m = 0.1$ and $K = 100$. There is no particular significance in our choice of $N = 1$ for the lower constraint; similar families of curves are obtained at other values of *N*, provided that these are nonzero and small in comparison with *K* (supporting online text).

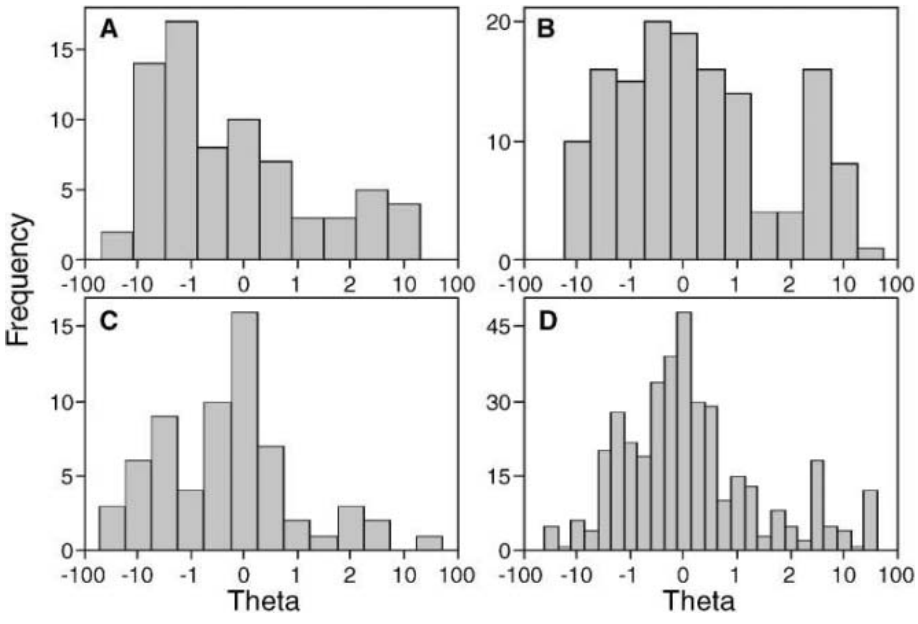

Fig. 3. Histograms of θ for the four major taxonomic groups in the GPDD database: (**A**) mammals, (**B**) birds, (**C**) fish, and (**D**) insects. A hybrid scale is used for θ, linear between –1 and 2 and $\log_{10}$ elsewhere. This scale is used to give similar weights to each of the principal regions of interest in Fig. 2. Where there existed within-species replication, we used the average value, so that each species is here represented only once.

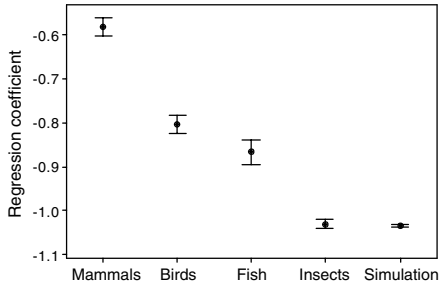

Fig. 4. Slopes of regressions of *pgr* versus $\log_e$ density, showing that the observed relationships are not simply a result of measurement error. Measurement error alone predicts a slope of –1 in regressions of *pgr* against $\log_e$ density, in marked contrast to fitted slopes, except in the case of the insects. For comparison, we also show the effects of measurement error simulated with 3920 time series of length 30 and processed as for the GPDD data sets. Bars show one standard error of the mean. Frequency distributions of these regression coefficients are shown in fig. S3.

Values of θ around zero can arise from measurement error (*24*), and so it is important to exclude that possibility here (*25*). If all variation in population size arises from random measurement error, it is straightforward to derive the predicted relationship between *pgr* and the logarithm of population density. The relationship is linear with slope –1.0. We analysed the slope of the relationship between *pgr* and the logarithm of population density within each of our four taxonomic groups and for simulated data in which all variation in density was random (Fig. 4). In three of our four groups, the slopes differed markedly from –1.0 (*t* tests, $P \ll 0.001$), suggesting that measurement error does not have a dominant role in these groups. The simulated data have, as expected, a mean very close to –1.0, and our insect populations also fall close to –1.0, possibly suggesting that measurement error has affected the estimates of θ in these populations. As a further check, we used the GPDD grading of time series to indicate perceived quality, which may in some cases be affected by measurement error (*21*). Restricting our analysis to the top two grades out of five did not affect our conclusions.

An important implication of our finding, that the relationship between *pgr* and density is generally concave, is that many animals may spend most of their time at or above carrying capacity. To see this, consider the effects of variations in population size induced by density-independent environmental factors. Assume that increases and decreases occur with similar magnitudes and frequencies and that $\theta < 1$. For $\theta < 1$, returns to carrying capacity are faster if the population is below than if it is above carrying capacity. The rate of return is given by the absolute value of *pgr*, and the rate of return is faster from a point below carrying capacity than from a point an equivalent distance above carrying capacity. This is seen in the dynamics of the population of *Xylena vetusta* (Fig. 1C) for which the estimated carrying capacity (where $pgr = 0$) is 512. Note that upward steps are generally larger than downward. The result is that populations spend more time above than below carrying capacity. This process will produce a tail extending to the right in the frequency distribution of population size. In line with this prediction, 88% of the 1849 GPDD cases analyzed here are positively skewed ($P < 0.001$, mean skewness 1.08 ± 0.024). Halley and Inchausti (*26*) obtained a similar result. Because bird and mammal populations may generally be regulated by their food supplies (*27*–*29*), our finding that most individuals live in environments above carrying capacity suggests they have less food than is needed for population replacement. However, other factors, such as predation and social interactions within the species, may in some circumstances override the role of food.

Factors whose effects are not felt immediately may also be important in determining population growth or decline (*30*), and we considered carefully the possibility of including time delays in our analysis. Adding two time lags would have added a minimum of two extra parameters to be estimated. Our conclusion was that the additional complexity to the model was not warranted, given the quality of data sets in our analysis. However, we believe it would be interesting to explore the possibility of including time lags in future studies.

Our conclusion that the most common *pgr*-density relationships are concave in birds, mammals, fish, and insects should have wide implications for understanding how the abundance and dynamics of populations are controlled and for our practical ability to make predictions about how such species respond to environmental change. For example, if a linear relationship is assumed and values of r_m and K are estimated from other sources—for instance, r_m is sometimes estimated from life-history data in optimal environments—then concavity means that *pgr* is overestimated when the population is below carrying capacity (Fig. 2). This would have dangerous consequences in wildlife and fisheries management, because populations would recover from disturbances more slowly than predicted. Pest control, by contrast, would be more successful than expected. Knowledge of the shapes of the *pgr*-density relationship is required in all areas of population ecology to make projections as to future abundance and population dynamics (*18*, *28*, *29*, *31*).

References and Notes

1. A. Tsoularis, J. Wallace, *Math. Biosci.* **179**, 21 (2002).
2. P. Turchin, *Complex Population Dynamics* (Princeton Univ. Press, Princeton, NJ, 2003).
3. P. A. Stephens, W. J. Sutherland, *Trends Ecol. Evol.* **14**, 401 (1999).
4. F. Courchamp, T. Clutton-Brock, B. Grenfell, *Trends Ecol. Evol.* **14**, 405 (1999).
5. B.-E. Saether, S. Engen, E. Matthysen, *Science* **295**, 2070 (2002).
6. T. Royama, *Analytical Population Dynamics* (Chapman & Hall, London, 1992).
7. C. W. Fowler, *Ecology* **62**, 602 (1981).
8. M. E. Gilpin, F. J. Ayala, *Proc. Natl. Acad. Sci. U.S.A.* **70**, 3590 (1973).
9. A. R. E. Sinclair, *Philos. Trans. R. Soc. London Ser. B* **358**, 1729 (2003).
10. P. Bayliss, D. Choquenot, *Philos. Trans. R. Soc. London Ser. B* **357**, 1233 (2002).
11. J. Lindstrom, H. Kokko, *Ecol. Lett.* **5**, 338 (2002).
12. R. Lande, B.-E. Saether, S. Engen, *Ecology* **78**, 1341 (1997).

13. B.-E. Saether, *Trends Ecol. Evol.* **12**, 143 (1997).
14. T. H. Clutton-Brock *et al.*, *Am. Nat.* **149**, 195 (1997).
15. R. M. Sibly, J. Hone, *Philos. Trans. R. Soc. London Ser. B* **357**, 1153 (2002).
16. S. R. Beissinger, D. R. McCullough, Eds., *Population Viability Analysis* (Univ. of Chicago Press, Chicago, 2002).
17. G. Caughley, A. R. E. Sinclair, *Wildlife Ecology and Management* (Blackwell Science, Cambridge, MA, 1994).
18. R. A. Pastorok, S. M. Bartell, S. Ferson, L. R. Ginzburg, Eds., *Ecological Modeling in Risk Assessment* (CRC/Lewis, London, 2002).
19. R. M. Anderson, R. M. May, *Infectious Diseases of Humans: Dynamics and Control* (Oxford Univ. Press, Oxford, 1991).
20. P. Turchin, *Oikos* **84**, 153 (1999).
21. National Environment Research Council (NERC) Centre for Population Biology, Imperial College (1999), Global Population Dynamics Database, available at www.sw.ic.ac.uk/cpb/cpb/gpdd.html
22. Materials and methods are available as supporting material on *Science* Online.
23. B.-E. Saether, T. H. Ringsby, E. Roskaft, *Oikos* **77**, 217 (1996).
24. T. M. Shenk, G. C. White, K. P. Burnham, *Ecol. Monogr.* **68**, 445 (1998).
25. To identify the effects of measurement error on θ estimation, we carried out computer simulations of time series governed by Eq. 1 but subject to log-normal environmental perturbations and with measurement errors also being log-normally distributed. Preliminary results suggested that over the range of parameters of interest, θ can be recovered without appreciable bias, provided that measurement error is less than half of environmental variation, and that useful information is still obtainable when measurement error and environmental variation are equal.
26. J. Halley, P. Inchausti, *Oikos* **99**, 518 (2002).
27. A. R. E. Sinclair, in *Ecological Concepts*, J. M. Cherrett, Ed. (Blackwell Scientific, Oxford, 1989), pp. 197–241.
28. A. R. E. Sinclair, in *Frontiers of Population Ecology*, R. B. Floyd, A. W. Sheppard, P. J. De Barro, Eds. (CSIRO, Melbourne, 1996), pp. 127–154.
29. A. R. E. Sinclair, C. J. Krebs, *Philos. Trans. R. Soc. London Ser. B* **357**, 1221 (2002).
30. R. Lande, S. Engen, B.-E. Saether, *Stochastic Population Dynamics in Ecology and Conservation* (Oxford Univ. Press, Oxford, 2003).
31. S. Jennings, M. J. Kaiser, J. D. Reynolds, *Marine Fisheries Ecology* (Blackwell Science, Oxford, 2001).
32. C. J. Krebs, *Philos. Trans. R. Soc. London Ser. B* **357**, 1211 (2002).
33. We are grateful to E. Bazely-White and the NERC Centre for Population Biology at Silwood Park for generous and efficient help in supplying the data and to B.-E. Saether and A. Berryman for extensive constructive comments on an earlier version of the manuscript. Supported by NERC grant no. NER/B/S/2001/00867 (R.M.S. and M.P.).

Supporting Online Material
www.sciencemag.org/cgi/content/full/309/5734/607/DC1
Materials and Methods
SOM Text
Figs. S1 to S3
Table S1

7 February 2005; accepted 18 May 2005
10.1126/science.1110760

Host Suppression and Stability in a Parasitoid-Host System: Experimental Demonstration

William Murdoch,[1]* Cheryl J. Briggs,[2] Susan Swarbrick[1]

We elucidate the mechanisms causing stability and severe resource suppression in a consumer-resource system. The consumer, the parasitoid *Aphytis*, rapidly controlled an experimentally induced outbreak of the resource, California red scale, an agricultural pest, and imposed a low, stable pest equilibrium. The results are well predicted by a mechanistic, independently parameterized model. The key mechanisms are widespread in nature: an invulnerable adult stage in the resource population and rapid consumer development. Stability in this biologically nondiverse agricultural system is a property of the local interaction between these two species, not of spatial processes or of the larger ecological community.

Although some consumer-resource (e.g., predator-prey) populations famously cycle in abundance, most appear to be stable, even when the predator strongly suppresses prey abundance (*1*). Yet, any theory that includes only a few basic predator properties—time lags and limited killing capacity of individual predators—generally predicts instability, i.e., large-amplitude oscillations or even predator-driven extinction of the prey (*2*, *3*). Model stability is particularly difficult to achieve when the predator can drive the prey to densities far below the limits set by the prey's own resources [the "paradox of enrichment" (*4*)], and almost all theoretically stabilizing mechanisms achieve stability only by causing the prey density to increase close to that limit (*1*).

California red scale (*Aonidiella aurantii*), an insect pest of citrus worldwide, is controlled by the parasitoid *Aphytis melinus* (*5*). This system exemplifies in extreme the features—ecological simplicity, high productivity, and severe suppression of the pest—that should engender instability. (i) It is an almost pure specialist consumer-resource interaction. Citrus groves contain, in addition to red scale, only a few, scarce, herbivore species. Under biological control, red scale are attacked mainly by *Aphytis melinus*; one other parasitoid and one or two predator species are typically present but scarce. (ii) Citrus provides a rich resource for scale. deBach (*6*) showed that when dichloro-diphenyl-trichloroethane (DDT) was applied to citrus trees (which killed *Aphytis* but not the resistant scale), scale outbreak density reached several hundred times higher than controlled populations and was not brought back under control for more than 3 years (presumably, when *Aphytis* was able to re-invade the tree). Yet, in our study area, red scale under control have persisted for >40 years (80 scale generations) with little temporal variation, at densities <1% of the limit set by the citrus plant.

Over two decades, we and our colleagues have tested and ruled out many mechanisms by which *Aphytis* might achieve this remarkable control with stability, including parasitoid aggregation to, or independent of, local host density (*7*), as well as density-dependence in the parasitoid sex-ratio (*8*). Stability also does not depend on spatial processes, including metapopulation dynamics. Dynamics were not altered when a spatial refuge from parasitism was removed, or when populations in individual trees were isolated from the larger population in the grove (*9*): Control and stabilizing mechanisms act locally within a single tree. Feasible remaining mechanisms explored in models involve life-history details, e.g., a long adult host stage invulnerable to parasitism (*10*). In previous studies, we could not detect temporal density-dependence in parasitism, host-feeding, or predation (*11*), a difficult task within the narrow range of densities of a stable system near equilibrium (*12*). A density-perturbation experiment might uncover both density-dependence and the mechanisms causing return to equilibrium. Density manipulations at the appropriate spatial scale typically are logistically daunting, but in the *Aphytis*–red scale system, the appropriate spatial scale is the individual tree (*9*).

We created experimental red scale outbreaks (*13*). We caged individual trees and increased scale recruitment over a period somewhat longer than it takes scale to develop from birth to adult (this development period defines the time unit, t). We followed the dynamics of these outbreak populations, together with caged and uncaged control populations, over three to five scale development times. Three separate experiments gave the same result. We present only the third experiment, which had four outbreak trees.

Control of the outbreak and stability—return to equilibrium density—occurred rapidly (Fig. 1). Scale density began to decline even before crawler additions stopped and before one scale development period had passed, and most suppression occurred by $t = 2$; i.e., within 2 months after we added scale. By

[1]Department of Ecology, Evolution and Marine Biology, University of California, Santa Barbara, CA 93106, USA. [2]Department of Integrative Biology, University of California, Berkeley, CA 94720–3140, USA.

*To whom correspondence should be addressed. E-mail: murdoch@lifesci.ucsb.edu

$t = 3$, scale densities in outbreak trees almost exactly equaled control densities: This is dynamic stability. Little variation in density was seen in experimental and control populations thereafter.

The resident *Aphytis* populations controlled the outbreak by rapidly increasing in abundance. Scale stages suitable for parasitism ("host stages") became abundant only at the second sampling date, yet by the next sample (less than one scale development period into the experiment), the immature *Aphytis* population was >20 times denser than in control trees. Adult *Aphytis* density then increased with only a short delay. Between $t = 1$ and $t = 2$, the average host's lifetime probability of parasitism by *Aphytis* reached 95% in outbreak populations versus 66% in controls (*13*). Immature and adult *Aphytis* populations also returned rapidly to control densities as soon as the outbreak was suppressed (Fig. 1).

We developed and parameterized a detailed day-by-day stage-structured model of the system, based on extensive laboratory and field investigations (*13*). The model is an extension of a simpler one that distinguished major red scale life stages and their differential treatment by *Aphytis* and that suggested that stability might be achieved via three mechanisms. (i) There is a long-lived invulnerable adult scale stage. (ii) *Aphytis* develops (about 3 times) faster than scale. (iii) An attack on older immature scale yields a higher gain to the parasitoid than does an attack on younger immature scale (the "gain" mechanism); for example, older scale yield one or more female parasitoid offspring while the youngest scale are eaten, yielding nutrients for egg development (*1*, *10*).

The model recognizes every ecologically distinguishable scale stage and how it is used (or not used) by *Aphytis*, which can either feed on hosts or lay a clutch of one or two, male or female, eggs (Fig. 2). It classifies adult *Aphytis* by their egg load and "gut fullness"; both affect how the parasitoid responds to encountered scale. Egg load increases with a brief delay after a meal and decreases after oviposition. Gut and egg capacity are limited. The model runs on physiological time (degree-days), because in the field, development and search rates are temperature-dependent; simulations use the actual sequence of temperatures experienced during the experiment. Stage durations in degree-days are known, and the model keeps track of the physiological age of all groups. The model also contains two new potentially stabilizing processes discovered during other field experiments. (iv) Hosts containing an *Aphytis* egg can be reattacked; the existing egg is killed, and the new immature *Aphytis* survives about half as well as would the original. Subsequent reparasitizations do not produce live offspring. (v) *Aphytis* adults live longer when scale density is higher (*13*).

The model was parameterized independently of the outbreak experiment (*13*) and used to predict the experiment's outcome. It was run for $t > 20$, until the populations had reached their approximate long-term dynamics, then scale crawlers were added every day over the same period and at the same rate as in the experiment. The model predicted that, in the absence of *Aphytis*, live scale should reach a first-generation density about 80 times control density, then increase roughly threefold during each scale development time (Fig. 3A). This rate of increase is the maximum observed by deBach in the DDT experiment described above (*6*).

The model predicted the mean densities of the experimental populations with remarkable accuracy (Fig. 3B). Predicted peak adult parasitoid density is higher than the observed mean, but close to the peak in the densest tree. Increases or decreases by 10% in each parameter value or set of values (excluding scale development time, which sets the time scale that all other parameters relate to) change predictions little and are as likely to improve as to worsen predictions; Fig. 3B shows the lowest and highest densities induced by these changes.

More important, the general result is robust to substantial changes in the value of parameters we expected would affect dynamics most strongly, and even to changes in aspects of model structure. We doubled *Aphytis* development lag, immature death rates, adult longev-

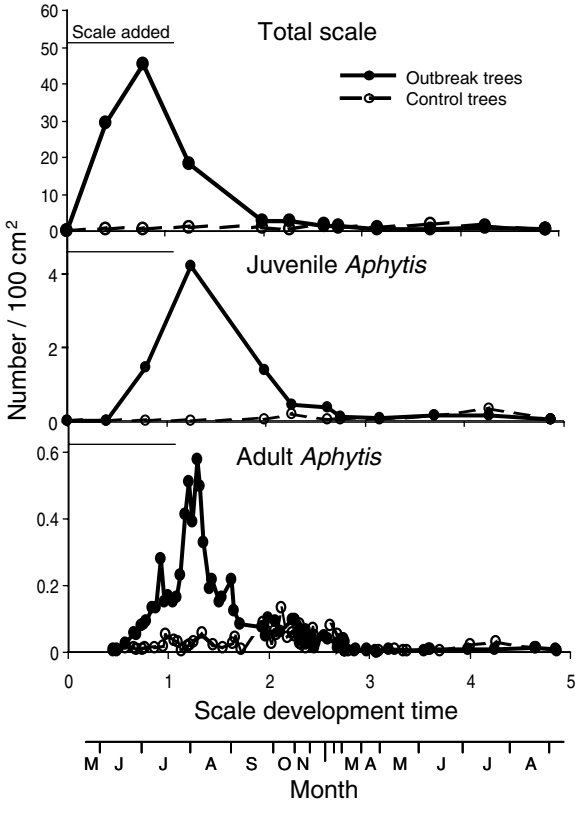

Fig. 1. Mean densities in four outbreak and 10 control trees over five scale development times (16 months).

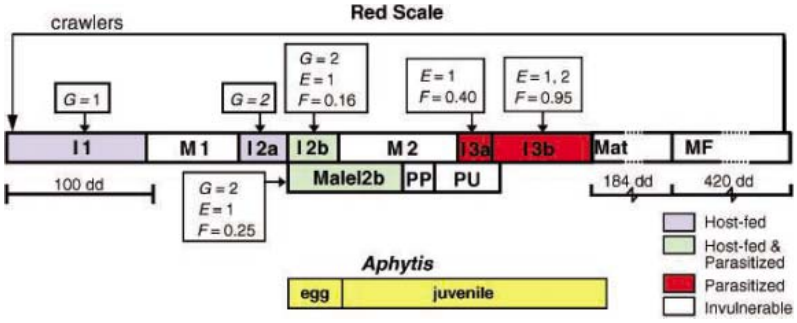

Fig. 2. Red scale and *Aphytis* stages. Width of stage indicates duration (degree-days). *G*, gain in egg-equivalents from a meal; *E*, number of eggs laid; *F*, fraction that are female; I, instar; M, molt; males and females distinguishable after I2a. Invulnerable adult females: Mat, mature females; MF, crawler-producers. PP, PU, prepupal and pupal males, respectively.

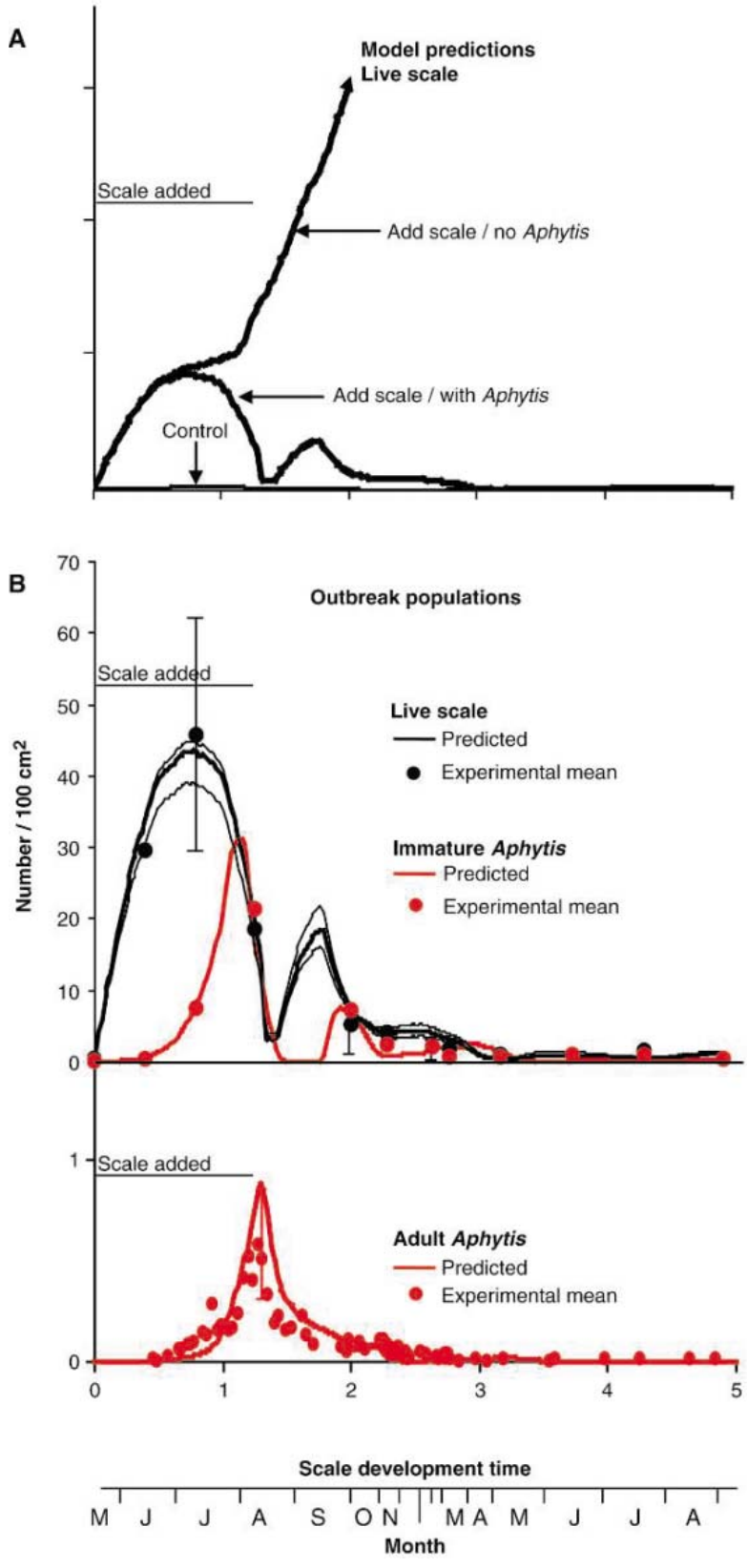

Fig. 3. (**A**) Density of live scale predicted by the model. Scale eventually increase exponentially in absence of *Aphytis*, but return to control density with *Aphytis* present. (**B**) (Top) Dark curves, model prediction; light curves, highest (*Aphytis* lag shorter) and lowest (immature scale death rates higher) densities predicted when parameters increased or decreased, individually, by 10%. Vertical lines, range of live scale densities (four experimental trees) on dates when prediction is furthest from observed mean. (Bottom) Vertical lines, range for date closest to peak when counts were made in all four trees. The model parameters were estimated independently of the experimental data.

ity, or attack rate; we doubled scale fecundity, or halved adult scale longevity or the attack rate on already parasitized scale. In all cases, model output is little different from that with the default parameters: The outbreak is brought under control by about $t = 3$, fluctuations in density remain small over the long run, and long-term average scale density changes little. The three worst cases are shown in Fig. 4: Doubling parasitoid lag slightly delays control; doubling *Aphytis* immature death rates roughly doubles long-term scale density; keeping *Aphytis* longevity fixed, independent of scale density, delays control until just after $t = 3$, but does not alter long-term dynamics. The pattern is also not altered when we remove the "gain" mechanism.

Considering the five mechanisms, stability is impossible if the adult invulnerable stage is brief, regardless of other parameter values. A large enough increase (fourfold) in parasitoid time lag causes instability. Changes in intensity of the other three stabilizing mechanisms generally have only small effects on stability. *Aphytis* longevity that increases with scale density, however, contributes strongly to timely control, especially when the parasitoid delay is long. Although these three mechanisms are individually less important, the combination of mechanisms creates a "fail-safe" system that is robust to variation in the environment (parameter values) and major life history properties.

Aphytis causes the low scale equilibrium density by efficiently producing female offspring, by means of its search rate and its ability to produce females from relatively small scale (*14*, *15*). Although stabilizing mechanisms in general increase prey density, rapid *Aphytis* development decreases pest prey density, and adult scale longevity has little effect (*1*).

The field experiment demonstrates remarkable stability in a consumer-resource interaction. The model uncovers the mechanisms that explain such stability, together with concomitant severe suppression of the resource (host) population far below the density set by its own resource (the citrus tree). A simpler version of the model explains how *Aphytis melinus* re-

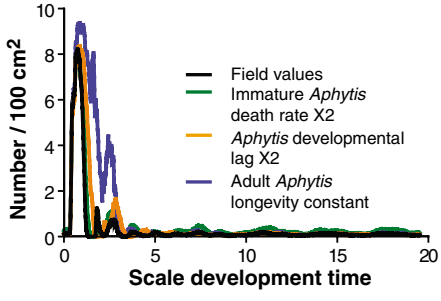

Fig. 4. Predicted long-term dynamics in the outbreak experiment when key parameter values were doubled (×2) or a mechanism was deleted from the model. Shown are the default prediction and the three worst cases.

placed a less effective agent (*A. lingnanensis*) (*15*), so we have confidence that the models capture the features that make *A. melinus* one of the most successful of biological control agents.

The life-history features most crucial to stability (an invulnerable adult stage and relatively rapid parasitoid development) are widespread in parasitoid-host systems with overlapping generations, and in many other consumer-resource interactions. Simple models suggest that, in general, differences in vulnerability among prey age classes, rather than absolute invulnerability, constitute the actual stabilizing mechanism (*1*, *16*, *17*). Such differential vulnerability occurs in all but the simplest organisms, and the reproductive stage is commonly least vulnerable. Probably most species of natural enemies (parasites, parasitoids, and disease organisms) develop faster than their prey. True predators, however, typically develop more slowly than their prey and must have countervailing stabilizing mechanisms.

The implications of these results go far beyond this system. The protagonists have long been removed (the scale from China and *Aphytis* from Iran) from their natural ecological communities and are now in an unnatural, species-poor, human-created system. Stability is achieved without diversity at any trophic level. Although appeal to spatial processes has come to dominate explanations of persistence and stability, they are not important to the stability or dynamics of this system. Instead, suppression and stability are consequences of the purely life-history and physiological properties of the interacting organisms.

References and Notes

1. W. W. Murdoch, C. J. Briggs, R. M. Nisbet, in *Consumer-Resource Dynamics,* S. Levin, Ed. (Monographs in Population Biology, Princeton Univ. Press, Princeton, NJ, 2003).
2. M. P. Hassell, *The Dynamics of Arthropod Predator-Prey Systems* (Monographs in Population Biology Princeton Univ. Press, Princeton, NJ, 1978), vol. 13, Fig. 2.7.
3. R. M. May, in *Theoretical Ecology: Principles and Applications*, R. M. May, Ed. (Blackwell Scientific, Oxford, 1976), pp. 49–70.
4. M. L. Rosenzweig, *Science* **171**, 385 (1971).
5. D. Rosen, P. DeBach, *Species of* Aphytis *of the World (Hymenoptera: Aphelinidae)* (Junk, Dordrecht, Netherlands, 1979).
6. P. deBach, D. Rosen, C. E. Kennett, in *Biological Control*, C. B. Huffaker, Ed. (Plenum, New York, 1971), pp. 165–194.
7. J. D. Reeve, W. W. Murdoch, *J. Anim. Ecol.* **54**, 797 (1985).
8. J. D. Reeve, W. W. Murdoch, *J. Anim. Ecol.* **55**, 1069 (1986).
9. W. W. Murdoch, S. L. Swarbrick, R. F. Luck, S. Walde, D. S. Yu, *Am. Nat.* **147**, 424 (1996).
10. W. W. Murdoch, R. M. Nisbet, R. F. Luck, H. C. J. Godfray, W. S. C. Gurney, *J. Anim. Ecol.* **61**, 533 (1992).
11. W. W. Murdoch *et al.*, *Ecology* **76**, 206 (1995).
12. W. W. Murdoch, *Ecology* **75**, 271 (1994).
13. Supplementary material is available at *Science* Online.
14. R. F. Luck, H. Podoler, *Ecology* **66**, 904 (1985).
15. W. W. Murdoch, C. J. Briggs, R. M. Nisbet, *Am. Nat.* **148**, 807 (1996).
16. R. H. Smith, R. Mead, *Theor. Popul. Biol.* **6**, 308 (1974).
17. J. N. McNair, *Theor. Popul. Biol.* **32**, 383 (1987).

18. Research supported by NSF grants DEB9629316 and DEB0089515, and National Research Initiative of the U.S. Department of Agriculture Cooperative State Research, Education and Extension Service, grant 98-35302-6877. We thank J. Latto and M. Daugherty for insightful comments and R. Nisbet and K. Shea for interactions on an earlier model.

Supporting Online Material

www.sciencemag.org/cgi/content/full/309/5734/610/DC1
Materials and Methods
Figs. S1 to S4
References and Notes

4 May 2005; accepted 17 June 2005
10.1126/science.1114426

Dynamics of Mammalian Chromosome Evolution Inferred from Multispecies Comparative Maps

William J. Murphy,[1,3*†] Denis M. Larkin,[5*] Annelie Everts-van der Wind,[5*] Guillaume Bourque,[8] Glenn Tesler,[9] Loretta Auvil,[6] Jonathan E. Beever,[5] Bhanu P. Chowdhary,[1] Francis Galibert,[11] Lisa Gatzke,[6] Christophe Hitte,[11] Stacey N. Meyers,[5] Denis Milan,[12] Elaine A. Ostrander,[13] Greg Pape,[6] Heidi G. Parker,[13] Terje Raudsepp,[1] Margarita B. Rogatcheva,[5] Lawrence B. Schook,[5,7] Loren C. Skow,[1] Michael Welge,[6] James E. Womack,[2] Stephen J. O'Brien,[4] Pavel A. Pevzner,[10] Harris A. Lewin[5,7†]

The genome organizations of eight phylogenetically distinct species from five mammalian orders were compared in order to address fundamental questions relating to mammalian chromosomal evolution. Rates of chromosome evolution within mammalian orders were found to increase since the Cretaceous-Tertiary boundary. Nearly 20% of chromosome breakpoint regions were reused during mammalian evolution; these reuse sites are also enriched for centromeres. Analysis of gene content in and around evolutionary breakpoint regions revealed increased gene density relative to the genome-wide average. We found that segmental duplications populate the majority of primate-specific breakpoints and often flank inverted chromosome segments, implicating their role in chromosomal rearrangement.

Whole-genome analysis of human, mouse, rat, and cattle genomes has indicated that breakpoints are reused (convergently) in karyotypic evolution, implying some bias for or against breakage in certain regions of mammalian genomes (*1*–*3*). To extend observations based on the few sequenced mammalian genomes (i.e., human, mouse, and rat) (*4*–*7*), we annotated homologous synteny blocks (HSBs) in the latest radiation hybrid (RH) genome maps of cat, cattle, dog, pig, and horse (*8*–*12*). The HSBs were defined for each species with the use of the human genome as a reference (NCBI Build 33) and required a minimum of two adjacent markers on the same chromosome in both species, without interruption by genes from other HSBs. Inversions were counted only if determined by three or more markers, each ≥1 million base pairs (Mbp) apart from its neighbors. We did not perform our analysis with the dog whole-genome sequence assembly because it was not available for analysis at the time. Furthermore, because of the low comparative resolution of many horse chromosome maps, only a subset of equine chromosomes was included for chromosome-specific analyses. We used the GRIMM-Synteny–based mouse-human and rat-human whole-genome sequence synteny blocks (*13*), but we allowed the threshold for considered rearrangements to be ≥1 Mbp to make resolution comparable to that of RH-based gene maps.

[1]Department of Veterinary Integrative Biosciences, [2]Department of Veterinary Pathobiology, Texas A&M University, College Station, TX 77843, USA. [3]SAIC-Frederick Inc., [4]Laboratory of Genomic Diversity, National Cancer Institute, Frederick, MD 21702, USA. [5]Department of Animal Sciences, [6]National Center for Supercomputing Applications, [7]Institute for Genomic Biology, University of Illinois at Urbana-Champaign, Urbana, IL 61801, USA. [8]Genome Institute of Singapore, 138672, Singapore. [9]Department of Mathematics, [10]Department of Computer Science and Engineering, University of California, San Diego, CA 92093, USA. [11]UMR6061-CNRS, Genetique et developpement, Université de Rennes 1, 35043 Rennes, France. [12]Laboratoire de Génétique Cellulaire, INRA, 31326 Castanet-Tolosan, France. [13]National Human Genome Research Institute, Bethesda, MD 20892, USA.

*These authors contributed equally to this work.
†To whom correspondence should be addressed. E-mail: wmurphy@cvm.tamu.edu; h-lewin@uiuc.edu

We identified 1159 pairwise HSBs between the genomes of human and the six nonprimate species (average size = 13.7 Mbp; median = 7.4 Mbp) (table S1). A bioinformatics tool (*14*) was designed to align and compare HSBs across species (Fig. 1) (fig. S1). Using the seven-species pairwise HSBs, we compiled multispecies HSBs (table S2) and constructed an evolutionary scenario depicting the rearrangements between all genomes and their ancestors (Fig. 2) (fig. S2). We were able to reconstruct a genome for the ferungulate ancestor of Cetartiodactyla (pig and cattle) and Carnivora (cat and dog) (Fig. 2). Combining the putative ferungulate ancestor with the computed primate-rodent ancestor, we then estimated an ancestral boreoeutherian mammalian genome that contains 48% comparative coverage of the human genome (Fig. 2). The ferungulate and boreoeutherian ancestors had 24 pairs of chromosomes, and they contain the majority of the ancestral chromosomes expected on the basis of chromosome painting of diverse mammals (*15*). In contrast to these cytogenetic studies that largely reveal conservation of synteny but not gene order (*15*), we now have reliable reconstructions of internal chromosome structure for most ancestral chromosomes. Eleven of 24 boreoeutherian ancestor (BA) chromosomes contain large segments that are colinear with human chromosomes, whereas other chromosomes show more extensive rearrangement in each mammalian lineage (e.g., BA11, BA15, and BA19, Fig. 2 and fig. S2).

We defined an evolutionary breakpoint region as an interval between two HSBs that is demarcated by the end-sequence coordinates of those HSBs on each side. We identified 492 breakpoint regions in our data set (table S3); 367 of these were refined to <4 Mbp in size (average = 1.2 Mbp; median = 1.0 Mbp). We focused on these to avoid any possible errors in regions of low comparative coverage. Breakpoints were further categorized as lineage-specific (found in only one species), order-specific (overlapping between species of the same order), superordinal (overlapping in all representatives of a superordinal clade), and reuse (occurring in the same breakpoint region in different species).

Early comparative mapping studies concluded that there were three phases of chromosome evolution: (i) an early phase, 100 to 300 million years ago (Ma), with a slow rate of rearrangement; (ii) a second phase, 65 to 100 Ma, when there was an overall rate increase in mammalian lineages; and (iii) a reduction of mammalian rates during the Cenozoic Era (*16*). Other studies based primarily on chromosome painting data (unordered comparative maps) suggest a more dichotomous view of rearrangements during the Cenozoic (*17*), although recent studies based on chromosome painting of more genomes and a refined phylogeny (*18*) did not lend support to the bimodal model (*15*).

We looked for trends in the ordered genome data by examining rates of chromosome breakage throughout mammalian history. An evolutionary time scale (*19*) was used to infer rates (and assess confidence intervals) of breakage over time (Fig. 3). In contrast to previous studies (*16*), our results suggest an increase in breakage rates after the Cretaceous-Tertiary (K-T) boundary. Superordinal lineages predating the K-T boundary (i.e., the beginning of the Cenozoic) evolved at a rate of roughly 0.11 to 0.43 breaks per million years,

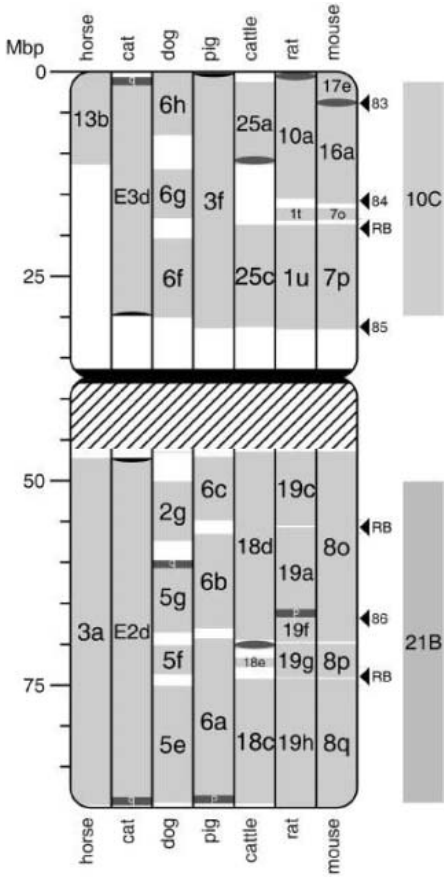

Fig. 1. Multispecies comparative chromosome architecture of human chromosome 16 (HSA16). Gray blocks indicate HSBs, with the chromosomal identity indicated by either a number or an uppercase letter and a number. Lowercase letters indicate order of the HSB in that species' chromosome (in alphabetical order). Telomere and centromere positions are indicated by dark gray rectangles and ovals, respectively. Reuse breakpoints are indicated with arrowheads labeled RB on the right side of the chromosome ideogram. Positions of cancer-associated breakpoints (10 or more confirmed cases) (*32*) are indicated with arrowheads followed by a number indicating the associated gene: 83 = *CREBBP*, 84 = *MYH11*, 85 = *FUS*, 86 = *CBFB*. See table S9 for details of all numbered cancer breakpoints and their occurrences. Computed boreoeutherian ancestral HSBs aligned to HSA16 (BA10c and BA21b) are shown on the right. For visualization of all chromosomes, see fig. S1 and (*14*).

whereas in ordinal and familial evolutionary lineages during the Cenozoic we find rate increases by factors of 2 to 4 in carnivores, primates, and cetartiodactyls, and by as much as a factor of 5 in rodents (Fig. 3). The only exception is the cat lineage, whose lower rate is partly a by-product of reduced map resolution relative to other species (*20*). Furthermore, our taxon sampling masks the fact that the rodent and primate rate increase occurred even later than shown in Fig. 3, because early primate and rodent ancestors, with origins around 75 Ma, had very conserved genome organizations (*15*). Thus, both ordered and unordered mapping data support the contention that early eutherian ancestors retained fairly conserved genomes.

Nearly 20% of all classified breakpoints were categorized as reuse (Fig. 1), suggesting a high frequency of independent rearrangements occurring at the same regions of the genome in different mammalian lineages. A majority of reuse breakpoints (71%) involve the two rodents and one or two other species; in most cases the two other most rapidly evolving genomes were cattle or dog (fig. S3), confirming and extending previous findings (*1*, *2*). Multispecies alignments also afforded an examination of the relationship between evolutionary and cancer-associated chromosome breakpoints (Fig. 1) (figs. S1 and S5). The more frequent cancer-associated chromosome aberrations (more than nine human cases) fell within or near (±0.4 Mbp) evolutionary breakpoint regions three times as often as did the less frequent cancer-associated aberrations (two to nine human cases), whereas outside of the evolutionary breakpoint regions their distributions were not different. These data, and the complete absence of cancer-associated breakpoints in the three longest HSBs con-

Fig. 2. Genome architecture of the ancestors of three mammalian lineages computed by MGR (*33*) from the seven starting genomes and compared to the human genome (far left). Each human chromosome is assigned a unique color and is divided into blocks corresponding to the seven-way HSBs common to all species. The size of each block is approximately proportional to the actual size of the block in human. Physical gaps between blocks are shown in human to give an indication of the coverage. Also in human, the heterochromatic/centromere regions are denoted by hatched gray boxes. Numbers above the reconstructed ancestral chromosomes indicate the human chromosome homolog. Diagonal lines within each block (from top left to bottom right) indicate the relative order and orientation of genes within the block. Black arrowheads under the ancestral chromosomes indicate that the two adjacent HSBs separated by the arrowhead were not found in every one of the most parsimonious solutions explored; these are considered "weak" adjacencies. Arrowheads at the ends of HSB chromosomes indicate that some alternative solutions placed these chromosome-end HSBs adjacent to HSBs from other chromosomes.

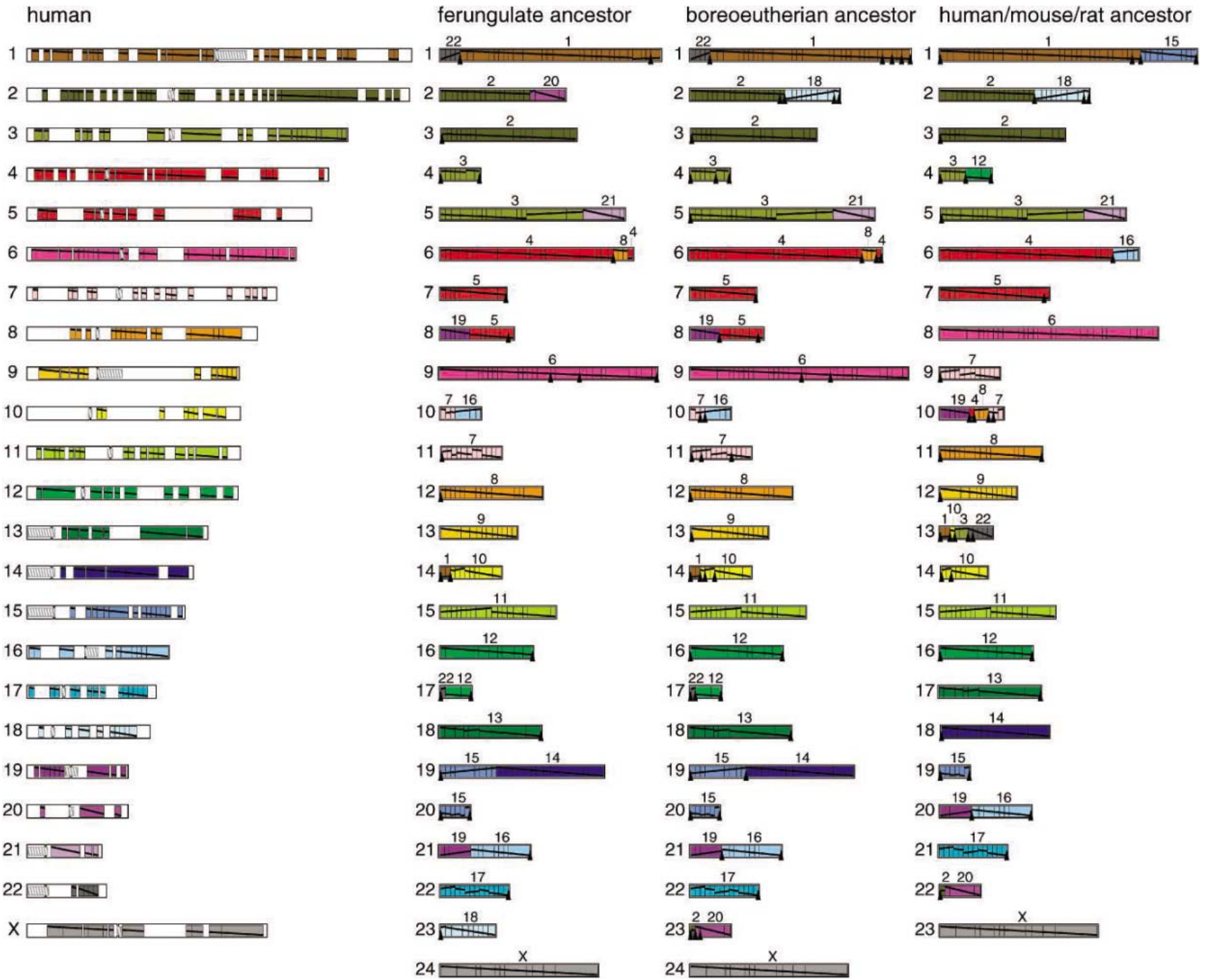
human
ferungulate ancestor
boreoeutherian ancestor
human/mouse/rat ancestor
1
2
3
4
5
6
7
8
9
10
11
12
13
14
15
16
17
18
19
20
21
22
X
23
24

served across all the mammalian genomes studied (on HSA3, HSA13, and HSA20, fig. S1), suggest a link between meiotic and mitotic chromosome instability.

We analyzed the human gene content of all evolutionary chromosomal breakpoint regions that could be refined to <4 Mbp. We defined the narrowest interval (usually defined by rat and mouse) of the breakpoint region as a "core breakpoint," and then analyzed gene density (NCBI Build 33 RefSeq + predicted genes) in windows surrounding the midpoint of the core breakpoint (table S4). When the central 1 Mbp around the core breakpoint was compared to the overall gene density per Mbp outside of the breakpoint regions, there was a significant increase in gene density ($P < 0.0001$) (genome-wide average 12.3 genes per Mbp versus 17.6 genes per Mbp in breakpoints) (table S5). One of the most gene-dense regions of the human genome, the major histocompatibility complex (~26 genes per Mbp), is also characterized by recurrent breaks in different mammalian lineages (e.g., dog, cat, cattle, murid rodents), marked amounts of gene turnover (*21*), and variation in centromere placement (*22*).

Recent segmental duplications annotated in the human genome arose during the last 40 million years of primate evolution (*23*, *24*). However, early studies of human-mouse evolutionary breakpoints (*25*, *26*) were unable to distinguish breakpoints that occurred during primate evolution from those that occurred on the rodent lineage—a necessary piece of evidence to implicate segmental duplication as a potential cause of primate chromosome rearrangements. We considered a chromosome breakpoint shared by all or nearly all non-human species, when aligned with the human genome sequence, to be evidence of a rearrangement occurring in the human lineage (fig. S1). We identified 40 breakpoints that could be classified as primate-specific (table S6); that is, they occurred somewhere after divergence of primates and rodents at 85 Ma (*19*). We cannot rule out, however, that some of these breaks preceded the basal divergence of primates from tree shrews and flying lemurs (*18*, *19*). For primate-specific breakpoints, 98% contained segmental duplications (table S6). On the basis of comparison to the reconstructed ancestor (Fig. 2), we could infer that many of the primate-specific breaks involved inversions. Roughly 85% of the primate-specific breakpoint regions were populated by intrachromosomal duplications (table S6). In 62% of the cases, these intrachromosomal duplications flanked the inverted HSBs. Therefore, we suggest that in these cases duplications promoted nonallelic homologous recombination, and thus a chromosome rearrangement (*23*, *27*). Because hundreds of regions across the human genome are occupied by primate-specific segmental duplications, whereas only a few dozen of these co-occur with primate-specific chromosomal rearrangements, such duplications are more likely to have promoted chromosomal rearrangements than to have resulted from them (*23*).

As chromosomes evolve by breakage and fusion, telomeres must be able to form de novo for meiosis and mitosis to occur normally. Extreme examples of conservation of telomere position are found at HSA14qter and HSA20qter (fig. S1), where conservation exists in chromosomes from four and five other species, respectively. On a genome-wide basis, 70% of telomere positions ($N = 254$) are conserved in more than one species (table S7). Within Rodentia, 34% of telomere positions are conserved (fig. S4), although this is not surprising given the relatively recent divergence of mouse and rat. By contrast, the longer evolutionary time separating cat and dog, and cattle and pig, is reflected by a very small fraction (<5%) of telomere positions being conserved exclusively within both orders (fig. S4). Conversely, a much larger fraction (40 to 50%) of carnivore and cetartiodactyl telomere positions are conserved with other orders, consistent with their slower overall rate of chromosomal evolution relative to mouse and rat. Although the dog genome is evolving more rapidly than the cat genome (Fig. 3) (*28*), dog telomere positions are often more conserved with homologous positions on chromosomes of other species (table S7). Our data show that sites of ancient telomere fusions, which would be signified by a telomere being "replaced" by a centromere in the new species, are likely to be quite rare. Most cases of telomere-to-centromere "conversions" appear to result from an internal breakage followed by centromerization of the former telomere. As an example, the telomeric region of ancestral chromosome 9a (HSA6p) may have become a centromere in an ancestral carnivore by the internal breakage of the segment followed by the de novo appearance of a centromere and a telomere, as represented on CFA35a and FCAB2a (fig. S1).

In contrast to telomeres, centromeres are more dynamic, rapidly evolving structures that can be repositioned among closely related species (*29*). In primates, a relatively large number of cryptic "neocentromeres" can develop into functional centromeres de novo, are associated with chromosomal abnormalities (*30*), and have evolutionary importance in karyotype evolution and speciation (*31*). For the multispecies analysis, the positions of 85 centromeres could be unambiguously determined. Of these, 52 (61%) show conservation of position in two or more species (table S8). The positions of 20 are conserved within Carnivora ($N = 14$) and Cetartiodactyla ($N = 6$), supporting a slower rate of chromosome evolution within these mammalian orders (table S8). The two rodent genomes were not included in the analysis of centromere conservation within and among orders because reliable positions for many metacentric rat centromeres in the sequence assembly were not available. For a given species, 39% of all centromere positions were found to be unique. Thus, a large fraction of centromeres analyzed were repositioned either by independent chromosomal rearrangements or by de novo centromere emergence, affirming the rapid evolution of centromeres.

Our analyses further revealed that telomere and centromere positions tend to cluster at sites of evolutionary breakages (fig. S1).

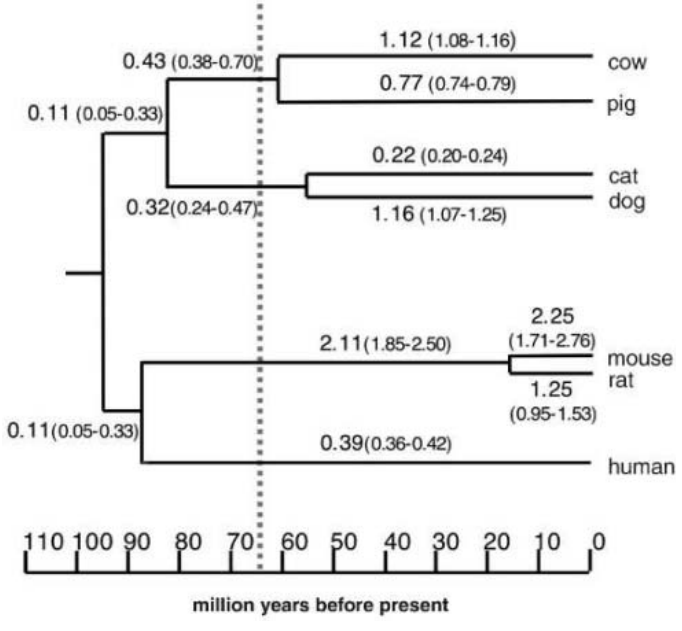

Fig. 3. Rates of chromosome breakage during mammalian evolution. The time scale is based on molecular divergence estimates (*19*). Rates (above the branches, in breaks per million years and 95% confidence intervals) were calculated using the total number of lineage, order, or superordinal breakpoints defined by the multispecies breakpoint analysis, and dividing these by the estimated time on the branch of the tree. The vertical gray dashed line indicates the K-T boundary, marking the abrupt extinction of the dinosaurs at ~65 Ma and preceding the appearance of most crown-group placental mammal orders in the Cenozoic Era (*19*).

Among the 85 centromere positions that could be classified, 38 were unambiguously assigned to HSBs, of which 28 (74%) occurred at the boundaries of evolutionary breakpoints. Furthermore, all 216 nonhuman telomeres appeared at the boundaries of evolutionary breakpoints or at the ends of computed ancestral chromosomes. These observations are logical given the requirement that the viability of a gamete containing the breakage is dependent on proper chromosome segregation in daughter cells as well as in subsequent meioses in an offspring. Another apparently related phenomenon is the joint clustering of centromeres and telomeres around evolutionary breakpoints. For example, there are 20 positions of clustering of telomere/centromere positions across the entire multispecies comparative landscape (fig. S1). Of these, 11 are clusters found in multiple species. Most of the centromeres that appear at evolutionary breakpoints as defined on the human genome are associated with the formation of acrocentric centromeres in other species.

The association between reuse breakpoints and the positions of centromeres or telomeres was significant ($\chi^2 = 14.5$, $P < 0.001$, 1 df). When telomeres and centromeres were analyzed separately, only centromeres were found to be significantly associated with reuse breakpoints ($P < 0.01$; table S8). This observation suggests a possible mechanism for chromosome evolution and the appearance of reuse breakpoints, whereby these evolutionary breakages preferentially occur at sites of ancestral centromeres or neocentromeres in independent lineages. Alternatively, reuse breakpoints may represent unstable chromosomal sites that, after breakage, will tend to form a new centromere or telomere.

We have shown that tremendous evolutionary activity exists at breakpoint regions, including reuse, increased gene density, segmental duplication accumulation, and the emergence of centromeres and telomeres. Taken together with our identification of reuse breakage occurring at the highest frequency between species with the most accelerated rates of chromosome evolution, our data suggest that there exist a limited and nonrandom number of regions in mammalian genomes that can be disrupted by these various dynamic processes. Given sufficient evolutionary time, these sites become "recycled" in different species. Future challenges lie in more fully interpreting the structure and function of breakpoint regions across a broader range of mammalian taxa, with the use of whole-genome sequence-based maps from phylogenetically divergent species.

References and Notes

1. P. Pevzner, G. Tesler, *Proc. Natl. Acad. Sci. U.S.A.* **100**, 7672 (2003).
2. D. M. Larkin *et al.*, *Genome Res.* **13**, 1966 (2003).
3. S. Zhao *et al.*, *Genome Res.* **14**, 1851 (2004).
4. E. S. Lander *et al.*, *Nature* **409**, 860 (2001).
5. J. C. Venter *et al.*, *Science* **291**, 1304 (2001).
6. R. H. Waterston, *Nature* **420**, 520 (2002).
7. R. A. Gibbs, *Nature* **428**, 493 (2004).
8. R. Guyon *et al.*, *Proc. Natl. Acad. Sci. U.S.A.* **100**, 5296 (2003).
9. M. Menotti-Raymond *et al.*, *Cytogenet. Genome Res.* **102**, 272 (2003).
10. B. P. Chowdhary *et al.*, *Genome Res.* **13**, 742 (2003).
11. A. Everts-van der Wind, *Genome Res.* **14**, 1424 (2004).
12. S. N. Meyers *et al.*, *Genomics,* in press.
13. G. Bourque, P. A. Pevzner, G. Tesler, *Genome Res.* **14**, 507 (2004).
14. Evolution Highway (http://evolutionhighway.ncsa.uiuc.edu).
15. L. Froenicke, *Cytogenet. Genome Res.* **108**, 122 (2005).
16. D. W. Burt *et al.*, *Nature* **402**, 411 (1999).
17. S. J. O'Brien *et al.*, *Science* **286**, 458 (1999).
18. W. J. Murphy *et al.*, *Science* **294**, 2348 (2001).
19. M. S. Springer, W. J. Murphy, E. Eizirik, S. J. O'Brien, *Proc. Natl. Acad. Sci. U.S.A.* **100**, 1056 (2003).
20. See supporting data on *Science* Online.
21. N. Yuhki *et al.*, *Genome Res.* **13**, 1169 (2003).
22. T. W. Beck *et al.*, *Immunogenetics* **56**, 702 (2005).
23. R. V. Samonte, E. E. Eichler, *Nat. Rev. Genet.* **3**, 65 (2002).
24. J. A. Bailey *et al.*, *Science* **297**, 1003 (2002).
25. L. Armengol, M. A. Pujana, J. Cheung, S. W. Scherer, X. Estivill, *Hum. Mol. Genet.* **12**, 2201 (2003).
26. J. A. Bailey, R. Baertsch, W. J. Kent, D. Haussler, E. Eichler, *Genome Biol.* **5**, R23 (2004).
27. B. K. Dennehey, D. G. Gutches, E. H. McConkey, K. S. Krauter, *Genomics* **83**, 493 (2004).
28. W. G. Nash *et al.*, *Cytogenet. Cell Genet.* **95**, 210 (2001).
29. V. Eder *et al.*, *Mol. Biol. Evol.* **20**, 1506 (2003).
30. D. J. Amor, K. H. Choo, *Am. J. Hum. Genet.* **71**, 695 (2002).
31. D. J. Amor *et al.*, *Proc. Natl. Acad. Sci. U.S.A.* **101**, 6542 (2004).
32. Mitelman Database of Chromosome Aberrations in Cancer (http://cgap.nci.nih.gov/Chromosomes/Mitelman).
33. G. Bourque, P. A. Pevzner, *Genome Res.* **12**, 26 (2002).

34. Supported by the Agency for Science, Technology and Research, Singapore (G.B.); the American Kennel Club Canine Health Foundation and NIH grant R01CA-92167 (E.A.O., F.G.); USDA National Research Initiative grant AG2004-3520-14196 (H.A.L., J.E.W.); USDA Cooperative State Research, Education and Extension Service grant AG2004-34480-14417, the Livestock Genome Sequencing Initiative (H.A.L., L.B.S., J.E.B.) to support comparative mapping; and the National Cancer Institute under contract N01-CO-12400 (W.J.M., S.J.O.). We thank K. Worley and M. Jensen-Seaman for providing data on rat centromere positions.

Supporting Online Material

www.sciencemag.org/cgi/content/full/309/5734/613/DC1
Materials and Methods
Figs. S1 to S5
Tables S1 to S9

22 February 2005; accepted 1 June 2005
10.1126/science.1111387

Extreme Reversed Sexual Dichromatism in a Bird Without Sex Role Reversal

Robert Heinsohn,[1]* Sarah Legge,[2] John A. Endler[3,4]

Brilliant plumage is typical of male birds, reflecting differential enhancement of male traits when females are the limiting sex. Brighter females are thought to evolve exclusively in response to sex role reversal. The striking reversed plumage dichromatism of *Eclectus roratus* parrots does not fit this pattern. We quantify plumage color in this species and show that very different selection pressures are acting on males and females. Male plumage reflects a compromise between the conflicting requirements for camouflage from predators while foraging and conspicuousness during display. Females are liberated from the need for camouflage but compete for rare nest hollows.

The operational sex ratio and sexual differences in potential reproductive rate lead to gender-biased mate competition, gender-biased sexual selection, and sexual dimorphism (*1*, *2*). These, along with ecological factors such as limited nesting sites (*3*), can result in sex role reversal (SRR), in which males care for offspring and females compete for mates (*2*, *4*). Reversed sexual dichromatism (females brighter than males) is usually associated with SRR and often with reversed size dimorphism (females larger than males (*5*), because sexual selection is stronger on females in SRR species (*1*, *4*). Phalaropes, sandpipers, and button quail are examples (*4*). Here we describe a case of extreme reversed sexual dichromatism in *Eclectus* parrots (*Eclectus roratus*), which is not associated with classic SRR but results from sex-based differences in visual predation and female competition for nest hollows.

The green male and bright red and blue female *E. roratus* are so different that they were originally regarded as separate species

[1]Centre for Resource and Environmental Studies, [2]School of Botany and Zoology, Australian National University, Canberra, ACT 0200 Australia. [3]Department of Ecology, Evolution and Marine Biology, University of California, Santa Barbara, CA 93106–9610, USA. [4]Department of Zoology and Tropical Ecology, James Cook University, Townsville QLD 4811, Australia.

*To whom correspondence should be addressed. E-mail: Robert.Heinsohn@anu.edu.au

(*6*), and their unusual dichromatism has puzzled biologists for decades (*7*, *8*). SRR does not explain the brilliant plumage of the females. Unlike most classic SRR birds (*1*, *9*), the reproductive rate of female *E. roratus* is limited because they have retained the role of incubating eggs and protecting young, and do not lay again until their chicks have fledged. The operational sex ratio may also be male-biased as a result of a strongly biased adult sex ratio (approximately 67% males) caused by higher mortality of juvenile females (*10*). Thus, *E. roratus* challenges the existing view of the evolution of reversed sexual dichromatism (*8*).

Our 8-year study in northern Australia has revealed a rare polygynandrous mating system in which males and females have diverged from the social monogamy and shared parental duties seen in most parrots (*6*, *11*) into entirely separate roles during breeding. *E. roratus* compete vigorously with both their own and other species for scarce nest hollows (approximately one hollow per square kilometer) (*12*, *13*). Intrasexual competition is intense in both sexes; females compete for nest hollows and males for access to breeding females. Females remain in their nest tree for up to 11 months each season (mean = 9.30 ± 0.11 SE, n = 212 female years), and apart from periods of display in the canopy, spend most of this time guarding their hollows from conspecifics that attempt to crush eggs or kill large chicks (*14*). Females may kill each other in disputes over hollows (*14*). Up to five males (mean = 1.97 ± 0.18 SE, n = 208 nest years) attend each nest, and they travel many kilometers to fruiting trees to provide all food for the females and their young over the breeding period (*10*).

The divergence in life-style between the sexes suggests that male *E. roratus* are more likely to be targeted by visually mediated predators than are females. Whereas males forage in the canopy for several hours every day throughout the year, breeding females only face this risk while they display before nesting and when they forage for themselves during the short nonbreeding period. Thus, one possible explanation for the divergence in color between the sexes is that it reflects the male's need for crypsis when foraging and the female's need to be conspicuous during displays of hollow ownership. Human vision is entirely different from that of birds, so it is important to score color objectively and from the observers' (conspecifics' and predators') perspective (*15*, *16*). To assess visibility to conspecifics and predators, we collected optical data on birds and their backgrounds. We applied established models of avian vision and calculated a disparity index that estimates the difference or visual contrast between two color patterns (*17*, *18*).

The analysis confirmed that males and females differ very strongly in their color patterns as sensed by birds. It unexpectedly revealed that females are more conspicuous than males against a visual background of leaves but not against trunks. Females occupied their nest trees up to 45 days before egg-laying (mean = 22.2 ± 1.92 SE, n = 174 female years). Before their confinement to the hollow during breeding, they preferred to display in branches high in the canopy, where other birds viewed them against a leafy rather than woody background (mean proportion of displays against leaves = 0.84 ± 0.032 SE, n = 10 females, 9 to 17 observations per individual). Birds flying toward the nest tree generally get their first view of the hollow owner from above. Females were more conspicuous from this angle against both visual backgrounds (Fig. 1, A and B). They were also significantly more conspicuous in open/cloudy light conditions (*19*) than in the woodland shade lower in the tree (Fig. 1, C and D). This choice of light and background colors by females to maximize conspicuousness during display is similar to that shown by males of some neotropical lekking species (*20*). However, females continued to call and show themselves from the entrance of the nest hollow throughout incubation. Although females are also conspicuous against tree trunks, our data suggest that their red and blue colors have been selected because these spectra are complementary to leaf green and therefore provide the greatest contrast against the background preferred for displays.

In contrast, males are more conspicuous against tree trunks than against leaves and are more conspicuous than females against tree trunks. Their color appears to serve the dual function of being conspicuous in intrasexual conflict near trunks but relatively inconspicuous when foraging. Most male competition for females occurred at the entrance to the nest hollow, where they displayed, fought, and physically dislodged each other (mean proportion of displays against tree trunk = 0.85 ± 0.033 SE, n = 11 males, 7 to 15 observations per individual). At most other times, especially while foraging, they either fly above or sit among foliage. Like females, they are more conspicuous from the angle at which arriving competitors first see them (from above, against tree trunks). Unlike females, they are less conspicuous from the angle at which aerial predators might observe them (from above, against leaves) (Fig. 1, A and B). The plumage of males against leaves is also less conspicuous to raptors than to other parrots (Fig. 1, E and F), suggesting that their colors are selected to exploit the difference between their color vision and that of their aerial predators (*21*). This appears to be adaptive because more of their lifetime is spent potentially being seen by predators than is spent by females, and more of this time will be against leaves than against trunks. Juvenile males and females both display adult colors, probably in readiness for breeding as early as their second year (*10*). The male-biased sex ratio among adults may reflect high mortality of juvenile females, who do not have the protection of their own nest hollows.

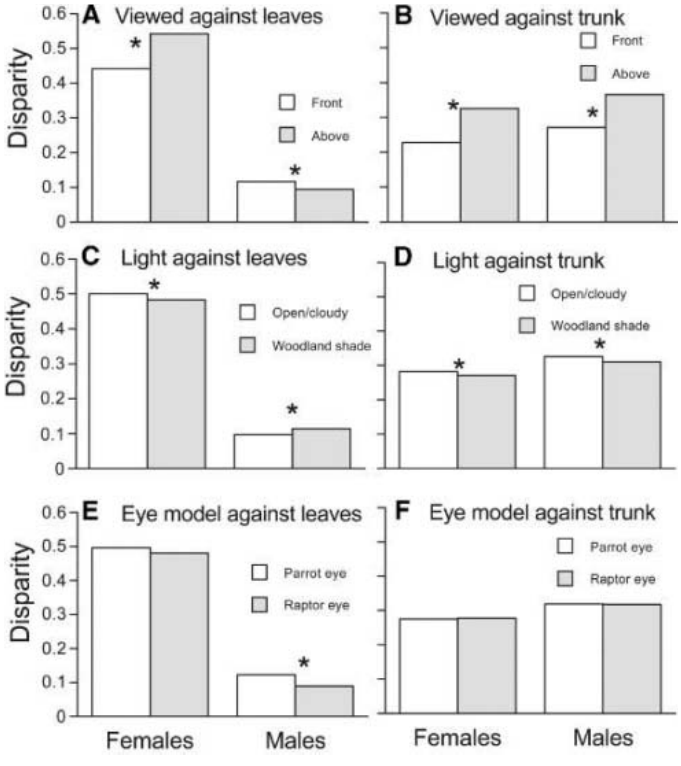

Fig. 1. (**A** and **B**) Effect of the observer's view (*17*) against leaves and trunks for females and males [linear mixed model, 3-way interaction, X^2_1 = 269.5, P < 0.001, standard error of difference (SED) = 0.004]. Disparity is a measure of the overall visual contrast between the two color patterns (*17*). (**C** and **D**) Effect of light environment (linear mixed model, 3-way interaction, X^2_1 = 27.8, P < 0.001, SED = 0.006). (**E** and **F**) Effect of parrot versus raptor eye model (linear mixed model, 3-way interaction, X^2_1 = 6.8, P = 0.009, SED = 0.006). An asterisk above adjacent bars indicates that they are significantly different. Males and females differ significantly in all cases.

Our analysis offers insights into the selective forces that shape coloration. Unlike open-nesting birds, in which the incubating females need to be inconspicuous to avoid predation, females of hollow-nesting species usually have similar colors to males. The sharing of parental duties and similar exposure to predation (during incubation and foraging) suggest that natural selection affects color similarly in both sexes in most species (*22*, *23*). In contrast, the colors of male and female *E. roratus* appear to be under independent selection. Whereas females are more conspicuous than males against leaves, they also have the nest hollow nearby as a refuge against predators. However, foraging males cannot retreat to a nest hollow whenever a predator approaches, and consequently their colors need to be less conspicuous against the leafy background. Ready access to a refuge from predators may also explain why females are not less conspicuous from above (Fig. 1A) or why they do not have colors that are significantly less conspicuous to their aerial predators (Fig. 1E).

The continuous occupation of the nest hollow by female *E. roratus* is atypical for parrots (*11*) but strikingly similar to that seen in hornbills (Bucerotiformes) (*24*). Females in most hornbill species are sealed into the nest hollow during the incubation and nestling phases and are fed by their mates and other group members. However, strong sexual dichromatism is rare in this group (*24*). Unlike *E. roratus*, most hornbill species (25 out of 33 known) are territorial, and the males and females of all 41 species on which sufficient data have been gathered have been observed to locate, prepare, and defend the nest site together. Further, female hornbills often leave the nest and help provision young before the young have fledged (*24*) and overall do not remain at the hollow for as long (66 to 142 days as compared with 279 days in *E. roratus*) (*24*). Similar sex roles both before and during breeding, and less total time spent at the nest by females, may reduce any independent selection on each sex in hornbills.

In *E. roratus*, a rare combination of intrasexual competition for a scarce resource in females, the separation of parental duties, and visually mediated predation appears to have shifted the balance of natural and sexual selection from the expected monomorphism in hollow nesters toward reversed dichromatism. These parrots provide an example of how conspicuous colors, like complex song (*25*), can result from strong intrasexual competition. The dichromatism of these parrots is also highly unusual among birds (*8*) because the sexes have acquired different color patterns for different purposes, and each is more conspicuous under specific conditions. Females compete for nest hollows and males compete for females at nest hollows, and thus both sexes are conspicuous against the tree trunks. However, males differ from females by spending a much larger proportion of their time foraging among the rainforest canopy. This favors reduced visibility to predators against leaves and, as a result, the balance between sexual selection and predation (*26*, *27*) differs in the two sexes and represents a reversal of the usual pattern. Although theory successfully predicts the direction of sexual selection (*9*, *26*–*29*), and mutual mate choice can account for similarly adorned sexes (*30*), *E. roratus* shows that bright coloration can evolve independently and simultaneously in both sexes. *Erectus* parrots emphasize the crucial interaction between natural selection and the lifestyle of males and females in modifying colors, even if they primarily result from sexual selection.

References and Notes

1. M. Andersson, *Sexual Selection* (Princeton Univ. Press, Princeton, NJ, 1994).
2. C. Kvarnemo, I. Ahnesjo, *Trends Ecol. Evol.* **11**, 404 (1996).
3. V. C. Almada, E. J. Goncalves, R. F. Oliveira, A. J. Santos, *Anim. Behav.* **49**, 1125 (1995).
4. M. Eens, R. Pinxten, *Behav. Processes* **51**, 135 (2000).
5. T. Székely, R. P. Freckleton, J. D. Reynolds, *Proc. Natl. Acad. Sci. U.S.A.* **101**, 12224 (2004).
6. J. M. Forshaw, W. D. Cooper, *Parrots of the World* (Lansdowne Press, Willoughby, Australia, 1989), pp. 616.
7. A. Grafen, *The Guardian*, 9 March 2000, p. 27.
8. T. Amundsen, H. Parn, in *Avian Coloration*, G. E. Hill, K. J. McGraw, Eds. (Harvard Univ. Press, Boston, in press).
9. S. T. Emlen, L. W. Oring, *Science* **197**, 215 (1977).
10. R. Heinsohn, S. Legge, *J. Zool.* **259**, 197 (2003).
11. T. Juniper, M. Parr, *Parrots: A Guide to Parrots of the World* (Pica Press, Sussex, UK, 1998).
12. S. Legge, R. G. Heinsohn, S. Garnett, *Wildl. Res.* **31**, 149 (2004).
13. R. Heinsohn, S. Murphy, S. Legge, *Aust. J. Zool.* **51**, 81 (2003).
14. We found eggs crushed but not eaten in 33 out of 421 clutches. In seven cases, the crushed eggs were found immediately after we saw an intruding female leave the nest hole. Ovicide was inferred in the remaining 26 cases. A 21-day-old nestling was found dead with wounds apparently inflicted by a parrot beak after an intruding male left the nest. We inferred infanticide in 15 further nests where nestlings aged from 1 to 15 days were found dead with similar wounds. One adult female was found dead in her hollow with extensive wounds on her head after an extended fight with an intruding female. Thirteen other uneaten corpses of adult females were found in the vicinity of nest trees in 210 female-years. Ten of these had wounds consistent with fighting.
15. J. A. Endler, *Biol. J. Linn. Soc.* **41**, 315 (1990).
16. A. T. D. Bennett, I. C. Cuthill, *Vision Res.* **34**, 1471 (1994).
17. Materials and methods are available as supporting material on *Science* Online.
18. J. A. Endler, P. W. Mielke, *Biol. J. Linn. Soc.*, in press.
19. J. A. Endler, *Ecol. Monogr.* **63**, 1 (1993).
20. J. A. Endler, M. Thery, *Am. Nat.* **148**, 421 (1996).
21. J. A. Endler, *Vision Res.* **31**, 587 (1991).
22. A. R. Wallace, *Darwinism* (Macmillan, London, ed. 2, 1889).
23. R. R. Baker, G. A. Parker, *Philos. Trans. R. Soc. London Ser. B* **287**, 63 (1979).
24. A. Kemp, *The Hornbills* (Oxford Univ. Press, Oxford, 1995).
25. N. E. Langmore, *Trends Ecol. Evol.* **13**, 136 (1998).
26. J. A. Endler, *Evol. Biol.* **11**, 319 (1978).
27. J. A. Endler, *Evol. Int. J. Org. Evol.* **34**, 76 (1980).
28. T. H. Clutton-Brock, A. C. J. Vincent, *Nature* **351**, 58 (1991).
29. H. Kokko, P. Monaghan, *Ecol. Lett.* **4**, 159 (2001).
30. I. L. Jones, F. M. Hunter, *Nature* **362**, 238 (1993).

31. We thank C. Blackman, A. Cockburn, N. Doerr, M. Hall, P. and E. Huybers, M. Jennions, N. Langmore, S. Murphy, A. Nathan, S. Rothstein, D. Storch, and D. Wilson, and the Australian Research Council and National Geographic Society.

Supporting Online Material

www.sciencemag.org/cgi/content/full/309/5734/617/DC1
Materials and Methods
Fig. S1
Table S1
References

25 March 2005; accepted 17 May 2005
10.1126/science.1112774

Independent Codes for Spatial and Episodic Memory in Hippocampal Neuronal Ensembles

Stefan Leutgeb,[1] Jill K. Leutgeb,[1] Carol A. Barnes,[1,2] Edward I. Moser,[1] Bruce L. McNaughton,[1,2]* May-Britt Moser[1]

Hippocampal neurons were recorded under conditions in which the recording chamber was varied but its location remained unchanged versus conditions in which an identical chamber was encountered in different places. Two forms of neuronal pattern separation occurred. In the variable cue-constant place condition, the firing rates of active cells varied, often over more than an order of magnitude, whereas the location of firing remained constant. In the variable place-constant cue condition, both location and rates changed, so that population vectors for a given location in the chamber were statistically independent. These independent encoding schemes may enable simultaneous representation of spatial and episodic memory information.

Hippocampal neuronal ensemble activity appears to play an important role in the establishment of both spatial and nonspatial episodic memories, but there has long been controversy as to which of these parameters best characterizes the role of the hippocampal formation in mnemonic processes (*1*, *2*). Although hippocampal neurons fire in a sparse

(*3*), spatially selective (*4*, *5*) manner, this activity can be weakly or strongly affected by other variables such as directional orientation (*6*, *7*), specific sensory inputs (*8*–*11*), behavioral context (*12*–*17*), and working memory (*11*, *14*–*17*). "Place fields" of a given neuron may change in magnitude, shift in position, or appear or disappear under different circumstances. All of these effects have been subsumed under the general terms "remapping" (*18*–*20*) or "orthogonalization" (*3*, *21*, *22*), but it has not been determined whether these effects can occur independently across simultaneously recorded neurons. Here, we show that the hippocampal population vector can undergo two essentially independent forms of remapping: rate remapping, in which the locations of place fields remain unchanged but the firing rates of the cells change, and global remapping, in which the distributions of location and rate both take on statistically independent values. In vector terms, rate remapping implies that the population vectors span the same subspace and hence preserve information about location, whereas in global remapping the population vectors span statistically independent subspaces. In principle, rate remapping permits the generation of representations of unique episodes of experience while maintaining the integrity of the code for spatial location, whereas global remapping permits the distinction between similar experiences that occur in different spatial contexts.

Ensemble activity was recorded from 330 cells in CA3 and 487 cells in CA1 of the dorsal hippocampus in 10 freely moving rats by using arrays of 12 tetrodes, about half of which were located in CA3 and half in CA1 (*23*). Two experimental conditions were studied. In the variable cue-constant place condition (Fig. 1), the recordings were conducted in a single room, but the actual recording chamber was varied, either by changing the shape (circular versus square) or by changing the wall color (black versus white). In the variable place-constant cue condition (Fig. 2), geometrically identical (square) chambers of the same color (black) were used in two distinct rooms. All rats were familiarized with the experimental protocols and conditions before recording (*24*).

For each cell whose mean firing rate in at least one environmental condition was above an estimate of background noise (*25*), we compared the location and rate of firing in the different experimental configurations. Spatial similarity was expressed by computing the correlations between pairs of rate maps and comparing their centers of mass. These measures are independent of the relative magnitude of firing. Rate similarity was expressed by dividing the relative change in mean rate by the sum of the mean rates.

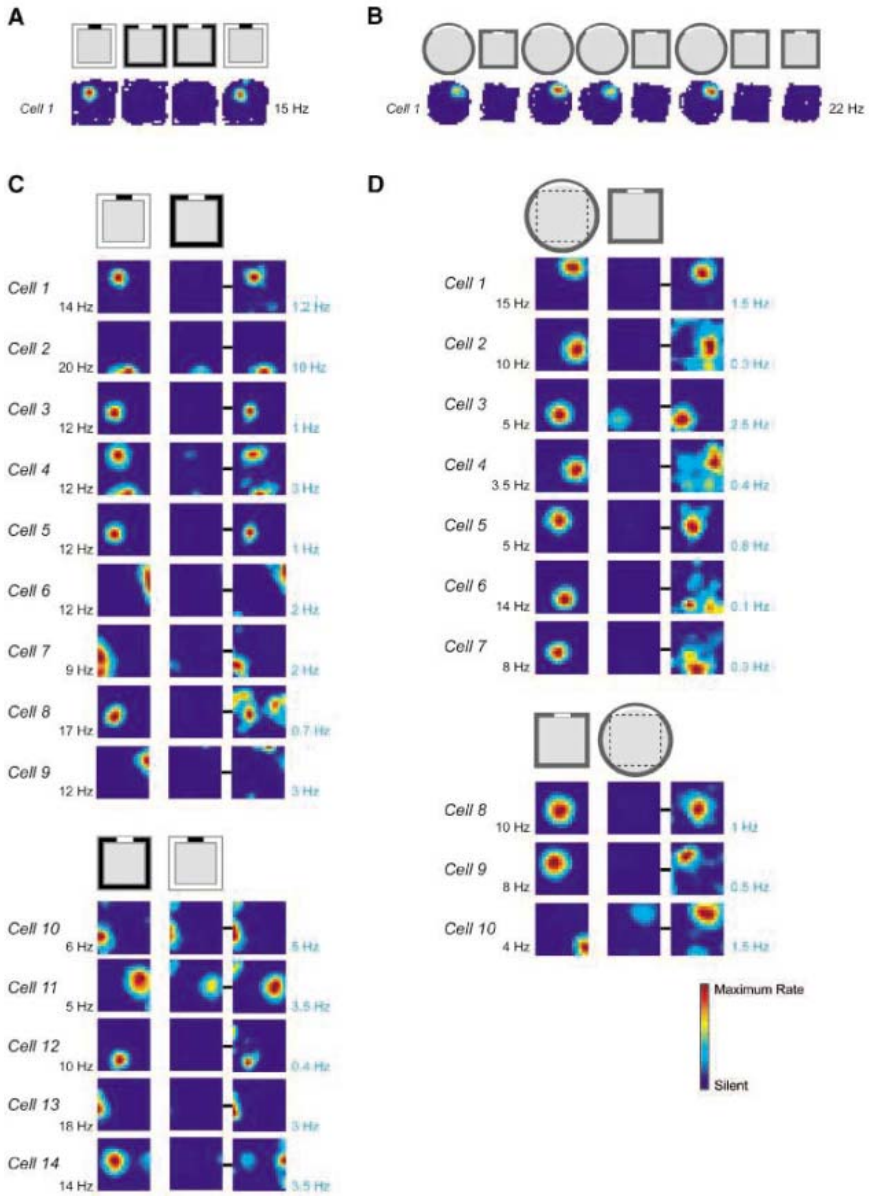

Fig. 1. Constant place-variable cue condition. Color-coded rate maps for cells recorded when the cue configuration was changed by switching either between two colors (**A** and **C**) or between two shapes (**B** and **D**) at a constant location. (A and B) Recording sequence with the rate maps of the first cell in (C) and (D) as an example. Rate is coded on a color scale from blue (silent) to red (maximum rate). Pixels not sampled are white. The symbols above the maps indicate color and shape of the box and the cue card (cue card in contrasting color). (C and D) Rate maps for two complete sets of simultaneously recorded CA3 neurons [(C) rat 10708, day 3; (D) rat 10683, day 16]. Repeated trials with the same cues are now averaged. In (D), only the area common to both shapes is shown (indicated by the dotted square in the circle). Only the area common to both shapes is depicted. Each row shows data from one active neuron. Silent cells [six in (C) and six in (D)] are not shown. The left columns show data for the condition that gave maximal firing. For each cell, the rate scale corresponds to the peak firing rate in that condition (indicated to the left of the rate map). In the middle columns, the data from the opposite condition are plotted at the same firing-rate scale. The right columns contain the same data as the middle but are scaled to their own maximum values (indicated to the right of the rate maps). Symbols above columns indicate which color or shape gave the higher and lower rate (left and middle, respectively) for the cells underneath. Note that different experiences in the same place resulted in place fields similar in location and shape, but with strikingly different firing intensities, sufficient, in many cases, to make it appear that the field was absent when plotted at the same scale. See fig. S2 for rate maps of individual trials and fig. S4, A and B, for rate maps of simultaneously recorded CA1 cells.

[1]Centre for the Biology of Memory, Medical-Technical Research Centre, Norwegian University of Science and Technology, 7489 Trondheim, Norway. [2]Arizona Research Laboratories Division of Neural Systems, Memory, and Aging, University of Arizona, Tucson, AZ 85724, USA.

*To whom correspondence should be addressed.

Lastly, representational similarity in the population as a whole was estimated by stacking all rate maps (including those of the silent cells) into a three-dimensional matrix with the two spatial dimensions on the x and y axes and cell identity on the z axis (fig. S1C). The distribution of mean rates along the z axis for a given x-y location represents the population vector for that location. Comparing the entire set of population vectors between two trials provides an estimate of how much the ensemble code changed.

For both CA3 and CA1, the distributions of spatial correlations in the two variable cue-constant place conditions (i.e., black square versus white square and circle versus square) were so similar to the control conditions (first versus second exposure in the same box) that, without closer analysis, one might have concluded that there had been no substantive effect of cue-condition or environmental shape on the hippocampal code (Figs. 1 and 3A and Table 1). In CA3, the median spatial correlations in the black-white and square-circle conditions were 0.82 and 0.83, respectively. In CA1, spatial correlations were similar to those obtained in CA3 (black-white: 0.78, $Z = 1.54$, not significant) or slightly lower (square-circle: 0.65, $Z = 3.92$, $P < 0.001$). In both areas, there were only minor shifts in center of mass of the place fields (Table 1).

In contrast, although the location of firing remained almost constant, the distributions of mean firing rates changed, especially in CA3. In this subfield, a substantial proportion of cells showed pronounced rate differences between conditions, with little or no change in the shape or location of the place field (Figs. 1 and 3A and Table 1). The median rate change between the black and white chambers was 3.9-fold; between square and circle, it was 6.9-fold. The median rate change was significantly higher than that for repeated tests with the same cues (difference/sum ratios; black-white, $Z = 8.58$ and $P < 0.001$; square-circle, $Z = 7.54$ and $P < 0.001$). The change in individual firing rates was also reflected as a pronounced shift toward lower values in the population vector correlations (Fig. 3A and Table 1) (black-white: $Z = 22.48$, $P < 0.001$; square-circle: $Z = 19.40$, $P < 0.001$). In CA1, the changes in relative firing rate were less pronounced (CA3 versus CA1: Z was 6.39 and 5.49 for black-white and square-circle, $P < 0.001$) and the population vectors were less different (Z was 11.14 and 13.72, respectively, $P < 0.001$) (Fig. 3B and Table 1).

Table 1. Spatial firing rate statistics.

Condition	CA3	CA1
Median place field correlation		
Constant cue and place	0.94	0.88
Color	0.93	0.87
Shape	0.97	0.93
Room	0.92	0.84
Black-white	0.82	0.78
Circle-square	0.83	0.65
Room1-room2	–0.10	0.00
Median center of mass change (cm)		
Constant cue and place	3.3	5.6
Color	4.3	5.9
Shape	2.3	4.1
Room	3.6	6.9
Black-white	9.8	8.6
Circle-square	7.4	10.2
Room1-room2	34.5	26.8
Median relative firing rate change (unsigned rate difference divided by rate sum)		
Constant cue and place	0.12 (1.3-fold)	0.14 (1.3-fold)
Color	0.10 (1.2-fold)	0.13 (1.3-fold)
Shape	0.12 (1.3-fold)	0.13 (1.3-fold)
Room	0.14 (1.3-fold)	0.16 (1.4-fold)
Black-white	0.59 (3.9-fold)	0.19 (1.5-fold)
Circle-square	0.74 (6.9-fold)	0.30 (1.9-fold)
Room1-room2	0.97 (61.6-fold)	0.42 (2.4-fold)
Median population vector correlation		
Constant cue and place	0.91	0.83
Color	0.91	0.85
Shape	0.94	0.85
Room	0.91	0.75
Black-white	0.58	0.73
Circle-square	0.24	0.57
Room1-room2	–0.03	0.25

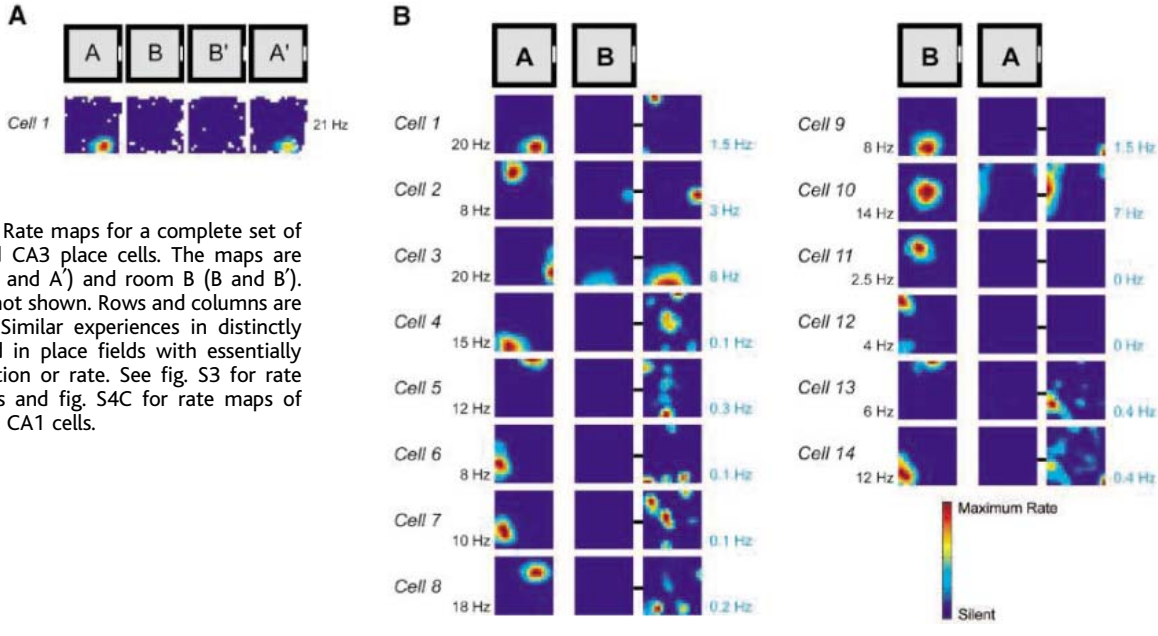

Fig. 2. Variable place-constant cue condition. Color-coded rate maps for tests in identical boxes in two different rooms (rat 10968, day 9). (**A**) Recording sequence and rate maps with the first cell in (B) as an example. (**B**) Rate maps for a complete set of simultaneously recorded CA3 place cells. The maps are averages for room A (A and A′) and room B (B and B′). Silent cells ($n = 16$) are not shown. Rows and columns are organized as in Fig. 1. Similar experiences in distinctly different places resulted in place fields with essentially zero correlation in location or rate. See fig. S3 for rate maps of individual trials and fig. S4C for rate maps of simultaneously recorded CA1 cells.

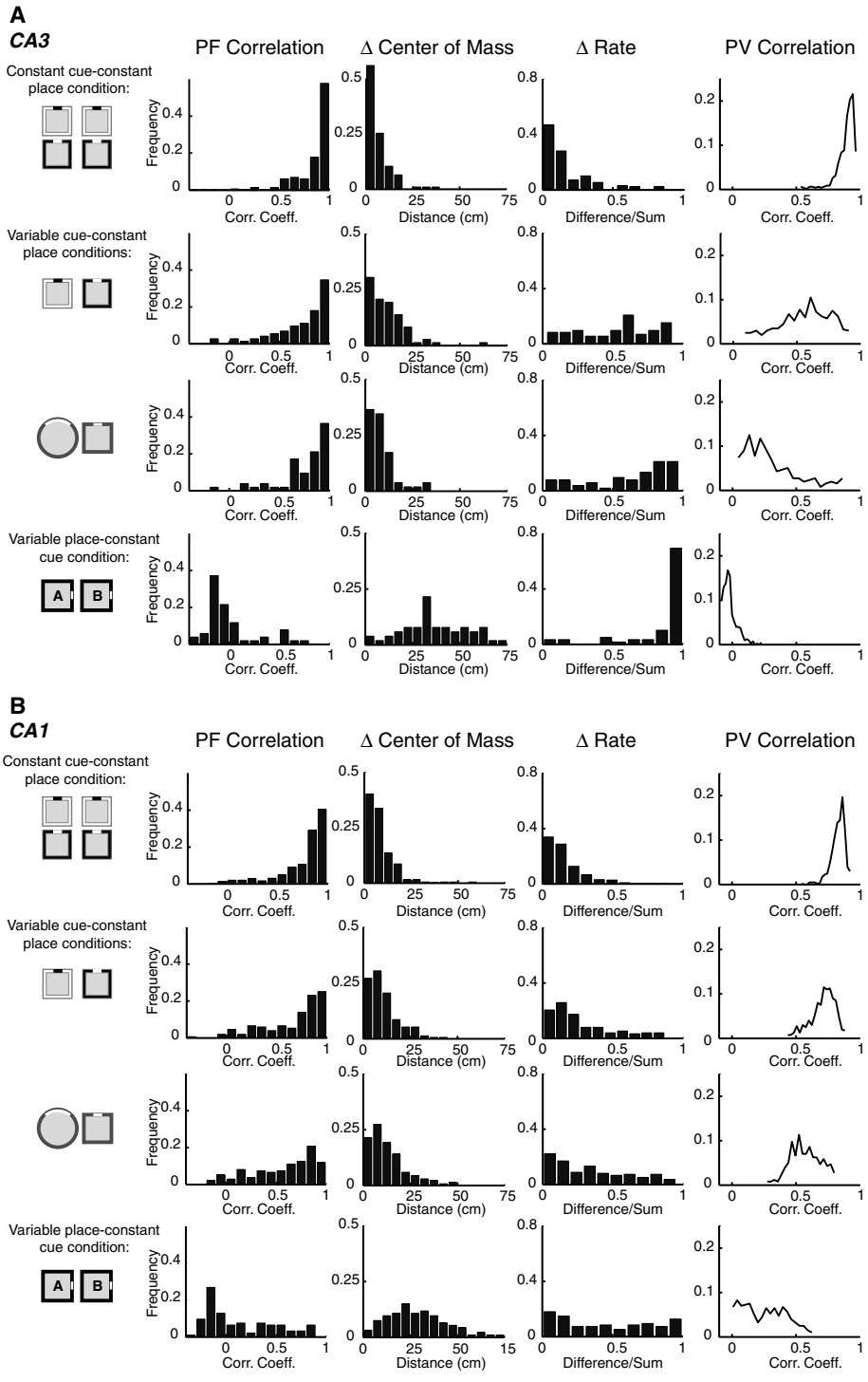

Fig. 3. Spatial firing rate statistics for ensembles of hippocampal CA3 (**A**) and CA1 (**B**) neurons comparing the following conditions: two visits to the same box in a constant location, visits to black and white boxes in a constant location, visits to circular and square boxes in a constant location, and visits to identical boxes located in two distinctly different places. For each pair of conditions, columns from left to right show frequency distributions for correlations in the spatial firing patterns (PF correlation), shifts of the place-field centers (Δ center of mass), changes in the mean firing rates (Δ rate), and correlations between spatial population vectors (PV correlation). Rate change is expressed as the unsigned difference between the rates in the two conditions, divided by their sum. On this asymptotic scale, 0.5 corresponds to a threefold difference, whereas 0.8 represents a ninefold difference. Whereas a variable place exerted a marked influence on both rate and firing location, changes in sensory cues in a fixed place resulted only in substantial changes in the firing rates, especially in CA3, with little change in the relative spatial firing distribution, implying that cues and locations are coded independently. See fig. S5 for additional comparisons in the constant cue-constant place configuration.

In the variable place-constant cue condition, the distributions of spatial and population vector correlations were both shifted to values near zero, and the overall firing rate differences were large (Figs. 2 and 3 and Table 1). In CA3, firing locations in the two boxes were totally uncorrelated. Place field correlations were also skewed toward zero in CA1, albeit with a significant tail toward higher values (Fig. 3A) (Kolmogorov-Smirnov test, $P < 0.05$) (Fig. 3B). The change in firing locations was accompanied by pronounced rate changes in the same cells. In CA3, the majority of neurons showed more than 10-fold rate changes, and the population vector correlations for different locations were clustered around zero. In CA1, the extent of rate change varied widely within the population, and population vector correlations ranged between 0 and 0.5. In each animal, the population vectors were more dissimilar in CA3 than CA1.

To summarize, when the same prominent environmental features were encountered in two distinct places, the CA3 population vectors for locations (relative to the reference frame of the constant feature) were uncorrelated. This is consistent with previous studies reporting orthogonalization of hippocampal population activity, especially in CA3, after dislocation of the local reference frame (*22*, *26–28*). When the rats experienced changes in prominent features in the same spatial context, however, the hippocampus encoded these changes primarily by changing the values of the components of the spatial population vectors, without much, if any, change in the distribution of the firing locations (*29*). The latter finding raises the possibility that much of the previous evidence for single-location remapping is rate-based. Rate remapping may be the cause of direction-specific (*6*, *30*) and trajectory-specific (*14–16*) firing as well as task-induced changes in population activity (*12*, *13*, *31*). However, certain training regimes may provoke global remapping even in a single spatial environment (*18–20*, *32*). Whether the environments are then encoded as distinct spatial reference frames remains to be determined.

The existence of independent population codes for location and cue configurations implies that hippocampal cell ensembles may simultaneously convey information related to where an animal is located and what is currently present in that location. Presynaptic dynamics (*33*) as well as nonlinear postsynaptic responses may render some neurons sensitive to which inputs are active but not to presynaptic firing rate per se. Cells with such properties might be able to transmit information about the location of the animal irrespective of current sensory input. In contrast, cells that are sensitive to the rate function of afferent neurons might discriminate different events occurring at a given location. The pres-

ervation of both types of information in the hippocampal output may form the basis of its key role in episodic memory (*2*, *34*).

References and Notes

1. J. O'Keefe, L. Nadel, *The Hippocampus as a Cognitive Map* (Clarendon, Oxford, 1978).
2. H. Eichenbaum, P. Dudchenko, E. Wood, M. Shapiro, H. Tanila, *Neuron* **23**, 209 (1999).
3. B. L. McNaughton, R. G. M. Morris, *Trends Neurosci.* **10**, 408 (1987).
4. J. O'Keefe, J. Dostrovsky, *Brain Res.* **34**, 171 (1971).
5. R. U. Muller, J. L. Kubie, J. B. Ranck, *J. Neurosci.* **7**, 1935 (1987).
6. B. L. McNaughton, C. A. Barnes, J. O'Keefe, *Exp. Brain Res.* **52**, 41 (1983).
7. J. J. Knierim, H. S. Kudrimoti, B. L. McNaughton, *J. Neurosci.* **15**, 1648 (1995).
8. J. O'Keefe, D. H. Conway, *Exp. Brain Res.* **31**, 573 (1978).
9. K. M. Gothard, W. E. Skaggs, B. L. McNaughton, *J. Neurosci.* **16**, 8027 (1996).
10. M. L. Shapiro, H. Tanila, H. Eichenbaum, *Hippocampus* **7**, 624 (1997).
11. E. R. Wood, P. A. Dudchenko, H. Eichenbaum, *Nature* **397**, 613 (1999).
12. E. J. Markus *et al.*, *J. Neurosci.* **15**, 7079 (1995).
13. M. A. Moita, S. Rosis, Y. Zhou, J. E. LeDoux, H. T. Blair, *J. Neurosci.* **24**, 7015 (2004).
14. E. R. Wood, P. A. Dudchenko, R. J. Robitsek, H. Eichenbaum, *Neuron* **27**, 623 (2000).
15. J. Ferbinteanu, M. L. Shapiro, *Neuron* **40**, 1227 (2003).
16. M. R. Bower, D. R. Euston, B. L. McNaughton, *J. Neurosci.* **25**, 1313 (2005).
17. S. A. Hollup, S. Molden, J. G. Donnett, M.-B. Moser, E. I. Moser, *J. Neurosci.* **21**, 1635 (2001).
18. E. Bostock, R. U. Muller, J. L. Kubie, *Hippocampus* **1**, 193 (1991).
19. C. Kentros *et al.*, *Science* **280**, 2121 (1998).
20. A. Cressant, R. U. Muller, B. Poucet, *Exp. Brain Res.* **143**, 470 (2002).
21. D. Marr, *J. Physiol.* **202**, 437 (1969).
22. S. Leutgeb, J. K. Leutgeb, A. Treves, M.-B. Moser, E. I. Moser, *Science* **305**, 1295 (2004); published online 22 July 2004 (10.1126/science.1100265).
23. Materials and methods are available as supporting material on *Science* Online.
24. The mean number of pretraining days in the test environment was 17 (square-circle), 14 (two rooms), and 4 (black-white).
25. The rate threshold was 0.27 Hz. Similar results were obtained with rate thresholds of 0.10 Hz and 0.50 Hz (tables S1 and S2) (*23*).
26. K. M. Gothard, W. E. Skaggs, K. M. Moore, B. L. McNaughton, *J. Neurosci.* **16**, 823 (1996).
27. W. E. Skaggs, B. L. McNaughton, *J. Neurosci.* **18**, 8455 (1998).
28. H. Tanila, *Hippocampus* **9**, 235 (1999).
29. If the external spatial input is strong enough, it is theoretically possible for large changes to occur in the firing rates of some cells, whereas intrinsic attractor dynamics of the network maintain the relative relations between the place fields of the ensemble (*35*).
30. S. A. Hollup, S. Molden, J. G. Donnett, M.-B. Moser, E. I. Moser, *Eur. J. Neurosci.* **13**, 1197 (2001).
31. In these studies, which all focused on CA1, much of the residual activity in the less active condition appeared inside the cell's place field in the more active condition [e.g., figure 8 in (*30*), figures 3 to 5 in (*14*), figures 2 to 6 in (*15*), figure 6 in (*16*), figures 6B and 9 in (*12*), and figure 4 in (*13*)], as expected if the remapping was primarily rate-based. In (*30*), 70% of the cells exhibited peak activity in the same quadrant in the two directions.
32. T. J. Wills, C. Lever, F. Cacucci, N. Burgess, J. O'Keefe, *Science* **308**, 873 (2005).
33. H. Markram, M. Tsodyks, *Nature* **382**, 807 (1996).
34. E. Tulving, *Annu. Rev. Psychol.* **53**, 1 (2002).
35. A. Samsonovich, B. L. McNaughton, *J. Neurosci.* **17**, 5900 (1997).

36. We thank R. G. M. Morris and M. P. Witter for discussion and A. M. Amundsgård, I. M. F. Hammer, K. Haugen, K. Jenssen, R. Skjerpeng, E. Sjulstad, B. H. Solem, and H. Waade for technical assistance. The work was supported by a Centre of Excellence grant from the Norwegian Research Council.

Supporting Online Material

www.sciencemag.org/cgi/content/full/309/5734/619/DC1
Materials and Methods
Figs. S1 to S5
Tables S1 and S2

25 April 2005; accepted 10 June 2005
10.1126/science.1114037

Complete Replication of Hepatitis C Virus in Cell Culture

Brett D. Lindenbach,[1] Matthew J. Evans,[1] Andrew J. Syder,[1] Benno Wölk,[1] Timothy L. Tellinghuisen,[1] Christopher C. Liu,[2] Toshiaki Maruyama,[3]* Richard O. Hynes,[2] Dennis R. Burton,[3] Jane A. McKeating,[1]† Charles M. Rice[1]‡

Many aspects of the hepatitis C virus (HCV) life cycle have not been reproduced in cell culture, which has slowed research progress on this important human pathogen. Here, we describe a full-length HCV genome that replicates and produces virus particles that are infectious in cell culture (HCVcc). Replication of HCVcc was robust, producing nearly 10^5 infectious units per milliliter within 48 hours. Virus particles were filterable and neutralized with a monoclonal antibody against the viral glycoprotein E2. Viral entry was dependent on cellular expression of a putative HCV receptor, CD81. HCVcc replication was inhibited by interferon-α and by several HCV-specific antiviral compounds, suggesting that this in vitro system will aid in the search for improved antivirals.

HCV is a major cause of chronic liver disease, with over 170 million persistently infected individuals worldwide (*1*). HCV-associated liver disease frequently progresses to cirrhosis, which can lead to liver failure and hepatocellular carcinoma. Current drug therapies are often poorly tolerated and effective in only a fraction of patients; there is no vaccine for HCV. A major obstacle to understanding the virus life cycle and to developing improved therapeutics is the inability to efficiently grow HCV in cell culture.

HCV is an enveloped, positive-sense RNA virus of the family *Flaviviridae*. Naturally occurring variants of HCV are classified into six major genotypes. The 9.6-kb genome encodes one large polyprotein that is processed by viral and cellular proteinases to produce the virion structural proteins (core and glycoproteins E1 and E2) as well as nonstructural (NS) proteins (p7 through NS5B) (Fig. 1A). Subgenomic RNA replicons have been adapted for efficient RNA replication in the human hepatoma line Huh-7 and other cultured cells (*2*–*5*). However, full-length genomes containing cell culture–adaptive mutations do not produce infectious virus particles in culture and are severely attenuated in vivo (*6*–*8*). This led us to hypothesize that mutations that enhance RNA replication may have deleterious effects on virion production. To test this idea, we used a genotype 2a subgenomic replicon, SGR-JFH1, that efficiently replicates in cell culture without adaptive mutations (*4*). Full-length chimeric genomes were constructed with the use of the core-NS2 gene regions from the infectious J6 (genotype 2a) and H77 (genotype 1a) virus strains (Fig. 1A). Both full-length chimeras and the subgenomic RNA were competent for RNA replication, as seen by the accumulation of NS5A protein and viral RNA 48 hours after RNA transfection into the Huh-7.5 cell line (Fig. 1B). As expected, mutation of the NS5B RNA polymerase active site [GlyAspAsp to GlyAsnAsp (GND)] destroyed the ability of FL-J6/JFH to replicate (Fig. 1B). Within transfected cells, both full-length genomes expressed core, E2, and NS5A (Fig. 1C). As expected, SGR-JFH1 expressed NS5A but not core or E2. While ≈30% of cells were productively transfected with FL-J6/JFH, FL-H77/JFH, or SGR-JFH1 RNA (Fig. 1B), >95% of FL-J6/JFH–transfected cells were positive for NS5A by 96 hours (fig. S1). This suggested that FL-J6/JFH spread within the transfected cell cultures.

To test whether infectivity could be transferred to naïve cells, we clarified conditioned

[1]Center for the Study of Hepatitis C, The Rockefeller University, 1230 York Avenue, New York, NY 10021, USA. [2]Howard Hughes Medical Institute, Center for Cancer Research, Massachusetts Institute of Technology, Cambridge, MA 02139, USA. [3]Departments of Immunology and Molecular Biology, The Scripps Research Institute, La Jolla, CA 92037, USA.

*Present address: Alexion Antibody Technologies, San Diego, CA 92121, USA.
†Present address: Division of Immunity and Infection, Institute of Biomedical Research, University of Birmingham Medical School, Birmingham B15 2TT, UK.
‡To whom correspondence should be addressed. E-mail: ricec@rockefeller.edu

media from these cultures by centrifugation (*9*), filtered the supernatants (0.2 μm), and incubated them with naïve Huh-7.5 cells. NS5A expression could be transferred by the FL-J6/JFH–transfected culture media but not by media from cells transfected with FL-H77/JFH or SGR-JFH1 (Fig. 1B). Interestingly, the amount of FL-J6/JFH RNA released into the transfected cell culture media exceeded that of the other RNAs by a factor of >200, and only FL-J6/JFH produced an extracellular form of core (Fig. 1C, lower panel). Given that the infectivity of the genotype 2a chimera is filterable and is associated with the release of HCV RNA and core protein, we refer to this cell culture–produced virus as HCVcc. The ability of the genotype 1a/2a chimera to replicate but not spread suggests that interactions between the structural and nonstructural gene products may be important for HCVcc formation, as has been observed for other members of this virus family (*10*, *11*).

Limiting dilution assays for NS5A expression in electroporated cells showed that 30.3 ± 9.5% (n = 6) of cells were productively transfected with FL-J6/JFH, and of these, 55% produced infectivity that was detectable upon transfer to naïve cells. Thus, FL-J6/JFH RNA transcripts were highly infectious and formation of HCVcc did not depend on the emergence of rare variants. Limiting dilution assays were also used to quantitate the amount of HCVcc infectivity between samples as median tissue culture infectious units per milliliter ($TCID_{50}$/ml). The $TCID_{50}$ is the dilution that infects 50% of replicate cell cultures (*9*). After an eclipse phase (≥9 hours), FL-J6/JFH infectivity could be detected in the media by 18 hours posttransfection, and it continued to accumulate until 48 hours (Fig. 1D). Interestingly, FL-J6/JFH (H2476L), which contained a weakly adaptive mutation in NS5B (*4*), showed slightly delayed growth kinetics but also peaked to similar levels by 48 hours. Viruses could be serially passaged, infecting 50 to 90% of cells within 5 days after two rounds of passage at a low multiplicity of infection (MOI) of 0.1 to 1.0 (Fig. 1E). The expression and subcellular localization of core, E2, and NS5A within FL-J6/JFH–infected cells was consistent with what was previously seen in full-length and subgenomic replicon-bearing cells [supporting online material (SOM) text]. Taken together, these measurements show that HCVcc replication is robust and occurs with kinetics similar to those of other *Flaviviridae*.

A classic method in virus identification is to neutralize the suspected virus with specific antisera. As shown in Fig. 2A, an E2-specific human monoclonal antibody neutralized HCVcc infectivity in a dose-dependent manner, whereas an isotype-matched control antibody had no effect on HCVcc titer. These data affirm the viral nature of HCVcc infectivity and show that E2 is essential for virus entry.

HCV E2 has been shown to bind to the cellular surface protein CD81 (*12*), which is an essential coreceptor for the entry of HCV glycoprotein-pseudotyped retroviruses (*13*–*15*). We found that HCVcc infectivity could be blocked with a soluble recombinant form of the CD81 large extracellular loop (Fig. 2B).

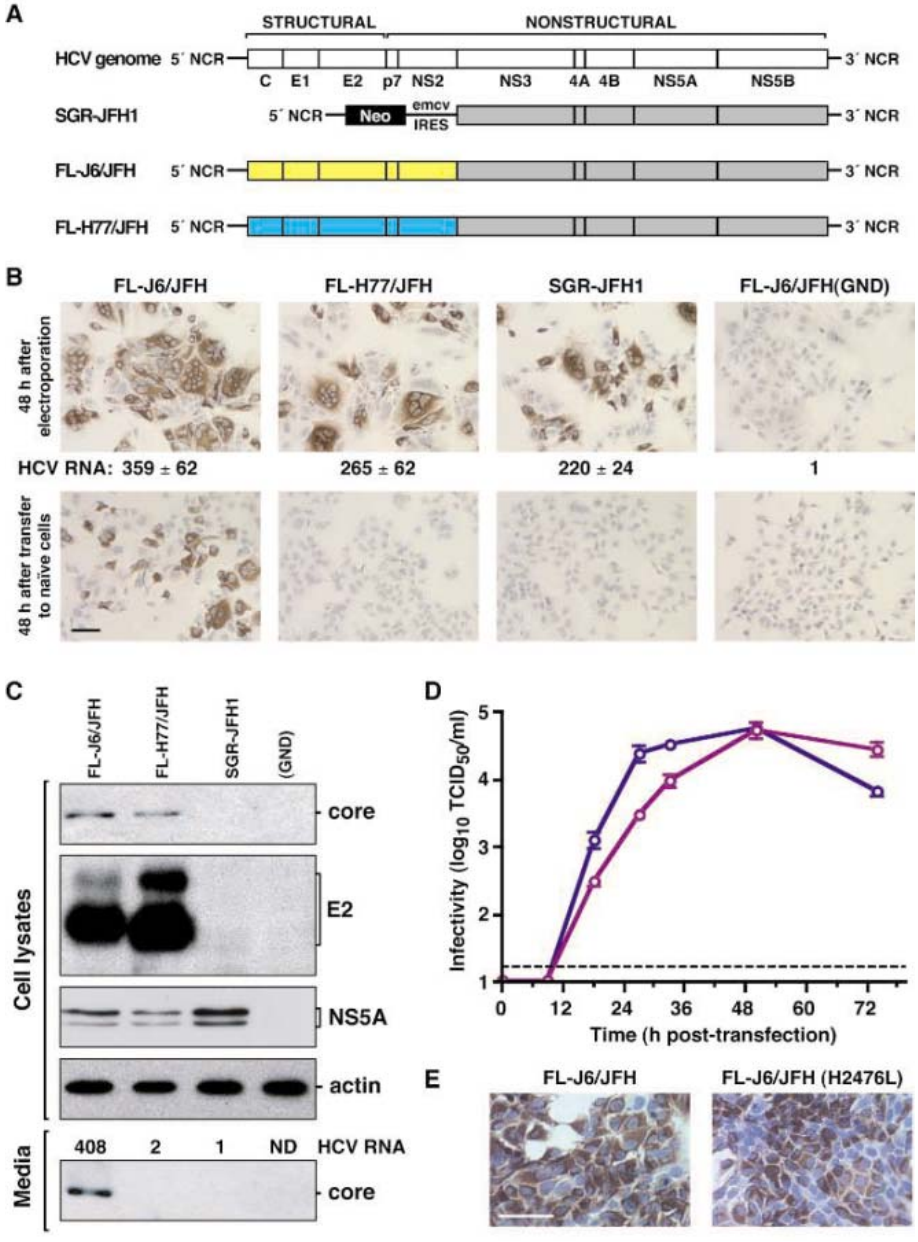

Fig. 1. Production of infectious HCV in cell culture. (**A**) The structures of the HCV RNA genome, the SGR-JFH1 replicon, and full-length chimeric genomes FL-J6/JFH and FL-H77/JFH. NCR, noncoding region; C, core; yellow, J6; cyan, H77. (**B**) Huh-7.5 cells were electroporated with RNA transcripts of the indicated genomes [or the RNA-polymerase defective mutant FL-J6/JFH(GND)] 48 hours before immunostaining for NS5A (brown, upper panel). Nuclei were counterstained with hematoxylin (blue). Below is the relative amount of HCV RNA detected in each transfected cell population at 48 hours by quantitative reverse transcription polymerase chain reaction (RT-PCR). Naïve Huh-7.5 cells were incubated for 48 hours with filtered, conditioned media from the transfected cells and immunostained for NS5A expression (lower panel). (**C**) Western blot for HCV core, E2, NS5A, or actin protein expression at 48 hours in RNA transfected Huh-7.5 cells. Below each lane is the relative amount of HCV RNA and core detected in cell culture media by quantitative RT-PCR and Western blot, respectively. ND, not determined. (**D**) The accumulation of HCVcc infectivity after electroporation of FL-J6/JFH (blue) or FL-J6/JFH (H2476L) (purple) into 6 × 10^5 cells/timepoint, assessed by a limiting dilution assay (mean ± SEM; n = 4). Dotted line, assay sensitivity. (**E**) Cells were immunostained for NS5A 5 days after infection with serially passaged virus. Scale bars, 100 μm.

To further examine the role of CD81 in virus entry we used HepG2 cells, which lack CD81 expression but are capable of supporting HCV RNA replication (*3*). As seen in Fig. 2C, normal HepG2 cells were not infected by FL-J6/JFH, whereas CD81-expressing HepG2 cells were infected under the same conditions, albeit with reduced efficiency (≈850 times less than Huh-7.5 cells). These data confirm that interactions between E2 and CD81 are important for HCV entry.

The physical nature of HCV particles has been difficult to study in the absence of an infectious culture system. In density gradients, clinical isolates of HCV exhibit a broad distribution and unusually low buoyant densities [reviewed in (*16*)]. These properties have been partly explained by the interaction of HCV with serum components such as immunoglobulins and β-lipoproteins. We examined the profiles of RNA and infectivity associated with HCVcc particles by equilibrium centrifugation in 10 to 40% iodixanol, an iso-osmotic gradient material. A series of controls confirmed that this method accurately measured the buoyant density of HCVcc (SOM text). HCV RNA was broadly distributed through the top of the gradient, with a peak in fractions 16 and 17 (1.13 to 1.14 g/ml), and was not found beyond fraction 20 (1.18 g/ml) (Fig. 3A). HCVcc infectivity was also broadly distributed among fractions 1 to 15 (1.01 to 1.12 g/ml), and infectivity was not seen beyond fraction 18 (1.17 g/ml). Surprisingly, fractions 16 and 17, which contained the highest levels of HCV RNA, had little infectivity associated with them. The specific infectivity of a virus preparation relates the amount of infectivity to the total number of virus particles or genomes in the preparation. Interestingly, a plot of HCVcc-specific infectivity versus buoyant density indicates that the most infectious material is at 1.09 to 1.10 g/ml (Fig. 3B), which is similar to the peak of infectivity (1.09 to 1.11 g/ml) previously seen in chimpanzees (*17*). In contrast, RNA-containing material with a buoyant density of 1.14 g/ml (fraction 17) had a low specific infectivity, with ≈300,000 RNA molecules per infectious unit. Many groups have reported an HCV RNA peak near this density (*18*–*20*), although infectivity could not be assessed.

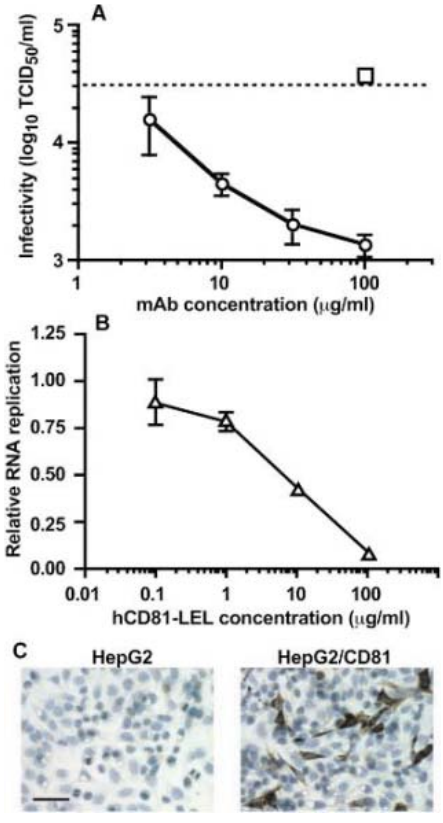

Fig. 2. HCVcc infection is dependent on HCV glycoprotein functions. (**A**) FL-J6/JFH (H2476L) was pre-incubated for 1 hour at 37°C with the indicated concentrations of recombinant human anti-E2 C1 (circles) or anti-dengue virus NS1 (square) immunoglobulin G1 monoclonal antibodies (mAb), then titered by limiting dilution assay (mean ± SEM; $n = 3$). Assays for both antibodies were conducted in parallel. The dotted line indicates the titer of untreated virus. (**B**) FL-J6/JFH (H2476L) was preincubated with 12 μg/ml of a recombinant form of the large extracellular loop (LEL) of CD81 and used to infect naïve cells. The levels of HCV RNA, relative to an untreated control, were determined at 48 hours postinfection by quantitative RT-PCR (mean ± SEM; $n = 4$). (**C**) HepG2 or HepG2/CD81 cells were infected with FL-J6/JFH for 48 hours before immunostaining for NS5A expression. Scale bar, 100 μm.

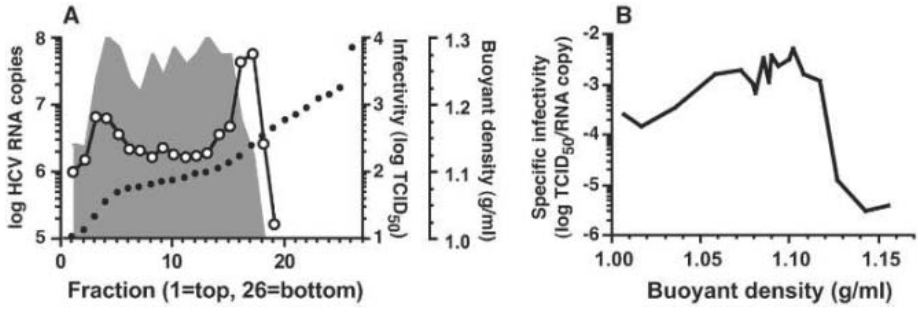

Fig. 3. Characterization of HCVcc particles. (**A**) The profiles of FL-J6/JFH (H2476L) RNA (open circles) and infectivity (solid gray) are shown after isopycnic centrifugation in a 10 to 40% iodixanol gradient. Closed circles indicate the buoyant density of each fraction. (**B**) The specific infectivity of each fraction in panel (A) was calculated as the infectivity per RNA copy and plotted against the buoyant density.

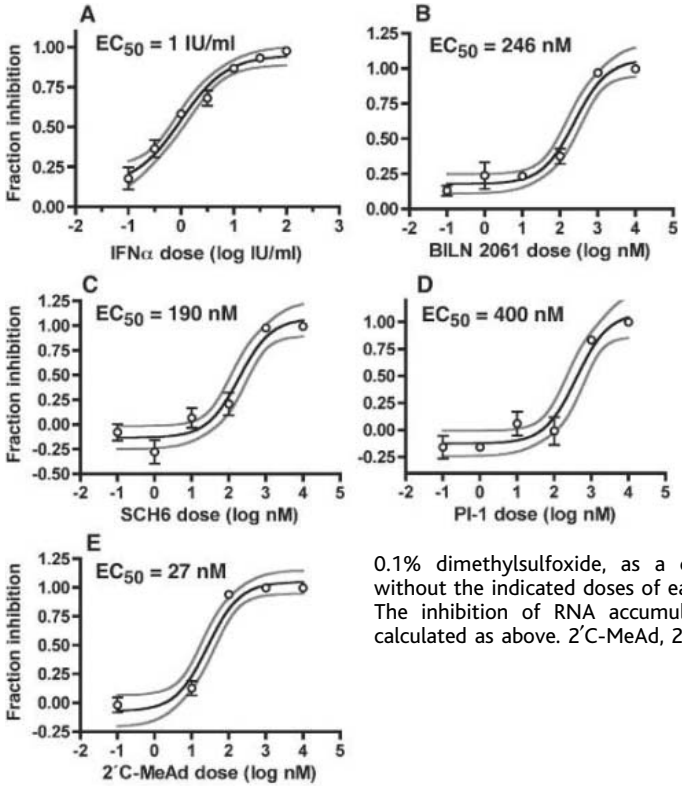

Fig. 4. Antiviral inhibition of HCVcc. (**A**) Huh-7.5 cells were incubated for 18 hours with the indicated doses of IFN before infection with FL-J6/JFH (H2476L) (MOI of 1.0). The fraction of inhibition was calculated from the levels of HCV RNA at 48 hours post-infection. The mean ± SEM ($n = 3$), best-fit curve (black), and 95% confidence interval (gray curves) are shown. (**B** to **E**) After 8 hours inoculation with FL-J6/JFH (H2476L) (MOI of 0.1), Huh-7.5 cells were washed and incubated in media containing 0.1% dimethylsulfoxide, as a carrier control, with or without the indicated doses of each anti-HCV compound. The inhibition of RNA accumulation at 48 hours was calculated as above. 2′C-MeAd, 2′C-methyladenosine.

Thus, HCVcc exhibits physical properties similar to those that have been previously described for natural isolates of HCV.

There is an urgent need for improved HCV drug therapies. The current standard treatment, pegylated interferon-α (IFNα) and ribavirin, leads to a sustained response in only ≈50% of genotype 1–infected patients. We examined the ability of HCVcc replication to be inhibited by IFNα and other antiviral compounds. Dose-response experiments showed that IFNα inhibited HCVcc RNA accumulation in infected cells with a median effective concentration (EC_{50}) of 1 international unit (IU)/ml (Fig. 4A). We also tested three HCV-specific inhibitors of the NS3 serine protease for their effects on HCVcc infection. As seen in Fig. 4, B to D, BILN 2061 (*21*), SCH6 (*22*), and PI-1 (*23*) all inhibited HCVcc RNA accumulation in the submicromolar range. In addition, a nucleoside analog inhibitor of the NS5B RNA polymerase, 2′C-methyladenosine (*24*), was found to inhibit HCVcc replication in the low nanomolar range (Fig. 4E). Thus, HCVcc infection can be inhibited by IFNα and several HCV-specific antiviral compounds. The specificity of these latter compounds further shows that HCVcc infection leads to authentic replication in target cells and demonstrates that this infectious system may be useful for testing current and future antiviral compounds.

We describe a full-length genotype 2a HCV genome that replicates and produces virus particles that are infectious in cell culture. This system lays a foundation for future in vitro studies to examine new aspects of the virus life cycle and to develop new drugs for combating HCV.

Note added in proof: Full-length JFH-1 has also been recently reported to produce infectious virus in cell culture (*25–27*), as has a genotype 1b Com1/JFH-1 chimera (*28*), albeit with lower efficiency and slower growth kinetics than the system reported here.

References and Notes

1. Anonymous, *Wkly. Epidemiol. Rec.* **75**, 18 (2000).
2. K. J. Blight, A. A. Kolykhalov, C. M. Rice, *Science* **290**, 1972 (2000).
3. T. Date *et al.*, *J. Biol. Chem.* **279**, 22371 (2004).
4. T. Kato *et al.*, *Gastroenterology* **125**, 1808 (2003).
5. V. Lohmann *et al.*, *Science* **285**, 110 (1999).
6. K. J. Blight, J. A. McKeating, C. M. Rice, *J. Virol.* **76**, 13001 (2002).
7. J. Bukh *et al.*, *Proc. Natl. Acad. Sci. U.S.A.* **99**, 14416 (2002).
8. T. Pietschmann *et al.*, *J. Virol.* **76**, 4008 (2002).
9. Materials and methods are available as supporting material on *Science* Online.
10. E. V. Agapov *et al.*, *J. Virol.* **78**, 2414 (2004).
11. B. M. Kümmerer, C. M. Rice, *J. Virol.* **76**, 4773 (2002).
12. P. Pileri *et al.*, *Science* **282**, 938 (1998).
13. B. Bartosch *et al.*, *J. Biol. Chem.* **278**, 41624 (2003).
14. E. G. Cormier *et al.*, *Proc. Natl. Acad. Sci. U.S.A.* **101**, 7270 (2004).
15. J. Zhang *et al.*, *J. Virol.* **78**, 1448 (2004).
16. R. Bartenschlager, M. Frese, T. Pietschmann, *Adv. Virus Res.* **63**, 71 (2004).
17. D. Bradley *et al.*, *J. Med. Virol.* **34**, 206 (1991).
18. N. Fujita *et al.*, *J. Med. Virol.* **63**, 108 (2001).
19. T. Heller *et al.*, *Proc. Natl. Acad. Sci. U.S.A.* **102**, 2579 (2005).
20. M. Hijikata *et al.*, *J. Virol.* **67**, 1953 (1993).
21. D. Lamarre *et al.*, *Nature* **426**, 186 (2003).
22. A. K. Saksena *et al.*, International Patent Application WO 02/008244 (2002).
23. K. Lin, A. D. Kwong, C. Lin, *Antimicrob. Agents Chemother.* **48**, 4784 (2004).
24. S. S. Carroll *et al.*, *J. Biol. Chem.* **278**, 11979 (2003).
25. T. Wakita, T. Kato, T. Date, M. Miyamoto, paper presented at the 11th International Symposium on HCV and Related Viruses, Heidelberg, Germany, 5 October 2004.
26. T. Wakita *et al.*, *Nat. Med.* 12 June 2005 (10.1038/nm1268).
27. J. Zhong *et al.*, *Proc. Natl. Acad. Sci. U.S.A.* 6 June 2005 (10.1073/pnas.0503596102).
28. T. Pietschmann *et al.*, paper presented at the 11th International Symposium on HCV and Related Viruses, Heidelberg, Germany, 5 October 2004.

29. We thank P. Holst, V. Kramer, and N. Torres for technical assistance; J. Bloom, A. Gauthier, L. Dustin, and D. Bernard for careful review of the manuscript; T. Wakita for SGR-JFH1, SGR-JFH (H2476L), and SGR-JFH(GND); J. Bukh for pJ6CF; D. Moradpour for C7-50 antibody; T. von Hahn and J. Zhang for HepG2/CD81 cells; Boehringer Ingelheim for BILN 2061; The Schering-Plough Research Institute for SCH6; C. Lin and A. Kwong of Vertex Pharmaceutical, Inc. for PI-1; and D. Olsen and S. Ludmerer at Merck for 2′C-methyladenosine. Funded by grants from NIH (CA57973, CA85883, AI40034 to C.M.R., CA10702 to B.D.L., DK70497 to A.J.S., AI51820 to T.L.T., AI50798 to J.A.M.) and the Greenberg Medical Research Institute. Additional support was provided by the Charles H. Revson Foundation (M.J.E.) and the German Science Foundation (Deutsche Forschungsgemeinschaft) (B.W.). B.D.L. is a recipient of the National Cancer Institute Howard Temin Award. C.M.R. is a manager of and has equity in Apath, LLC, which has an exclusive license for the Huh-7.5 cell line.

Supporting Online Material

www.sciencemag.org/cgi/content/full/1114016/DC1
Materials and Methods
SOM Text
Figs. S1 to S3
References and Notes

25 April 2005; accepted 31 May 2005
Published online 9 June 2005;
10.1126/science.1114016
Include this information when citing this paper.

Genome-Scale Identification of Nucleosome Positions in *S. cerevisiae*

Guo-Cheng Yuan, Yuen-Jong Liu,* Michael F. Dion, Michael D. Slack,† Lani F. Wu, Steven J. Altschuler, Oliver J. Rando‡

The positioning of nucleosomes along chromatin has been implicated in the regulation of gene expression in eukaryotic cells, because packaging DNA into nucleosomes affects sequence accessibility. We developed a tiled microarray approach to identify at high resolution the translational positions of 2278 nucleosomes over 482 kilobases of *Saccharomyces cerevisiae* DNA, including almost all of chromosome III and 223 additional regulatory regions. The majority of the nucleosomes identified were well-positioned. We found a stereotyped chromatin organization at Pol II promoters consisting of a nucleosome-free region ~200 base pairs upstream of the start codon flanked on both sides by positioned nucleosomes. The nucleosome-free sequences were evolutionarily conserved and were enriched in poly-deoxyadenosine or poly-deoxythymidine sequences. Most occupied transcription factor binding motifs were devoid of nucleosomes, strongly suggesting that nucleosome positioning is a global determinant of transcription factor access.

Nucleosomes prevent many DNA binding proteins from approaching their sites (*1–3*), whereas appropriately positioned nucleosomes can bring distant DNA sequences into close proximity to promote transcription (*4*). Current understanding of the primary structure of chromatin and its effects on gene expression comes from a handful of well-characterized loci (see examples below). High-resolution measurements of nucleosome positions over chromosome-scale distances would enhance our understanding of chromatin structure and function.

To measure nucleosome positions on a genomic scale, we developed a DNA microarray method (*5*) to identify nucleosomal and linker DNA sequences on the basis of susceptibility of linker DNA to micrococcal nuclease (fig. S1). Nucleosomal DNA was isolated, labeled with Cy3 fluorescent dye (green), and mixed with Cy5-labeled total genomic DNA (red). This mixture was hybridized to microarrays printed with overlapping 50-mer oligonucleotide probes tiled every 20 base pairs across chromosomal regions of interest (fig.

Bauer Center for Genomics Research, Harvard University, 7 Divinity Avenue, Cambridge, MA 02138, USA.

*Present address: Department of Molecular Biophysics and Biochemistry, Yale University, Post Office Box 208114, New Haven, CT 06520, USA.

†Present address: BAE Systems Advanced Information Technologies, 9655 Granite Ridge Drive, San Diego, CA 92123, USA.

‡To whom correspondence should be addressed. E-mail: orando@cgr.harvard.edu

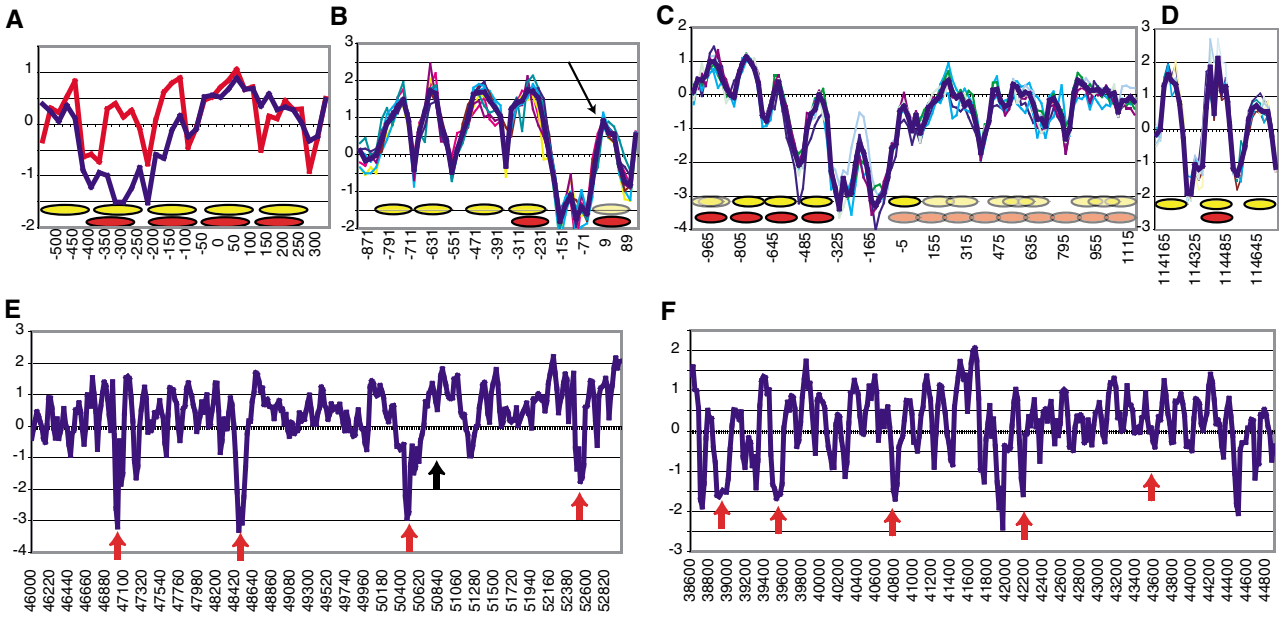

Fig. 1. Microarray data reproduce multiple sources of published data. The *y* axis represents the log(2) ratio of the hybridization values for Cy3 (nucleosomal DNA) versus Cy5 (genomic DNA), whereas the *x* axis represents the chromosomal coordinates of the microarray oligonucleotides. Yellow ovals represent nucleosomes inferred by HMM; red ovals give literature positions. The *x* axis in (A) to (C) shows distance to ATG, whereas the *x* axis in (D) to (F) shows chromosome III coordinate. (**A**) *MFA2* promoter. Blue line indicates data from BY4741 (MATa), whereas the red line shows data from BY4742 (MATα). Data are taken from a proof-of-concept array, where tiling was every 25 base pairs, and represent average of three experiments. (**B**) *HIS3* promoter. Thick blue line shows the median of eight independent microarrays for BY4741. Individual replicates are shown as thin lines. Arrow indicates "low" nucleosome only identified in detrended data. (**C**) *CHA1* promoter as in (B). Delocalized nucleosomes shown as overlapping pale ovals. (**D**) Chromosome III centromere as in (B). (**E** and **F**) Published DNase I hypersensitive sites (*11*) are indicated with arrows. Red arrows represent strong bands in the published study, whereas black arrow represents a dubious band.

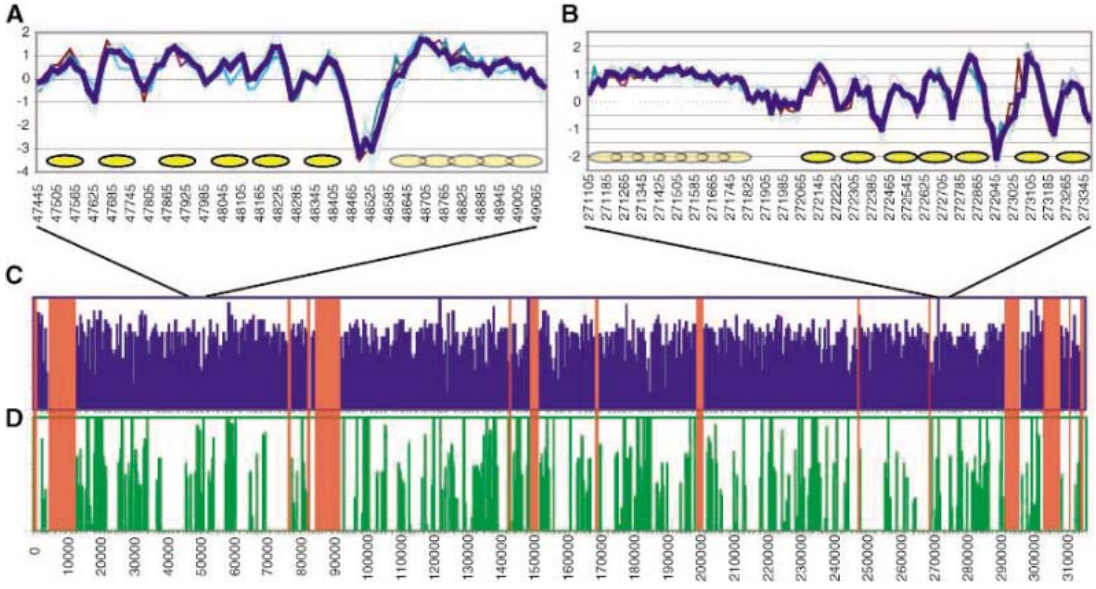

Fig. 2. Local and global views of delocalized nucleosomes. (**A** and **B**) Well-positioned and delocalized nucleosomes. Data graphed as in Fig. 1. (**C**) Global nucleosome occupancy on chromosome III. Nucleosome density was calculated from HMM calls, and a 500–base pair running average was plotted. Red rectangles indicate regions not tiled. (**D**) Delocalized nucleosomes are inhomogeneously distributed on chromosome III. Fraction of nucleosomal probes found in delocalized nucleosomes plotted as in (C).

S1B). A graph of green:red ratio values for spots along the chromosome is expected to show nucleosomes as peaks about 140 base pairs long (*6*), or six to eight microarray spots, surrounded by lower ratio values corresponding to linker regions (fig. S1C).

To objectively compare our data to published nucleosome positions, we developed a hidden Markov model (HMM) (*7*) to determine nucleosome/linker boundaries (fig. S1, D to G). HMMs use observable data to infer hidden states responsible for generating the signal. Here, observable signals are hybridization values of the tiled probes (fig. S1, C and D), and the hidden states are nucleosomal and linker states (fig. S1E). Well-positioned nucleosomes should cover ~140 base pairs or six to eight probes (fig. S1E, N1 to N8) and have a high green:red ratio, whereas stretches of ≥nine probes were classified as "fuzzy" or delocalized nucleosomes (fig. S1E, DN1 to DN9). Linkers are expected to have lower ratios (fig. S1D) and may have variable length (fig. S1E, return arrow on node L). The model calculates the probability that a given probe on the array corresponded to nucleosomal, fuzzy nucleosomal, or linker DNA (fig. S1F) and identifies the most likely nucleosome positions (fig. S1G). To capture nucleosome peaks with low maxima (see arrow, Fig. 1B), we detrended data by using a peak-to-trough measure and analyzed it with the HMM. Nucleosomes identified exclusively from the detrended data were annotated as "low" nucleo-

somes and may correspond to nucleosomes found only in a subpopulation of cells (Fig. 1B and Materials and Methods).

We characterized nucleosome positions by using two microarrays. We first used a proof-of-concept array covering the *MFA2* and *PHO5* promoters (Fig. 1A and fig. S4).

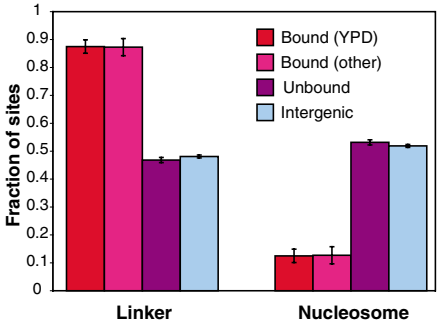

Fig. 3. Functional transcription factor binding motifs are more accessible than unbound motifs. Oligonucleotide probes were separated into all intergenic probes (background), unbound motifs under all conditions tested, motifs bound in YPD, and motifs bound in any other condition but unbound in YPD (*21*). The percentage of each group of probes determined in this work to be nucleosomal is shown. Error bars indicate SEM.

With information gained from this array, we designed a microarray to measure nucleosome positions over half a megabase of the *S. cerevisiae* genome. Chromosome III was tiled, except for regions of extensive cross-hybridization, with 50-mers overlapping every 20 base pairs, leaving 30 overlapping continuous sequences (contigs) covering 278,960 base pairs. In addition, one kilobase of promoter sequence was tiled for 223 genes on other chromosomes.

Nucleosomal DNA from eight independent cultures of log-phase yeast was hybridized to this microarray. We validated the microarray by comparing nucleosome positions determined with our approach to published nucleosome positions. We correctly identified nucleosomes at the *MFA2*, *HIS3*, *PHO5*, and *CHA1* promoters, over the chromosome III centromere, and over the silent mating type loci (Fig. 1 and figs. S4 and S5) (*8*–*10*). We also found that 27 of 32 deoxyribonuclease (DNase) hypersensitive sites on chromosome III (*11*) fall in long linkers identified by our method (Fig. 1, E and F, and fig. S4). Lastly, a coarse-grained view of our high-resolution data reproduced recent genome-wide chromatin immunoprecipitation studies at ~1-kb resolution (*12*, *13*) (fig. S6). Thus, our method faithfully reproduced high- and low-resolution characteristics of chromatin previously described with the use of three distinct assay types: micrococcal nuclease sensitivity, DNase I sensitivity, and histone occupancy.

The availability of thousands of nucleosome positions facilitates the elucidation of global chromatin properties, such as the fraction of nucleosomes that are well-positioned (Fig. 2 and table S1). Nucleosomes might be expected to occupy multiple positions in ensemble measurements, because there is little thermodynamic preference of the histone octamer for most genomic DNA (*14*). In addition, yeast growing exponentially are a heterogeneous mixture of cells in different cell cycle and epigenetic states (*15*, *16*). However, examination of our data revealed pervasive examples of well-positioned nucleosomes. Global HMM identification of well-positioned and delocalized nucleosomes revealed that 65 to 69% of nucleosomal DNA was found in well-positioned nucleosomes (table S1).

Although average nucleosome density is relatively constant over chromosome III, delocalized nucleosomes are inhomogeneously distributed (Fig. 2, C and D). Passage of RNA

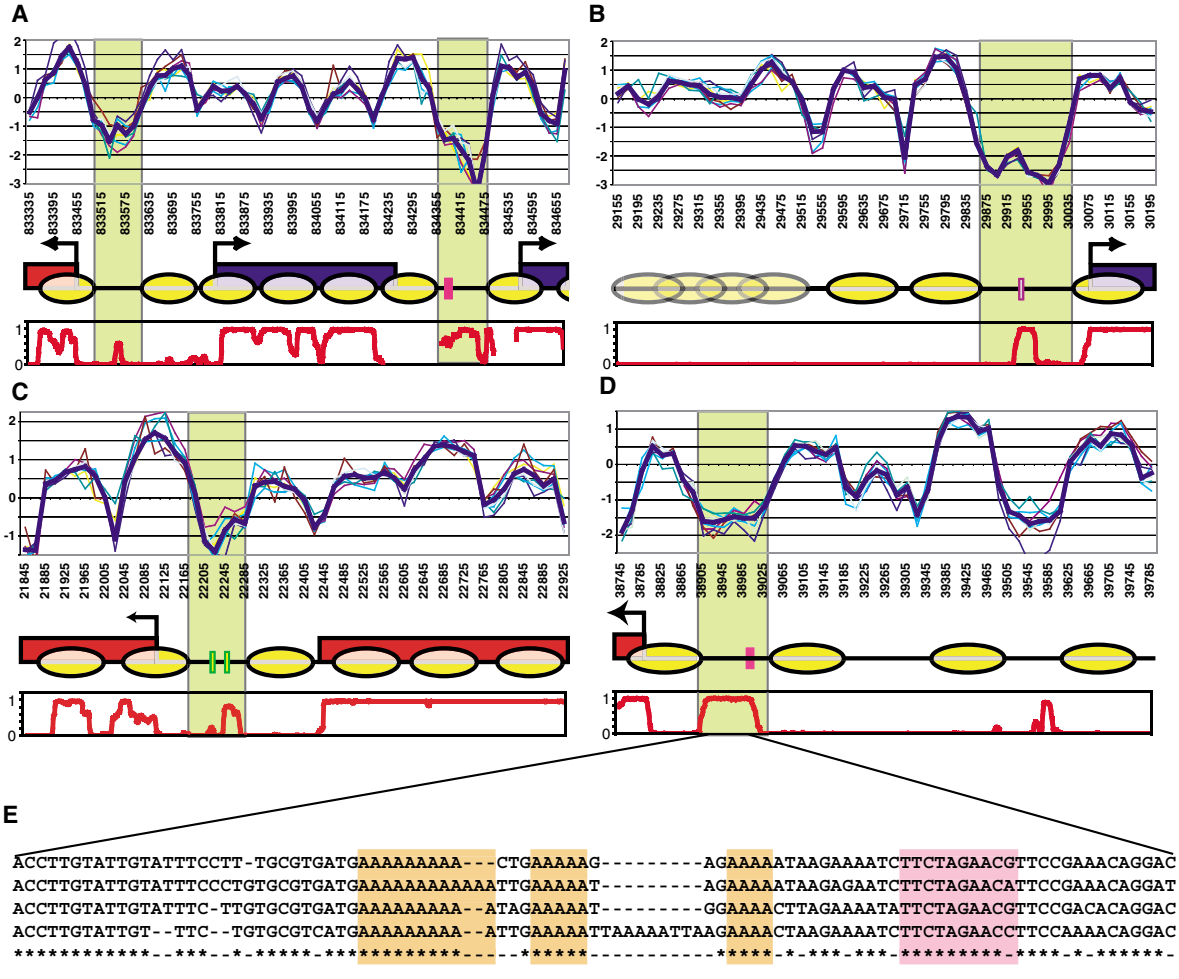

Fig. 4. Long NFRs are common in promoters. (**A** to **D**) Top graphs show microarray data. Middle images show gene annotation (Crick genes are red and Watson genes are blue), bound transcription factor motifs from (*21*) (colored rectangles), and inferred nucleosome positions (ovals). Bottom graphs show an aggregate sequence conservation score (*29*). Green rectangles highlight upstream NFRs. Individual examples: (A) Chr XVI 833335-834655, (B) Chr XVI 29155-30195, (C) Chr III 21845-22925, and (D) Chr III 38745-39785. (**E**) Expanded view of conserved sequence. Sequences are shown for *S. cerevisiae*, *S. mikatae*, *S. paradoxus*, and *S. bayanus*. Hsf1 binding site is outlined in purple; polyA stretches are highlighted in orange.

polymerase through coding regions temporarily disrupts nucleosomes (*17*, *18*), which rapidly reassemble behind the polymerase (*19*). High transcription rates may cause nucleosomes to appear delocalized, because polymerases (and transiently disassembled nucleosomes) occupy distinct positions in the ensemble (see *CHA1* above). We found that highly expressed genes were enriched for delocalized nucleosomes (P = 0.007) (fig. S7). Furthermore, delocalized nucleosomes were found farther from transcriptional start sites than were well-positioned nucleosomes (fig. S8).

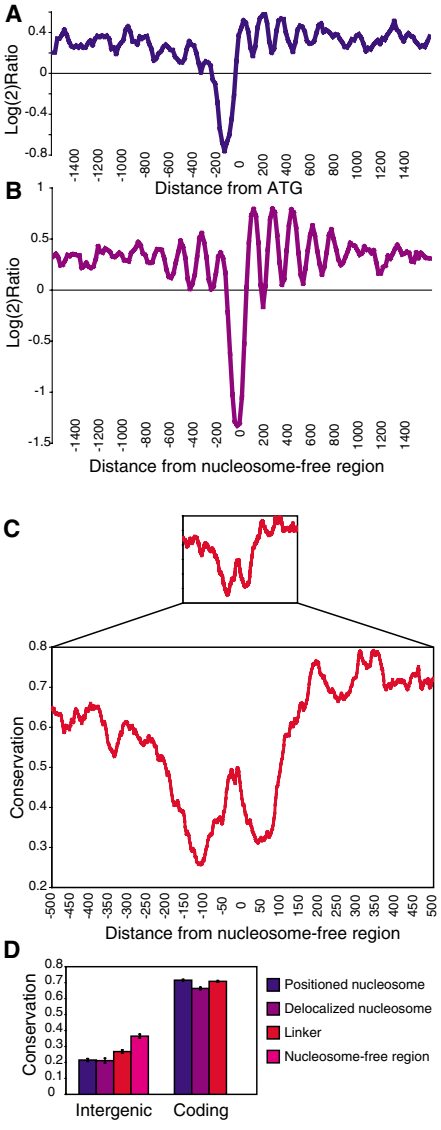

Fig. 5. NFRs are pervasive in promoters and occur over conserved sequences. (**A**) Promoters were aligned by start codon, and microarray data were averaged and plotted. The *x* axis shows distance from ATG. (**B**) After alignment by NFR, data from 90% of tiled promoters were averaged. The *x* axis shows distance from NFR. (**C**) Chromosome III promoters were aligned as in (B), and conservation values were averaged for one kilobase around NFR. Top graph has the same *x* axis scale as (B); bottom graph shows expanded view. (**D**) Chromosome III probes were separated into groups as indicated, and sequence conservation was averaged and plotted. For intergenic regions, linkers were separated into NFRs and all other linkers. Error bars indicate SEM.

Nucleosome occupancy has been proposed to exclude transcription factors from a subset of their specific consensus motifs (*1*–*3*, *20*), and recent work demonstrated that promoters bound by many transcription factors are grossly nucleosome-depleted (*13*). To investigate this phenomenon at high resolution, we compared our data to a database of transcription factor motifs bound under a variety of conditions (*21*). We plotted the fractions of bound and unbound motifs that were in nucleosomes or in linkers (Fig. 3). A total of 47% of unbound motifs were found in linker DNA sequences, very close to the baseline measurement of 48% for all intergenic sequences. In contrast, over 87% of the motifs that are associated with transcription factors under our growth conditions were depleted of nucleosomes. Thus, functional transcription factor binding sites are predominantly nucleosome-free in vivo. Furthermore, the set of functional motifs that are unbound under our assay conditions showed the same linker enrichment as motifs that are bound (Fig. 3). For example, the promoter upstream of *YCL050C* (Fig. 4D), which is not bound by any transcription factors at standard growth temperatures, is bound by Hsf1 in heat-stressed yeast (*21*). Our measurements indicated the Hsf1 binding motif was located in a linker (and thus accessible for factor binding), even in the absence of heat stress.

Intergenic DNA in yeast is nucleosome-depleted relative to coding DNA (*12*, *13*). This could correspond to decreased population occupancy of several nucleosomes or high population occupancy of sparse nucleosomes. Consistent with the latter possibility, nucleosome-free regions (NFRs) of ~150 base pairs were found about 200 base pairs upstream of many annotated coding sequences (Fig. 4, A to D). The pervasiveness of this signal can be seen by averaging data for all tiled genes (Fig. 5A): a long linker dominates the average. We iteratively aligned promoters by correlation to the average profile, thus aligning NFRs, and selected 90% of promoters to eliminate the noise introduced by rare promoters lacking an NFR. This averaged alignment shows several regularly spaced nucleosomes surrounding the NFR (Fig. 5B), with an internucleosome distance between 160 and 170 base pairs [an average internucleosomal distance of 160 to 165 base pairs was previously measured in yeast (*6*)].

Noting that functional transcription factor motifs are similarly found ~100 to 500 base pairs upstream of start codons (*21*), we identified NFRs as sites of 51% of bound motifs found on our array (Fig. 4). This suggested that NFRs are transcriptional start sites, predicting that the extent of the 5′ untranslated region of the genes assayed in this study could be identified by using these data. RNA (total RNA and mRNA) was isolated and hybridized to our microarray. As expected, 5′ ends of transcripts coincided with NFRs (fig. S9), identifying these regions as transcriptional start sites.

The conservation of functional transcription factor motifs between related *Saccharomyces* species (*22*) lead us to investigate sequence conservation in NFRs. The bottom graphs in Fig. 4, A to D, show an aggregate conservation score from seven sequenced *Saccharomyces* species. Coding DNA was highly conserved, but there was also marked conservation of intergenic sequence surrounding, but not limited to, transcription factor binding sites (Fig. 4E). To investigate this conservation globally, we aligned promoters by the NFR and averaged the conservation scores. Notable here is a peak of average sequence conservation in the NFR surrounded by valleys of poor conservation (Fig. 5C). We also investigated sequence conservation by partitioning probes containing coding or intergenic sequences into bins defined by the HMM output (Fig. 5D). Coding regions were highly conserved regardless of nucleosomal context. Conversely, intergenic sequences found in nucleosomes were poorly conserved, whereas those in NFRs were more highly conserved across evolution. Thus, biologically meaningful regulatory information in intergenic sequences falls into clusters that are accessible to the cell. This is not only due to conservation of transcription factor binding sites, because the region of conservation often includes a great deal of sequence beyond the transcription factor binding motif (Fig. 4E).

Conserved nucleosome-free sequences included not only transcription factor binding sites but also multiple stretches of poly-A or poly-T (Fig. 4E). Poly(dA-dT) stretches incorporate poorly into nucleosomes because of their relative rigidity (*23*–*25*). Globally, we found that NFRs were enriched for poly(dA-dT) (fig. S10A), as expected from the prevalence of these elements in yeast promoters (*26*). Conversely, these homopolymer stretches globally had increased likelihood of being in linkers (fig. S10B). This was not caused by sequence specificity of micrococcal nuclease (*27*), because hybridizations of micrococcal nuclease-treated naked DNA showed little correlation with nucleosomal data (r = 0.09). Our results suggest that poly(dA-dT) stretches play a causal role in establishing many NFRs.

Chromatin in yeast is well-ordered (over 69% of nucleosomal DNA was found in well-positioned nucleosomes), and delocalized nucleosomes are found distant from NFRs (fig. S8). Taken together, our results are consistent with a modified "statistical positioning" (*28*) mechanism underlying this global order, where nucleosomes are prevented from association with promoter regions either by sequence characteristics such as poly(dA-dT)

elements or by nucleosomal eviction by recruited proteins, and nucleosomes are subsequently well-positioned between nearby NFRs because of structural constraints imposed by packaging short stretches of sequence with nucleosomes.

It will be interesting to determine whether the accessible transcription factor binding sites, highly positioned nucleosomes, and stereotyped promoter architecture found in yeast chromatin will be conserved features of metazoan chromatin.

References and Notes

1. J. D. Anderson, J. Widom, *J. Mol. Biol.* **296**, 979 (2000).
2. L. L. Wallrath, Q. Lu, H. Granok, S. C. Elgin, *Bioessays* **16**, 165 (1994).
3. U. Venter, J. Svaren, J. Schmitz, A. Schmid, W. Horz, *EMBO J.* **13**, 4848 (1994).
4. W. Stunkel, I. Kober, K. H. Seifart, *Mol. Cell. Biol.* **17**, 4397 (1997).
5. J. L. DeRisi, V. R. Iyer, P. O. Brown, *Science* **278**, 680 (1997).
6. K. E. Van Holde, *Chromatin*, Springer series in molecular biology (Springer-Verlag, New York, 1989).
7. R. Durbin, *Biological Sequence Analysis: Probabalistic Models of Proteins and Nucleic Scids* (Cambridge Univ. Press, Cambridge, 1998).
8. Y. Teng, S. Yu, R. Waters, *Nucleic Acids Res.* **29**, E64 (2001).
9. M. J. Saunders, E. Yeh, M. Grunstein, K. Bloom, *Mol. Cell. Biol.* **10**, 5721 (1990).
10. J. M. Moreira, S. Holmberg, *EMBO J.* **17**, 6028 (1998).
11. S. Ercan, R. T. Simpson, *Mol. Cell. Biol.* **24**, 10026 (2004).
12. C. K. Lee, Y. Shibata, B. Rao, B. D. Strahl, J. D. Lieb, *Nat. Genet.* **36**, 900 (2004).
13. B. E. Bernstein, C. L. Liu, E. L. Humphrey, E. O. Perlstein, S. L. Schreiber, *Genome Biol.* **5**, R62 (2004).
14. P. T. Lowary, J. Widom, *Proc. Natl. Acad. Sci. U.S.A.* **94**, 1183 (1997).
15. D. E. Gottschling, O. M. Aparicio, B. L. Billington, V. A. Zakian, *Cell* **63**, 751 (1990).
16. L. Z. Osherovich, J. S. Weissman, *Dev. Cell* **2**, 143 (2002).
17. M. A. Schwabish, K. Struhl, *Mol. Cell. Biol.* **24**, 10111 (2004).
18. A. Kristjuhan, J. Q. Svejstrup, *EMBO J.* **23**, 4243 (2004).
19. R. Belotserkovskaya *et al.*, *Science* **301**, 1090 (2003).
20. J. D. Lieb, X. Liu, D. Botstein, P. O. Brown, *Nat. Genet.* **28**, 327 (2001).
21. C. T. Harbison *et al.*, *Nature* **431**, 99 (2004).
22. M. Kellis, N. Patterson, M. Endrizzi, B. Birren, E. S. Lander, *Nature* **423**, 241 (2003).
23. K. Struhl, *Proc. Natl. Acad. Sci. U.S.A.* **82**, 8419 (1985).
24. J. D. Anderson, J. Widom, *Mol. Cell. Biol.* **21**, 3830 (2001).
25. H. C. Nelson, J. T. Finch, B. F. Luisi, A. Klug, *Nature* **330**, 221 (1987).
26. S. Karlin, B. E. Blaisdell, R. J. Sapolsky, L. Cardon, C. Burge, *Nucleic Acids Res.* **21**, 703 (1993).
27. W. Horz, W. Altenburger, *Nucleic Acids Res.* **9**, 2643 (1981).
28. R. D. Kornberg, L. Stryer, *Nucleic Acids Res.* **16**, 6677 (1988).
29. Alignment scores were downloaded from http://genome.ucsc.edu.

30. We thank N. Francis, T. Maniatis, K. Thorn, N. Friedman, J. Oshiro, T. Kaplan, J. Rinn, H. Chang, J. Lieb, and A. Gasch for critical reading of the manuscript; T. Aldredge, C. Reardon, and C. Daly for technical help; and A. Murray and the Bauer Center community for advice and support. This work was supported by the Bauer Center and by National Institute of General Medical Sciences.

Supporting Online Material

www.sciencemag.org/cgi/content/full/1112178/DC1
Materials and Methods
SOM Text
Figs. S1 to S10
Table S1
References and Notes

14 March 2005; accepted 2 June 2005
Published online 16 June 2005;
10.1126/science.1112178
Include this information when citing this paper.

Plant Circadian Clocks Increase Photosynthesis, Growth, Survival, and Competitive Advantage

Antony N. Dodd,[1] Neeraj Salathia,[2]* Anthony Hall,[2]† Eva Kévei,[3] Réka Tóth,[3] Ferenc Nagy,[3] Julian M. Hibberd,[1] Andrew J. Millar,[2]‡ Alex A. R. Webb[1]§

Circadian clocks are believed to confer an advantage to plants, but the nature of that advantage has been unknown. We show that a substantial photosynthetic advantage is conferred by correct matching of the circadian clock period with that of the external light-dark cycle. In wild type and in long– and short–circadian period mutants of *Arabidopsis thaliana*, plants with a clock period matched to the environment contain more chlorophyll, fix more carbon, grow faster, and survive better than plants with circadian periods differing from their environment. This explains why plants gain advantage from circadian control.

Circadian clocks produce an internal estimate of time that synchronizes biological events with external day-night cycles (*1*). Clocks with similar properties and regulatory architecture have evolved at least four times, indicating that circadian rhythms confer a selective advantage (*2*). In plants, circadian rhythms control gene expression, stomatal opening, and the timing component of photoperiodism, which regulates seasonal reproduction, but the basis for their contribution to fitness during vegetative growth remains undetermined (*3*, *4*). Indirect evidence suggests a physiological benefit from circadian rhythms during growth under unnaturally short photoperiods (*5*). Cyanobacteria and higher plants gain an advantage when the endogenous period is matched to the light-dark cycle (*6*–*8*). Rhythmic growth inhibitor secretion might cause the growth advantage in cyanobacteria (*7*, *8*), but this hypothesis may not apply to multicellular eukaryotes. We demonstrate that when correctly tuned, the *Arabidopsis* circadian system enhances chlorophyll content, photosynthetic carbon fixation, and growth. We also show that circadian enhancement of photosynthesis leads to improved survival and competitive advantage.

Biological clocks have evolved so that clock outputs are in phase with the Earth's rotation. We wished to identify and quantify mechanisms by which the clock confers advantage in light-dark cycles. We hypothesized that matching the endogenous clock period (τ) with the period of exogenous light-dark cycles (T) [so called "circadian resonance" (*7*)] provides an advantage by optimizing the phase relation between clock-controlled biology and exogenous day-night cycles. Plants having clocks that are dissonant from the environment, therefore, may be disadvantaged. To test this hypothesis, we compared the performance of wild-type plants with lines having mutations that alter clock period length, in a range of environmental period lengths ("T cycles") that were either matched or unmatched to the endogenous clock period.

We used three experimental approaches to test this hypothesis (*9*). First, wild-type plants with a circadian period of about 24 hours were grown in 10 hours light–10 hours dark (T20), 12 hours light–12 hours dark (T24) and 14 hours light–14 hours dark (T28) cycles. Second, we grew the long- and short-period mutants *ztl-1* [τ = 27.1 hours–32.5 hours; (*10*)] and *toc1-1* [τ = 20.7 hours; (*11*)] in T cycles that were similar to, or dissimilar from, their endogenous clock periods (T20 and T28). In these T-cycle experiments, relative performance was measured within, not between, genotypes, which specifically quantified the benefit

[1]Department of Plant Sciences, University of Cambridge, Downing Street, Cambridge, CB2 3EA, UK. [2]Department of Biological Sciences, University of Warwick, Coventry, CV4 7AL, UK. [3]Plant Biology Institute, Biological Research Centre of the Hungarian Academy of Sciences, Post Office Box 521, H-6701 Szeged, Hungary.

*Present address: Bauer Center for Genomics Research, Harvard University, 7 Divinity Avenue, Cambridge, MA 02138, USA.
†Present address: School of Biological Sciences, University of Liverpool, Crown Street, Liverpool L69 7ZB, UK.
‡Present address: Institute of Molecular Plant Sciences, Mayfield Road, University of Edinburgh, Edinburgh EH9 3JH, UK.
§To whom correspondence should be addressed. E-mail: alex.webb@plantsci.cam.ac.uk

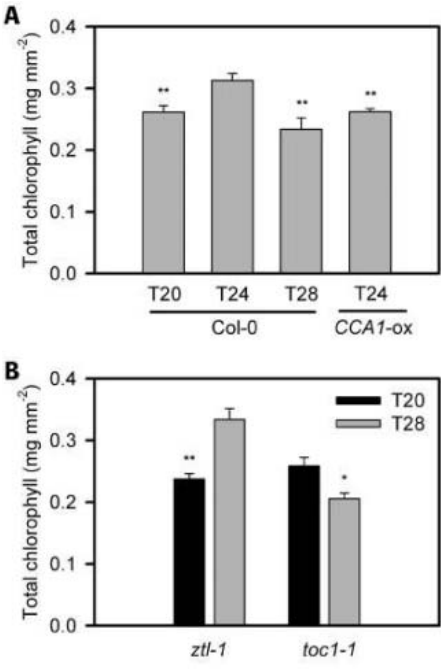

Fig. 1. Leaves contain more chlorophyll when their clock period matches the environmental period. (**A**) Total chlorophyll in Col-0 wild type grown under T20, T24, and T28, and in arrhythmic line *CCA1*-ox under T24. (**B**) Total chlorophyll in *ztl-1* (long-period mutant) and *toc1-1* (short-period mutant) grown in T20 and T28. For all groups, $n = 5$; data are means + SEM. In two-sample *t* tests comparing chlorophyll concentrations to the line having the period matched to the environment, significance of results: $*P < 0.05$, $**P < 0.01$.

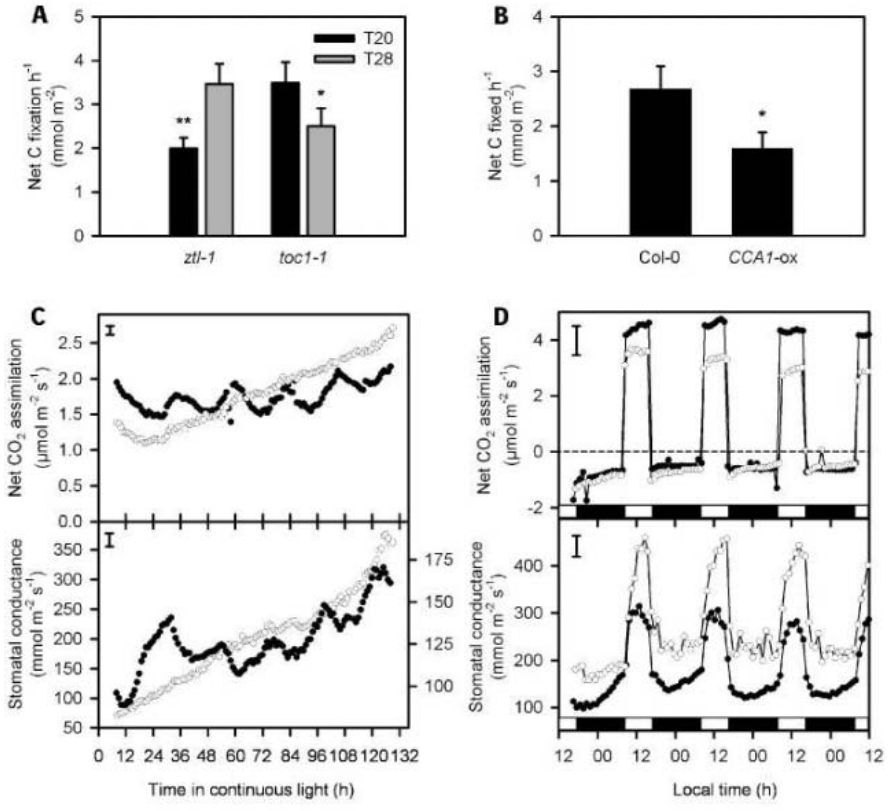

Fig. 2. The circadian clock enhances photosynthetic carbon fixation. (**A**) Mean C fixation per hour in *ztl-1* and *toc1-1* grown in T20 and T28. (**B**) Mean C fixation per hour in Col-0 wild type and arrhythmic *CCA1*-ox, in T24. (**C**) *CCA1* overexpression (open circles) abolishes the circadian rhythms of CO_2 fixation and stomatal opening that occur in Col-0 wild type (filled circles). (**D**) CO_2 assimilation and stomatal conductance in *CCA1*-ox (open circles) and Col-0 wild type (filled circles) under light-dark cycles (indicated by bars on the *x* axis). For these experiments, $n = 6$; data are means ± SEM (A and B) or largest standard error (C and D). In two-sample *t* tests comparing net C fixation per hour to the line with the clock period matched to the environment, significance of results: $*P < 0.05$, $**P < 0.01$.

of circadian resonance and excluded effects not associated with the clock. Last, the effect of circadian arrhythmia on growth and physiology was investigated in well-characterized arrhythmic plants overexpressing the molecular oscillator component *CCA1* (*CCA1*-ox), and compared with rhythmic wild types (*8*, *12*). Experiments were conducted during vegetative growth, to assess the contribution of circadian resonance to growth and fitness, and to eliminate pleiotropic effects on life history due to the flowering time alterations that arise in circadian period mutants (*13*). We assessed the contribution of circadian resonance to carbon fixation, biomass, and leaf chlorophyll. Carbon fixation rates (*14*–*16*) and biomass (*17*) are traits associated with plant fitness; therefore, our study provides information concerning specific mechanisms by which the clock contributes to fitness.

In wild type and in short- and long-period mutants, leaves contained more chlorophyll when the oscillator period matched that of the environment. Leaves of Columbia-0 (Col-0) wild-type plants grown for 30 days in T24 contained more chlorophyll than Col-0 grown in T20 or T28 (Fig. 1A). When *ztl-1* and *toc1-1* were grown under T20 and T28, the long-period mutant *ztl-1* contained more chlorophyll after growth in T28 than T20, whereas the short-period mutant *toc1-1* contained more chlorophyll after growth in T20 than T28 (Fig. 1B). Therefore, correct matching of the circadian period with the external period increases chlorophyll accumulation. When the Col-0 clock was stopped by *CCA1* overexpression, less chlorophyll was present compared with wild-type Col-0 under T24, which confirmed the dependence of chlorophyll accumulation on clock function (Fig. 1A).

There are circadian rhythms in transcript abundance of genes associated with chlorophyll synthesis, heme production, chlorophyll accumulation, and synthesis of chlorophyll-binding proteins (*11*, *18*–*20*). Virtually all clock-controlled genes associated with chlorophyll synthesis and the light-harvesting apparatus exhibit peak circadian transcript abundance 4 hours after subjective dawn (*18*), which suggests that circadian expression of these genes could be important for enhancing light-harvesting capacity. Although the amount of light-harvesting complex pigments and proteins remains uniform over the diel cycle (*19*), the clock might sustain steady-state levels of proteins that exhibit light-induced degradation, by way of circadian changes in turnover. This could explain why chlorosis can occur under very long photoperiods (*21*), because the duration of light-induced degradation of light-harvesting complex proteins extends beyond their period of clock-enhanced transcription.

Because chlorophyll content was greatest under circumstances of matched endogenous and environmental periods, we examined whether circadian resonance improves photosynthesis. We compared net carbon fixation of long- and short-period mutants and *CCA1*-ox, under T20, T24, and T28. The long-period mutant *ztl1* fixed 42% more carbon under T28 than T20, whereas the short-period mutant *toc1-1* fixed 40% more carbon under T20 than T28 (Fig. 2A). Circadian resonance, therefore, increases CO_2 fixation. Col-0 wild type fixed 67% more carbon than arrhythmic *CCA1*-ox (Fig. 2B). The reduction in carbon fixation associated with circadian arrhythmia was, therefore, greater than the disadvantage caused by the ~8-hour period mismatch with the environment that occurred in *ztl1* and *toc1-1*. Under continuous light, the rate of CO_2 fixation was lower in *CCA1*-ox than wild type for the first 48 hours

of continuous light, but during prolonged constant light, assimilation was higher in *CCA1*-ox than wild type (Fig. 2C). This was reminiscent of the outcompetition of rhythmic cyanobacterial lines by the arrhythmic line CLAb under continuous light (*8*). *CCA1* overexpression abolished circadian rhythms of CO_2 fixation and stomatal opening in constant conditions. Fourier analysis (*22*) estimated period lengths of 24.1 ± 0.6 hours and 23.5 ± 0.3 hours for stomatal conductance and carbon assimilation, respectively, in Col-0 wild type, but failed to detect circadian regulation for *CCA1*-ox. Similarly, the *toc1-1* and *ztl1* mutations cause respective shortening and extension of the circadian period of CO_2 fixation and stomatal opening rhythms that occur in continuous light (*23*, *24*).

Under light-dark cycles, rhythmic stomatal opening and closure was restored in *CCA1*-ox, but anticipation of dawn and dusk was absent, which demonstrated that the clock remained stopped in *CCA1*-ox, even in light-dark cycles (Fig. 2D). The stomata continued to open for the entire photoperiod in *CCA1*-ox, whereas in Col-0, stomatal opening ceased around midday. *CCA1*-ox, therefore, had higher total transpiration than Col-0 during the light period (Fig. 2D). Thus, the clock allows stomata to anticipate dusk and might participate in enhancement of water-use efficiency.

Because photosynthesis increased when exogenous and endogenous periods were similar (Fig. 2) and because long-term carbon fixation is correlated to leaf chlorophyll content (*25*), we reasoned that circadian resonance might increase vegetative growth. Col-0 wild type grown under T20, T24, and T28 had greatest vegetative biomass in T24 (Fig. 3, A and B). Under T20, aerial biomass was reduced by 47% relative to T24, and growth under T28 resulted in 42% less biomass relative to T24. When the long- and short-period mutants *ztl1* and *toc1-1* were grown under T20 and T28, *ztl1* had maximum aerial biomass and leaf area under T28. In *toc1-1*, aerial biomass and leaf area were maximal under T20 (Fig. 3, C and D). These measures of growth were lower in *toc1-1* than *ztl1-1* under all conditions. Separately, we compared growth of Col-0 and CCA1-ox under T24. After 32 days, the aerial biomass of *CCA1*-ox was 53% lower than that of Col-0 (Fig. 3, E and F). We did not compare growth of *CCA1*-ox and Col-0 in continuous light, because wild-type plants become arrhythmic under extended continuous light (*26*). Therefore, circadian resonance enhances growth in wild-type plants and mutants with altered circadian period, and stopping the clock further reduces growth. Enhancement of biomass and photosynthesis by the circadian clock consequently indicates processes by which the clock increases fitness (*14*–*17*).

Fitness arising from circadian resonance might be reported by seedset (*5*). We compared seedset from short- and long-period mutants and wild type, under T24. In a single experiment, there were no large or consistent differences in mean seed production (*toc1-1*, 16200 seeds per plant; wild type, 15757 seeds per plant; *ztl-1*, 15005 seeds per plant; $n = 15$). Because the clock determines flowering time, which becomes altered in period mutants (*13*), seedset is likely to be an ambiguous marker for the fitness implications of circadian resonance. However, we have demonstrated that circadian resonance increases the established fitness traits of photosynthesis and biomass (Figs. 1 to 3) (*14*–*17*).

We performed reciprocal competitions between long- and short-period plants (*7*), using two short-period mutants of *TOC1* [*toc1-1* and *toc1-2*, $\tau \approx 20$ hours (*27*)] and two long-period mutants of *ZTL* [*ztl-1* and *ztl-27*, $\tau \approx 28$ hours (*9*, *10*)]. Mixed populations of *toc1* and *ztl* were grown under T20 and T28, which generated a crowded lawn of plants. In these conditions, interactions among neighboring plants of differing genotypes affect physiological outcomes, in addition to the interaction between each plant and the light-dark cycle that we tested previously. We grew monocultures of each line, to assess the importance of differing growth rates among neighbors compared with growth rates among lines. Testing for competitive advantage derived from circadian resonance, using reciprocal competition, requires a mixed population of two period-length genotypes; therefore, it cannot be assessed in just wild type. The period-length mutants were appropriate for this experiment because the growth disadvantage that occurred when $T \neq \tau$ in wild type also occurred with the period mutants (Figs. 1 to 3).

In two separate competition experiments, using different *ZTL* and *TOC1* mutants, under T20, *TOC1* mutants grew more successfully than *ZTL* mutants, as indicated by multiple parameters including chlorophyll content, leaf number, rosette diameter, and aerial biomass (Fig. 4). Conversely, under T28, growth of *ZTL* mutants was enhanced compared with *TOC1*. This was similar to results obtained when plants were grown without competition (Figs. 1 to 3). However, competition caused mortality of some plants, which did not occur in the absence of competition. Mortality was greater in *ztl-27* under T20, and greater in *toc1-2* under T28 (Fig. 4B). Circadian resonance, therefore, en-

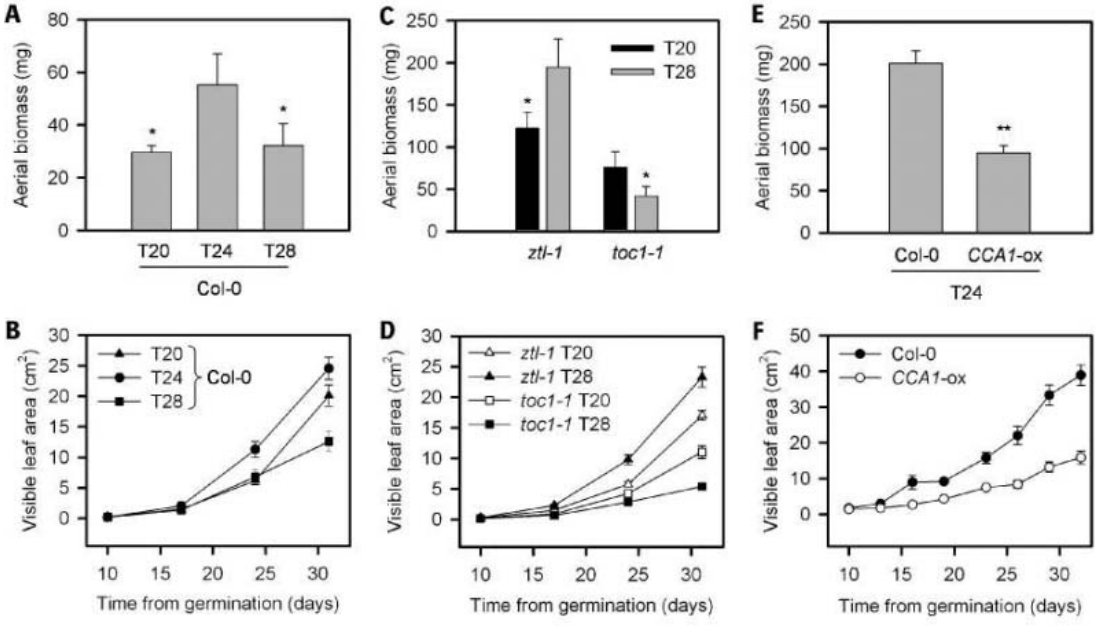

Fig. 3. Environmentally matched clock period enhances vegetative growth. (**A** and **B**) Dry aerial biomass (A) and visible leaf area (B) in Col-0 wild type after growth under T20, T24, and T28. (**C** and **D**) Dry aerial biomass (C) and visible leaf area (D) after growth of the long-period mutant *ztl-1* and short-period mutant *toc1-1* under T20 and T28. (**E** and **F**) Dry aerial biomass (E) and visible leaf area (F) after 35 days' growth of Col-0 wild type and arrhythmic *CCA1*-ox line in T24. Biomass was measured after 32 days (A and C) or 35 days (E). For all groups, $n = 5$; data are means + or ± SEM. (A, C, and E) In two-sample *t* tests comparing aerial biomass to the line with the clock period matched to the environment, significance of results: $^*P < 0.05$, $^{**}P < 0.01$.

hanced growth and survival, and this was more pronounced under competition than during monoculture (Fig. 4A). In two separate monoculture experiments, there was no consistent pattern of T cycle–dependent mortality (Fig. 4C). Therefore, both poor individual growth and outcompetition confer a disadvantage under dissonant T cycles. Our data underestimate the true growth advantage that occurs under competition, because physiological parameters were not measured in dead plants. Neither genotype had an advantage in all conditions, which implicated circadian effects of the mutations rather than secondary phenotypes. Competition between *toc1-1* and *ztl-1*, and between *toc1-1* or *toc1-2* and *ztl-27*, gave the same result, which discounts the likelihood of background mutations or allele-specific effects (*28*). *Arabidopsis* entrains stably to T cycles far from τ (*24*, *29*, *30*), so the long-term growth advantage was likely due to correct phasing of rhythmic processes relative to the environment in one genotype, and an incorrect phase in its competitor (*7*). This suggests that a correctly matched circadian clock confers a competitive advantage, whereas the enhancement of two key fitness traits [biomass and photosynthesis; (*14*–*17*)] by circadian resonance indicates that enhanced photosynthesis is one mechanism by which the clock increases fitness.

Our experiments demonstrate that the circadian clock allows plants to increase photosynthesis and that the clock underlies a doubling of *Arabidopsis* productivity. This may derive from correct anticipation of dawn and dusk, and synchronization of the synthesis of light-harvesting complex proteins and chlorophyll, both of which are unstable in their unbound state (*18*). Incorrect matching of endogenous rhythms to environmental rhythms reduced leaf chlorophyll content, reduced assimilation, reduced growth, and increased mortality. Optimization of these parameters by circadian resonance could represent one of the mechanisms that has selected for circadian clock function during plant evolution. We suggest that selective plant breeding for enhanced crop performance must be performed carefully, because phase and period changes could arise from the close genetic linkage of phase and period loci (*31*) to the trait under selection, and cause alterations to clock function that might reduce vegetative yield. Clock manipulation could enhance food production during exploration of space and other planets, where the light-dark cycle may differ from the terrestrial 24-hour period. Circadian resonance is likely to provide an advantage in all kingdoms, because resonance of the internal clock with the external light-dark cycle ensures an optimal phase relation between physiology and the day-night cycle and provides the basis for anticipation of changes in environmental conditions.

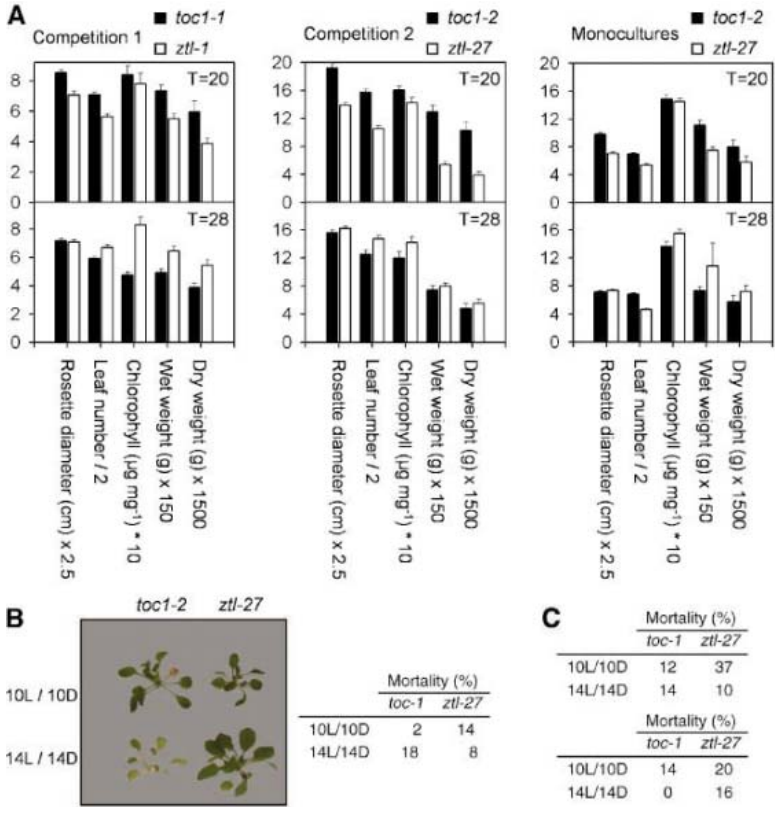

Fig. 4. Correct circadian period enhances growth and survival. (**A**) In two separate competition experiments using different mutant lines and one monoculture experiment, comparative growth and survival of *toc1* and *ztl* under T20 and T28; $n = 49$, except $n = 17$ to 20 for dry biomass values; data are means ± SEM. (**B**) Representative individuals from a competition experiment. Mortality in short- and long-period lines after competition (B) or monoculture (**C**) in T20 and T28.

References and Notes

1. C. H. Johnson, M. Knight, A. Trewavas, T. Kondo, in *Biological Rhythms and Photoperiodism in Plants*, P. L. Lumsden, A. J. Millar, Eds. (Bios Scientific, Oxford, 1998), pp. 1–34.
2. M. W. Young, S. A. Kay, *Nat. Rev. Genet.* **2**, 702 (2001).
3. M. J. Yanovsky, S. A. Kay, *Curr. Opin. Plant Biol.* **4**, 429 (2001).
4. T. P. Michael *et al.*, *Science* **302**, 1049 (2003).
5. R. M. Green, S. Tingay, Z. Y. Wang, E. M. Tobin, *Plant Physiol.* **129**, 576 (2002).
6. H. R. Highkin, J. B. Hanson, *Plant Physiol.* **29**, 301 (1954).
7. Y. Ouyang, C. R. Andersson, T. Kondo, S. S. Golden, C. H. Johnson, *Proc. Natl. Acad. Sci. U.S.A.* **95**, 8660 (1998).
8. M. A. Woelfle, Y. Ouyang, K. Phanvijhitsiri, C. H. Johnson, *Curr. Biol.* **14**, 1481 (2004).
9. Materials and methods are available on *Science* Online.
10. D. E. Somers, T. F. Schultz, M. Milnamow, S. A. Kay, *Cell* **101**, 319 (2000).
11. A. J. Millar, I. A. Carré, C. A. Strayer, N.-H. Chua, S. A. Kay, *Science* **267**, 1161 (1995).
12. Z. Y. Wang *et al.*, *Plant Cell* **9**, 491 (1997).
13. R. Hayama, G. Coupland, *Curr. Opin. Plant Biol.* **6**, 13 (2003).
14. A. M. Arntz, E. H. DeLucia, N. Jordan, *Ecology* **81**, 2567 (2000).
15. J. K. Ward, J. K. Kelly, *Ecol. Lett.* **7**, 427 (2004).
16. P. S. Curtis, X. Wang, *Oecologia* **113**, 299 (1998).
17. T. Mitchell-Olds, *Evol. Int. J. Org. Evol.* **50**, 140 (1996).
18. S. L. Harmer *et al.*, *Science* **290**, 2110 (suppl. data) (2000).
19. A. Prombona, J. Argyroudi-Akoyunoglou, *Plant Sci.* **167**, 117 (2004).
20. K. Kaasik, C.-C. Lee, *Nature* **430**, 467 (2004).
21. A. P. Withrow, R. B. Withrow, *Plant Physiol.* **24**, 657 (1949).
22. J. D. Plautz *et al.*, *J. Biol. Rhythms* **12**, 204 (1997).
23. A. N. Dodd, K. Parkinson, A. A. R. Webb, *New Phytol.* **162**, 63 (2004).
24. D. E. Somers, A. A. R. Webb, M. Pearson, S. A. Kay, *Development* **125**, 485 (1998).
25. H. Griffiths *et al.*, in *Physiological Plant Ecology*, M. C. Press, J. D. Scholes, M. G. Barker, Eds. (Blackwell, Oxford, 1998), pp. 415–441.
26. T. L. Hennessey, C. B. Field, *Plant Physiol.* **96**, 831 (1991).
27. D. Alabadí *et al.*, *Science* **293**, 880 (2001).
28. N. Salathia *et al.*, unpublished observations.
29. M. J. Yanovsky, S. A. Kay, *Nature* **419**, 308 (2002).
30. L. C. Roden, H. R. Song, S. Jackson, K. Morris, I. A. Carré, *Proc. Natl. Acad. Sci. U.S.A.* **99**, 13313 (2002).
31. D. E. Somers, W.-Y. Kim, R. Geng, *Plant Cell* **16**, 769 (2004).

32. Authors E.K., R.T., A.H., and A.J.M. identified *ztl-27*; N.S. and A.J.M. conceived and performed competition and seedset experiments with A.H.; A.N.D., J.M.H., and A.A.R.W. performed all other experiments. We thank the U.K. Biotechnology and Biological Sciences Research Council (A.A.R.W., J.M.H., and A.J.M.); the Royal Society of London and the Isaac Newton Trust (A.A.R.W.); and the Howard Hughes Medical Institute (F.N.). We are grateful to E. Tobin (UCLA) and S. Kay (Scripps) for collaboration and donation of *CCA1*-ox and *toc1-2*, respectively.

Supporting Online Material

www.sciencemag.org/cgi/content/full/309/5734/630/DC1
Materials and Methods
References and Notes

1 April 2005; accepted 7 June 2005
10.1126/science.1115581

Antibodies for Fluorescent Proteins

The BD Living Colors Anti-RCFP Polyclonal Pan Antibody detects any reef coral fluorescent proteins, including AmCyan, ZsGreen, ZsYellow, DsRed2, DsRed-Express, HcRed, and AsRed, in protein immunoblotting. Importantly, it does not recognize EGFP nor AcGFP1. The ZsGreen Polyclonal Antibody specifically detects *Zoanthus* green fluorescent protein (ZsGreen). It can be used to identify and confirm fusion constructs in bacteria and mammalian cells and does not cross-react with other fluorescent proteins.

BD Biosciences Clontech For information 877-232-8995 www.bdbiosciences.com

X-Ray Diffraction Detectors

New XRD^2 methodology for X-ray diffraction (XRD) represents a powerful solution for demanding applications in materials research, high-throughput screening, nanotechnology, and thin-film research. XRD^2 stands for X-ray analysis by means of a two-dimensional detector with large scattering angle coverage. XRD^2 allows simultaneous identification and quantification of all crystalline and amorphous phases in a sample, as well as the determination of their atomic arrangements and distortions with high speed and accuracy. Combining speed and accuracy without compromise is the major progress over traditional XRD systems, which are typically optimized for either high speed or high accuracy.

Bruker Biosciences For information 978-663-3660 www.bruker-biosciences.com

High-Performance Liquid Chromatography System

Expanded functionality doubles the throughput of the ExpressLC-800 rapid gradient high-performance liquid chromatography (HPLC) system. New software drivers and hardware accessories support CTC Analytics' TwinPAL Autosampler, ensuring sample delivery at a pace that fully optimizes the throughput of the eight-channel HPLC system. Suitable for a range of drug discovery applications that run up to thousands of samples per day, the ExpressLC-800's eight fully independent channels provide flexibility, time savings, and cost savings. Each chromatographic channel can deliver as much as six times the sample throughput of a conventional HPLC instrument and requires only 25% of the bench space. The dual autosampler capability is now standard, and existing systems can be upgraded. The ExpressLC-800 can now accept samples in two formats—regular 2 ml vials or 96-well microplates, either deep or shallow well.

Eksigent Technologies
For information 925-960-8869
www.eksigent.com

Graphing and Data Analysis Software

The latest version of KaleidaGraph has been designed to allow scientists, researchers, and engineers who need to graph, analyze, and communicate the results of their critical research the ability to greatly improve the visual impact of their data. The new version features significant axes improvements to provide researchers with a more effective tool for making their important data more visually representative on their graphs. Axes can now be broken down to allow a user to easily show a graph that contains large gaps in data. Linear and log scales can be used on both sides of the break. Axes can now be moved and placed at a set value. Offset axes can be created by dragging the x and y axes away from the plot. Two axes can even be positioned on the same side of the plot.

Synergy Software For information 610-779-0522 www.synergy.com

Liquid Chromatograph/Mass Spectrometer

The LCMS-IT-TOF Liquid Chromatograph/Mass Spectrometer (LC/MS) is a novel hybrid mass spectrometer for biomarker discovery, metabolite identification, and proteomics research. Coupling atmospheric pressure ionization with ion-trap (IT) and time-of-flight (TOF) technologies, the LCMS-IT-TOF delivers high mass accuracy and high mass resolution (10,000 at 1000 m/z) independent of MS mode. This instrument has been designed to maximize sensitivity and selectivity by optimizing the ion transport to the TOF analyzer and redefining the capability of the quadrupole ion trap. The ion trap is used not only to focus ions before ejection into the TOF, but it also supports fragmentation, MS^n analysis, and a high precursor ion selection (resolution >1,000 at 1,000 m/z). A high precursor ion selection allows specific ions to be isolated for further fragmentation, simplifying MS/MS data interpretation and enhancing the selectivity of detection, particularly from complex matrices.

Shimadzu For information 800-477-1227 www.ssi.shimadzu.com

Multibeam Tweezers

The mmi CellManipulator is an optical trap that enables precise, contact-free manipulation of microscopic particles. The optical tweezers make use of a focused laser beam to trap, move, and position single cells or subcellular and microscopic particles in a size range of approximately 0.1 to 200 μm. The instrument has applications in cell sorting, cell fusion, cell–cell interactions, measurement of binding forces or viscosities, and neuroscience-related applications.

MMI Molecular Machines & Industries
For information 603-629-9536
www.molecular-machines.com

Nucleic Acid Stain Kit

The SilverSure Nucleic Acid Stain Kit provides results in less than 30 min. The kit can be used for detecting either DNA or RNA in any type of agarose used for separation. There is no need for any chemical mutagens or ultraviolet transilluminators. The kit is less toxic than ethidium bromide, with equal sensitivity. It is compatible with most types of agarose and does not interfere with polymerase chain reaction or cloning of excised bands.

Amresco For information 800-448-4442 www.amresco-inc.com

Newly offered instrumentation, apparatus, and laboratory materials of interest to researchers in all disciplines in academic, industrial, and government organizations are featured in this space. Emphasis is given to purpose, chief characteristics, and availability of products and materials. Endorsement by *Science* or AAAS of any products or materials mentioned is not implied. Additional information may be obtained from the manufacturer or supplier by visiting www.science.labvelocity.com on the Web, where you can request that the information be sent to you by e-mail, fax, mail, or telephone.

ScienceCareers.org

Classified Advertising

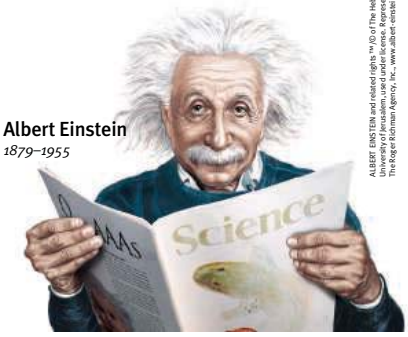

Albert Einstein
1879–1955

For full advertising details, go to **www.sciencecareers.org** and click on **How to Advertise,** or call one of our representatives.

United States & Canada

E-mail: advertise@sciencecareers.org
Fax: 202-289-6742

JILL DOWNING
(CT, DE, DC, FL, GA, MD, ME, MA, NH, NJ, NY, NC, PA, RI, SC, VT, VA)
Phone: 631-580-2445

KRISTINE VON ZEDLITZ
(AK, AZ, CA, CO, HI, ID, IA, KS, MT, NE, NV, NM, ND, OR, SD, TX, UT, WA, WY)
Phone: 415-956-2531

KATHLEEN CLARK
Employment: AR, IL, LA, MN, MO, OK, WI, Canada; Graduate Programs; Meetings & Announcements (U.S., Canada, Caribbean, Central and South America)
Phone: 510-271-8349

EMNET TESFAYE
(Display Ads: AL, IN, KY, MI, MS, OH, TN, WV; Line Ads)
Phone: 202-326-6740

BETH DWYER
(Internet Sales Manager)
Phone: 202-326-6534

Europe & International

E-mail: ads@science-int.co.uk
Fax: +44 (0) 1223-326-532

TRACY HOLMES
Phone: +44 (0) 1223-326-525

HELEN MORONEY
Phone: +44 (0) 1223-326-528

CHRISTINA HARRISON
Phone: +44 (0) 1223-326-510

JASON HANNAFORD
Phone: +81 (0) 52-789-1860

To subscribe to *Science*:
In U.S./Canada call 202-326-6417 or 1-800-731-4939
In the rest of the world call +44 (0) 1223-326-515

Science makes every effort to screen its ads for offensive and/or discriminatory language in accordance with U.S. and non-U.S. law. Since we are an international journal, you may see ads from non-U.S. countries that request applications from specific demographic groups. Since U.S. law does not apply to other countries we try to accommodate recruiting practices of other countries. However, we encourage our readers to alert us to any ads that they feel are discriminatory or offensive.

Largest bonus distribution of the year

Careers and Graduate Programs for

B.S. & M.S. Scientists

A *Science* Advertising Supplement

Issue date 26 August 2005
Reserve ad space by 9 August 2005

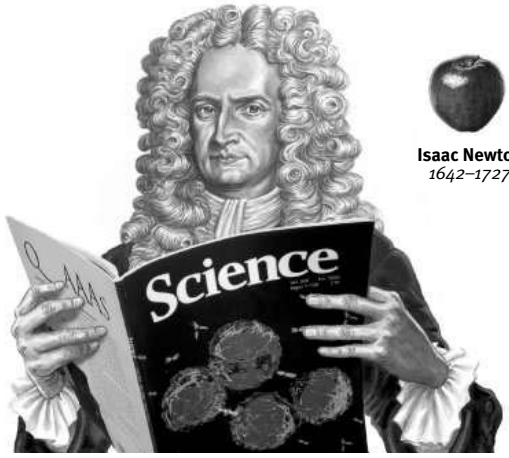

Isaac Newton
1642–1727

Largest Bonus Distribution of the Year!

Over 8,500 issues distributed to the top U.S. Biology and Chemistry programs. Total global weekly readership of over 710,000* that includes over 18,000 B.S. and M.S. level *Science* subscribers.

ScienceCareers.org postings available—7 websites for the price of one! If you post your job online, it is also searchable on these websites: Stanford University School of Medicine, National Postdoctoral Association (NPA), Biocompare, *Science*'s Signal Transduction Knowledge Environment (STKE), *Science*'s Aging Knowledge Environment (SAGE), and *Science*'s Next Wave.

1 *Science* June 2004 circulation of 129,590 as applied to 14 January 2000 Harvey Research Readership Survey and 2002 Harvey Research Cumulative Report, publisher's own data.

For more information, contact Daryl Anderson:
202-326-6543 – advertise@sciencecareers.org

ScienceCareers.org

Positions @ NIH
THE NATIONAL INSTITUTES OF HEALTH

National Institute of Neurological Disorders and Stroke
Office of Science Policy and Planning
Health Science Policy Analyst Position

The National Institute of Neurological Disorders and Stroke (NINDS), located in Bethesda, Maryland, part of the National Institutes of Health, Department of Health and Human Services, is seeking applications for a Health Science Policy Analyst vacancy in its Office of Science Policy and Planning (OSPP) in the Office of the Director. The incumbent is responsible for analyzing and monitoring developments in neuroscience as they affect NINDS programs; for furnishing policy and programmatic guidance and assistance as required to Institute scientific program staff; and for consulting with the Institute leadership and other key staff regarding the many policy issues relevant to NINDS, NIH, and DHHS. The ability to function independently in a staff capacity, and to develop collaborative relationships to prepare reports and analyses of research findings; to prepare written testimony and related briefing materials for Congressional hearings; to coordinate strategic planning efforts; to attend, plan, and coordinate meetings for the NINDS; and to evaluate Institute research agendas and scientific initiatives is essential.

The ideal candidate should have knowledge of current issues in neuroscience or a related scientific or clinical field comparable to the Ph.D. level; a good understanding of biomedical research administration and funding; experience in policy analysis and development; experience interacting and coordinating work efforts with a wide range of individuals including high-level program and administrative managers and scientists; and outstanding communication skills, including the ability to translate complex medical research concepts orally and in writing to a variety of audiences. This is a civil service position that will be filled at the GS-12 or GS-13 grade level; promotion potential to the GS-14 grade level is possible. The salary range of GS-12 is $62,886-$81,747; the GS-13 range is $74,782-$97,213. Please send a curriculum vitae, resume or an Optional Application for Federal Employment, OF-612 to: **Nicole Moore, 6120 Executive Plaza, Suite 200, Rockville, MD 20892**

Applicants are strongly encouraged to apply on-line through USA Jobs. Supporting documents may be faxed to **(301) 480-2503** or sent via e-mail to **mooren@mail.nih.gov**. Please be aware that if all the requested supporting documents are not submitted before the closing date, it will result in non consideration of your application. The NINDS has a strong commitment to the diversity of its workforce and a biomedical research environment that reflects the diversity of the American population **(http://oeo.od.nih.gov/)**. When applying for this vacancy, please make sure to reference which vacancy announcement number you are applying to. For information on how to apply for the Health Science Policy Analyst vacancy, and for the full vacancy announcement, please go to: **(http://jobsearch.usajobs.opm.gov/getjob.asp?JobID=31797224)**

Molecular Imaging Program

With nation-wide responsibility for improving the health and well being of all Americans, the Department of Health and Human Services (DHHS) oversees the biomedical research programs of the National Institutes of Health (NIH) and those of NIH's research Institutes.

The Molecular Imaging Program (MIP) of the Center for Cancer Research, National Cancer Institute (NCI), NIH is seeking applicants for the following positions:

- Staff Scientist, Molecular Biology
- Research Fellow, Synthetic Organic Chemistry and/or Radiochemistry

The MIP is a multidisciplinary program that designs, develops and tests imaging probes targeted to cancer for diagnosis and treatment. We are seeking individuals with expertise in Molecular Biology and experience in animal models of cancer, tumor vaccines, immunology and humanizing tumor antigens for a Staff Scientist Position. A Ph.D. and at least 10 years of independent research experience are required.

We are also seeking Research Fellows with training in molecular probe chemistry, optical imaging and/or radiochemistry with experience in linking molecular targets of biologic importance to imaging probes. A Ph.D. is required.

Salary for both positions commensurate with experience. Candidates should send a cover letter, curriculum vitae and names and addresses of three references to: **Peter L. Choyke, M.D. Chief, Molecular Imaging Program, Center for Cancer Research, NCI, NIH, Building 10, Room B3B69, Bethesda, Maryland 20892-1002. Electronic applications will be accepted at mip@nih.gov.**

Postdoctoral Training Positions
Translational Cancer Genomics

The Oncogenomics Section, at the National Cancer Institute, NIH, has two post-doctoral training positions available in translational genomics. Ongoing research efforts involve genomic and proteomic approaches to the investigation of Neuroblastoma. Using these approaches we have identified prognostic markers and potential new therapeutic targets in cancers. The candidate will work on combining molecular and genomic approaches to validate these targets both in vitro and animal models to bring these reagents to the clinic. The candidate should hold either a Ph.D. or M.D. degree and have an interest in oncology and significant experience in genomics and the microarray technology. Experience in mouse/animal models is preferred. Candidates should have less than five years post-doctoral experience.

Correspondence, names of references and CV should be sent to **Dr. Javed Khan, Advanced Technology Center, National Cancer Institute, Room 225B, 8717 Grovemont Circle, Gaithersburg, MD 20877, or via email at khanjav@mail.nih.gov**

WWW.NIH.GOV

National Institutes of Health

Virtual Career Center

at the tip of your mouse

www.training.nih.gov/careers

-EXPLORE CAREER OPTIONS
-CONTINUE YOUR EDUCATION
-SEARCH FOR A JOB

Careers in science, medicine, and beyond at the college, postbaccalaureate, graduate, and postdoctoral levels

Office of Intramural Training and Education
(800) 445-8283

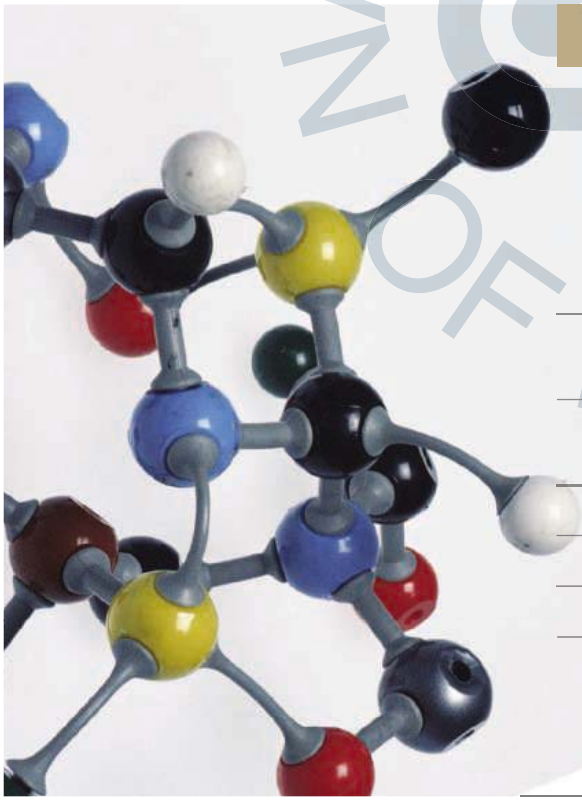

Postdoctoral Research Training at NIH

- Launch a career to improve human health
- Work in one of 1250 of the most innovative and well-equipped biomedical research laboratories in the world
- Explore new options in interdisciplinary and bench-to-bedside research
- Develop the professional skills essential for success
- Earn an excellent stipend and benefits
- Click on www.training.nih.gov

Office of Intramural Training and Education

GEORG-AUGUST-UNIVERSITY GÖTTINGEN
Bereich Humanmedizin

University Hospital – Faculty of Medicine

The following vacancy is available as of immediately in the Department of Biochemistry II, Centre for Biochemistry and Molecular Cell Biology at the Bereich Humanmedizin (University Hospital and Faculty of Medicine) of the Georg-August-University Göttingen:

UNIVERSITY PROFESSORSHIP FOR BIOCHEMISTRY
(SALARY GROUP W3)

In cooperation with the other departments at the Centre for Biochemistry and Molecular Cell Biology, the successful candidate will represent the entire subject area of Biochemistry in the medical curriculum. An outstanding record at international level in biochemical research is an essential prerequisite. It is expected that the successful candidate will contribute to and build upon the existing research foci of the department with his/her own thematic interests. Research cooperation with the clinical departments at the Faculty of Medicine is desired.

The departments at the Centre for Biochemistry and Molecular Cell Biology are involved in interdisciplinary initiatives in research and education, as well as profile-building research networks, in the area of Göttingen. The successful candidate will be expected to contribute to these activities.

In addition, a postdoctoral lecturer qualification (habilitation) or equivalent scientific achievements are required. A high level of commitment and experience in education is desirable.

The University of Göttingen is incorporated as a public trust. The requirements for the appointment to a professorship are enshrined in §25 of the Higher Education Act of Lower Saxony (NHG, Nds. GVBl 19/2002, S. 286 ff.). Details can be supplied on request.

The University of Göttingen aims to increase the percentage of female scientists employed and expressly invites applications from women. In the case of equal qualifications, women will be considered preferentially within the framework of the legal possibilities.

Persons with disabilities will be considered preferentially in cases of equal aptitude.

Part-time employment may be possible under certain circumstances.

Applications including Curriculum Vitae, a profile of the scientific career containing details of successful applications for third-party funding and experience in teaching, a structured index of publications together with six selected reprints are to be submitted within four weeks of this advertisement to the:

Dean of the Faculty of Medicine and Member of the Board of Directors for Research and Education, Bereich Humanmedizin, Georg-August-University Göttingen, Robert-Koch-Str. 42, D-37075 Göttingen.

GEORG-AUGUST-UNIVERSITÄT GÖTTINGEN
Stiftung Öffentlichen Rechts
Bereich Humanmedizin
Universitätsklinikum - Medizinische Fakultät
Zentrum Molekularphysiologie des Gehirns - CMPB

The Center of Molecular Physiology of the Brain (CMPB) in Göttingen, Germany, seeks applications for

PHD POSITIONS

to work in a team embedded in a dynamic and excellently equipped research environment on analysis of signalling pathways involved in regulation of specific neuronal functions (in particular neuronal morphology). The project will focuses on the quantitative analysis of protein-protein interaction within the living cells by using confocal microscopy combined with the foerster resonance energy transfer (FRET) techniques and will be partly supervised by Prof. Erwin Neher from Max-Plank-Institute for biophysical Chemistry.

CMPB is an excellence Research Center funded by the German Research Council (http://www.cmpb.org). The Center combines various university departments, the European Neuroscience Institute, the Max-Planck-Institutes for Biophysical Chemistry and Experimental Medicine as well as the German Primate Center.

Women are especially encouraged to apply. Handicapped applicants with equal qualifications will be given preferential treatment.

Motivated, enthusiastic individuals with an understanding of the neurosciences, biophysics and microscopy techniques send or email applications, incl. CV and names of references within four weeks after publication to:

University of Göttingen, Evgeni Ponimaskin, PhD, Associated Professor Center of Physiology, Humboldtallee 23, 37073 Göttingen, Germany. E-Mail: eponima@gwdg.de, Phone: + 49-551-397097; Fax + 49-551-396031.

UNIVERSITY OF OXFORD

Norman Collisson Professorship of Musculoskeletal Sciences

Applications are invited for the above post, tenable from 1st October 2006, or such later date as may be arranged. The Norman Collisson Professor of Musculoskeletal Sciences will be expected to play a leading role in the research activity of the Nuffield Department of Orthopaedic Surgery. The professorship is a key post in relation to the future management and success of the Botnar Research Centre based in the Nuffield Orthopaedic Centre. The successful candidate will have an outstanding track record in research in the musculoskeletal sciences and a demonstrable ability to compete for and to obtain substantial independent external grant support.

A non-stipendiary fellowship at St Peter's College is attached to the professorship.

The professor may or may not be clinically qualified.

Further particulars, including details of how to apply, are available from http://www.admin.ox.ac.uk/fp/ or from the Registrar, University Offices, Wellington Square, Oxford OX1 2JD, tel. (01865) 270200. The closing date for applications is 5th September 2005.

The University is an Equal Opportunities Employer.

DUPONT

The miracles of science™

TEAM LEADER, METABOLISM and MECHANISTIC TOXICOLOGIST

(Job #RES00310)

DuPont is seeking a Team Leader, Metabolism and Mechanistic Toxicologist, to work at Haskell Laboratory located in Newark, Delaware. Haskell Laboratory for Health and Environmental Sciences is a full service toxicology laboratory.

The successful candidate will:

(1) be responsible for the development of several technologies in biochemistry, genetics and computational toxicology, aimed at supporting the future toxicology needs of DuPont and potential third-party clients and alliances. These include computational metabolism and toxicity screening and in vitro approaches to assessing toxicology liabilities early in the product development path;
(2) design, conduct, and interpretation of appropriate studies to address potential human health or environmental hazard and risk of new or existing chemicals;
(3) effectively communicate findings to business and scientific audiences, through both oral presentations and written technical reports and manuscripts; and
(4) function as a scientific and team leader in a metabolism and mechanistic toxicology research group.

Minimum Requirements:

- PhD in Biomedical Science, Biochemistry, Metabolism, Computation Chemistry, or related field of study.
- Demonstrated expertise in mammalian metabolism chemistry and metabolite identification.
- Functional experience with in vitro assay and mammalian tissue culture techniques
- Functional experience and capability to conduct in-life dosing and tissue collection
- Experience in extraction technology and quantitative analytical separations chemistry such as GC and/or HPLC and methods of detection/analysis such as NMR, UV, radiometric and mass spectrometric techniques
- Excellent written and verbal communication skills
- Demonstrated ability to effectively function as a member of a high-performance toxicology team.

The following are highly desirable: proven scientific leadership, experience in quantitative risk assessment, ADME expertise, computational toxicology experience, molecular biochemistry experience.

DuPont offers an attractive salary and comprehensive benefits. Qualified candidates should apply through DuPont's career web page: **http://careers.dupont.com**. Click on Jobs by Region, United States, View US Job Listings. Then enter the job code (RES00310) in the Keyword Field (Use the new search button for successive searches)

DuPont is an Equal Opportunity Employer.

FACULTY POSITIONS DEPARTMENT OF PHYSICS THE UNIVERSITY OF TEXAS AT AUSTIN

The Department of Physics at The University of Texas at Austin is seeking candidates for tenure-track assistant professorship positions in physics starting in September, 2006. In special cases, appointments at more senior levels will be considered. Successful candidates will assume full teaching responsibilities for undergraduate and graduate courses in the Department of Physics and are also expected to conduct vigorous research programs. Research areas of current highest priority for the Department are Biophysics/Soft-Condensed Matter Experiment, Cosmology/Relativity Theory, AMO/Quantum Information Science, Condensed Matter/Nanoscience Experiment, and Particle/Astrophysics Experiment. Outstanding candidates in other areas of departmental focus will also be considered. Excellent English language communication skills are required. Applicants must have a Ph.D. (or equivalent) and a demonstrated potential for excellence in teaching and research.

Interested applicants should send a curriculum vitae, a list of publications, a statement of research interests, a research plan, and should arrange for at least five letters of recommendation to be sent to: **Prof. John T. Markert, Chair, Department of Physics, The University of Texas at Austin, 1 University Station C1600, Austin, TX 78712-0264**. Review of completed applications will begin in **October, 2005**.

The University of Texas at Austin is an Equal Opportunity/Affirmative Action Employer.

UNIVERSITY OF NOTRE DAME

Endowed Chair in Cell Biology
Department of Biological Sciences

The Department of Biological Sciences at the University of Notre Dame invites applications for a newly created Endowed Chair at the Full Professor rank. Applicants must demonstrate an exceptional record of research accomplishment based on publications, national/international recognition and extramural funding. We seek an outstanding scientist studying exciting problems in the general area of cell biology; including but not limited to cell signaling, cell adhesion and migration, membrane trafficking, the cell cycle, cell morphogenesis and host-pathogen interactions. The successful candidate will be a cooperative scientific leader who will strengthen the existing cell motility, endocrinology, neuroscience and/or infectious disease emphases within the Department and the College of Science. Ample opportunities exist for collaborations with multiple interdisciplinary Centers within the University, including the Walther Cancer Research Center, the Center for Tropical Diseases, the Keck Center for Transgene Research, and the Interdisciplinary Center for the Study of Biocomplexity. Additional information on the department, its faculty and facilities is available at **http://biology.nd.edu**.

Applications will be accepted until the position is filled, but review will commence immediately. Qualified individuals should send their curriculum vitae, the names and addresses of five references, a summary of current research and teaching interests, plus future research goals to:

Chair, Cell Biology Search Committee
Department of Biological Sciences
University of Notre Dame
Notre Dame, IN 46556-0369

For more information, email the search chair (**Dr. A.L. Johnson**) at **johnson.128@nd.edu**.

The University of Notre Dame is an Affirmative Action/Equal Opportunity Employer. Women and minority candidates are encouraged to apply.

UCSF

University of California, San Francisco
Post-doctoral Fellowship
Tissue Engineering

The Department of Orthopaedic Surgery at the UCSF announces an opening for a post-doctoral fellowship that will focus on musculoskeletal tissue engineering utilizing mesenchymal stem cells. The successful candidate will apply the principles of bioengineering and biology to generate/develop innovative technologies that restore, maintain, or improve the function of human skeletal and connective tissues. Research may include the design and growth of tissues outside the body for later implantation, the implantation of cell-containing or cell-free devices, or the development of external or internal devices containing human tissues designed to improve function. This position will be supported by two current NIH grants that focus on stem cell characterization and intervertegral disc regeneration.

Candidates should have background in bioengineering and molecular biology with a focus on biomaterials and cell/matrix interaction. He/she should have a strong record of research activity, the proven capacity to attract research funding, and will be expected to have leadership and administrative abilities in a multidisciplinary environment. Candidate will be expected to serve as a research supervisor for doctoral candidates, and interact with students and faculty at all levels.

Send curriculum vitae and names of references to: **Dr. J.C. Lotz, Department of Orthopaedic Surgery, University of California, San Francisco, 533 Parnassus Ave., San Francisco, CA 94143-0514; Fax: 415-476-1128; E-mail: jlotz@itsa.ucsf.edu**.

The **Department of Surgery at the University of California, San Francisco** is recruiting a basic scientist at the **Associate/Full Professor** level with interests in the broad area of regenerative medicine and tissue engineering. Individuals with interests in artificial matrices, three-dimensional organotypic models or stem cell biology/tissue regeneration are encouraged to apply. This individual is being recruited to lead a new initiative within the Department of Surgery to conduct translational research and interact with members in the Department of Surgery conducting research in skin, cardiovascular, islet, bone and liver regeneration.

The individual will also have the opportunity to train residents and fellows. In addition they will be expected to actively participate in the broader UCSF Regenerative Medicine initiative. The successful candidate will be a member of the Biomedical Sciences Graduate Program and will be jointly appointed in an appropriate basic science department.

Please submit curriculum vitae, statement of research interests and the names and addresses of three references to:

Tissue Engineering Search Committee
c/o Nancy Boudreau, Ph.D.
Department of Surgery
Box 1302
University of California
San Francisco CA 94143-1302

The University of Edinburgh

The University of Edinburgh is an exciting, vibrant, research-led academic community offering opportunities to work with leading international academics whose visions are shaping tomorrow's world.

Senior Fellow (Senior Lecturer equivalent in Vascular Biology, non clinical)

£34,227 – £42,573

This is an exciting opportunity to build upon the strengths of the Centre for Cardiovascular Sciences (5* rated in RAE) and the University's £100M plus investment in biomedical research in the New Research Institute, adjacent to the University facilities and the New Royal Infirmary. This is a substantive, not a short-term post.

The Centre for Cardiovascular Science (www.cvs.med.ed.ac.uk) hosts world-class research groups active in Molecular Physiology, Inflammation Research, Molecular Endocrinology, Vascular Injury and Endothelial Cell and Molecular Cardiology. Members of the Centre have access to excellent core facilities including Transgenesis, Radiotelemetry, *in vivo* Imaging and Post Genomic Research facilities. In addition, the group has been awarded funding for a new imaging facility (7T MRI), with links to the SHEFC Brain Imaging Research Centre for Scotland (www.dcn.ed.ac.uk/bic) and Optical Projection Tomography, allowing innovative approaches to translational research.

With a strong track record of research publication in the field of Vascular Biology, you will establish an internationally competitive research team.

Formal enquiries to Professor Keith A A Fox, tel: 0131 242 6378 or e-mail: k.a.a.fox@ed.ac.uk

Apply online, view further particulars or browse more jobs at our website. Alternatively, telephone the recruitment line on 0131 650 2511. Ref: 3004707SI. Closing date: 26 August 2005.

Committed to Equality of Opportunity

www.jobs.ed.ac.uk

UMDNJ - ROBERT WOOD JOHNSON MEDICAL SCHOOL

POST-DOCTORAL RESEARCH FELLOWSHIP

Translational Cancer Research

Post-doctoral fellowship opportunities are available in translational cancer research at the Cancer Institute of New Jersey, UMDNJ-Robert Wood Johnson Medical School. The fellowships are funded by the National Cancer Institute, National Institutes of Health (1 T32 CA099946-01). The primary objective of this postdoctoral training program in translational cancer research is to provide candidates with the highest quality training and research experience so that they will be competitive in developing research careers in academia, government, and the private sector. The program integrates the highest quality of basic science laboratory studies with a fundamental understanding of the unique requirements of clinical translation of the discoveries. Postdoctoral candidates will be either Ph.D. holders who wish to develop careers in clinically relevant research or M.D. (M.D./Ph.D.) finishing their training (following their residency and/or fellowship) who wish to prepare for careers in academic medicine. Graduates of the postdoctoral program will be expected to be competitive for academic faculty positions and should be competitive for entry level funding awards at the R01 level.

To apply or obtain additional information contact the Director, Research Education: **Sunita Chaudhary, Ph.D., The Cancer Institute of New Jersey, 195 Little Albany Street, New Brunswick, NJ 08901. Fax: 732-235-9888 or E-mail: sunita.chaudhary@umdnj.edu.** UMDNJ is an Affirmative Action/Equal Opportunity Employer.

The Cancer Institute of New Jersey™ — NCI CCC A Comprehensive Cancer Center Designated by the National Cancer Institute

UMDNJ Robert Wood Johnson Medical School — University of Medicine & Dentistry of New Jersey

University of Heidelberg

Tschira Foundation Chair in Modelling and Simulation of Biological Systems University of Heidelberg

The Department of Biosciences of the University of Heidelberg is opening the above position which should further strengthen its role as one of the leading departments in European biological research.

The successful candidate will have a strong international reputation in the above field, and will be expected to initiate a top-class externally-funded research program and to contribute to teaching in the university. The Habilitation degree is not essential although equivalent experience is required. The position will be funded by a private foundation, the Klaus Tschira Stiftung, and is initially for five years.

The University of Heidelberg and the Heidelberg scientific research environment offer outstanding opportunities for creative research and teaching. The field of research should be related to the new research network 'Quantitative analysis of molecular and cellular biosystems (BIOQUANT)'. Heidelberg's molecular research arena offers outstanding scientific opportunities for developing interdisciplinary research projects. Excellent start-up conditions and a competitive salary will be offered. For further information on the University of Heidelberg and the Faculty of Biosciences see http://www.uni-heidelberg.de.

Applications including curriculum vitae, list of publications, teaching activities, grant applications, names and addresses of referees, and a short description of future research plans should be sent by **31.08.2005** to: **Prof. Dr. Jeremy C. Smith (Search Committee Chair), IWR, Im Neuenheimer Feld 368, D-69120 Heidelberg (Tel: +49 6221-54 8857)**

The University of Heidelberg has a policy of raising the proportion of women in academic positions and therefore specifically invites the application of women scholars with the necessary qualifications. Under German law disabled applicants with full qualifications are to be preferred.

U.S. DEPARTMENT OF VETERANS AFFAIRS
BIOMEDICAL LABORATORY R&D SERVICE
HEALTH SCIENCE OFFICER

The VA's Biomedical Laboratory R&D Service, is recruiting for a full-time Health Science Officer to manage the Agency's basic science and preclinical oncology research program. The **HEALTH SCIENCE OFFICER** will be responsible for portfolio management and administration of VA research related to oncology and will assist with the proposal review process. Ideal candidates will have a Ph.D. degree with a research background in a relevant area. Experience in grant writing and/or review is desirable. The position is located at VA Central Office, Washington, DC.

Closing date: **August 5, 2005**. To view full vacancy announcement, go to site below and type in **AR366584** in keyword search.

http://jobsearch.usajobs.opm.gov/

Follow instructions in the announcement or contact the OPM office below to apply.

Office of Personnel Management
Raleigh Service Center
4407 Bland Road Suite 200
Raleigh, NC 27609
(919) 790-2864

EOE

Johnson & Johnson

Research & Development Scientific Positions Available in Rochester, NY

Ortho-Clinical Diagnostics, a Johnson & Johnson company, is a leading provider of high value diagnostic products and services for the global health care community. Committed to developing the most advanced tests for early detection or diagnosis of disease, the Company brings products to market that provide timely information and help to facilitate better medical decisions. Worldwide, health care professionals rely on Ortho-Clinical Diagnostics for innovative diagnostic solutions that promote effective diagnoses and enhanced patient care.

We are currently seeking forward thinking, passionate R&D Scientists in the fields of Assay Development, Assay Research, and Chemistry (Materials and Process Development) to support a number of cutting edge programs in Immunodiagnostics, Clinical Chemistry, and Immunohematology.

Job #: 0502015 **Sr. Scientist - Assay R&D**
0505586 **Research Fellow - Chemistry**
0502407 **Sr. Scientist - Chemistry**
0502735 **Sr. Scientist - Immunohematology**
0509174 **Principal Scientist - Clinical Chemistry**
0508091 **Principal Scientist - Assay R&D**

We are looking for candidates with a BS or advanced degree in Biological Sciences with industry experience in the development of medical diagnostic tests. Qualified candidates should apply for these and other challenging opportunities on: **https://www.jnj.com/careers/exp_search.html** and reference the appropriate job number. No phone calls please.

Ortho-Clinical Diagnostics is committed to providing Equal Opportunity to a diverse workforce.

The University of Montana

ASSOCIATE DEAN
Division of Biological Sciences
University of Montana

ASSOCIATE DEAN and **PROFESSOR** to lead the Division of Biological Sciences. The Division offers undergraduate, MS, and PhD degrees in a variety of biological disciplines (**http://biology.dbs.umt.edu/dbs/**). The 40 faculty are committed to excellence in teaching and research. The Division is a vigorous group; faculty received over $12 million in new grants last year. We are looking for someone with vision and leadership who has the desire and skills to enhance development of the Division. Applicants must have a doctoral degree in a biological science, evidence of excellence in teaching and research, and strong administrative and communication skills.

Send CV, contact information for five references, and letter of interest that includes a statement of leadership philosophy and career goals, as well as a description of research and teaching accomplishments to:

Chair
Assoc. Dean Search Committee
Division of Biological Sciences
University of Montana
Missoula, MT 59812

We will begin reviewing applications on **12 September 2005**. For more information see the web page above or contact **fred.allendorf@umontana.edu**. The University has been awarded an NSF ADVANCE grant to support an increase in the number of women faculty in the sciences and mathematics (**http://pace.dbs.umt.edu/default.aspx**).

AA/EOE.

Harvard School of Dental Medicine
Biomaterials Scientist
Stem Cell Biology and Regulation of Stem Cell Differentiation

The Harvard School of Dental Medicine is initiating a search for an established investigator in stem cell biology and regulation of stem cell differentiation to join the Faculty of Medicine of Harvard University on or before July 1, 2006.

Qualifications for this position include a DDS/DMD/MD degree or equivalent, and/or a PhD degree, postdoctoral experience and 3-5 years of funded research. Academic rank will be dependent upon the candidate's experience and achievement.

The successful candidate will be based in The Department of Restorative Dentistry and Biomaterials Sciences at the Harvard School of Dental Medicine, which has recently restructured and realigned departments to enhance its mission in research, teaching and patient care. A new Research and Education Building was completed in the fall of 2004. The building offers 25,000 square feet of new research space designed to foster innovative, interdisciplinary and interdepartmental research in mucosal and skeletal biology and pathology. The facilities are located in the Harvard Medical Area, with the basic science departments of Harvard Medical School and the recently founded Department of Systems Biology, as well as the research and clinical facilities of several Harvard teaching hospitals, a few steps away, providing unlimited opportunities for collaboration with leading investigators in stem cell biology and tissue engineering. Harvard University's Stem Cell Initiative and the potential for collaboration with MIT and other outstanding hospitals and institutions in Boston and Cambridge further add to the exceptionally rich scientific environment. The position offers the opportunity to work with and mentor outstanding students, postdoctoral fellows and junior faculty members.

Interested applicants should send *curriculum vitae* and names of 3 references to: **Dr. Hans-Peter Weber, Professor and Chair, Department of Restorative Dentistry and Biomaterials Sciences, Harvard School of Dental Medicine, 188 Longwood Avenue, Boston, MA 02115; (hpweber@hsdm.harvard.edu).**

Harvard is an Equal Opportunity Employer.

PIONEER
A DuPont Company

Director, Bioinformatics and Computational Biology – Research Information Management

Pioneer Hi-Bred International, Inc, a DuPont company, is the world leader in the discovery, development and delivery of elite crop genetics. We are seeking a Director of Bioinformatics and Computational Biology. This individual will provide leadership and direction for computer application development and user support for the Crop Genetics Research Discovery organization. This position will be located at either our Johnston, IA or Wilmington, DE location. A Ph.D. in molecular genetics, bioinformatics, plant biology, plant breeding/genetics, or related scientific field and 7+ years of relevant professional experience required. Demonstrated knowledge and experience in: developing and executing cross functional client-based IT strategies; managing and directing computer application development teams working in biological science; supporting laboratory and field scientists in application of Novel computer systems; developing innovative bioinformatics and system solutions to complex genetic problems; and familiarity with scientific technologies and analysis techniques of genomic data also required.

Req. ID for this position is **TA312**. To view a complete job description and to apply visit:
http://www.pioneer.com

EOE

Center Director
The Ecosystems Center
Marine Biological Laboratory

The Marine Biological Laboratory (MBL), an international research and educational institution founded in 1888 and located in Woods Hole, Massachusetts, invites applications and nominations for the position of Director of The Ecosystems Center.

Established in 1975, The Ecosystems Center is the largest of the MBL's resident research centers. It operates as a collegial association of scientists under the leadership of the center director and carries out research and education in systems ecology. Eleven senior terrestrial and aquatic scientists and their staffs work in a wide variety of ecosystems ranging from the streams, lakes, and tundra of the Alaskan Arctic to sediments of Massachusetts Bay, to forests in New England and South America, and to large estuaries in the Gulf of Maine. In addition, Center scientists are actively involved in a collaborative project between the MBL and Brown University that includes joint courses and an active Ph.D. program. Center faculty offer a semester-long educational program for undergraduates from a consortium of 60 colleges and universities nation-wide. More information available at **www.mbl.edu/jobs**.

Applicants must have a Ph.D. in ecology or an associated area of science, an excellent publication record, and a demonstrated ability to attract federal and private support for research. The successful candidate will also have administrative experience including managing research groups and educational programs, a demonstrated ability to form consensus among individuals with different perspectives, and an ability to look to the future and set the direction for the Center, ensuring that it maintains its leadership position in the field of ecological science.

Application materials should include a letter that outlines the candidate's research interests, how his/her experience matches the position requirements, a curriculum vitae, and contact information for 3 references. Send to: **Center Director Search Committee, Marine Biological Laboratory, c/o Human Resources, 7 MBL Street, Woods Hole, MA 02543** or **resume@mbl.edu**. Applications will be accepted and reviewed as received until a successful applicant is identified.

An Equal Opportunity/Affirmative Action Employer/
Non-smoking Workplace.

USDA ARS Agricultural Research Service
www.ars.usda.gov

Research Molecular Biologist
Postdoctoral Research Associate

The U.S. Department of Agriculture, Agricultural Research Service, Plant Genetics Research Unit, St. Louis, MO, has an IMMEDIATE OPENING for an innovative scientist for a TWO YEAR APPOINTMENT. Salary is commensurate with experience ($50,708 - $79,006) plus benefits. The research involves structure-function studies on legume plant proteins which are also food allergens, including soybean P34 and peanut. This project aims to understand the structural basis for allergenicity in these proteins and to re-engineer them to remove the allergenic epitopes. Recent Ph.D. in biological or chemical sciences with emphasis in molecular biology is required. Demonstrated experience in macromolecular crystallography, including protein purification, protein crystallization, X-ray data collection, and subsequent structure determination is necessary.

Refer to **http://www.afm.ars.usda.gov/hrd/jobs** for further information and complete application instructions (**RA-05-065H**). Send application materials and references to: **Dr. Eliot Herman, Donald Danforth Plant Science Center, 975 North Warson Rd., St. Louis, MO 63132** or e-mail to: **eherman@danforthcenter.org**.

USDA/ARS is an Equal Opportunity Provider and Employer.

UCLA

University of California
Los Angeles
Faculty Position
in
Condensed Matter Theory

The Department of Physics and Astronomy at the University of California, Los Angeles invites applications for a new faculty position in condensed matter theory with an anticipated starting date of July 1, 2006. The department is seeking outstanding candidates with the potential for exceptional research and excellence in teaching. The search is focused at the tenure-track assistant professor level, but outstanding candidates at all levels will be considered. Special attention will be paid to candidates whose work is in the general field of correlated electron physics, either computational or analytical. The UCLA Department of Physics and Astronomy has very active research programs that span the range of condensed matter physics, including superconductivity, superfluidity, quantum magnetism, quantum phase transitions, the quantum Hall effect, disordered systems, dissipative quantum systems, quantum computation and statistical mechanics.

Prospective applicants should submit a curriculum vitae, statement of research interests, and publication list, and arrange to have at least three letters of recommendation sent to: **Chair, Physics Search Committee, Department of Physics and Astronomy, University of California, Los Angeles, CA 90095-1547** by the deadline of **December 1, 2005**. Applications received after the deadline will be considered on a case-by-case basis until the position is filled.

The University of California is an Equal Opportunity/Affirmative Action Employer.

POSITIONS OPEN

POSTDOCTORAL RESEARCH FELLOWSHIPS IN BLOOD CELL BIOLOGY
Joint Program in Transfusion Medicine
Harvard Medical School Affiliated Institutions
Boston, Massachusetts

Applications are now being accepted for Postdoctoral (M.D. or Ph.D.) Fellows who desire research careers in the expanding, multidisciplinary field of blood cell biology. The program offers a stimulating environment with various basic science and applied research opportunities, and is supported by senior faculty in the Departments of Pediatrics, Pathology, Hematology/Oncology, and Genetics. Fellows will conduct independent research for two years under the direction of one mentor, with opportunities for collaborative and inter-laboratory projects. The principal research fields include stem cell biology including immune modulation, gene therapy, cancer immunology, platelet biology, and hematopoiesis. Publication in an international peer-reviewed journal is a prerequisite for acceptance into the program. Send curriculum vitae, statement of interest, and three references to: **Leslie E. Silberstein, M.D., Director, Joint Program in Transfusion Medicine, c/o Blair Owren, Children's Hospital, Boston, Karp Family Research Building, 10th Floor, Room 10217, 1 Blackfan Circle, Boston, MA 02115** or via **e-mail: blair.owren@childrens.harvard.edu.**

Affirmative Action/Equal Opportunity Employer.

LANDSCAPE ECOLOGIST, ASSISTANT OR ASSOCIATE PROFESSOR
Center for Environmental Science Appalachian Laboratory
University of Maryland

The Appalachian Laboratory (AL), University of Maryland Center for Environmental Science (UMCES), solicits applications for a Landscape Ecologist using a combination of geographic information system, remote sensing, modeling, and field experimentation to understand population, community, or ecosystem processes at broad spatial scales. We are especially interested in applicants who study the effects of land use (history, pattern, or change) on the functioning, sustainability, or restoration of forest ecosystems. Applicants should be willing to collaborate with UMCES faculty in multidisciplinary research focused on the Chesapeake Bay watershed. UMCES faculty members are also expected to participate in graduate education. The successful candidate must have completed a Ph.D. at the time of appointment, and must be able to generate external research funding. We anticipate making this appointment at the Assistant Professor level, but will consider exceptional candidates for appointment at the Associate Professor level.

To apply, send curriculum vitae, cover letter, research statement, selected reprints, and a list of four references (name, address, telephone, fax, and e-mail) to: **J. Edward Gates, Search Chair, Appalachian Laboratory, UMCES, 301 Braddock Road, Frostburg, MD 21532.** Review of applications will begin September 15, 2005, and will continue until the position is filled. Salary and benefits are competitive and dependent on qualifications.

UMCES is an Affirmative Action/Equal Opportunity Employer. We promote excellence through diversity and encourage all qualified individuals to apply.

Two NIH-funded **POSTDOCTORAL POSITIONS** are available immediately in the Department of Pediatrics, University of Southern California School of Medicine for qualified candidates to study molecular biology of lung development and disease in murine models. A Ph.D. or equivalent degree is required. Possibility for promotion to junior faculty for more advanced candidates. Competitive salary and benefits. Please apply to: **Parviz Minoo** at **e-mail: minoo@usc.edu** or **Changgong Li** at **e-mail: changgon@usc.edu.**

TENURE-TRACK FACULTY POSITION MICROBIOLOGY

The Department of Molecular and Cell Biology of The University of Texas at Dallas (UTD) (**website: http://www.utdallas.edu/biology/**) is now recruiting a tenure-track Microbiologist at any rank. Preference will be for an investigator who complements existing strengths in microbiology and microbial physiology (metabolism and mechanisms of signal transduction) and who shows evidence of a vigorous research program that is or will be externally supported. We are especially interested in the areas of bacterial agents important for biodefense, emerging infections, and/or host response to infection. The Department is actively involved in interdisciplinary research, graduate training at the doctoral level, and educating a select group of undergraduate students. The School of Natural Sciences and Mathematics and the School of Engineering and Computer Sciences are undertaking a major expansion, with an emphasis on recruiting faculty who can foster interdisciplinary interactions. This expansion includes the construction of a new building for science and engineering research, equipped with state-of-the-art facilities, including a BSL-3 laboratory. Applicants would desirably have at least two years of postdoctoral experience. The candidate will be expected to fully participate in graduate and undergraduate education. Review of all applications will begin immediately and will continue until the position is filled. Indication of sex and ethnicity for affirmative action statistical purposes is requested as part of the application but not required. Interested individuals should submit a letter of application, curriculum vitae, a statement of research plans and teaching interests, and have three letters of reference sent to:

Academic Search #2074
The University of Texas at Dallas
P.O. Box 830688, AD 23
Richardson, TX 75083-0688

UTD is an Affirmative Action/Equal Opportunity Employer.

POSTDOCTORAL POSITIONS IMMUNOLOGY

Postdoctoral positions in immunology are available to study the molecular and cellular basis by which interleukin (IL)–2 contributes to the development of CD4+CD25+ T regulatory cells. Other work seeks to establish high throughput methodology to evaluate the antigen-specificity of natural T regulatory cells. These projects offer the opportunity to develop new mouse models to investigate the contribution of T cell receptor and IL-2 signals for the thymic production of T regulatory cells. Candidates must have a Ph.D. or an M.D. degree. Prior experience in immunology and/or receptor signal transduction is preferred. Send curriculum vitae, description of research interests, and names of three references to: **Dr. Thomas Malek, Department of Microbiology and Immunology, University of Miami School of Medicine, P.O. Box 016960, Miami, FL 33101. E-mail: tmalek@med.miami.edu.**

ASSISTANT OR ASSOCIATE PROFESSOR

A full-time position at the Assistant or Associate Professor level is available in the Department of Pathology of the College of Medical Sciences/Health Professions Division at Nova Southeastern University in Ft. Lauderdale, Florida. The candidate's responsibilities will include participation in teaching of pathology courses to students of Health Professions Division, faculty development and service. Individuals with teaching experience in general and systematic pathology at the medical school level will be given special consideration. The position requires a D.O., M.D., or Ph.D. degree. Although primarily a teaching position, opportunities for research do exist. Salary is dependent on qualifications. Please apply online to position #998761 at **website: http://www.nsujobs.com.** *Affirmative Action/Equal Opportunity Employer.*

PURDUE UNIVERSITY

ASSISTANT PROFESSOR
Forest Entomology

The Department of Entomology at Purdue University invites outstanding candidates specializing in insect-plant interactions of forest systems to apply for an academic year, tenure-track faculty position. Individuals with a strong research background and novel experience are urged to submit their applications. Visit **website: http://www.entm.purdue.edu/employment/forest>** for details. To apply send curriculum vitae, relevant reprints, transcripts, a statement of research and teaching goals, and contact information of five references to: **C. S. Sadof, Search Chair, Department of Entomology, 901 W. State Street, Smith Hall, Purdue University, West Lafayette, IN 47907-2089. Telephone: 765-494-5983; fax: 765-494-2152; e-mail: csadof@purdue.edu.** Screening of applicants will begin on September 1, 2005, and continue until the position is filled. *Purdue University is an Equal Opportunity/Equal Access/Affirmative Action Employer.*

The Department of Infectious Diseases, College of Veterinary Medicine, University of Georgia, invites applications for a tenure-track **ASSISTANT PROFESSOR** position in bacterial pathogenesis focusing on zoonotic or other emerging infectious diseases. Applicants must have a D.V.M. and/or Ph.D. and evidence of research accomplishments. The successful candidate will be expected to establish a nationally recognized and externally funded research program and contribute to teaching in the professional, graduate, or undergraduate curricula. The University of Georgia and the College of Veterinary Medicine are currently undergoing major expansions including BSL-3 and BSL-2 biocontainment animal health research facilities, the Paul C. Coverdell Biomedical Health Research Center, Center for Tropical and Emerging Global Diseases, and the Center for Disease Intervention. These units provide a state-of-the-art research environment. Interested applicants should submit a letter of application including a statement of research plans and career goals, curriculum vitae, and the names and addresses of three references to:

Dr. Frederick D. Quinn
Chair of the Search Committee
Department of Infectious Diseases
College of Veterinary Medicine
University of Georgia
Athens, GA 30602

Applications received before September 30, 2005, are assured full consideration. *The University of Georgia is an Equal Opportunity/Affirmative Action Employer.*

A **NONTENURE-TRACK FACULTY POSITION** is available at the Albert Einstein College of Medicine to develop high throughput capabilities for the global analysis of protein interactions, function, regulation, and integration. Appropriate areas of expertise include, but are not limited to, high throughput yeast two-hybrid and synthetic genetic array technologies, functional cloning of genes involved in secondary metabolic pathways and natural product biosynthesis, and biomedical microelectromechanical systems and nanostructure technologies. The position would be part of a new Integrated Genetics and Systems Biology Initiative and would complement existing strengths in mammalian genetics, microbiology, cancer biology, mechanistic enzymology, and structural genomics. Interested candidates should forward curriculum vitae, a brief one-page research plan, and the names of three references to: **Dr. Steven C. Almo, Department of Biochemistry, Albert Einstein College of Medicine, Jack and Pearl Resnick Campus, 1300 Morris Park Avenue, Bronx, NY 10461; e-mail: almo@aecom.yu.edu.** *Equal Opportunity Employer.*

POSITIONS OPEN

TENURE-TRACK FACULTY POSITION CELL BIOLOGY

The Department of Molecular and Cell Biology of The University of Texas at Dallas (UTD) (**website: http://www.utdallas.edu/biology/**) invites applications for a tenure-track Faculty appointment at any rank in the broad area of molecular cell biology. Preference will be for an investigator whose expertise complements existing strengths in the Department, which include neuronal apoptosis, gene regulation, sickle cell disease, and membrane trafficking. The School of Natural Sciences and Mathematics and the School of Engineering and Computer Sciences are expanding, with an emphasis on recruiting faculty who can foster interdisciplinary interactions. Candidates whose teaching and research link areas of cell biology with other disciplines, such as chemistry, physics, neuroscience, nanotechnology, and bioengineering, are encouraged to apply. Successful candidates will have had at least two years of postdoctoral experience, and have or show evidence they can develop externally funded research programs. Teaching responsibilities will include participation in appropriate graduate and undergraduate courses. Review of applications will begin immediately and will continue until the position is filled. Indication of sex and ethnicity for affirmative action statistical purposes is requested as part of the application but is not required. Forward curriculum vitae and short descriptions of research plans and teaching interests, and have three letters of reference sent to:

Academic Search #2073
The University of Texas at Dallas
P.O. Box 830688, AD 23
Richardson, TX 75083-0688

UTD is an Affirmative Action/Equal Opportunity Employer.

ASSISTANT/ASSOCIATE PROFESSOR

The Department of Comparative Biomedical Sciences is seeking a tenure-track Assistant/Associate Professor (Physiologist). The Department has numerous well-funded investigators in cell and molecular biology. Required qualifications: Ph.D. or equivalent degree in physiology and/or biological/biomedical sciences. Additional qualifications desired: D.V.M. degree; postdoctoral experience; ability to teach comparative vertebrate physiology of multiple-organ systems. Primary responsibilities: coordinates a two-semester, team-taught, physiology course in the veterinary professional curriculum; maintains a competitive, extramurally funded research program. Salary and rank will be commensurate with qualifications. Application deadline is August 26, 2005, or until candidate is selected. Submit letter of application and resume (including e-mail address) to:

Dr. Gary E. Wise, Professor and Head
Comparative Biomedical Sciences
School of Veterinary Medicine
Louisiana State University
Reference #000097
Baton Rouge, LA 70803
Telephone: 225-578-9889
E-mail: gwise@vetmed.lsu.edu

Louisiana State University is an Equal Opportunity/Equal Access Employer.

ASSISTANT RESEARCH PROFESSOR position available for one year to study mechanisms of cancer chemoprevention. Work in our laboratory is directed toward studying the effects of UVB-induced changes in DNA structure and mechanisms of effects of chemopreventive agents. Candidates with experience in molecular mechanisms of carcinogenesis, DNA sequencing, and fidelity of DNA polymerases are encouraged to send their curriculum vitae, statement of research interests, and list of three references to: **Allan H. Conney, Susan Lehman Cullman Laboratory for Cancer Research, School of Pharmacy, Rutgers, The State University of New Jersey, 164 Frelinghuysen Road, Piscataway, NJ 08854-8020. Fax: 732-445-0687; e-mail: bachorik@rci.rutgers.edu.**

POSITIONS OPEN

University of Michigan Health System

The University of Michigan Health System, Department of Ophthalmology, has the following openings: **RESEARCH LABORATORY SPECIALIST INTERMEDIATE.** We are seeking a candidate who can perform compound isolation, mass spectroscopy (MS), nuclear magnetic resonance (NMR) spectroscopy, and organic synthesis.

A Ph.D. is strongly desired. Experience with high performance liquid chromatography, MS, NMR carbohydrates, and lipids are preferred. Background in organic synthesis preferred. Will consider combination of education, experience and ability, with a minimum of a Master's degree in a related science curriculum.

RESEARCH FELLOW. A Postdoctoral position is available to study signaling using imaging techniques. Studies will focus on cell analysis using several microscope-based methodologies. Duties include preparation of cells, reagents, image processing, and writing manuscripts.

Ph.D. in cell biology or immunology with experience in electrophysiology or experience in imaging or immunologic inflammation or retinal biology is required. Must be able to function independently, good communication skills, and evidence of previous publication are essential.

Send resumes to: **Dr. Howard Petty, The University of Michigan, Kellogg Eye Center, 1000 Wall Street, Ann Arbor, MI 48105-0714.** *A nondiscriminatory, Affirmative Action Employer.*

The Department of Infectious Diseases, College of Veterinary Medicine, University of Georgia, invites applications for a tenure-track **ASSISTANT** or **ASSOCIATE PROFESSOR** position in parasitology. Applicants must have a D.V.M. and/or Ph.D., postdoctoral experience, and evidence of research accomplishments. Of special interest are investigators with research programs in molecular helminthology, but individuals in a broad range of parasitology-related disciplines are encouraged to apply. The successful candidate will be expected to establish a nationally recognized and externally funded research program and contribute to teaching in the professional and graduate curricula. The University of Georgia and the College of Veterinary Medicine offer a highly innovative and vigorous research environment including biocontainment animal health research facilities, the Biomedical Health Research Center, the Center for Tropical and Emerging Global Diseases, and the Filariasis Research Reagent Resource Center. For more information, log onto **website: http://www.vet.uga.edu/id/parasitology_search.htm.** Interested applicants should submit a letter of application including a statement of research plans, career goals, and teaching interests, along with curriculum vitae and three references to:

Dr. John W. McCall
Chair of the Search Committee
Department of Infectious Diseases
College of Veterinary Medicine
University of Georgia
Athens, GA 30602

Applications received before August 1, 2005, are assured consideration. *The University of Georgia is an Equal Opportunity/Affirmative Action Employer.*

POSTDOCTORAL FELLOWSHIPS

Michigan Society of Fellows postdoctoral fellowships program is offering three-year Fellowships at the University of Michigan to begin September 2006. Annual stipend will be $47,271. Application postal deadline: September 30, 2005. Information and applications are available online at **website: http://www.rackham.umich.edu/Faculty/society.html,** or by writing: **Society of Fellows, 3572 Rackham Building, University of Michigan, 915 E. Washington Street, Ann Arbor, MI 48109-1070. E-mail: society.of.fellows@umich.edu.** No e-mail applications accepted.

POSITIONS OPEN

TENURE-TRACK FACULTY POSITION BIOMOLECULAR STRUCTURE

The Department of Molecular and Cell Biology of The University of Texas at Dallas (UTD) (**website: http://www.utdallas.edu/biology/**) invites applications for a tenure-track Faculty appointment at any rank in the broad area of biomolecular structure. Preference will be for an investigator who complements existing strengths in investigating nucleic acid-protein interactions and who shows evidence of a vigorous and independent research program that is or will be externally supported. The Department is actively involved in interdisciplinary research, graduate training at the doctoral level, and educating a select group of undergraduate students. The School of Natural Sciences and Mathematics and the School of Engineering and Computer Sciences are undertaking a major expansion, with an emphasis on recruiting faculty who can foster interdisciplinary interactions. This expansion includes the construction of a new building for science and engineering research, equipped with state-of-the-art facilities. Applicants would desirably have at least two years of postdoctoral experience. The candidate will be expected to fully participate in graduate and undergraduate education. Review of applications will begin immediately and will continue until the position is filled. Indication of sex and ethnicity for affirmative action statistical purposes is requested as part of the application but not required. Interested individuals should submit curriculum vitae, a statement of research plans and teaching interests, and have three letters of reference sent to:

Academic Search #2072
The University of Texas at Dallas
P.O. Box 830688, AD 23
Richardson, TX 75083-0688

UTD is an Affirmative Action/Equal Opportunity Employer.

The Institute of Atomic and Molecular Sciences, Academia Sinica, invites qualified candidates to apply for **TENURE-TRACK RESEARCH FELLOW POSITIONS** in the following research fields: surface science, biophysical science, nano-science, theoretical molecular dynamics, experimental atomic physics, and ultrafast and high-field optics. Please visit **website: http://www.iams.sinica.edu.tw** for detailed academia activities of the Institute. Successful candidates must show excellent academic achievements and abilities to establish a successful research program within the Institute in the above research fields. Collaborations with other research fellows are strongly encouraged. Interested applicants should send full curriculum vitae by airmail, including a list of publications, a research proposal, and at least three letters of recommendation to: **Dr. Szu-yuan Chen, Room 325, P.O. Box 23-166, Institute of Atomic and Molecular Sciences, Academia Sinica, Taipei, Taiwan. E-mail: sychen@ltl.iams.sinica.edu.tw; fax: 886-2-2362-7064.** To ensure timely processing, all application materials must be received by September 30, 2005.

POSTDOCTORAL POSITIONS: Several Postdoctoral positions funded by the National Institutes of Health are available, to study the roles of insulin, nitric oxide, and protein tyrosine phosphatases in regulation of vascular smooth muscle cell signaling and neointima formation in vascular injury. Our projects address important basic science questions and also have relevance to clinical problems. Experience in molecular biology and/or rat and mouse surgery is essential. Competitive salaries are offered. Please send curriculum vitae and the names of three references to: **Dr. Aviv Hassid, Department of Physiology, University of Tennessee, 894 Union Avenue, Memphis, TN 38163. E-mail: ahassid@tennessee.edu; fax: 901-448-7126.** *The University of Tennessee is an Equal Employment Opportunity/Affirmative Action/Title IV/Title IX/Section 504/ADA/ADEA Institution in the provision of its education and employment programs and services.*

Sponsored by MERCK

Attend the next *Science* Career Fair

10 August 2005
11:00 a.m.–4:00 p.m.
Boston Convention Center
Room 253
Boston, MA

Science is hosting this career fair in conjunction with **Drug Discovery Technology™ 2005**

Scientists

Scientists at all levels are invited to meet recruiters face to face.

Attendance is free.

Visit ScienceCareers.org and click on Career Fairs for more information and a list of exhibitors.

Experts will be on hand to help you refine your resume.

Post your resume

Exhibitors have access to *Science*'s Resume/CV Database prior to the event, so post your resume today at ScienceCareers.org.

Exhibitors

Meet scientists with varying experience and backgrounds.

Exhibitor rate: $3,000

Free access to *Science*'s Resume/CV Database through 31 August when you sign up to exhibit at the career fair.

To exhibit, contact Daryl Anderson:
Phone ..... (202) 326-6543
Fax ..... (202) 289-6742
E-mail ... advertise@sciencecareers.org

ScienceCareers.org
We know science AAAS

POSITIONS OPEN

RESEARCH STAFF SCIENTIST

Applications are invited for a Research Scientist position in the Oncology Research Institute (ORI) at Sioux Falls, South Dakota. ORI is part of the South Dakota Health Research Foundation (SDHRF), which is a partnership between the University of South Dakota School of Medicine and Sioux Valley Hospitals and Health System. This particular position is in the Gynecologic Oncology Laboratory that focuses on human papilloma virus (HPV)/cervical cancer research. An academic appointment with the University of South Dakota School of Medicine is available for this position based on qualifications and experience.

Applicants must have a Ph.D. or equivalent in biomedical sciences with at least three years of postdoctoral research training in molecular biology. Prior experience in HPV research is a plus as well as previous experience doing research with a clinician. Excellent oral and written communication and personnel skills are essential in addition to being highly self-motivated and disciplined.

Applicants should submit a letter of interest, curriculum vitae, and the contact information of three references to: **Human Resources, South Dakota Health Research Foundation, 1100 East 21st Street, Suite 700, Sioux Falls, SD 57105. Fax: 605-328-1355; e-mail: bpoppens@usd.edu.**

Applications will be accepted until the position is filled. Review of applications will begin on July 25, 2005, until a suitable candidate is found.

SDHRF is an Equal Opportunity/Affirmative Action Employer.

DIRECTOR
National Oceanic and Atmospheric Administration
Fisheries Service
Office of Science and Technology

As Director, Office of Science and Technology, National Oceanic and Atmospheric Administration (NOAA) Fisheries Service, the incumbent is responsible for developing national standards, policies, and operational guidelines for research programs and scientific activities, reviewing and evaluating scientific and technical aspects for the collection of fishery statistics and fisheries research, overseeing the management and collection of fisheries statistics and social and economic data, development of long-term science and technology policy and strategy, and other duties. The position is located in NOAA headquarters in Silver Spring, Maryland. As a member of the Senior Executive Service, this is a science leadership position within the Agency. Full description of duties, qualifications, and application procedures can be found at **website: http://www.usajobs.gov** (announcement NOAA#05-06.NJH). For further information contact: **Ms. Norma Hughes** at **telephone: 301-713-0530, extension 205. E-mail: norma.j.hughes@noaa.gov.** Closing date is August 5, 2005.

POSTDOCTORAL POSITIONS
Protein Synthesis and Synthetic Biology
Vanderbilt University

Join the Pharmacology Department ranked no. 1 nationally in citations per faculty: **website: http://www.vanderbilt.edu/pharmacology.** For details see laboratory **website: https://medschool.mc.vanderbilt.edu/forster.** Minimal qualifications include expertise in molecular biology and two first-authored research papers in international peer-reviewed journals. Experience with translation or RNA is a plus. The University is located on a single, beautiful campus in the livable "Music City." Please e-mail a letter of interest, curriculum vitae, and names, e-mail addresses, telephone numbers of three references to: **Anthony C. Forster, M.D., Ph.D., Department Pharmacology and Vanderbilt Institute of Chemical Biology, PRB 459, Vanderbilt University Medical Center, 23rd Avenue South at Pierce, Nashville, TN 37232, U.S.A.** *Vanderbilt University is an Affirmative Action/Equal Opportunity Employer. Women and minority candidates are encouraged to apply.*

POSITIONS OPEN

Seeking a **JUNIOR-LEVEL FACULTY MEMBER** to join an interactive and growing group of basic and clinical scientists. Requires a doctoral degree (Ph.D., D.V.M., or M.D.) with at least two years of postdoctoral training and the ability to develop an independent research program that focuses on one or more aspects of women's reproductive health. Prefer candidate with experience in ovarian biology and function, and with a record of extramural funding. Salary and Harvard Medical School academic appointment is commensurate with experience. Send current curriculum vitae and contact information for three references (names, address, telephone, e-mail) to: **Vincent Center for Reproductive Biology at Massachusetts General Hospital, VBK121, 55 Fruit Street, Boston MA 02114.** Send electronic applications to (**e-mail: sgilligan@partners.org**). Additional information is available on the Vincent Center for Reproductive Biology **website: http://www.vcrb.org.** *Massachusetts General Hospital is a teaching affiliate of Harvard Medical School and an Equal Opportunity Employer.*

BIOLOGY DEPARTMENT POSITION
University of Louisville

The Department of Biology at the University of Louisville, **website: http://www.louisville.edu/a-s/biology,** invites applications for a position in conservation biology. **ENDOWED CHAIR:** The Wallace Endowment fund is supporting a Chair (rank open) in conservation biology who will complement existing strengths of the Department in ecosystem, restoration, and organismal ecology. Conservation biologists with interests and expertise in landscape ecology (ecological impacts of fragmentation, disturbance, and land-use change), geographic information system, or simulation modeling are especially encouraged to apply. The successful candidate is expected to contribute to undergraduate and graduate programs and to maintain an excellent record of research productivity and external funding. Applicants should submit curriculum vitae, statements of research and teaching interests, representative reprints, and contact information for three references to: **Department of Biology, University of Louisville, Louisville, KY 40292.** Review of applications will begin on October 1, 2005, and will continue until the position is filled. *Women and minorities are encouraged to apply. The University of Louisville is an Affirmative Action/Equal Opportunity Employer.*

VISITING ASSISTANT PROFESSOR

The Department of Biological Sciences at the University of Illinois at Chicago (UIC) invites applications for a Visiting Assistant Professor position. This is a one AY appointment, effective August 15, 2005, through May 15, 2006, with the possibility of renewing for one additional year. Duties include teaching two courses per semester. Minimum requirements are Ph.D. in neurobiology or a related science field and relevant teaching experience. This is a nontenured position. The salary is $50,000. Please send resume and three reference letters to: **Ms. Stephanie Davis, Department of Biological Sciences, University of Illinois at Chicago, 845 W. Taylor Street m/c 066, Chicago, IL 60607** or **e-mail: sydavis@uic.edu.** Application deadline is July 31, 2005. *UIC is an Affirmative Action/Equal Opportunity Employer.*

POSTDOCTORAL POSITION is available immediately at the Medical University of South Carolina to participate in the NIH Training Program on the mechanisms of autoimmunity and fibrosis. The candidate should have a Ph.D. degree and a strong background in molecular biology, cell biology, or immunology. Submit curriculum vitae and names of three references to: **Maria Trojanowska, Ph.D., Division of Rheumatology and Immunology, Medical University of South Carolina, 96 Jonathan Lucas Street, Suite 912, Charleston, SC 29425. E-mail: trojanme@musc.edu.**

POSITIONS OPEN

ECOLOGY SEARCH REOPENED
Tennessee

The Department of Ecology and Evolutionary Biology at the University of Tennessee seeks to fill a tenure-track position with a Field Ecologist interested in research across spatial scales or at broad spatial scales, to start August 1, 2006. The position is at the **ASSISTANT** (or, in exceptional circumstances, **ASSOCIATE**) **PROFESSOR** level. We especially seek applicants who will develop a vigorous field-based research program, in part within the southern Appalachians. Teaching will include an upper-division course in ecology and an advanced course in the applicant's specialty.

For more information visit **website: http://eeb.bio.utk.edu.** Candidates should apply to:

Dr. Dan Simberloff
Department of Ecology and Evolutionary Biology
University of Tennessee
Knoxville, TN 37996

Applicants should send curriculum vitae, statements of research and teaching goals, and arrange for three reference letters to be submitted. Applications will be reviewed beginning 26 September 2005. *The University of Tennessee is an Equal Employment Opportunity/Affirmative Action/Title VI/TitleIX/Section 504/Americans with Disabilities Act/Age Discrimination in Employment Act Institution in the provision of its Education and Employment programs and services.*

Two **POSTDOCTORAL POSITIONS:** Electrophysiologist/Molecular Biologist: One position is to study calcium sparks, calcium channels, and potassium channels in arterial smooth muscle cells. Experience with cardiovascular physiology, electrophysiology, and/or calcium imaging preferred. A second Postdoctoral position requires expertise with molecular biology, including cloning, western blotting, reverse transcription polymerase chain reaction, and pinpoint mutagenesis. Required qualifications for both positions include a Ph.D. or M.D. Send curriculum vitae and names and addresses of three references to: **Jonathan H. Jaggar, Ph.D., Department of Physiology, University of Tennessee Health Science Center, 894 Union Avenue, Memphis, TN 38163, U.S.A. E-mail: jjaggar@physio1.utmem.edu.**

The University of Tennessee is an Equal Employment Opportunity/Affirmative Action/Title IV/Title IX/Section 504/ADA/ADEA Institution in the provision of its education and employment programs and services.

ASSISTANT PROFESSOR position available in the Department of Neurosurgery at Yale University School of Medicine. Applicants should demonstrate considerable expertise in the early embryonic development of sensory systems and the underlying mechanisms. Outstanding skills in protein detection, confocal microscopy, and the ability to successfully compete for extramural funding will be important in selecting the final candidates. Curricula vitae and the names and e-mail addresses of references can be submitted to: **Charles A. Greer, Ph.D., Department of Neurosurgery, Yale University School of Medicine, P.O. Box 208082, New Haven, CT 06520-8082;** or by **e-mail: charles.greer@yale.edu.** Deadline for applications is August 21, 2005.

Yale University is an Affirmative Action/Equal Opportunity Employer. Minorities and women are encouraged to apply.

Additional job postings not featured in this issue can be viewed online at **website: http://www.sciencecareers.org.** New jobs are added daily!

Manage your job search more effectively by creating an account at **website: http://www.sciencecareers.org.** You can post your resume (open or confidentially) in our database and use it to apply to multiple jobs simultaneously. Track the jobs you have applied to in special tracking folders. Plus, you can create Job Alerts that will e-mail you notification of jobs that match your search criteria.

COURSE

ADVANCED BIOLOGY TRAINING COURSE IN ANTARCTICA

Integrative Biology and Adaptation of Antarctic Marine Organisms

This National Science Foundation sponsored course will be held in Antarctica at the United States' McMurdo Station for one month, starting January 2006. This is an international course, open to all nationalities. Applications are invited from graduate students, postdoctoral fellows, and other research scientists who are interested in the study of extreme environments and the biology of Antarctic organisms.

The course will accommodate up to 20 students. Full scholarships are available to each student accepted into the course to cover the cost of travel from home institution to Antarctica, and room and board while in Antarctica. The emphasis of the Antarctic Biology Course is on integrative biology, with laboratory- and field-based projects focused on adaptations in an extreme polar environment. A diverse teaching faculty will offer students the possibility of working on a wide range of Antarctic organisms (bacteria, algae, invertebrates, and fish), as well as working at several different levels of biological analysis (molecular biology, physiological ecology, species diversity, and evolution).

Deadline for receipt of completed applications is **September 1, 2005**.

For more information and on-line applications, please see:
http://antarctica.usc.edu

GRANTS

› **Research on biology and/or pathology of malaria parasites**

› **Up to €100,000 a year for up to 3 years**

These grants provide scientists who are early in their careers the opportunity to integrate in the EU Network on basic malaria research and to strengthen research infrastructure in the African institution.

Grants are supported by the EU Network on Biology and Pathology of Malaria Parasites (BioMalPar), in collaboration with Multilateral Initiative on Malaria and Tropical Diseases Research (MIM/TDR).

› Go to **www.biomalpar.org** for complete details.

PRIZES

MARCH OF DIMES PRIZE IN DEVELOPMENTAL BIOLOGY

Nominations of candidates are solicited for the 11th annual prize to be awarded in 2006. Please make your recommendations on or before **September 15, 2005**.

The March of Dimes Prize in Developmental Biology, a cash award of $250,000 and a silver medal in the design of the Roosevelt dime, is awarded to investigators whose research has profoundly advanced the science that underlies our understanding of birth defects.

Nomination forms are available upon request from:

Michael Katz, M.D.
Senior Vice President for Research and Global Programs
March of Dimes
1275 Mamaroneck Avenue
White Plains, NY 10605
Telephone: (914) 997-4555
Facsimile: (914) 997-4560
mkatz@marchofdimes.com

The previous recipients were:

2005 - Mario R. Capecchi and Oliver Smithies
2004 - Mary F. Lyon
2003 - Pierre Chambon and Ronald M. Evans
2002 - Seymour Benzer and Sydney Brenner
2001 - Corey S. Goodman and Thomas M. Jessell
2000 - H. Robert Horvitz
1999 - Sir Martin J. Evans and Richard L. Gardner
1998 - Davor Solter
1997 - Walter J. Gehring and David S. Hogness
1996 - Ralph L. Brinster and Beatrice Mintz

CONFERENCE

Conference and Exhibition

Keynote Speakers

Dr. John J. Rossi
City of Hope National Medical Center

Ronald H.A. Plasterk PhD.
Netherlands Institute for Developmental Biology

Amsterdam, Netherlands
28-29 September 2005

The location of RNAi Europe 2005 is the Hilton Amsterdam, allowing easy access from both Europe and North America. This luxurious hotel is in one of the city's most exclusive areas, close to Amsterdam's best shopping streets and the city's commercial and financial centre. It is located 15 minutes drive from Schiphol Airport and downtown is only 10 minutes away.

www.RNAiEurope.com

Corporate Sponsors:

QIAGEN · invitrogen · DHARMACON · IDT INTEGRATED DNA TECHNOLOGIES, INC.

Believe it!

DNA Sequencing for $2.50 per reaction.

- Read length up to 900 bases.
- High quality electropherograms.
- Fast turnaround.
- Plasmid and PCR purification available.

POLYMORPHIC
Polymorphic DNA Technologies, Inc.℠

www.polymorphicdna.com
info@polymorphicdna.com

1125 Atlantic Ave., Ste. 102
Alameda, CA 94501

Polymorphic exclusively uses ABI 3730XL sequencers.
Data delivered via secure FTP, email or CD.
No charge for standard sequencing primers.
96 sample minimum order.
96 well plates only- no tubes.

888.362.0888

For more information please visit
www.polymorphicdna.com